AWARD NUMBER: W81XWH-16-1-0179

TITLE: Targeting Extracellular Histones with Novel RNA Bio-drugs for the Treatment of Acute Lung Injury

PRINCIPAL INVESTIGATOR: Francis Miller

CONTRACTING ORGANIZATION: Duke University

REPORT DATE: July 2020

TYPE OF REPORT: Final progress report

PREPARED FOR: U.S. Army Medical Research and Materiel Command
Fort Detrick, Maryland 21702-5012

REPORT DOCUMENTATION PAGE

Form Approved
OMB No. 0704-0188

1. REPORT DATE	2. REPORT TYPE	3. DATES COVERED
July 2020	Final	09/15/2016 - 03/14/2020

4. TITLE AND SUBTITLE
Targeting Extracellular Histones with Novel RNA Bio-drugs for the Treatment of Acute Lung Injury

5a. CONTRACT NUMBER

5b. GRANT NUMBER
W81XWH-16-1-0179

5c. PROGRAM ELEMENT NUMBER

6. AUTHOR(S)
Francis J Miller, MD

E-Mail: francis.miller@duke.edu;

5d. PROJECT NUMBER

5e. TASK NUMBER

5f. WORK UNIT NUMBER

7. PERFORMING ORGANIZATION NAME(S) AND ADDRESS(ES)

Duke University
200 West Main St
Suite 820 Erwin Square Plaza
Durham, NC 27705-0000

Subcontract to:
UNIVERSITY OF IOWA, THE
105 JESSUP HALL
IOWA CITY IA 52242-1316

8. PERFORMING ORGANIZATION REPORT NUMBER

9. SPONSORING / MONITORING AGENCY NAME(S) AND ADDRESS(ES)

U.S. Army Medical Research and Materiel Command
Fort Detrick, Maryland 21702-5012

10. SPONSOR/MONITOR'S ACRONYM(S)

11. SPONSOR/MONITOR'S REPORT NUMBER(S)

12. DISTRIBUTION / AVAILABILITY STATEMENT

Approved for public release; distribution unlimited

13. SUPPLEMENTARY NOTES

14. ABSTRACT

Extracellular histones have been proposed as a causative agent of acute lung injury (ALI). The goal of this proposal was to develop a therapeutic to neutralize (inactivate) circulating histones and prevent the multiple organ dysfunction/acute respiratory distress syndrome (MODS/ARDS) occurring with ALI. To accomplish this goal, we developed synthetic oligonucleotides (RNA aptamers) that bind to extracellular histones known to cause MODS/ARDS but do not bind to other serum proteins. In vitro studies showed that selected RNA aptamers protected from histone-mediate cytotoxicity, platelet aggregation, inflammatory activation, and calcium influx. In a murine model of histone-mediated ALI, aptamers attenuated pulmonary toxicity and improved survival. In a smoke inhalation model of ALI, RNA aptamer protected mice from alveolar barrier disruption, decreased cytokine activation, and neutrophil infiltration. RNA aptamer attenuated weight loss, barrier disruption and inflammation in the lungs in a murine model of H1N1 influenza. The RNA aptamers did not activate innate immunity and caused no abnormalities of general clinical chemistries, or of liver and kidney function.

15. SUBJECT TERMS
Acute lung injury (ALI), acute respiratory distress syndrome (ARDS), extracellular histones, circulating histones, aptamers, oligonucleotides, smoke inhalation injury, influenza

16. SECURITY CLASSIFICATION OF:			17. LIMITATION OF ABSTRACT	18. NUMBER OF PAGES	19a. NAME OF RESPONSIBLE PERSON
a. REPORT	b. ABSTRACT	c. THIS PAGE			USAMRMC
Unclassified	Unclassified	Unclassified	Unclassified	139	19b. TELEPHONE NUMBER *(include area code)*

TABLE OF CONTENTS

1. INTRODUCTION:

A challenging medical problem often observed in critically ill patients is that following a severe injury or illness, even those organs not directly affected by the original problem subsequently become dysfunctional. This condition, known as multiple organ dysfunction syndrome (MODS), may be reversible, but there is no treatment to prevent it from happening, and of those that develop MODS, the risk of death is 40%. The most common organ involved in MODS is the lungs (referred to as acute respiratory distress syndrome or ARDS). Trauma (blast and explosive) has obvious relevance to the military; however, other equally relevant causes of MODS/ARDS are acute lung injury (ALI) from smoke/chlorine gas inhalation, burns, radiation, influenza, and severe infection. Only recently have investigators recognized that each of these various conditions is caused by damaged tissues releasing histones into the circulation. Histones typically reside in the nucleus and partner with the DNA, but when extracellular histones have toxic effects on the lungs and other organs. The goal of this proposal was to develop a therapeutic to neutralize (inactivate) circulating histones and prevent the morbidity and mortality associated with MODS/ARDS caused by ALI that can be quickly delivered in combat and field situations. To accomplish this goal, we first identified synthetic oligonucleotides (RNA aptamers) that bind to histones but not to other circulating proteins. The studies performed here were designed to perform in vitro and in vivo experiments to test the efficacy of these histone-specific RNA aptamers. Studies were performed in human cultured cells and murine models of acute lung injury, including chlorine gas inhalation injury, smoke inhalation injury, and influenza infection. Since histones are highly conserved across species from yeast to humans, the bio-reagents developed and validated in this proposal can be immediately tested in preclinical animal models and human clinical trials. Furthermore, as a drug to prevent the development of MODS/ARDS and ALI in high-risk patients, these bio-reagents have significant advantages as compared to other possible therapeutics because they are very stable and not as susceptible to fluctuations in temperature, do not require special handling conditions, do not cause allergic responses, and will be easy to deliver. In addition to having relevance to military situations, the therapeutics derived from this application would have broad benefits to the general population in reducing morbidity and mortality associated with MODS/ARDS.

2. KEYWORDS:

Acute lung injury (ALI), acute respiratory distress syndrome (ARDS), extracellular histones, circulating histones, aptamers, oligonucleotides, smoke inhalation injury, influenza.

3. ACCOMPLISHMENTS:

What were the major goals of the project?

The primary goal of this project was to test the efficacy of selective RNA aptamers to inactivate circulating histones and prevent the morbidity and mortality associated with acute lung injury. More specifically, the major goals of this project, as outlined in the approved SOW were:

Major Task 1:	Local IRB/IACUC Approval	100% completed
Major Task 2:	In vitro functional efficacy of aptamers	100% completed
Major Task 3:	Evaluation of efficacy in inhalation injury models	100% completed
Major Task 4:	Evaluation of efficacy in influenza injury model	100% completed
Major Task 5:	Evaluation of safety.	100% completed

What was accomplished under these goals?

The methodology and summary data supporting the accomplishments listed below are described in our *Nature Communications*. Manuscript. Figure numbers refer to the figure in the manuscript (see appendix). We have also identified the major findings that support the Major Tasks outlined in the SOW.

- Identification of histone-specific RNA aptamers – Figure 1 and Supplemental Figures 1 and 2.
- High specificity binding of RNA aptamers to histones but not to serum proteins - Figure 2.
- Stability of RNA aptamers in human serum - Supplementary Figure 3.
- RNA aptamers inhibit histone-induced platelet aggregation – Figure 3 and Supplementary Figure 4. (SOW Major task 2)
- RNA aptamers inhibit histone-induced Toll like receptor (TLR) activation - Figure 3 and Supplementary Figure 4. (SOW Major task 2)
- RNA aptamers inhibit histone-mediated toxicity of endothelial cells - Figure 3. (SOW Major task 2)
- RNA aptamers inhibit histone-mediated extracellular calcium influx into endothelial cells - Figure 3. (SOW Major task 2)
- RNA aptamers prevent death in a murine model of MODS – Figure 4.
- RNA aptamers attenuate the histologic findings of vascular congestion, multifocal neutrophilic aggregates in vessels, thrombi, and in the lung in response to intravenous histones in mice – Figure 4 and Supplementary Figure 5.
- RNA aptamers partially attenuate TLR activation in the liver but not in lung or spleen in response to intravenous histones – Figure 4.
- Aptamers bind and neutralize histones generated in NETosis of human neutrophils – Figure 6.

Manuscripts are currently under preparation (refs 2 and 3 below) that report the following accomplishments:

- Development of an aptamer-based histone detection assay more sensitive than currently available methods for detection of extracellular histones in blood and biologic fluids. (SOW Major task 2)
- RNA aptamers detect low levels (< 10 μg/mL) of circulating histones in blood from critically ill patient samples. (SOW Major task 2)
- Validation of the aptamer-based detection assay showing that serum histone levels in ICU patients are associated with severity of illness (APACHE II score). (SOW Major task 2)
- Confirmed the efficacy of aptamers pre- and post- histone exposure in cultured cells.
- RNA aptamers inhibit histone-mediated TLR activation and apoptosis of human pulmonary microvascular endothelial cells and human epithelial cells in culture. (SOW Major task 2)
- RNA aptamers inhibit histone-induced endothelial cell dysfunction in culture. (SOW Major task 2)
- Characterized histone-mediated ALI in mice following oropharyngeal aspiration of calf thymus-derived histones, resulting in increased levels of neutrophils, albumin and cytokines in

bronchoalveolar lavage fluid (BALF) and histologic evidence of alveolar edema, inflammatory infiltrate, and alveolar disruption.

- Evaluated the retention and distribution of RNA aptamers in the lung by delivery of a fluorescent-labeled RNA aptamer by oropharyngeal aspiration in mice. The aptamer was distributed throughout all segments of the lung and remained present in BALF and the alveoli at 24 hours without causing inflammatory cell infiltration or alveolar injury. (SOW Major task 3)
- RNA aptamer 30 minutes before or 30 minutes after histone-mediated ALI markedly attenuated barrier disruption, interstitial edema, and inflammatory cell infiltration in the lungs of mice. (SOW Major task 3)
- Development of smoke inhalation model in mice. Intratracheal delivery of smoke particulate matter when derived from flammable wood increases extracellular histones, albumin, and inflammatory cell infiltration in the BALF, induced lung edema and weight loss. (SOW Major task 3)
- RNA aptamer attenuated weight loss, cytokine activation, alveolar barrier disruption and neutrophil infiltration in mice after exposure to wood smoke particulate matter. (SOW Major task 3)
- Secondary to the small caliber of airways, the inhalation of chlorine gas by mice predominantly causes large airway sloughing and irritation but not the increased alveolar-capillary permeability characteristic of ALI. Larger animal models are necessary for testing chlorine gas ALI. (SOW Major task 3)
- Adapted influenza lung infection model in mice. Influenza infection increased extracellular histones, alveolar permeability, and inflammation in BALF. RNA aptamer attenuated weight loss, barrier disruption and inflammation in lungs in a murine model of H1N1 influenza. (SOW Major task 4)
- RNA aptamer alone does not cause an inflammatory response when administered to the lungs of mice. (SOW Major task 5)
- Aptamers did not activate innate immunity (no increase of 2’5’-oligoadenylate synthetase, interleukin-6, type I interferon, interferon beta or gamma) in kidney, liver, lung, or spleen. (SOW Major task 5)
- Aptamers caused no abnormalities of a general clinical chemistry panel (included liver function and renal function). (SOW Major task 5)

The data supporting each of these conclusions is discussed in more detail below and in the appendix. The SOW table directly below has the addition of a column that indicates where the supporting data can be found.

Approved SOW :		
Specific Aim 1: In vitro characterization and optimization of RNA aptamers that selectively bind to human histone.	**Work Completed**	**DATA**
Major Task 1L Local IRB/IACUC Approval		
Local IRB approval	100%	N/A
Local IACUC approval	100%	N/A
Major Task 2: In vitro - functional efficacy of aptamers		
Measurement of calcium influx by fura-2 in human pulmonary microvascular endothelial cells.	100%	Urak et al. Figures 3D, 5B
Measurement of TLR activation in human pulmonary microvascular endothelial cells	100%	Urak et al. Figure 3B And Figure 2 below
Detection of cell toxicity Cell lines used: human pulmonary microvascular endothelial cells	100%	Urak et al. Figures 3C, 5A And Figures 1, 3 below
Measure platelet thrombi formation Human platelets (healthy donors)	100%	Urak et al. Figures 3A, and Suppl Fig 3A,B
Measure platelet surface marker expression in human platelets (healthy donors)	100%	Figure 3E below, MHSRS poster Fig 5
Ex vivo experiment using blood from patients with ALI	100%	Shubham et al. Figure 4
Specific Aim 2: Evaluate efficacy and safety of histone-specific RNA aptamers in vivo		
Major Task 3: Evaluation of efficacy in inhalation injury model (chlorine inhalation and smoke inhalation models)		
Assessment of minimal effective dose (MED) C57/BL6 mice	100%	See text and Figure 4 and 5 below
Assessment of alveoloar permeability and inflammation by bronchoalveolar lavage	100%	See text and Figure 4 and 5 below
Lung histology by histopathologic staining and analysis	100%	See text and Figure 4 and 5 below
Major Task 4: Evaluation of efficacy in influenza lung injury model		
Assessment of minimal effective dose (MED) C57/BL6 mice.	100%	Figure 7 below
Assessment of alveoloar permeability and inflammation by bronchoalveolar lavage	100%	Figure 7 below
Lung histology by histopathologic staining and analysis	100%	Figure 7 below
Major Task 5: Evaluation of safety		
Rising dose and repeated dose toxicology studies to establish a no observed adverse event level (NOAEL) in vitro and in vivo	100%	See appendix and Figure 8 below
Assessment of potential immunostimulation in humanized mice	100%	See appendix and Figure 8 below

We assessed three distinct murine models of ALI relevant to military situations: (1) chlorine gas inhalation, (2*)* wood smoke inhalation, and *3)* influenza infection. The predominant site of injury of chlorine gas in mice was the trachea and bronchi, with the alveoli showing unreliable injury, likely due to the small caliber of airways that absorb chlorine before it reaches the alveoli. Larger animal models are necessary to test chlorine gas ALI. Wood smoke inhalation was tested by intratracheal administration of flaming eucalyptus particulate matter. Influenza infection (Flu) was tested by intranasal inoculation of influenza A/Puerto Rico/8/34, H1N1 virus.

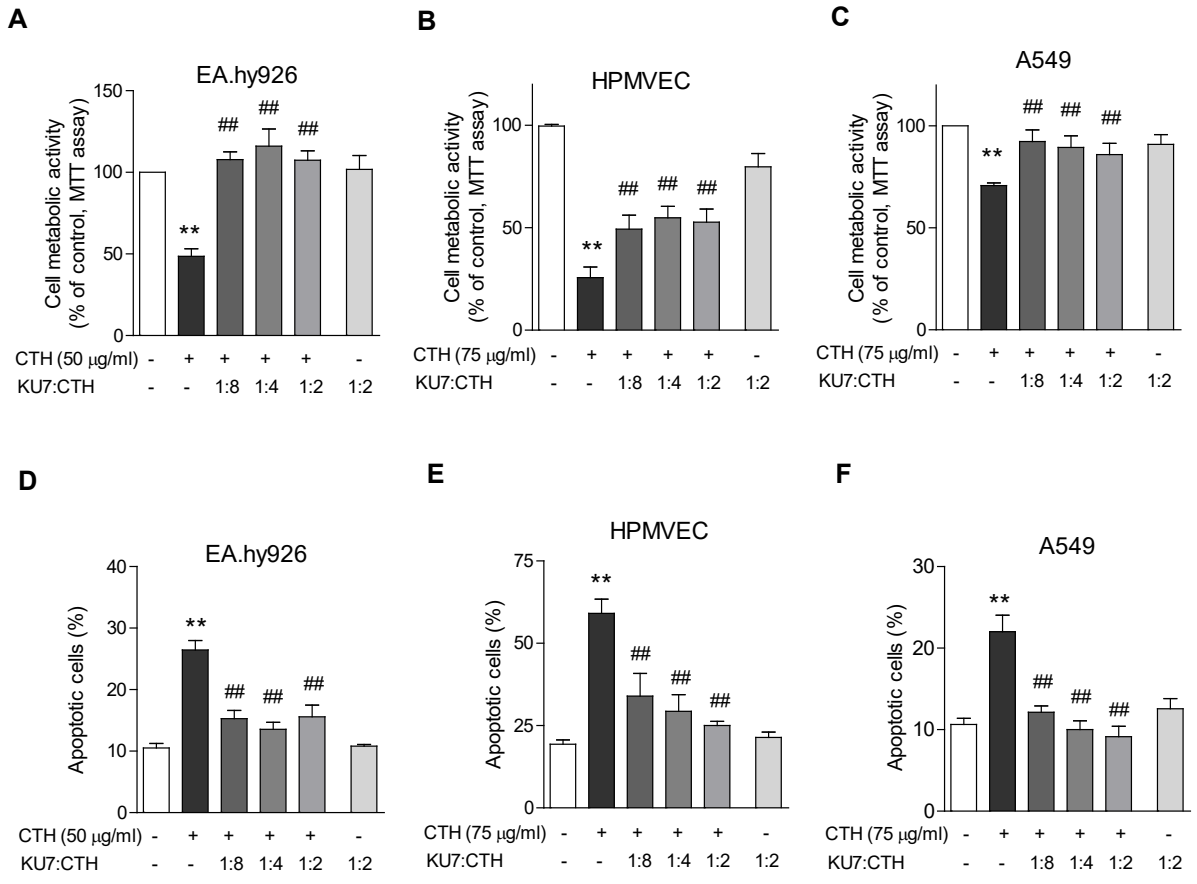

Figure 1. RNA aptamer KU7 prevents histone-induced cytotoxicity. Calf thymus histones (CTH) reduced cellular metabolic activity of (A) human endothelial EA.hy926 cells (24 hours), (B) human pulmonary microvascular endothelial cells (HPMVEC, 4 hours) and (C) human epithelial A549 cells (24 hours) as measured by MTT assay. CTH also caused apoptosis of (D) EA.hy926, (E) HPMVEC and (F) A549 cells as measured by Annexin V staining. The addition of aptamer KU7 30 minutes after CTH prevented histone-mediated toxicity. Ratio refers to molar ratio of KU7 to CTH. N = 4-8. **P < 0.01 vs control; ##P < 0.01 vs CTH.

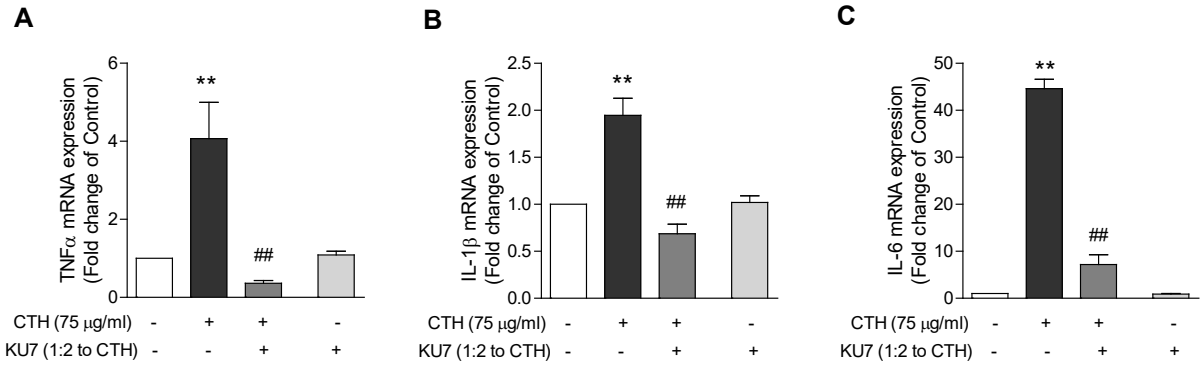

Figure 2. KU7 prevents histone-mediated upregulation of pro-inflammatory cytokines. Calf thymus histones (CTH, 75 μg/ml) for 4 hours increased mRNA expression of cytokines in human pulmonary microvascular endothelial cells (HPMVEC), as measured by RT-PCR. The addition of aptamer KU7 30 minutes after CTH prevented histone-mediated cytokine activation. Ratio refers to molar ratio of KU7 to CTH. N = 3-4. **P < 0.01 vs control; ##P < 0.01 vs CTH.

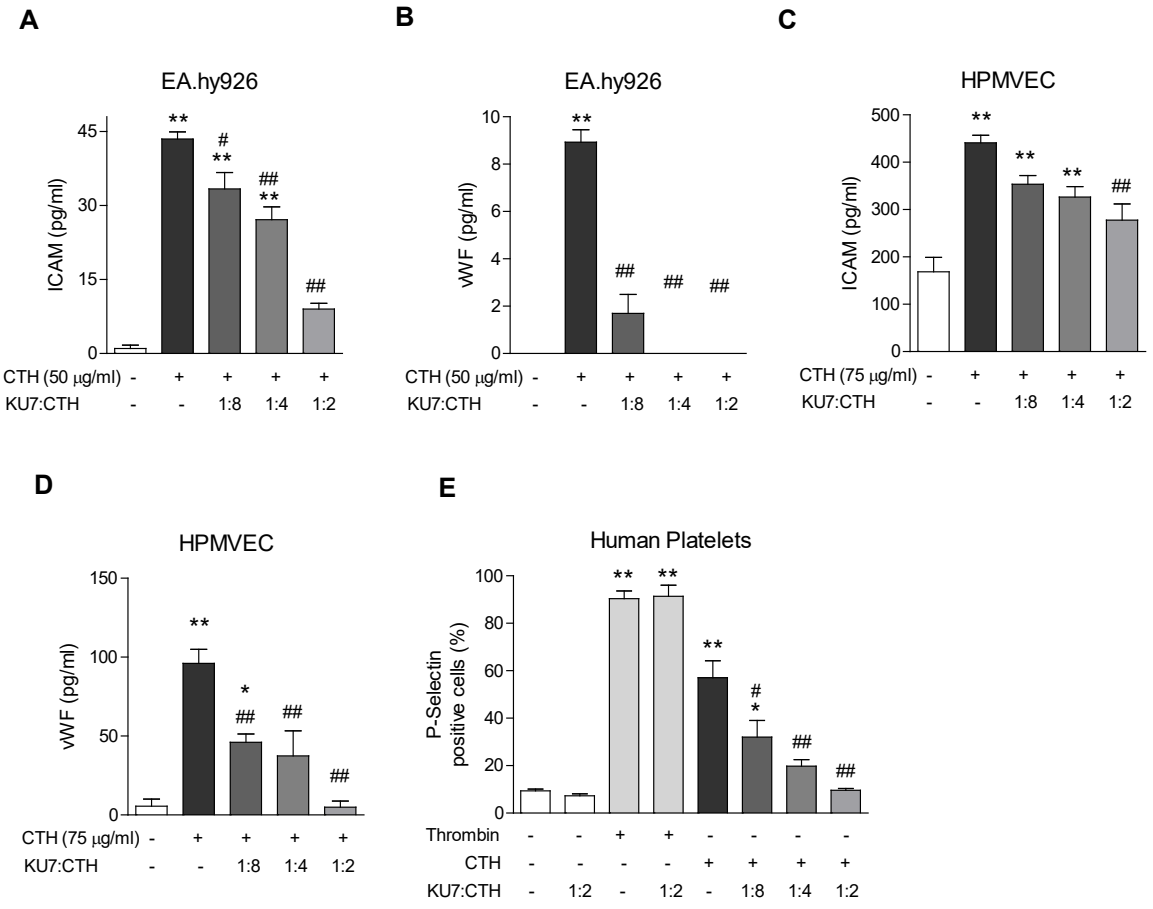

Figure 3. KU7 prevents histone-mediated endothelial cell dysfunction and platelet activation. Markers of endothelial cell dysfunction were measured by ELISA of supernatant of human endothelial EA.hy926 cells (A, B) 6 hours after calf thymus histones (CTH) or of HPMVECs (C, D) 4 hours after CTH exposure. Aptamer KU7 was added 30-60 minutes after CTH. Ratio refers to molar ratio of KU7 to CTH. N = 4. (E) KU7 prevents histone-mediated platelet activation. Human platelets were exposed to CTH (50 μg/ml) for 15 minutes and platelet activation marker P-selectin expression was measured by flow cytometry. Aptamer KU7 was added at the same time as the CTH. Ratio refers to molar ratio of KU7 to CTH. N = 3-5. *P < 0.05, **P < 0.01 vs control; #P < 0.05, ##P < 0.01 vs CTH.

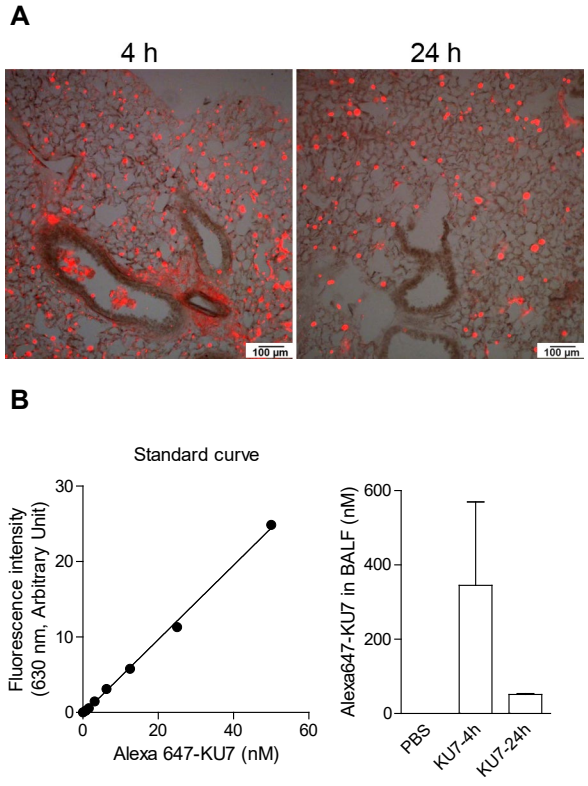

Figure 4. Lung distribution and retention of inhaled Alexa 647-KU7 in mice. The fluorescent tagged aptamer Alexa 647-KU7 (1.7 nmole, 30 µg) was delivered to C57BL/6 male mice via oropharyngeal aspiration and tissues and bronchoalveolar fluid (BALF) were collected at 4 h and 24 h after aptamer administration. (A) Microscopy images showed lung distribution of Alexa 647-KU7 at 4 and 24 h after delivery. (B) KU7 retention in the BALF was estimated via fluorescence intensity measurement at 630 nm. (C) KU7 retention in the lung was determined by the recovery of KU7 from lung tissue via RT-PCR. N = 2.

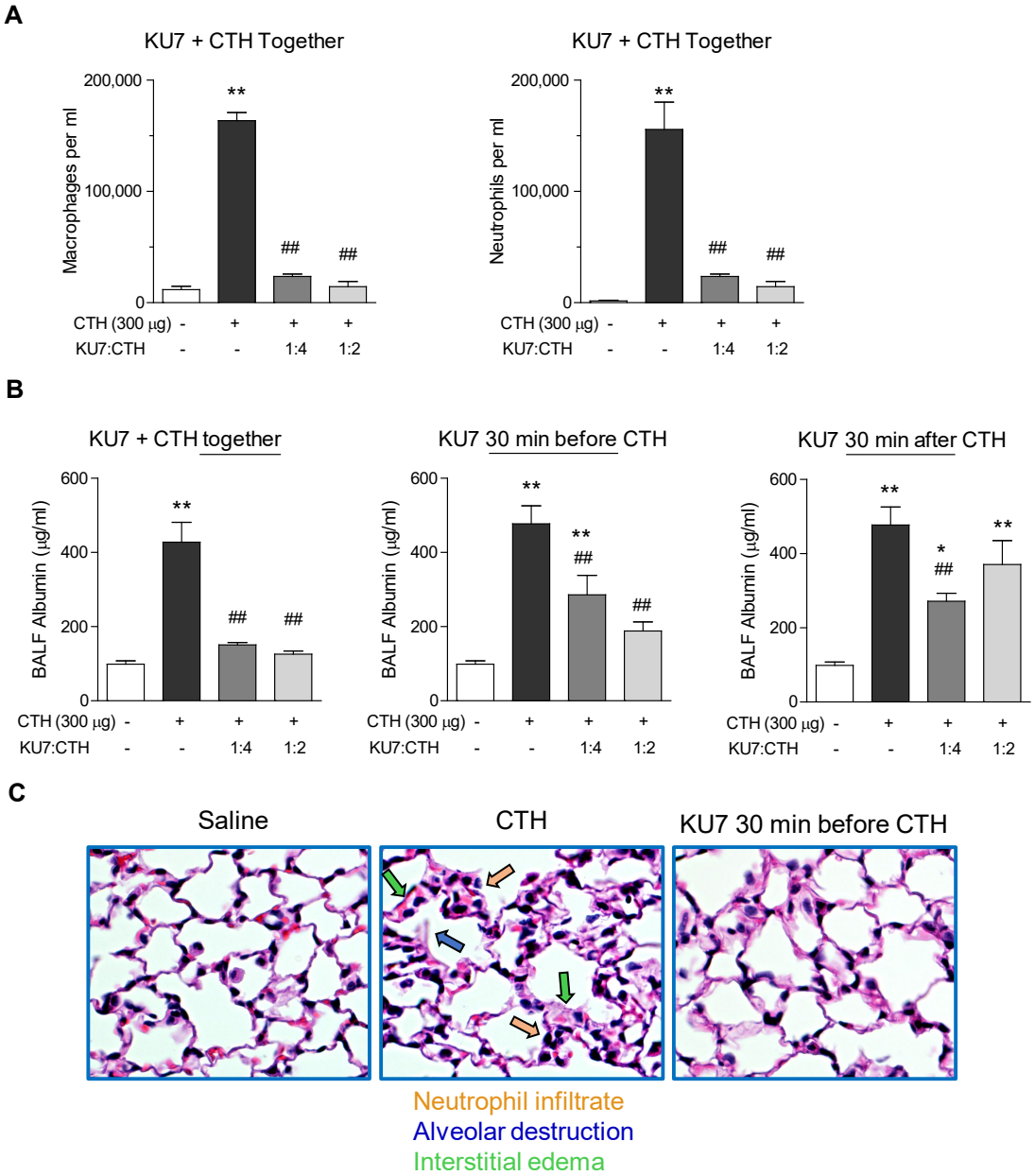

Figure 5. Inhalation of KU7 protects from histone-mediated acute lung injury in mice. C57BL/6 male mice were subjected to oropharyngeal aspiration of calf thymus histones (CTH, 300 µg). KU7 was delivered by a similar method at the indicated times. Tissues and bronchoalveolar fluid (BALF) were collected at 8 hours after CTH challenge. Alveolar inflammatory cell infiltration and barrier disruption Lung inflammation was evaluated by alveolar inflammatory cell infiltration, as measured by white blood cell counts and differential in BALF (A). Alveolar barrier disruption was assessed by BALF albumin ELISA (B). Lung histology was performed, representative images from HE stain were shown (C) and histopathology was scored in a blinded fashion (D). Ratio refers to molar ratio of KU7 to CTH. N = 3-11. *P < 0.05, **P < 0.01 vs control; #P < 0.05, ##P < 0.01 vs CTH.

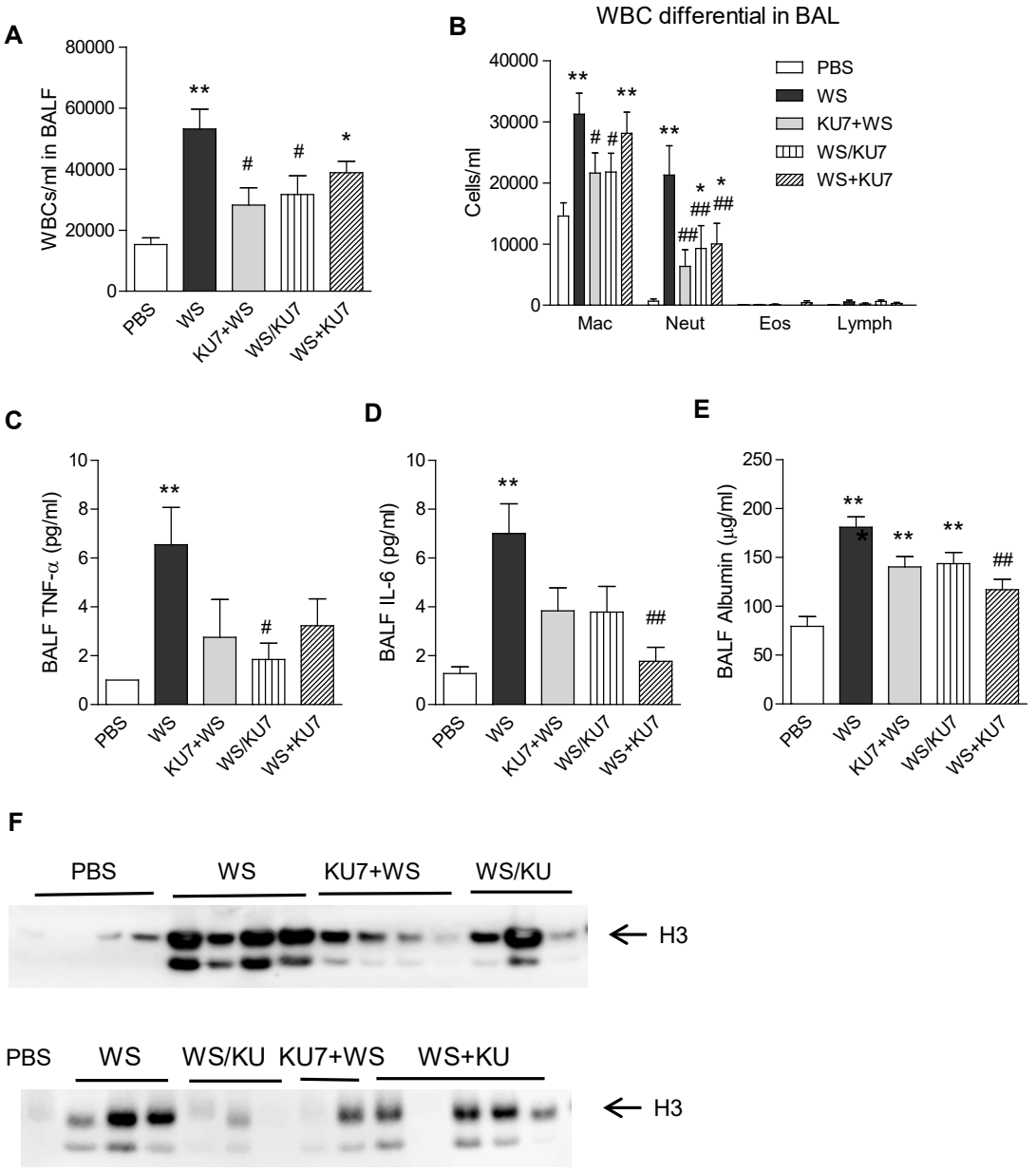

Figure 6. Inhalation of KU7 reduces smoke particulate matter-mediated lung inflammation and histone accumulation in mice. Smoke particulate matter (150 μg) was inhaled by C57BL/6 male mice via oropharyngeal aspiration. White blood cell counts (A) and differential (B), cytokines TNFα (C) and IL-6 (D), albumin (E), and histone H3 (F, G) were measured in bronchoalveolar fluid (BALF) 24 hours after wood smoke challenge. KU7 (86 μg) was delivered by similar method at 30 min before (KU7+WS), at the same time of (WS/KU7) or 30 min after (WS+KU7) smoke matter exposure. N=6-8. *P < 0.05, **P < 0.01 vs control; #P < 0.05, ##P < 0.01 vs CTH.

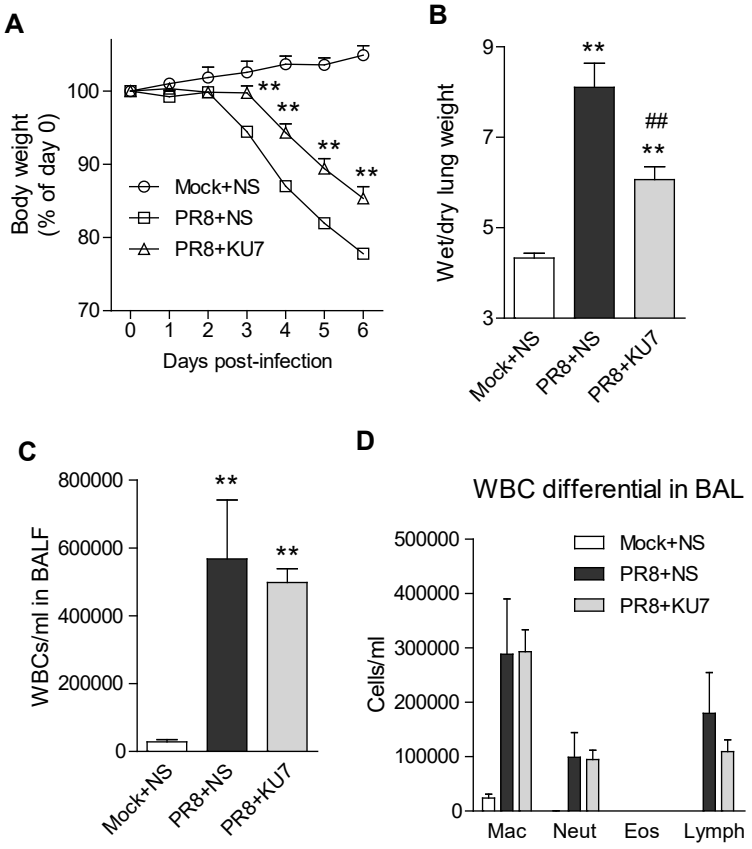

Figure 7. Efficacy of inhaled aptamer KU7 in a murine model of influenza. Female BALB/c mice were intranasally challenged with 250 PFU of influenza A/Puerto Rico/8/34 H1N1 virus (PR8) or heat-inactivated virus mock infection. Single dose of KU7 (100 μg) or vehicle was administrated via oropharyngeal aspiration 24 hours after infection. Body weight was monitored daily (A). Tissues and bronchoalveolar fluid (BALF) were collected at day 7 post infection. Lung edema was assessed by lung wet to dry weight ratio (B). White blood cell counts (C) and differential (Din bronchoalveolar fluid (BALF) were measured to evaluate lung inflammation and injury. N=3-10. *P < 0.05, **P < 0.01 vs control; #P < 0.05, ##P < 0.01 vs CTH.

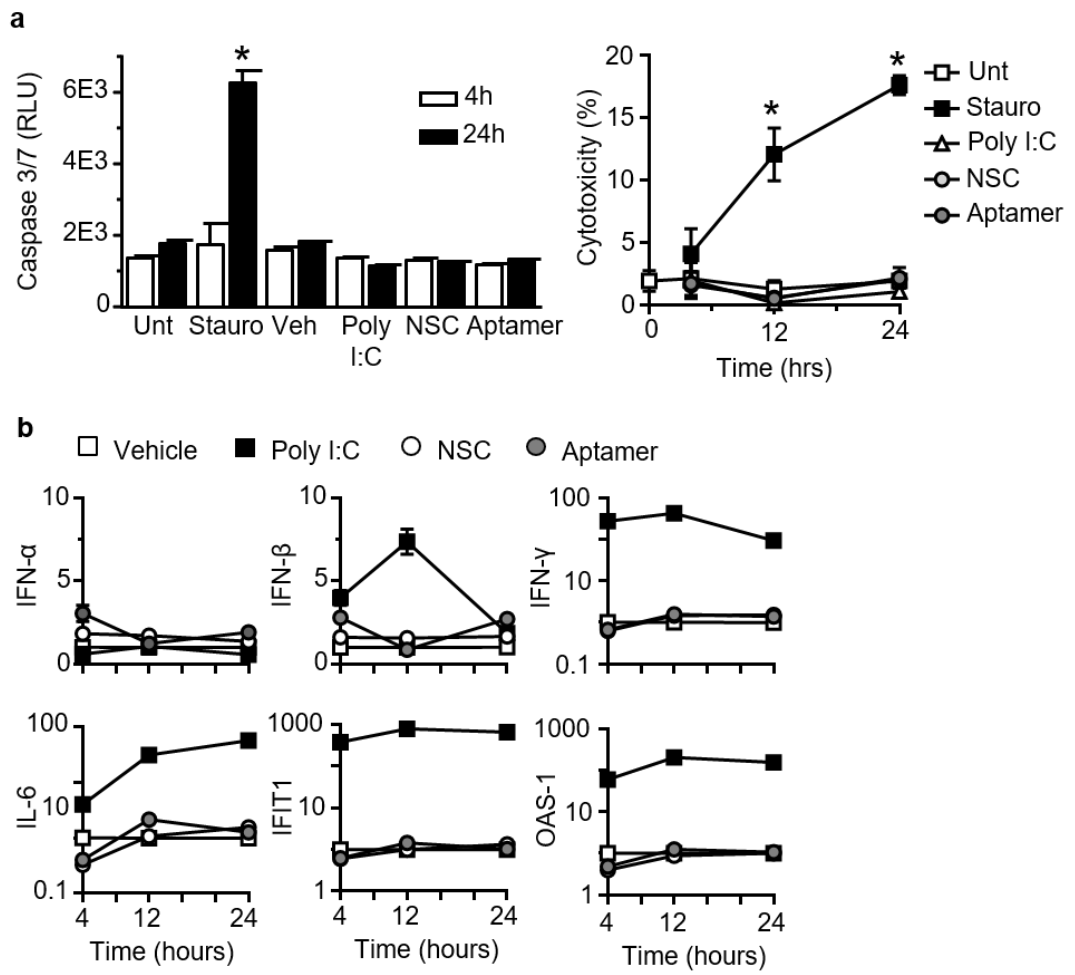

Figure 9 (a) Assessment of aptamer (150 nM) toxicity in human peripheral blood mononuclear cells (PBMCs). Measurement of Caspase 3/7 activation (left panel), measurement of lactate dehydrogenase (LDH) release (right panel). Percent cytotoxicity was determined by measuring LDH release as compared to maximum LDH release at each time point. * $p<0.05$ vs. untreated (Unt) for same time point. **(b)** Assessment of immunostimulatory effect of aptamers (150 nM; 14 or NSC). Staurosporine: positive control for apoptosis / cytotoxicity; Poly I:C: positive control for immune stimulation. OAS-1: 2'-5' oligoadenylate synthetase 1A, INF-α: interferon alpha, IFN-β: interferon beta 1, IFN-γ: interferon gamma, IL-6: interleukin 6, and IFIT1: interferon-induced protein with tetratricopeptide repeats 1.

We performed studies examining the safety of the aptamer (SOW Major task 5). Given the expense of humanized mice, our studies tested safety in C57BL6 mice (see appendix for detailed safety data). In addition, we assessed potential cell cytotoxicity and activation of the innate immune system by RNA aptamer Treatment of human peripheral blood mononuclear cells (PBMCs) with RNA aptamer did not induce activation of Caspase 3 or7 (markers of apoptosis) or the release of lactate dehydrogenase (LDH) over a 24 hour incubation (**Fig.9a**). In contrast, cytotoxicity was observed following treatment of PBMCs with staurosporine, a positive control for activation of caspase-dependent and independent apoptotic pathways[26] (**Fig. 9a**). Finally, as a measure of

immune stimulation, treatment of human PBMCs with RNA aptamer for 24 hours did not increase inflammatory cytokines (Il-6), type I (IFN-β) and type II (IFN-γ) interferons, or viral RNA recognition genes (2'-5'-oligoadenylate synthetase 1, OAS-1; interferon-induced protein with tetratricopeptide repeats, IFIT1) (**Fig. 9b**). Together, these studies suggest that the RNA aptamer is stable in human serum and has an acceptable safety profile

Approved SOW :

Specific Aim 1: In vitro characterization and optimization of RNA aptamers that selectively bind to human histone.	**Proposed Completion**	**Work Completed**	**Site 1 Initiating PI**	**Site 2 Partnering PI**
Major Task 1L Local IRB/IACUC Approval				
Local IRB approval		100%	Miller	Giangrande
Local IACUC approval		100%	Miller	Giangrande
Major Task 2: In vitro - functional efficacy of aptamers	*Months*	*Percent*	*Team*	*Team*
Measurement of calcium influx by fura-2 in human pulmonary microvascular endothelial cells.	1-12	100%	Miller	Giangrande
Measurement of TLR activation in human pulmonary microvascular endothelial cells	1-12	100%		Giangrande
Detection of cell toxicity Cell lines used: human pulmonary microvascular endothelial cells	1-12	100%	Miller	Giangrande
Measure platelet thrombi formation Human platelets (health donors)	6-18	100%		Giangrande Dayal
Measure platelet surface marker expression in human platelets (healthy donors)	6-18	100%	Miller	Giangrande
Ex vivo experiment using blood from patients with ALI	6-24	100%		Giangrande
Specific Aim 2: Evaluate efficacy and safety of histone-specific RNA aptamers in vivo	**Proposed Completion**	**Work Completed**	**Site 1 Initiating PI**	**Site 2 Partnering PI**
Major Task 3: Evaluation of efficacy in inhalation injury model (chlorine inhalation and smoke inhalation models)	*Months*	*Percent*	*Team*	*Team*
Assessment of minimal effective dose (MED) C57/BL6 mice	18-26	100%	Miller Tighe Gunn	
Assessment of alveoloar permeability and inflammation by bronchoalveolar lavage	18-26	100%	Miller Tighe	Giangrande
Lung histology by histopathologic staining and analysis	26-30	100%	Miller Tighe	Giangrande
Major Task 4: Evaluation of efficacy in influenza lung injury model	*Months*	*Percent*	*Team*	*Team*
Assessment of minimal effective dose (MED) C57/BL6 mice.	18-26	100%	Miller Tighe	Giangrande
Assessment of alveoloar permeability and inflammation by bronchoalveolar lavage	18-26	100%	Miller Tighe	Giangrande
Lung histology by histopathologic staining and analysis	26-30	100%	Miller Tighe	Giangrande
Major Task 5: Evaluation of safety	*Months*	*Percent*	*Team*	*Team*
Rising dose and repeated dose toxicology studies to establish a no observed adverse event level (NOAEL) in vitro and in vivo studies.	30-36	100%	Miller	Giangrande
Assessment of potential immunostimulation in humanized mice	30-36	100%		Giangrande

What opportunities for training and professional development has the project provided?

This project served as the thesis project for Kevin Urak, a graduate student in Dr. Giangrande's research laboratory, and he successfully defended his thesis in December 2018. Furthermore, the project is providing opportunities for new knowledge and training in techniques for members in both Drs. Giangrande and Miller's laboratories (see #7 Participants below). Professional development included attendance and presentation of data at the research conferences American Society of Gene and Cell Therapy (ASGCT) meeting in 2018 and 2019, and the Military Health System Research Symposium (MHSRS) annual meeting in 2018 and 2019.

How were the results disseminated to communities of interest?

Results have been presented at local, regional, and national scientific seminars. Research data has been presented in oral and poster abstracts at the American Society of Gene and Cell Therapy (ASGCT) meeting in 2018 and 2019 and the Military Health System Research Symposium (MHSRS) annual meeting in 2018 and 2019. One manuscript was published in *Nature Communication* and an additional two manuscripts are under preparation and will be submitted soon.

What do you plan to do during the next reporting period to accomplish the goals?

Nothing to report.

4. IMPACT:

What was the impact on the development of the principal discipline(s) of the project?

Of relevance to the military, a challenging problem in individuals with severe tissue injury or critical illness is the potential that even those organs not directly affected by the original problem subsequently become dysfunctional (multiple organ dysfunction syndrome, or MODS). The example of trauma has obvious relevance to the military; however, other equally relevant causes of ALI leading to MODS/ARDS include smoke and chlorine gas inhalation, burns, radiation, and infection. The incidence of MODS/ARDS in military situations is difficult to assess because there are so many causes of it. For example, in burn patients, a recent study found an incidence of MODS/ARDS of 60% with a mortality of 65%. In patients with severe sepsis, MODS/ARDS develops in 50% and is responsible for most of the associated death. There is no effective pharmacotherapy to treat the underlying cause of MODS/ARDS directly, and current therapy is limited to supportive care. However, the RNA aptamers tested in this study were found to be efficacious in reducing morbidity and mortality of ALI/ARDs. Safety studies were also promising. Based on these results, the next step with follow on funding would be to test the RNA aptamers in a porcine model of smoke inhalation injury and influenza. If successful, studies will move into human trials as a drug to prevent the development of MODS/ARDS and ALI in high-risk patients. These bio-reagents have significant advantages as compared to other possible therapeutics because they are stable and not as susceptible to fluctuations in temperature, do not require special handling conditions, do not cause allergic responses, and will be easy to deliver.

What was the impact on other disciplines?

Since histones are responsible for multiple diverse causes of MODS/ARDS, including trauma, burns, major surgery, pancreatitis, sepsis, ischemia/reperfusion, etc., the results from this study have potentially broad application to many other diseases beyond ALI..

What was the impact on technology transfer?

Nothing to report.

What was the impact on society beyond science and technology?

Nothing to report

5. CHANGES/PROBLEMS:

Changes in approach and reasons for change?

Nothing to report.

Actual or anticipated problems or delays and actions or plans to resolve them

We initially proposed studies in mice using the chlorine gas model of acute lung injury. The major site of injury of chlorine gas in mice was the trachea and bronchi, with the alveoli showing unreliable damage, likely due to the small caliber of airways that absorb chlorine before it reaches the alveoli. This was not anticipated. Larger animal models are necessary to test chlorine gas acute lung injury.

Experiments involving the animal models of acute lung injury took longer than anticipated because of prolonged time to schedule experiments with the Duke Rodent Inhalation Facility and for the processing and interpretation of histologic samples. Dr. Miller redistributed personnel effort in an attempt to complete these studies, however, continued delays with scheduling, availability of smoke inhalation and influenza virus reagents, and processing required that the experiments proceed beyond the originally scheduled completion date and a six month no-cost extension was provided.

Changes that had a significant impact on expenditures

Nothing to report.

Significant changes in use or care of human subjects, vertebrate animals, biohazards, and/or select agents

Nothing to report.

Significant changes in use or care of human subjects

Nothing to report.

Significant changes in use or care of vertebrate animals.

Nothing to report.

Significant changes in use of biohazards and/or select agents

Nothing to report.

6. PRODUCTS:

Journal publications.

1 Urak KT, Blanco GN, Shubham S, Lin L, Dassie JP, Thiel WH, Chen Y, Sonkar VK, Lei B, Murthy S, Gutierrez WR, Wilson ME, Stiber JA, Klesney-Tait J, Dayal S, Miller Jr FJ*, Giangrande PH.* (*co-corresponding authors, equal contribution). RNA inhibitors of nuclear proteins responsible for multiple organ dysfunction syndrome. *Nature Communications*, 2019 Jan 10(1). PMID 30631065. Acknowledgment of federal support- Yes.

2 Shubham S, Lin LH, Contreras P, Urak KT, Blanco G, Miller Jr FJ, Klesney-Tait J, Giangrande PH. Detection of extracellular histones in serum using RNA aptamers. (in preparation). Acknowledgment of federal support- Yes.

3 Lei B, Urak KT, Shubham S, Snow K, Klesney-Tait J, Stiber JA, Giangrande PH, Miller Jr FJ. RNA aptamers in the treatment of acute lung injury. (in preparation). Acknowledgment of federal support- Yes.

Books or other non-periodical.

Nothing to report.

Other publications, conference papers, and presentations.

Oral Presentations

1 Urak KT, Blanco G, Lin LH, Dassie J, Shubham S, Thiel WT, Chen Y, Sonkar V, Lei B, Gutierrez W, Wilson M, Stiber JA, Klesney-Tait J, Dayal S, Miller Jr FJ, Giangrande PH. RNA Inhibitors of Nuclear Proteins Implicated in Multiple Organ Dysfunction Syndrome. American Society of Gene and Cell Therapy (ASGCT) annual meeting in Chicago IL, April 2018.

2 Urak KT, Blanco G, Lin LH, Dassie J, Shubham S, Thiel WT, Chen Y, Sonkar V, Lei B, Gutierrez W, Wilson M, Stiber JA, Klesney-Tait J, Dayal S, Miller Jr FJ, Giangrande PH. RNA Inhibitors of Nuclear Proteins Implicated in Multiple Organ Dysfunction Syndrome. University of Iowa Internal Medicine Research Day Award Presentations, Iowa City, IA. January 2018.

3 Urak KT, Blanco G, Lin LH, Dassie J, Shubham S, Thiel WT, Chen Y, Sonkar V, Lei B, Gutierrez W, Wilson M, Stiber JA, Klesney-Tait J, Dayal S, Miller Jr FJ, Giangrande PH. RNA Inhibitors of Nuclear Proteins Implicated in Multiple Organ Dysfunction Syndrome. Univ of Iowa Molecular Medicine Seminar, Iowa City, IA. January 2018.

4 Lei B, Snow K, Fang J, Tighe RM, Giangrande PH, Miller Jr, FJ. Inhalation of an RNA aptamer targeting extracellular histones protects from acute lung injury. Molecular Therapy, 2019 May (accepted for presentation at American Society of Gene and Cell Therapy (ASGCT) annual meeting in Washington DC, April 2019.

Poster Presentations

1 Urak KT, Blanco G, Lin LH, Dassie J, Shubham S, Thiel WT, Chen Y, Sonkar V, Lei B, Gutierrez W, Wilson M, Stiber JA, Klesney-Tait J, Dayal S, Miller Jr FJ, Giangrande PH. RNA Inhibitors of Nuclear Proteins Implicated in Multiple Organ Dysfunction Syndrome. RNA Consortium, Iowa City, IA, 2018.

2 Urak KT, Blanco G, Lin LH, Dassie J, Shubham S, Thiel WT, Chen Y, Sonkar V, Lei B, Gutierrez W, Wilson M, Stiber JA, Klesney-Tait J, Dayal S, Miller Jr FJ, Giangrande PH. RNA Inhibitors of Nuclear Proteins Implicated in Multiple Organ Dysfunction Syndrome. Univ of Iowa, Iowa City, IA. 2017.

3 Miller Jr FJ, Urak KT, Blanco G, Lin LH, Lei B, Giangrande PH. RNA inhibitors of extracellular histones to prevent multiple organ dysfunction syndrome. Military Health System Research Symposium (MHSRS) annual meeting, Orlando, FL, August 2018.

4 Miller Jr FJ, Lei B, Snow K, Tighe RM, Giangrande PH. Inhalation of RNA Biodrug Targeting Extracellular Histones Protects from Acute Lung Injury. Military Health System

Research Symposium (MHSRS) annual meeting, Orlando, FL, August 2019. Poster presentation.

Published abstracts

1. Urak KT, Blanco G, Lin LH, Dassie J, Shubham S, Thiel WT, Chen Y, Sonkar V, Lei B, Gutierrez W, Wilson M, Stiber JA, Klesney-Tait J, Dayal S, Miller Jr FJ, Giangrande PH. RNA Inhibitors of Nuclear Proteins Implicated in Multiple Organ Dysfunction Syndrome. Molecular Therapy, 2018 May 1,Vol. 26, No. 5, pp. 37-37.
2. Miller Jr FJ, Urak KT, Blanco G, Lin LH, Lei B, Giangrande PH. RNA inhibitors of extracellular histones to prevent multiple organ dysfunction syndrome. Military Health System Research Symposium (MHSRS), 2018.

Website(s) or other Internet site(s)

Nothing to report.

Technologies or techniques

Nothing to report.

Inventions, patent applications, and/or licenses

Nothing to report.

Other Products

Nothing to report.

5. PARTICIPANTS & OTHER COLLABORATING ORGANIZATIONS

What individuals have worked on the project?

Name: Francis Miller, MD
No change.

Name: Kamie Snow
No change.

Name: Beilei Lei, PhD
No change.

Name: Michael Gunn, MD
No change.

Name: Alejandro Comellas, MD
No change.

Name: Sanjana Dayal, PhD
No change.

Has there been a change in the active other support of the PD/PI(s) or senior/key personnel since the last reporting period?

Nothing to report.

What other organizations were involved as partners?

Nothing to report.

6. SPECIAL REPORTING REQUIREMENTS

Collaborative award.

Independent reports are submitted for both the Initiating PI (Miller) and the Partnering PI (Giangrande). Specific tasks are indicated with the PI and research site in the table of "Research Specific Tasks" found in Section #3.

7. APPENDICES:

Appendices materials have been included.

nature COMMUNICATIONS

ARTICLE

https://doi.org/10.1038/s41467-018-08030-y OPEN

RNA inhibitors of nuclear proteins responsible for multiple organ dysfunction syndrome

Kevin T. Urak[1,2], Giselle N. Blanco[1], Shambhavi Shubham[1], Li-Hsien Lin[1], Justin P. Dassie[1], William H. Thiel[1,3], Yani Chen[1], Vijay Kumar Sonkar[1], Beilei Lei[4], Shubha Murthy[1], Wade R. Gutierrez[5], Mary E. Wilson[1,6,7], Jonathan A. Stiber[4], Julia Klesney-Tait[1], Sanjana Dayal[1], Francis J. Miller Jr[4,8,9] & Paloma H. Giangrande[1,2,3,10,11,12,13]

The development of multiple organ dysfunction syndrome (MODS) following infection or tissue injury is associated with increased patient morbidity and mortality. Extensive cellular injury results in the release of nuclear proteins, of which histones are the most abundant, into the circulation. Circulating histones are implicated as essential mediators of MODS. Available anti-histone therapies have failed in clinical trials due to off-target effects such as bleeding and toxicity. Here, we describe a therapeutic strategy for MODS based on the neutralization of histones by chemically stabilized nucleic acid bio-drugs (aptamers). Systematic evolution of ligands by exponential enrichment technology identified aptamers that selectively bind those histones responsible for MODS and do not bind to serum proteins. We demonstrate the efficacy of histone-specific aptamers in human cells and in a murine model of MODS. These aptamers could have a significant therapeutic benefit in the treatment of multiple diverse clinical conditions associated with MODS.

[1] Internal Medicine, University of Iowa, Iowa City, IA 52242, USA. [2] Molecular & Cellular Biology Program, University of Iowa, Iowa City, IA 52242, USA. [3] Abboud Cardiovascular Research Center, University of Iowa, Iowa City, IA 52242, USA. [4] Department of Medicine, Duke University, Durham, NC 27708, USA. [5] Medical Scientist Training Program, University of Iowa, Iowa City, IA 52242, USA. [6] Department of Microbiology, University of Iowa, Iowa City, IA 52242, USA. [7] Veteran's Affairs Medical Center, University of Iowa, Iowa City, IA 52241, USA. [8] Pharmacology and Cancer Biology Program, Duke University, Durham, NC 27708, USA. [9] Deptartment of Medicine, Veterans Administration Medical Center, Durham, NC 27705, USA. [10] Interdisciplinary Graduate Program in Genetics, University of Iowa, Iowa City, IA 52242, USA. [11] Holden Comprehensive Cancer Center, University of Iowa, Iowa City, IA 52242, USA. [12] Radiation Oncology, University of Iowa, Iowa City, IA 52242, USA. [13] Environmental Health Sciences Research Center (EHSRC), University of Iowa, Iowa City, IA 52242, USA. These authors contributed equally: Kevin T. Urak, Giselle N. Blanco, Shambhavi Shubham. Correspondence and requests for materials should be addressed to F.J.M.Jr. (email: francis.miller@duke.edu) or to P.H.G. (email: paloma-giangrande@uiowa.edu)

Approximately 45% of patients who develop multiple organ dysfunction syndrome (MODS) will die due to acute secondary organ injury/failure[1]. Survivors are at risk of developing persistent mental and physical impairments. MODS occurs after a severe cytotoxic insult such as sepsis, trauma, ischemia/reperfusion injury, pancreatitis, peritonitis, stroke, thrombosis and autoimmune disease[2–4]. MODS is characterized by the release of molecular mediators from damaged tissues which create a domino effect including capillary leak, interstitial edema, hemorrhage and systemic inflammation[5]. MODS is primarily managed with supportive care, as there is no approved treatment to prevent or reverse it. The realization that damaged cells release their nuclear content into the circulation suggests nuclear proteins as potential therapeutic targets for MODS[2,6]. Since histones are the most abundant proteins in the nucleus, they have been identified as potential therapeutic targets for MODS.

Histones are highly cationic intra-nuclear proteins that support the normal structural development of chromatin and regulation of gene expression. Histones and DNA-bound histones (nucleosomes) are released into the extracellular space during cell death processes including necrosis, apoptosis and neutrophil extracellular trap-induced cell death (NETosis). In the extracellular space, histones act as cytotoxic damage-associated molecular pattern proteins by activating Toll-like receptors (TLRs), promoting pro-inflammatory cytokine pathways and altering phospholipid membrane permeability[3,7–9]. In humans, the normal serum level of histones is very low (estimated at <0.6 ng mL^{-1})[10–12]. However, serum levels as high as 3 ng mL^{-1} have been reported in critically ill patients, and correlate with hallmark features of MODS including, coagulopathy, endothelial dysfunction and inflammation[13–16].

Several animal studies demonstrate that intravenous administration of exogenous histones is sufficient to cause a MODS-like phenotype[3,7,17]. Importantly, anti-histone treatments (e.g., histone neutralizing antibodies, activated protein C (APC), recombinant thrombomodulin and heparin) protect mice against secondary organ failure due to lethal endotoxemia, sepsis, ischemia/reperfusion injury, trauma, pancreatitis, peritonitis, stroke and thrombosis[2–4,18,19]. However, therapeutic approaches currently pursued in experimental models have marked limitations. For example, despite their use in laboratory experiments, TLR2/4 monoclonal antibodies (mAbs) to block extracellular histone signaling would cause substantial immunodeficiency in humans by inhibiting innate immune defenses after host infection. Similarly, anti-histone mAbs have been implicated in autoimmunity[20,21]. Several other biologics that have demonstrated efficacy in animal models failed to provide therapeutic benefit in clinical trials (e.g., APC) and are associated with increased risk of bleeding (e.g., heparin and APC) or systemic toxicity (e.g., histone deacetylase inhibitors)[22,23]. In addition, many biologics require restrictive handling and storage, special dosing considerations and risk allergic reactions (recombinant proteins and antibodies), which limit their use in field situations or small regional health clinics[24,25]. Thus, the development of specific histone inhibitors is a unique clinical opportunity to interrupt a pathophysiologic cascade responsible for significant morbidity and mortality associated with MODS.

Chemically stabilized nucleic acid bio-drugs (aptamers) are synthetic structure RNA or DNA oligonucleotide ligands that bind with high affinity and specificity to their targets[26–28]. As a therapeutic, aptamers possess several key advantages over other biologics, including the following. (1) They are self-refolding, single chain and redox insensitive. Unlike proteins, aptamers tolerate pH and temperatures that proteins do not. (2) They act as selective inhibitors of their target, eliminating potential for off-target effects. (3) They are easy and economical to produce. Their production does not depend on bacteria, cell cultures or animals. (4) Their small size leads to a high number of moles of target substance bound per gram of aptamer. Additionally, their transport properties allow for improved tissue penetration. (5) They are stable at ambient temperature, yielding a much longer shelf-life than other biologics, and can tolerate transportation without refrigeration. (6) Cross-species reactive aptamers can be easily engineered, thus expediting testing of the same reagent in preclinical animal models and in future human clinical trials. The clinical potential of aptamers is also highlighted by the Food and Drug Administration (FDA) approval of an aptamer-based drug for the treatment of macular degeneration and by clinical trials demonstrating the safety and efficacy of systemically administered aptamers[29–35].

In this study, we develop an anti-histone therapeutic strategy to selectively neutralize extracellular histones implicated in MODS, based on aptamers. Because histones (cationic proteins) normally associate with DNA in the nucleosome, oligonucleotides such as aptamers (anionic molecules) have intrinsic high affinity for histones, making them an excellent reagent for binding and neutralizing extracellular histones and reducing the morbidity and mortality associated with MODS. In this study, we develop nuclease-resistant, 2′ fluoro-modified RNA aptamers with high affinity (K_D = nanomolar (nM)) for histones implicated in MODS (H3 and H4) with systematic evolution of ligands by exponential enrichment (SELEX)[36,37]. A key stringent negative selection step was introduced during the selection process to favor the identification of aptamers that bound to histones, but not other proteins in human serum, thereby reducing potential side effects. We show that the aptamers inhibit histone-induced human platelet aggregation and endothelial cell death in culture. In addition, we demonstrate efficacy of anti-histone aptamers in a murine model of MODS. Because extracellular histones have been implicated in the development of many different disease conditions, the anti-histone aptamer bio-drugs could potentially impact the treatment of numerous MODS-inducing clinical conditions.

Results

Identification of histone-specific RNA aptamers using SELEX. Two parallel selections were performed using the in vitro SELEX protocol to isolate RNA aptamers (51 nucleotides in length) that selectively bind to human histones implicated in MODS (H3 and H4) (Fig. 1a). To identify RNA sequences that specifically bind to histones, but not to proteins in serum, we introduced a stringent negative selection step against bovine serum albumin (BSA) and human IgG (Fig. 1a; step 2). RNAs that bound to serum proteins were removed (Fig. 1a; step 3) and unbound RNA was recovered. To ensure the isolation of high-affinity binding RNAs to human histones, a positive selection step was performed using human recombinant histones H3 and H4 proteins (Fig. 1a; step 3). Eight rounds of selection (against target histones H3 or H4) and negative selection (against BSA and human IgG) were performed (see Supplementary Table 1). Binding of the round 0 (R0) and round 8 (R8) RNA pools to histones H3 and H4 was verified using the double-filter binding assay (Fig. 1b; top panels). A leftward shift in the binding curve of the R8 RNA pools compared to the R0 RNA pools for both selections is indicative of enrichment of high-affinity binding RNA sequences. Importantly, the enriched R8 RNA pools did not bind to serum proteins (Fig. 1b; bottom panels) confirming specificity for histones. Equilibrium dissociation constants (K_D) for R0 and R8 RNA pools were determined using one site binding nonlinear regression curve fit (see Supplementary Table 2).

High-throughput sequencing (Illumina) and bioinformatics analysis of selected RNA sequences from the selection rounds

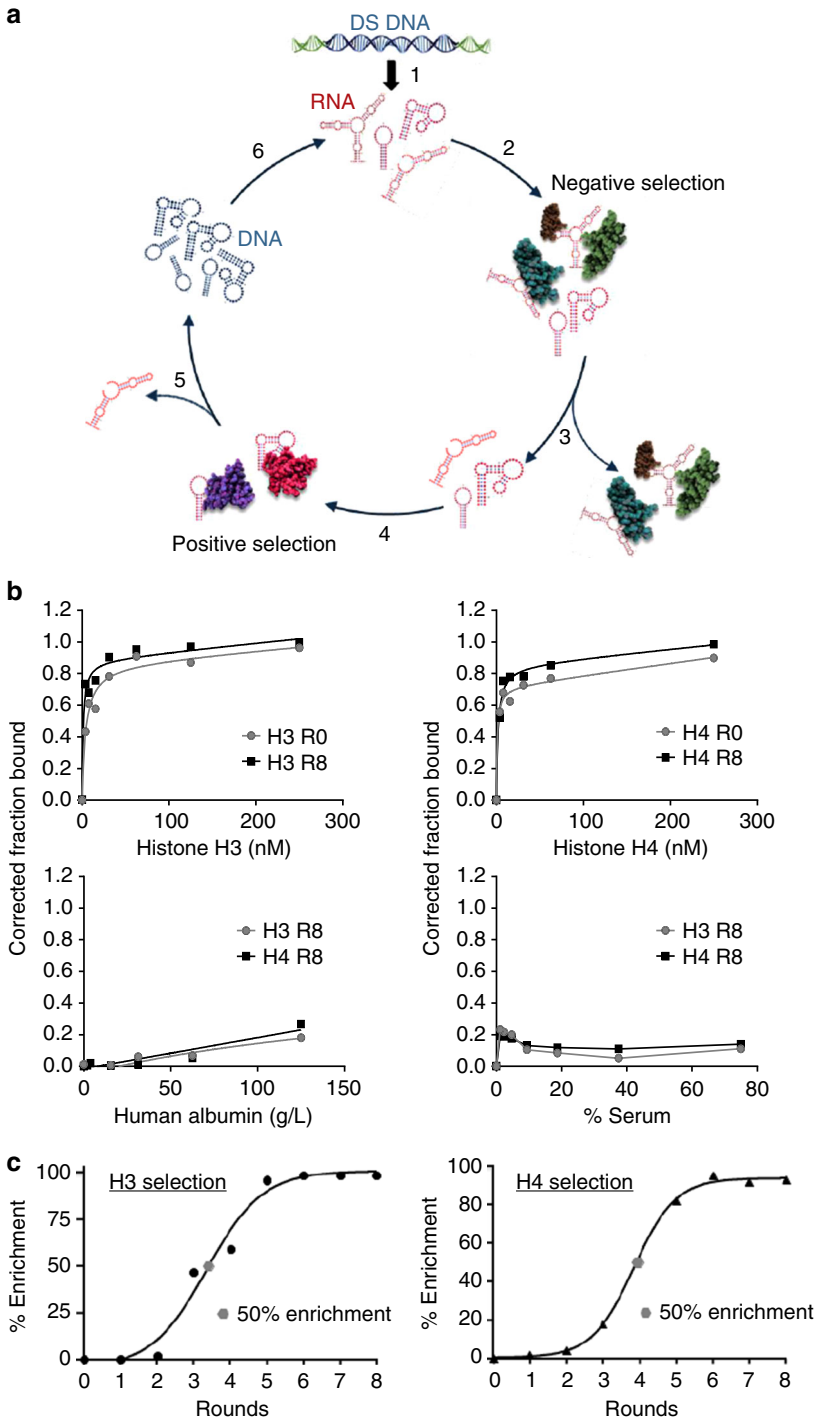

Fig. 1 Identification of histone-specific RNA aptamers using SELEX. **a** Schematic of the in vitro Systematic Evolution of Ligands by Exponential Enrichment (SELEX) procedure. Step 1. Double-stranded DNA (DS DNA) template library (Sel2N20) is in vitro transcribed in the presence of 2′ Fluoro pyrimidines and 2′ OH purines to generate the 2′ Fluoro-modified Round 0 RNA library (RNA). Step 2. The round 0 RNA library was incubated with human albumin and human IgG to remove RNAs that bind to human serum proteins (Negative selection). Step 3. RNA bound to serum proteins was discarded. Step 4. RNA not bound to serum proteins was incubated with human histones H3 and H4, respectively. Step 5. Histone-bound aptamers were collected and reverse-transcribed into DNA. Step 6. Round 1 DNA was then transcribed into RNA for the subsequent round of selection. A total of eight rounds of selection were performed for each histone selection (see Supplementary Table 1). **b** Binding of Round 0 (R0) and Round 8 (R8) RNA to recombinant human histone H3 (top, left panel) and H4 (top, right panel) proteins. Binding of R8 RNA to human albumin (bottom, left panel) and human serum (bottom, right panel). **c** Percent sequence enrichment (% Enrichment) at each round of selection (black circle). The 50% sequence enrichment point (gray circle) is indicated for each selection

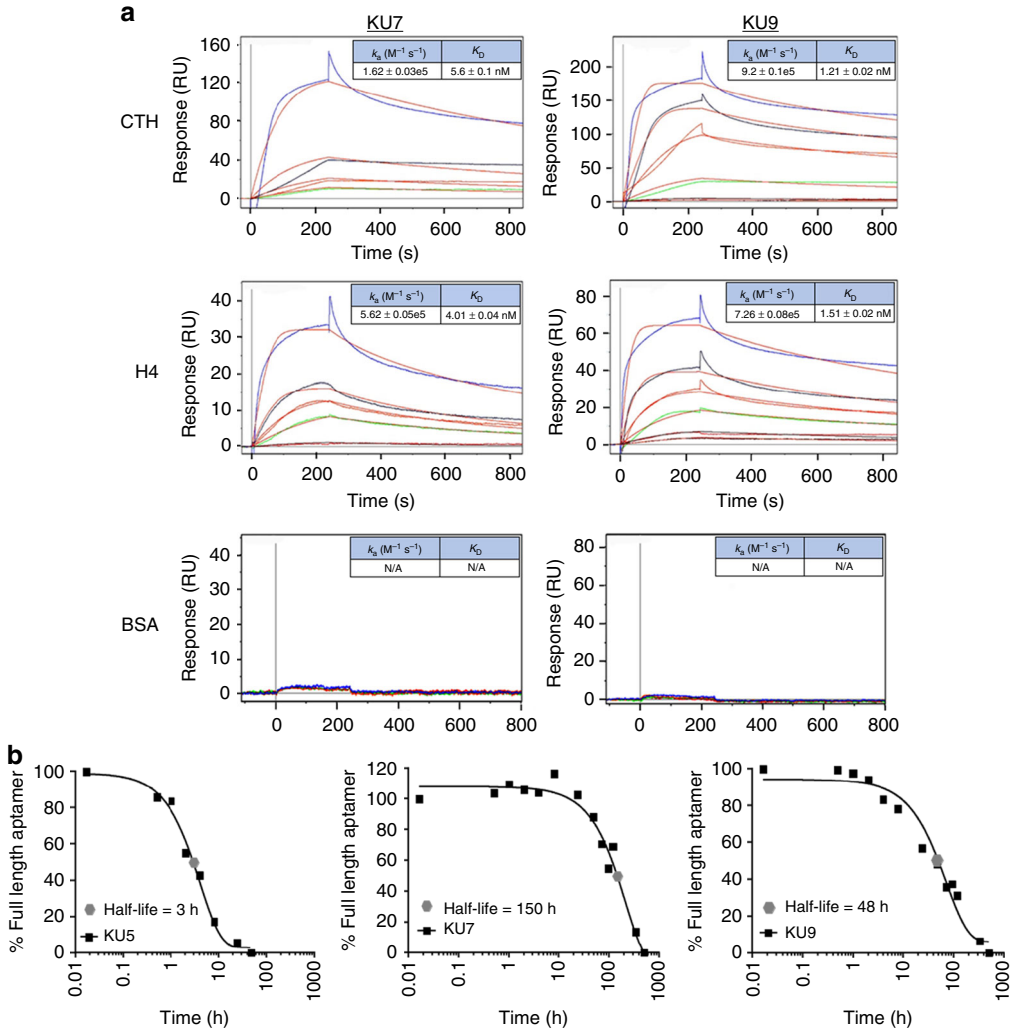

Fig. 2 Binding characterization and stability measurements of individual histone RNA aptamer sequences. **a** Binding kinetic rate constants (k_a and K_D) determined for aptamers KU7 (left panels) and KU9 (right panels) binding to CTH (top panels), H4 (middle panels) and BSA (bottom panels). Aptamers concentrations tested: 100 nM (blue), 50 nM (black), 25 nM (red), 12.5 nM (green), 10 nM (magenta). **b** Serum stability measurements for aptamers KU7 and KU9 (5 μM) in 50% human serum. $T_{1/2}$ KU7 = 150 h. $T_{1/2}$ KU9 = 48 h

revealed that the selections converged between rounds 5 and 8 (Fig. 1c). Percent sequence enrichment (% enrichment) was measured to determine the evolution of each sequence family at the later rounds of selection. Percent sequence enrichment at each round of selection was measured by taking the total number of unique sequences in each round and dividing by the total number of sequences obtained in each round. For each selection, the 50% enrichment point is indicated by a gray dot (Fig. 1c). The top three RNA sequences from each selection (H3 selection: KU4–KU6; H4 selection: KU7–KU9) were selected based on the following criteria: sequences that increase in abundance during the positive selection rounds (against target histones H3 or H4) but do not decrease in abundance during the negative selection rounds (against BSA and human IgG) (see Supplementary Table 1 for details on selection conditions). Individual RNA sequences are listed in Supplementary Table 3. Theoretical secondary structures for each of the six RNA aptamers were generated using Mfold[38] (Supplementary Fig. 1).

Next, the binding of single RNA aptamers isolated from the histone H3 and H4 selections was evaluated with surface plasmon resonance (SPR) (Fig. 2a) and double-filter binding assay (Supplementary Fig. 2; data shown for aptamers KU7 and KU9). RNA aptamers were incubated with either calf thymus-derived histones (CTH) (top panels), recombinant human histone H4 (middle panels) or BSA (bottom panels) (Fig. 2a). As predicted, the RNA aptamers bound with high affinity to both CTH histones and recombinant human histone H4, but not to BSA (Fig. 2a). Importantly, the aptamers bound equally well to both CTH and recombinant human histone H4 suggesting that the aptamers bind irrespective of post-translational modifications and are not species specific. While aptamers KU7 and KU9 were derived from the H3 selection, we also evaluated binding of the RNAs to all histone subunits using the double-filter binding assay (Supplementary Fig. 2A). Of note, both aptamers bound with low nM affinity to histones, H1, H3 and H4 (major histones implicated in MODS). In contrast, while only aptamer KU7 bound to histone H2B, neither aptamer bound to histone H2A. In addition, equilibrium binding kinetics were determined for one of the aptamers (KU7) using the double-filter binding assay. We observed similar (low nM) binding affinities at various time intervals (Supplementary Fig. 2B). Finally, as observed with SPR analysis (Fig. 2), no significant binding was observed to human serum or human albumin (Supplementary Fig. 2C), confirming specificity of the aptamers for histone proteins vs. serum proteins. Of note, differences in the binding constants generated using the double-filter binding and SPR assays could be due to

inherent differences with the assays and binding buffers used. For example, the double-filter binding assay is performed in solution (e.g., histone and aptamers are free to interact in solution). In contrast, binding with SPR is assessed by immobilizing the ligand (e.g., histones) on a solid surface. Together, these data highlight the potential safety of this approach for targeting extracellular histones, while minimizing unwanted off-target effects.

Based on the predicted secondary structures of the RNA aptamers (see Supplementary Fig. 1), we reasoned that two of the aptamers (KU7 and KU9) would be more stable in human serum compared to the other four aptamers (KU4, KU5, KU6 and KU8) and thus better suited for clinical applications. To assess their serum stability, RNA aptamers were incubated with 50% human serum for up to 28 days. Aliquots of the aptamer-serum solution, obtained at various time points, were resolved on a denaturing polyacrylamide gel electrophoresis (PAGE) gel (8 M urea 10% acrylamide) following staining with SYBR gold to visualize the RNAs (Supplementary Fig. 3). The amount of full-length aptamer was quantified for each time point by comparing the intensity of the bands to the "0 h" time point using the Image Lab software. (Fig. 2b; data shown for aptamers KU5, KU7 and KU9). As predicted, aptamers KU7 and KU9 had superior serum stability profiles compared to the other aptamers tested (comparison shown for KU5 only).

In vitro efficacy of RNA aptamers. The release of histones from dying cells is associated with microvascular thrombosis and tissue ischemia[4,39]. Histone H4 and, to a lesser extent H3, are responsible for directly inducing aggregation of human platelets. To determine whether the selected RNA aptamers inhibit adverse effects of extracellular histones, aptamers KU7 and KU9 were incubated with platelets derived from healthy human donors in the absence or presence of histone H4. We show that anti-histone aptamers KU7 and KU9 inhibit histone H4-induced platelet aggregation in a dose-dependent manner (Fig. 3a). In contrast, the aptamers did not inhibit platelet aggregation induced by collagen, even at the highest aptamer dose tested (Fig. 3a). Importantly, histone-induced platelet aggregation was significantly inhibited by aptamers KU7 and KU9 at a molar ratio of histone to aptamer of 1:1, 2:1 and, to a lesser extent, 4:1 (Fig. 3a). Platelet aggregometer graphs for the individual aptamers and RNA round pools are shown in Supplementary Fig. 4A and B.

In vivo, the release of extracellular histones in circulation results in an amplifying effect by promoting additional cell death and nuclear content release, as well as activation of TLRs resulting in pro-inflammatory cytokine production (interleukin-6 (IL-6)), enhanced inflammation and coagulation activation[7,13–15]. We show that aptamers KU7 and KU9 inhibit CTH-induced TLR activation as measured by IL-6 production (Fig. 3b and Supplementary Fig. 4C; left panel). Importantly, histone-induced TLR activation was significantly inhibited by aptamers KU7 and KU9 at a molar ratio of histone to aptamer of 1:1, 2:1, 4:1 (Fig. 3b). In contrast, the aptamers have no effect on lipopolysaccharide-induced TLR activation (Supplementary Fig. 4C; right panel).

In addition to a heightened inflammatory response, high levels of extracellular histones are cytotoxic to endothelial and epithelial cells as well as several other cell types[2,19,40,41]. We confirmed that administration of calf thymus histones to a human hybrid endothelial cell line (EA.hy926) causes dose-dependent cell death (Fig. 3c; left panel). Aptamers (KU7 and KU9) have a dose-dependent protective effect in neutralizing histone-induced cytotoxicity (Fig. 3c; right panel).

Extracellular histones appear to induce cytotoxicity through their interaction with phospholipids in the plasma membrane, leading to transmembrane conductance, calcium influx, cell swelling and cytolysis[42–44]. We confirmed that administration of calf thymus histones to EA.hy926 cells resulted in increased intracellular calcium [Ca^{2+}] levels^{+}]) calcium influx (Fig. 3d). Importantly, aptamers significantly inhibit the histone-induced increase of intracellular calcium at molar ratio of histone to aptamer up to 4:1 with KU7 and 6:1 with KU9 as measured using the calcium indicator Fura 2-acetoxymethyl ester (Fura 2-AM). The aptamers alone had no effect on intracellular calcium levels (Fig. 3d). Together, these data confirm that the aptamers can prevent the functional effect of histones in vitro and provide the rationale for proposing that these aptamers have the potential to attenuate histone-mediated injury in vivo.

Efficacy of histone aptamer in a murine model of MODS. Histone administration causes neutrophil migration, endothelial injury and dysfunction, hemorrhage and thrombosis and often results in death at levels as low as 50 mg kg^{-1} body weight. Intravenous injection of histones into mice leads to organ dysfunction and death (Fig. 4). Death occurred between 1 and 3 h in the mice treated with histones alone, but was inhibited by administration of aptamer (Fig. 4a). Injection of histones resulted in an increase in organ weight that was only partially reversed by the aptamer treatment (Fig. 4b). The increase in organ weight is likely a result of an increase in vascular congestion, multifocal neutrophilic aggregates in vessels, thrombi and hemorrhage (Fig. 4c, d; the liver, lung and spleen shown in Supplementary Fig. 5). Importantly, while no significant change in organ weight was observed with aptamer treatment, pathologic evidence of histone toxicity, as determined by hematoxylin and eosin (H&E) staining and immunostaining for presence of platelets and neutrophils in the various tissues, was inhibited by aptamer KU7 at a ratio of histone to aptamer of 2:1 and 4:1 (Fig. 4c, d). As predicted, injection of histones into the circulation of mice also resulted in an increase in TLR activation via IL-6 (Fig. 4e). The increase in TLR activation was partially attenuated by aptamer treatment in the liver but not in lung or spleen, and is likely due to the retention of aptamer–histone complexes in these organs. Together, these data confirm that aptamers that bind to the histones implicated in MODS can attenuate histone-mediated injury in vivo.

The experimental protocol of the in vivo efficacy study described above (Fig. 4) is consistent with all previous studies performed in preclinical models of MODS with histone inhibitors[16,45,46], such that the therapeutic treatment is administered prior to, or in conjunction with, the histones. To better represent the clinical scenario where the drug is administered after tissue injury, we evaluated the ability of anti-histone aptamers to rescue histone-induced toxicity as a function of time (Fig. 5). Anti-histone aptamers were added to EA.hy926 cells in culture at different time points following the addition of histones. Anti-histone aptamers prevented cytotoxicity in a time-dependent manner when administered after the histones, demonstrating the ability to protect from histone-induced cell death 2 h after histone administration (Fig. 5a). The administration of KU7 rescued the increase in intracellular [Ca^{2+}] after histones had already induced an increase of [Ca^{2+}] (Fig. 5b). As shown in Fig. 4a, intravenous injection of histones resulted in death of mice within 3 h; however, mice treated with anti-histone aptamer KU9 at 30 min following histone injection had markedly improved survival as compared to vehicle-treated mice (Fig. 5c; left panel) and a reduction in lung weight (Fig. 5c; right panel).

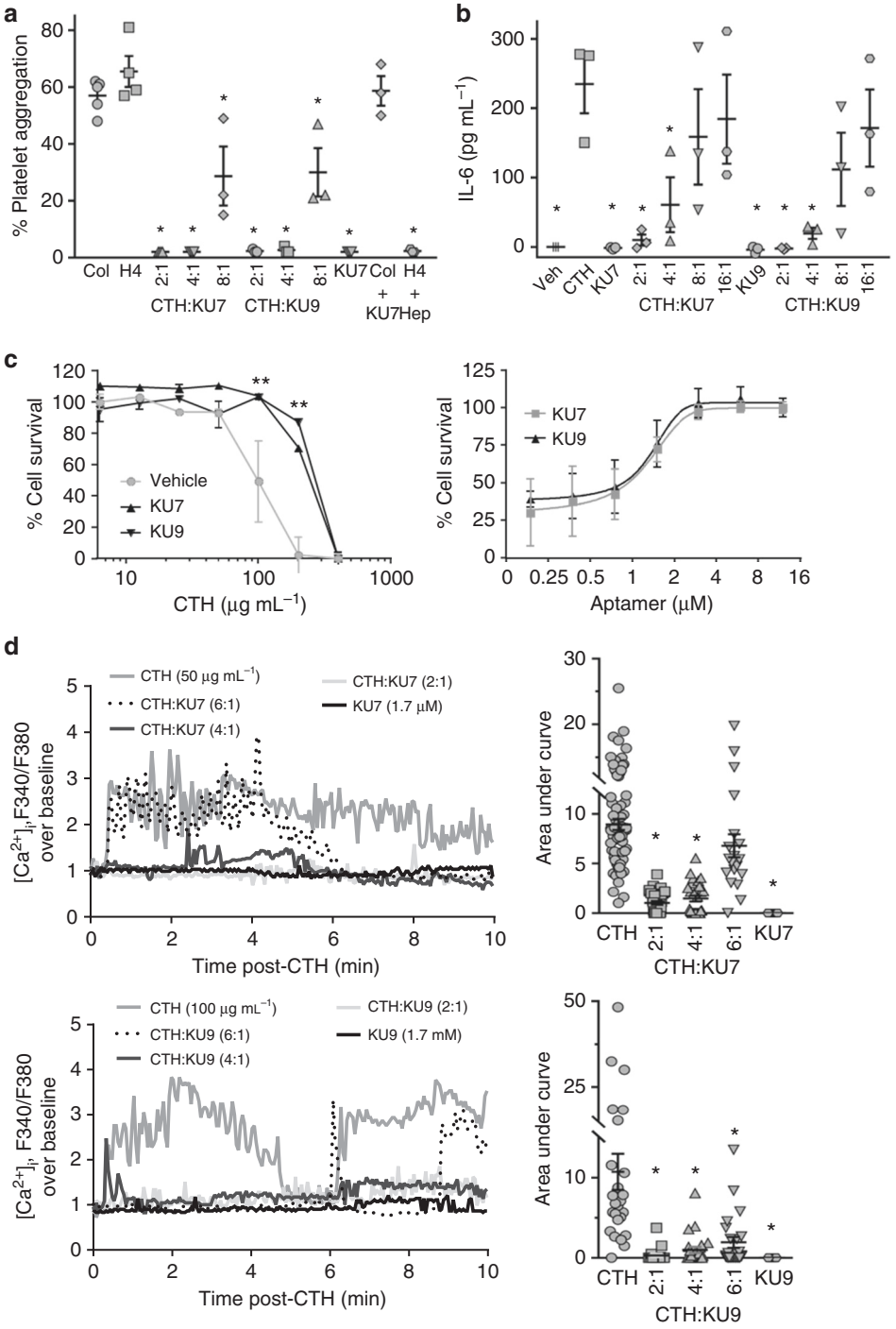

Fig. 3 In vitro efficacy of RNA aptamers. **a** Human platelet aggregation measurements using platelets derived from three independent healthy donors. Collagen (Col), histone H4 (H4), histone aptamers (KU7 and KU9), calf thymus histones (CTH), heparin (Hep); $^{*}p < 0.01$ vs. H4, one-way ANOVA corrected for multiple comparisons (Dunnett testing), $n = 3$–5. **b** TLR activation: IL-6 ELISA detection of IL-6 protein levels (as a measurement of TLR activation) in supernatants of EA.Hy926 cells treated with media alone (Veh), calf thymus histones (CTH), histone aptamers (KU7 and KU9) alone or in combination; $^{*}p < 0.01$ vs. CTH, one-way ANOVA corrected for multiple comparisons (Dunnett testing), $n = 3$. **c** Cytotoxicity measurements: aptamer inhibition of histone-mediated cytotoxicity of endothelial cells determined by MTS assay. (Left panel) EA.hy926 cells treated with 1.2 μM of aptamers (KU7 or KU9) and varying amounts (0 to 1000 μg mL^{-1}) of calf thymus histones (CTH). (Right panel) EA.hy926 cells treated with 180 μg mL^{-1} of CTH and increasing amounts (0 to 16 μM) of aptamers (KU7 or KU9); $^{**}p < 0.01$ vs. vehicle (100 μg mL^{-1}), $n = 4$. **d** Dynamic changes of intracellular calcium levels in Fura 2-AM-loaded EA.hy926 cells using fluorescence microscopy. (Left panel) Representative intracellular calcium elevation traces (F340/F380) of EA.hy926 treated with CTH alone, aptamer KU7 alone (25 μg mL^{-1}, top panels), aptamer KU9 alone (25 μg mL^{-1}, bottom panels) or in the presence of varying aptamer amounts (Molar ratio of CTH to aptamer indicated). (Right panel) Summary of data from multiple EA.hy926 cells ($n = 19$–69 cells per bar); $^{**}p < 0.01$ vs. CTH, one-way ANOVA corrected for multiple comparisons (Tukey's testing), $n = 3$. Data represent mean ± SEM

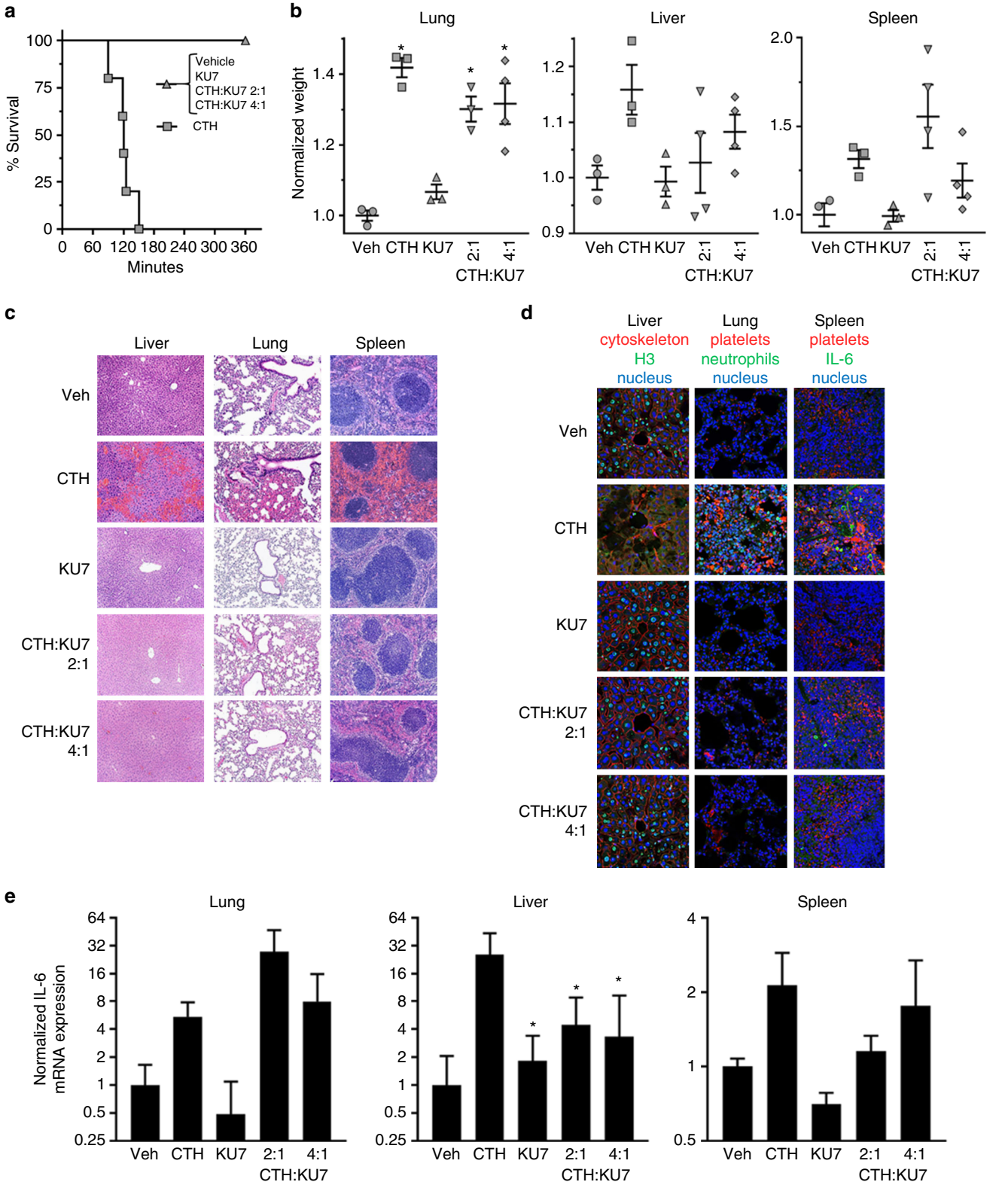

Fig. 4 Efficacy of histone aptamer in murine model of MODS. **a** Survival curves of mice injected IV with CTH in the presence or absence of aptamer treatment; $n = 6$ per group. Molar ratio of CTH to aptamer indicated. **b** Weights of the liver, lung and spleen normalized to pre-treatment body weight; $^*p < 0.05$ vs. Veh, one-way ANOVA corrected for multiple comparisons (Dunnett testing), $n = 4$–6 per group, data represent mean ± SEM. **c** Histology of the liver, lung and spleen of vehicle, CTH, KU7, CTH+KU7 (2:1), and CTH + KU7 (4:1) treated mice. Vascular congestion, thrombi and hemorrhaging are observed in the CTH mice. Scale bar = 100 µm. **d** Immunostaining of mouse liver, lung and spleen stained to identify nucleus (pseudo blue), cytoskeleton and platelets (pseudo red), histone H3, neutrophils and IL-6 (pseudo green) (see Supplementary Fig. 4 for quantitative analysis of immunostaining data). Scale bar = 25 µm. **e** Normalized IL-6 mRNA expression levels in the liver, lung and spleen of mice. Normalized IL-6 mRNA expression was determined using the following equation: $2^{\wedge}(\Delta\text{-}\Delta CT)$. ΔCT = beta actin − IL-6, $\Delta\text{-}\Delta CT$ = Vehicle ΔCT − Treatment ΔCT. Error bars represent the lower limit (LL) and upper limit (UL) of the standard deviation from the $\Delta\text{-}\Delta CT$ [$2^{\wedge}$(LL $\Delta\text{-}\Delta CT$) and $2^{\wedge}$(UL $\Delta\text{-}\Delta CT$)]; $^*p < 0.05$ vs. CTH (50 mg kg^{-1})

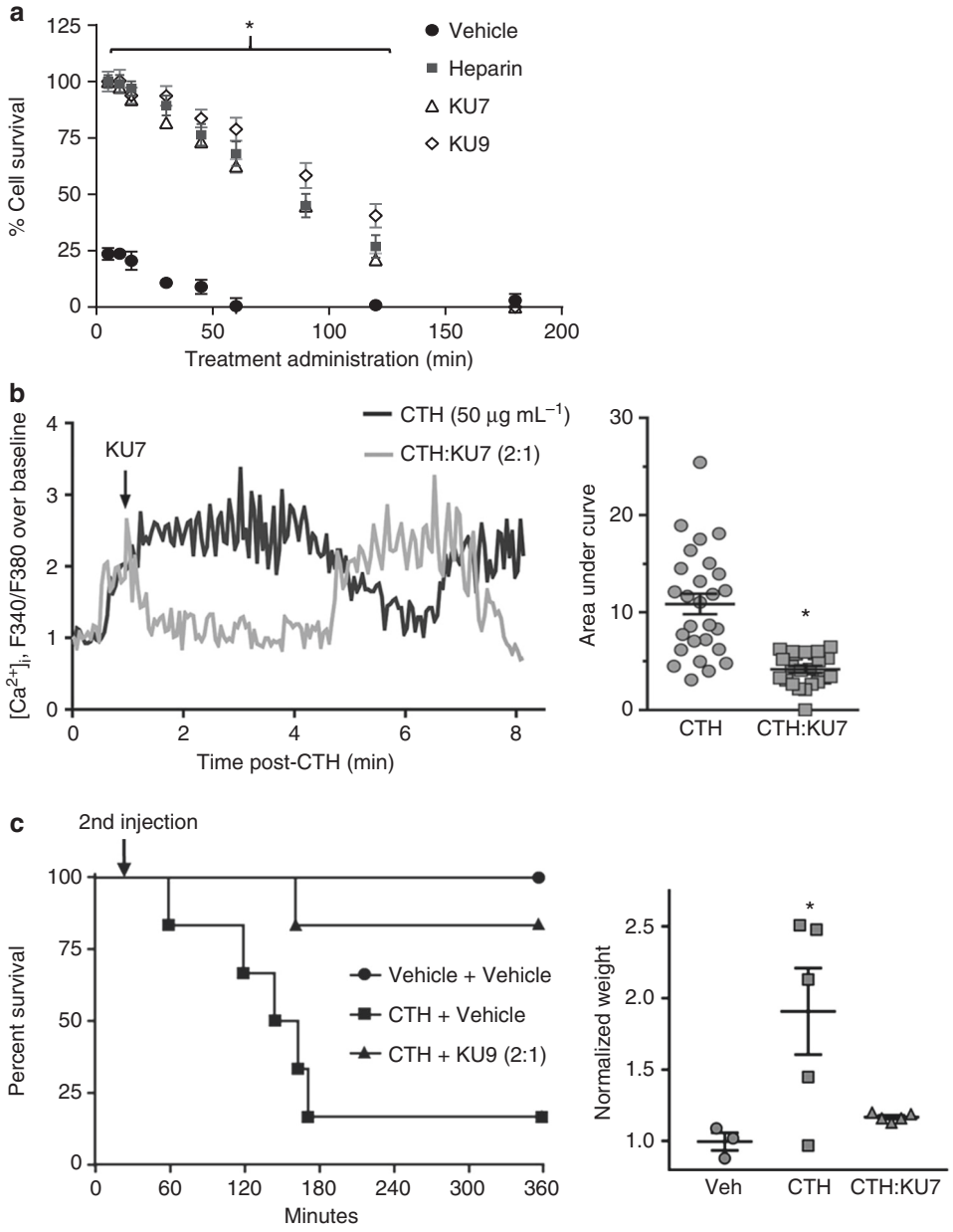

Fig. 5 Efficacy of anti-histone aptamers when administered after histones. **a** Aptamer inhibition of histone-mediated cytotoxicity of endothelial cells determined by MTS assay. EA.hy926 cells treated with 200 µg mL^{-1} of calf thymus histones followed by administration of either vehicle (negative control), heparin (positive control, 1:1), KU7 aptamer (1:2) or KU9 aptamer (1:2) at time points of 0, 5, 10, 15, 30, 45, 60, 90, 120 and 180 min after CTH; $n = 3$ biological replicates; *$p < 0.0025$ vs. vehicle. **b** Dynamic changes of intracellular calcium levels in Fura 2-AM-loaded EA.hy926 cells using fluorescence microscopy. (Left panel) Representative intracellular calcium elevation traces (F340/F380) of EA.hy926 treated with CTH (50 µg mL^{-1}) then followed by addition of vehicle or aptamer KU7 (Molar ratio of CTH to aptamer 2:1) added 1 min after CTH. (Right panel) Summary of data (*$p < 0.0001$ vs. CTH, unpaired two-tailed *t*-test, $n = 23$–27 cells). **c** Efficacy of anti-histone aptamers in murine model of MODS. Survival curves of mice injected IV with vehicle, or CTH (62.5 mg kg^{-1}), followed in 30 min by IV injection of vehicle or aptamer KU9 (31.25 mg kg^{-1}, indicated as 2nd injection); $n = 6$ biological replicates; *$p < 0.05$ vs. CTH+vehicle. Lung weight normalized to pre-treatment body weight. *$p < 0.05$ vs. Veh, one-way ANOVA corrected for multiple comparisons (Dunnett testing), $n = 3$–5 per group, data represent mean ± SEM

Aptamers bind and neutralize NET toxicity. Recent data demonstrate the importance of NETs as an important source of extracellular histones in a variety of clinical disease including MODS, sepsis, rheumatologic diseases and thrombosis[16,47–49]. We therefore assessed whether our anti-histone aptamers could prevent NET-associated cell toxicity. Human neutrophils were isolated, stimulated with phorbol myristate acetate (PMA) and NETs were generated for immunofluorescence microscopy and cell toxicity assays (Fig. 6). The 4′,6-diamidino-2-phenylindole (DAPI) stain demonstrates the formation of extracellular NETs (Fig. 6a; top, left panel) displaying histones (Fig. 6a; top, right panel). As shown in Fig. 6a, aptamer KU7 binds to human neutrophil-derived NETs (Fig. 6a, bottom, right panel). White color areas in the merged images demonstrate the close approximation of the aptamer KU7 with NETs (Fig. 6a; bottom, right panel). Importantly, anti-histone aptamer KU7 also attenuated NET-induced cell death (Fig. 6b), confirming their potential as a viable therapeutic option for clinical conditions (e.g., sepsis)

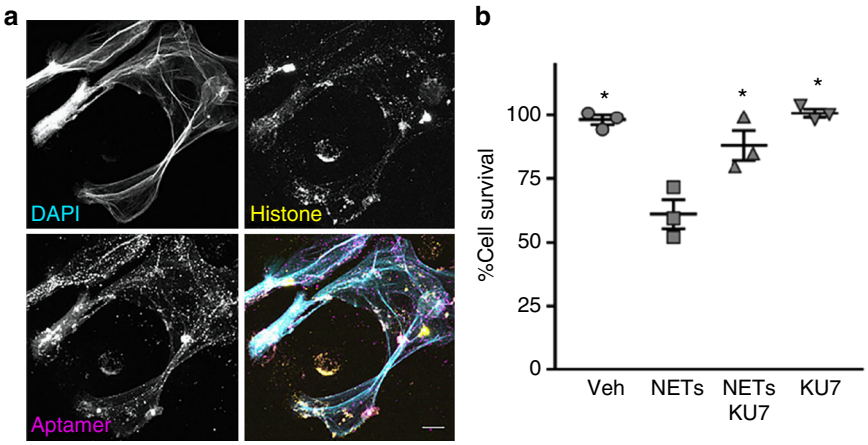

Fig. 6 Aptamers bind to human neutrophil-derived NETs and inhibit NET-induced cytotoxicity. **a** Confocal microscopy of human neutrophil-derived NETs. Single images are shown in gray scale. DAPI (top, left); histones (top, right); aptamer KU7 (bottom, left); merged images show: cyan, DAPI labeling of DNA, yellow, histones, and magenta, aptamer KU7-647 (bottom, right). White areas in the merged image represent close proximity of DNA, histone and aptamer. Representative images, captured with 40× oil and 2.8× zoom. Scale is equivalent to 10 µm. **b** Aptamer inhibition of NETs-mediated cytotoxicity of endothelial cells determined by MTS assay. EA.hy926 cells treated with 8 µg per well of NETs material (based on DNA concentration) and/or 8 µg per well (10.66 µM) of aptamer (KU7); $*p < 0.01$ vs. NETs, one-way ANOVA corrected for multiple comparisons (Tukey), $n = 3$, data represent mean ± SEM

leading to MODS. Although previous reports of histone inhibitors have demonstrated efficacy in the MODS via simultaneous administration of anti-histone therapy, this is the first report of an anti-histone therapy capable of rescuing the damaging cellular effects of extracellular histones in vitro and in vivo.

Discussion

This is the first report of an aptamer-based therapeutic approach for MODS. In this study, we developed nuclease-resistant RNA aptamers that bind with high affinity and specificity to human histones H3 and H4 implicated in MODS. Importantly, the aptamers do not bind to other proteins in human serum, and thus are expected to be safe for use in humans. We show that the aptamers inhibit histone-induced platelet aggregation (Fig. 3a), TLR activation (Fig. 3b) and endothelial cell death (Fig. 3c) and calcium influx (Fig. 3d) in human cells in culture. Importantly, these aptamers bind human NETs and neutralize their toxicity in vitro (Fig. 6). Finally, we demonstrate efficacy of one of the anti-histone aptamers (KU7) in a murine model of MODS (Figs. 4 and 5).

A key consideration when developing a drug that targets histones directly is that the drug must act exclusively in the extracellular space. Indeed, histone neutralizing drugs that obtain intracellular access could potentially disrupt DNA structure or function, and result in catastrophic side effects. To this end, oligonucleotide aptamers are highly anionic, and thus membrane impermeable which would negate any concerns with regards to toxicity due to targeting chromatin. An additional safety feature engineered into our anti-histone aptamers was the minimization of potential interactions between the aptamers and serum proteins. This was achieved by performing a stringent negative selection step (against human IgG and BSA) at every round of selection. An additional benefit imparted by the negative selection step was the maximization of the fraction of the aptamer drug that binds histones in circulation, thereby reducing the therapeutic dose of the aptamer. While binding of oligonucleotide-based drugs to serum proteins is normally viewed as a benefit to improve the pharmacokinetic properties of the drug and prolong circulating times, previous therapeutic aptamers to specific serum proteins (e.g., thrombin and factor IX) which have shown efficacy in humans were developed to minimize off-target interactions with non-target proteins in serum[26,50,51]. In addition, binding of the histone aptamers to multiple histone subtypes could also have a therapeutic advantage by enabling the inactivation of several histone proteins implicated in MODS with one aptamer drug. Similarly, a pool of (unselected) 2′ F-modified RNA aptamers, with low affinity for serum proteins, could be used to neutralize all cationic nuclear proteins (including all histones subtypes) released in circulation following extensive cell injury, thereby maximizing therapeutic efficacy.

Three distinct therapeutic approaches have been described to target extracellular histones. These include pharmacological agents to block histone release (e.g., PAD4 inhibitors and DNAse 1)[52,53] or downstream signaling (e.g., TLR blocking mAb or C reactive protein) or agents that directly neutralize extracellular histones (e.g., anti-histone mAb, APC and heparin)[7,19,48,54,55]. Although these approaches have shown promise in animal models of MODS, further research is necessary to warrant their safe application in a clinical setting. Indeed, one of the common problems with many of these anti-histone approaches is their propensity for nonspecific, off-target effects resulting in systemic toxicity.

Oligonucleotide-based drugs have been under clinical development for the past 30 years, starting with anti-sense oligos and followed by aptamers and small interfering RNAs. One of the key factors contributing to the approval of six oligonucleotide drugs over recent years has been the advent of nucleic acid chemistry to improve the safety and stability of these drugs. For example, the anti-vascular endothelial growth factor ($VEGF_{165}$) aptamer drug Macugen (formerly pegaptanib), which was approved by the FDA in 2004 to treat age-related macular degeneration of the retina, contains a phosphorothioate 3′—3′ deoxythymidine cap to promote nuclease stability, 2′-*O*-methylated purines and 2′-fluorinated pyrimidines. Finally, a 40 kDa molecular weight polyethylene glycol substituent was linked to the 5′ terminus of the aptamer to increase retention time in the eye[56,57]. Another safety consideration when developing the pegaptanib aptamer was enhancing target specificity. The pegaptanib aptamer was selected to be highly specific for $VEGF_{165}$, the predominant VEGF isoform in the human eye, thereby reducing potential systemic effects and greatly boosting the safety profile of the drug. The anti-histone aptamers developed in this study, which are modified with 2′-fluoro chemistry, were shown to be extremely

stable in human serum ($T_{1/2}$ KU7 = 150 h and $T_{1/2}$ KU9 = 48 h) (Fig. 2b) and safe in vivo (Fig. 4). In addition, as discussed above, the anti-histone aptamers were engineered to selectively bind histones in serum.

One additional benefit of the modification of the 2′-position of the ribose is increased duplex stability (T_m). 2'F modification in particular polarize the bases more significantly and contribute to strengthening of Watson-Crick base pairing[58]. For example, in the RNA interference field the combined use of 2′-fluoro pyrimidines with 2′-*O*-methyl purines results in RNA duplexes with extreme stability in serum and improved in vivo performance. Chemically engineered oligonucleotides with 2′-chemistry have also been used as efficient and specific silencers of endogenous microRNAs (miRNAs) in mice[59,60]. This is attributed to the ability of these modified oligos to compete with endogenous miRNAs for binding to their target mRNAs[60]. Similarly, post-selection modification of the 2′-position of aptamers increases binding to the target[61–63] and possibly favors binding of the anti-histone aptamers to both free histones and DNA-bound histones (nucleosomes) in serum (also see binding of aptamers to human neutrophil-derived NETs, Fig. 6a). Since free histones and DNA-bound histones are both pro-inflammatory[9], a single drug capable of neutralizing both forms is optimal.

In summary, we describe a approach using nuclease stabilized RNA aptamers to neutralize the toxic effects of extracellular histones implicated in MODS. Our approach overcomes many of the limitations of other experimental anti-histone treatments and provides a promising avenue for clinical implementation of a robust therapeutic for MODS in combination with other interventions (anti-inflammatory and supportive care). Because extracellular histones have been implicated in the development of many different disease conditions, the anti-histone aptamer biodrugs could potentially impact the treatment of numerous MODS-inducing clinical conditions including acute lung injury, transfusion-related acute lung injury, sepsis, trauma, burns, stroke, cancer, autoimmune/inflammatory disorders and ischemia/reperfusion and drug-mediated tissue injury.

Methods

Cell lines and cell culture reagents. Ea.Hy926 cells (ATCC®, CRL-2922, Manassas, VA) were maintained in Dulbecco's modified Eagle's medium (GIBCO, Gaithersburg, MD) supplemented with 10% fetal bovine serum (Atlanta Biologicals, Flowery Branch, GA) at 37 °C under 5% CO_2. The medium was changed every 2 to 3 days until confluent. During passaging, cells were trypsinized with Trypsin-EDTA (0.25%) (GIBCO, Gaithersburg, MD) and re-plated at a 1 to 4 ratio.

Selection protocol. The protocol for the generation of the initial (round 0) RNA Library has been described elsewhere. Step 1: Generation of double-stranded DNA (dsDNA) template by elongation. Elongation Solution 1 components: 9 µL of 100 mM Tris-HCl, pH 8.0 (Sigma-Aldrich, St. Louis, MO), 15 µL of 50 mM $MgCl_2$ (Sigma-Aldrich, St. Louis, MO), 1000 pmol of Sel2N20 template oligo (5′-TCGGGCGAGTCGTCTG-N20-CCGCATCGTCCTCCC-3′) (IDT, Coralville, IA), 2000 pmol Sel2 5′ primer (5′-TAATACGACTCACTA-TAGGGAGGACGATGCGG-3′) (IDT, Coralville, IA) and UltraPure distilled H_2O (diH_2O) (ThermoFisher, Waltham, MA) to a final volume of 90 µL. The Elongation Solution 1 was heated to 95 °C for 5 min and then 25 °C for 20 min. Elongation Solution 2 components: 50 µL of 10× PCR buffer (Denville Scientific, Charlotte, NC), 10 µL of 10 mM dNTP mix (New England Biolabs, Ipswich, MA), 4 µL of Choice Taq (Denville Scientific, Charlotte, NC), and diH_2O to a final volume of 410 µL. The Elongation Solution 2 was heated to 95 °C for 5 min then cooled to room temperature for 20 min. Elongation Solutions 1 and 2 were combined and placed in a thermal cycler. Cycling conditions for elongation were as follows: 72 °C for 30 min; 25 °C for 10 min; and held at 4 °C. Step 2: To generate the round 0 RNA library, the round 0 dsDNA template was transcribed in vitro using the mutant Y639F T7 RNA polymerase. The in vitro transcription reaction conditions were as follows: a total reaction volume of 250 µL was composed of 250 pmol of the dsDNA template library, 25 µL of a 10× rNTP solution (10× rNTP solution: 10 mM 2′-OH purines (Roche, Indianapolis, IN; GTP and ATP) and 30 mM 2′-Fluoro pyrimidines (TriLink BioTechnologies, LLC, San Diego, CA; 2′-Fluoro-2′-dCTP, 2′-Fluoro-2′-dUTP)) with 50 µL of a 5× Transcription Buffer (5× Transcription Buffer: 20% w/v Peg-8000 (Sigma-Aldrich, St. Louis, MO), 200 mM Tris-HCL, pH 8.0 (Life Technologies, Carlsbad, CA), 60 mM $MgCl_2$ (Sigma-Aldrich, St. Louis, MO), 5 mM spermidine HCl (Sigma-Aldrich, St. Louis, MO), 25 mM DTT (Sigma-Aldrich, St. Louis, MO), 2 µL of Inorganic pyrophosphatase (IPPI), ThermoFisher Scientific, Waltham, MA)) and diH_2O to 250 µL. The in vitro transcription reaction was incubated overnight at 37 °C. Removal of the dsDNA template was performed by addition of 1 µL (10 units) DNase I (Roche, Indianapolis IN) for 30 min at 37 °C followed by chloroform extraction. Step 3: The in vitro transcribed round 0 RNA was purified using PAGE. The RNA was run on a denaturing PAGE gel (10% acrylamide (Bio-Rad, Hercules, CA); 8 M urea (RPI, Mount Prospect, IL)) for 30 min at 24 watts. The round 0 RNA band was detected by ultraviolet (UV) shadowing, excised and eluted from the gel with TE low-EDTA buffer (0.1 mM EDTA (Sigma-Aldrich, St. Louis, MO), 10 mM TE pH 7.5 (Sigma-Aldrich, St. Louis, MO)) for 1 h at 37 °C in a rotator (Labnet, Edison, NJ). The eluted round 0 RNA was run through a 0.2 µM Cellulose Acetate Centricon (Sigma-Aldrich, St. Louis, MO) to remove any residual gel fragments. A 10,000 Molecular Weight Cut-Off Amicon Ultra-4 Centrifugal Filter Unit (Millipore, Burlington, MA) was used to concentrate the RNA solution. RNA OD_{260} and 260/280 ratio were determined by NanoDrop 2000 (ThermoFisher, Waltham, MA) to assess quantity and purity of round 0 RNA library.

For each round of selection, we performed a negative selection step (to remove nonspecific binding aptamers) and positive selection step (to enrich for histone binding aptamers). The round 0 RNA library was first incubated with human IgG (negative selection) (Sigma-Aldrich, St. Louis, MO) in 1× binding buffer (BB) at 37 °C ((1× BB: 20 mM HEPES (Sigma-Aldrich, St. Louis, MO), 0.15 M NaCl (Sigma-Aldrich, St. Louis, MO), 2 mM $CaCl_2$ (Sigma-Aldrich, St. Louis, MO)). Human IgG and human IgG binding aptamers were removed using a 0.2 µm nitrocellulose filter (GE, Chicago, IL). This was performed by incubating a 2 cm × 2 cm filter with the RNA solution for 20 min at 37 °C. Unbound RNA aptamers were transferred to a fresh tube containing (1000 pmol) of either human histone H3 or H4 (New England Biolabs, Ipswich, MA) and were incubated at 37 °C for 10 min. The histone-bound RNA aptamers were isolated by capturing the histones and RNAs on a nitrocellulose filter as described above. Histone-bound aptamers were eluted from the nitrocellulose filter by extraction with phenol/chloroform/isoamyl alcohol extraction. Specifically, the nitrocellulose disk containing the histones and histone-bound aptamers was submerged in phenol/chloroform/isoamyl alcohol (Fisher Scientific, Hampton, NH) and vortexed for 1 min. The solution was separated into two phases by adding an equal volume of diH_2O, vortexed for 1 min and centrifuging at 17,000 × *g* for 10 min. The aqueous layer (top layer containing the RNA aptamers) was collected and placed into an RNAse and DNAse-free 1.5 mL microcentrifuge tube (USA Scientific, Ocala, FL). An equal volume of chloroform (Fisher Scientific, Hampton, NH) was added to the aqueous layer to remove any trace of phenol, the solution was vortexed for 1 min, and centrifuged at 17,000 × *g* for 10 min. The aqueous layer (top layer containing the RNA aptamers) was collected and placed into a clean 1.5 mL microcentrifuge tube. The RNA aptamers were then ethanol precipitated by adding 5 µL of linear acrylamide (ThermoFisher, Waltham, MA), 1/10 volume of 10 M ammonium acetate (Fisher Scientific, Hampton, NH) and 2.5 volume of 100% ethanol (Pharmco-Aaper, Shelbyville, KY) followed by a 2 s vortex and centrifugation at 17,000 × *g* for 15 min. The solution was incubated at −20 °C overnight, and then centrifuged for 15 min at 17,000 × *g*. The supernatant was removed, and the pellet washed with 1 mL of 95% ethanol. The solution was centrifuged at 4 °C for 5 min at 17,000 × *g*, and the supernatant removed and the RNA pellet air dried at room temperature. The RNA pellet was then resuspended in 25 µL of diH_2O. The RNA was then reverse-transcribed by combining 10 µL of 5× FS buffer (ThermoFisher Scientific, Waltham, MA), 1 µL 0.1 M DTT (Sigma-Aldrich, St. Louis, MO), 1 µL 100 µM Sel2 3'primer (5'-TCGGGCGAGTCGTCTG-3' (IDT, Coralville, IA)), 31 µL diH_2O and 5 µL of recovered RNA in a polymerase chain reaction (PCR) tube (USA Scientific, Ocala, FL). Reaction conditions were as follows: 65 °C for 5 min, 22 °C for 5 min (annealing step) and room temperature for 10 min (cooling step). Then, 1 µL of 10 mM dNTP mix and 1 µL of Superscript III Reverse Transcriptase (ThermoFisher Scientific, Waltham, MA) was added to the mix followed by an incubation of 60 min at 55 °C, then 72 °C for 15 min and cooled to 4 °C. Next, 25 µL of the transcribed material was added to 50 µL of 10× Taq Polymerase Buffer (Denville Scientific, Charlotte, NC), 20 µL of 10 mM dNTP mix, 5 µL of 100 µM Sel2 5′ primer, 5 µL of 100 µM Sel2 3′-primer, 25 units of Taq polymerase (Denville Scientific, Charlotte, NC), and brought up to 500 µL with diH_2O. The reaction was separated into five PCR tubes and ran at 95 °C for 2 min, 22–25 cycles of 95 °C for 30 s, 55 °C for 30 s and 72 °C for 5 s, followed by 72 °C for 5 min, and then held at 4 °C. The amplified DNA (round 1 DNA) was utilized as the template for the subsequent round of selection as described above to generate the round 1 RNA pool. Selection conditions for each round of selection are provided in Supplemental Table 1.

Double-filter binding assay. Double-filter nitrocellulose binding assay was performed to determine the binding affinity (K_D) of the aptamers for their target. Briefly, the transcribed RNA from RD0 and RD8 of selection were dephosphorylated using Bacterial Alkaline Phosphatase (ThermoFisher, Waltham, MA). The dephosphorylating conditions were as follows: 100 pmol of RD0 or RD8 RNA was combined with 5 µL of 1 M Tris-HCL, pH 8.0, 1 µL BAP, and supplemented with diH_2O to reach 100 µL. The solution was then incubated at 55 °C for 60 min,

followed by adding 10 µL of 10× Dephosphorylation Stop Mixture ((20 mM Tris-HCl, pH 8.0, 40 mM EDTA, 200 mM NaCl (RPI, Mount Prospect, IL), 1% SDS (RPI, Mount Prospect, IL) (w/v)). Then, 300 µL of low-EDTA buffer was added to the reaction and purified using the phenol/chloroform/isoamyl alcohol extraction described above.

The dephosphorylated RNA and synthetic aptamers (KU7 and KU9) were radiolabeled with gamma-^{32}P-ATP using T4 polynucleotide kinase (PNK) as follows. A total reaction volume of 20 µL was made up of 20 pmol of aptamer RNA, 2 µL PNK (New England Biolabs, Ipswich, MA), 2 µL PNK reaction buffer (New England Biolabs, Ipswich, MA), 2 µL gamma-^{32}P-ATP (PerkinElmer, Waltham, MA) and diH_2O. The mixture was then incubated at 37 °C for 30 min and 65 °C for 20 min to heat inactivate the PNK. Then, 20 µL of 1× BB was added to the reaction followed by a centrifugation step through a G25 purification column (GE Healthcare, Little Chalfont, UK) according to the manufacturer's instructions. Labeling efficiency was determined by a scintillation counter. All radiolabeled RNAs were diluted in 1× BB to 2000 cpm mL^{-1}. Then, 5 µL of 2000 cpm mL^{-1} radiolabeled RNA were incubated at 37 °C for 5 min with 15 µL of either human histone H3.2 or H4 (positive selection targets) or human albumin (Sigma-Aldrich, St. Louis, MO) or serum (Sigma-Aldrich, St. Louis, MO) (negative control proteins) serially diluted in 1× BB. The binding reactions were loaded onto a dot blot apparatus (composed of nitrocellulose membrane on the top, nylon membrane (Sigma-Aldrich, St. Louis, MO) in the middle and Whatman paper (Sigma-Aldrich, St. Louis, MO) on the bottom). Treatment of the nitrocellulose membrane was as follows: pretreated with 0.5 M KOH (Sigma-Aldrich, St. Louis, MO) for 20 min, quick wash with diH_2O and equilibrated in 0.1 M Tris-HCl 7.5 for 45 min, washed with diH_2O and transferred to 1× BB for 20 min before l (Sigma-Aldrich, St. Louis, MO). The nylon was also incubated in 1× BB for 20 min before being loaded on the manifold. Before loading the RNA/protein samples, the wells were washed with 100 µL of 1× BB. The amount of RNA bound (nitrocellulose) versus unbound (nylon) was determined by densitometry of imaged membrane on a Fuji Phosphor imager.

Illumina high-throughput sequencing and sample preparation. The RNA pools from all rounds of selection were reverse-transcribed using Superscript III Reverse Transcriptase and the Sel2 3′ primer. Briefly, the RNA from each selection round was heated for 60 min at 55 °C followed by 72 °C for 15 min. The DNA product was then PCR-amplified using Choice Taq DNA Polymerase with barcoded Illumina primers (Supplementary Table 4). The DNA product with the Illumina barcode was heated for 2 min at 95 °C, followed by 10 cycles of 95 °C for 30 s, 55 °C for 30 s and 72 °C for 30 s with a final extension step at 72 °C for 5 min. The PCR product was then run on a 2% agarose gel and the appropriate bands (approximately 151 base pairs) were excised. The gel fragment was purified using the Qiagen Gel Extraction kit (Hilden, Germany) and quantified using NanoDrop 2000. Qualitative analysis of the samples was performed on an Agilent Model 2100 Bioanalyzer (Agilent, Santa Clara, CA). The samples were combined at equal molar amounts and submitted for Illumina sequencing (University of Iowa Genomic core, Iowa City, IA; Illumina Genome Analyzer II)[64].

The Illumina base calls (sequence reads) were pre-processed and filtered to identify the Sel2N20 aptamer library variable region sequence. For each round of selection, all unique variable region sequences were enumerated with the repeat sequences being counted. The sequenced DNA code was converted to RNA and the 5' and 3' constant regions were added.

Surface plasmon resonance. pH scouting was performed with all proteins. Coating of histone H4 and BSA to the COOHV biosensor was performed at pH 4.7. Coating of calf thymus histone to the COOHV biosensor was performed at pH 6.0. To prevent nonspecific binding to the vial and sensor surface, a small concentration (~0.01%) of Tween-20 was added to these solutions. The proteins were immobilized following a standard amine coupling procedure where a mixture of EDC (1-ethyl-3-(3-dimethylaminopropyl) carbodiimide) and NHS (*N*-hydroxysuccinimide) was injected to activate the surface carboxyl groups and protein was injected to react with and be coupled to the sensor surface. Then, 1 M Tris pH 8 was injected last to deactivate remaining active carboxyl groups.

A twofold dilution series (ranging from 10 to 100 nM) was prepared for each aptamer in buffer. Each sample was injected over all three flow channels for 4 min at a flow rate of 30 µL min^{-1} and dissociation was monitored for 10 min. The sensor surface was regenerated after each analyte cycle by injecting 1 M NaCl for 1 min. Data were processed by subtracting the reference channel signal and buffer blank responses (double referencing method). A two-compartment kinetic (mass transport limited) model was fit to the data to determine rate constants of association (k_a) and dissociation (k_d). A local R_{max} was provided in the fit due to an apparent concentration-dependent surface activity.

Serum stability measurements. Human blood was collected from healthy volunteers after obtaining written informed consent with protocols conducted in accordance to global ethical standards and approved by the University of Iowa Institutional Review Board. Chemically synthesized aptamers KU7 and KU9 were incubated at 37 °C under 5% CO_2 at a concentration of 5 µmol L^{-1} in 50% human serum. Incubation times ranged from 0 min to 28 days. At each time point, 10 pmol of aptamer (2 µL) was removed and added to 8 µL of 1× Tris base, Boric Acid, EDTA (TBE) (Fisher Scientific, Hampton, NH) and 2 µl of 2× Urea RNA loading dye (0.01 g Xylene Cyanol, 0.01 g bromophenol blue (Sigma-Aldrich, St. Louis, MO), 500 µl of 10× TBE and 10 mL of formamide (Amresco, Solon, OH)). The samples were then heat-inactivated at 95 °C for 5 min and stored at −20 °C. All samples (10 µL per lane = 8 pmol aptamer RNA) were loaded into a denaturing PAGE gel (8 M urea 10% acrylamide) and separated by electrophoresis at 10 watts for 30 min. The gel was stained with SYBR Gold (Invitrogen, Carlsbad, CA) at a 1:10,000 dilution in phosphate-buffered saline (PBS) for 30 min and visualized by UV light using a Chemidoc (Bio-Rad, Hercules, CA). Briefly, the quantification area of the aptamers at each time point was set to the height and size of the band at the 0 min time point. The band intensity of each time point was then calculated and normalized to 0 min, which was set at 100%.

Platelet isolation. Healthy donor blood (20 mL) was collected in 3.2% sodium citrate (9:1, v/v) vacutainer tubes (BD Scientific, San Jose, CA). The blood was pooled into 15 mL conical tubes (CellTreat, Pepperell, MA) and centrifuged at 100 × *g* for 15 min (without brakes) at room temperature. Platelet-rich plasma (PRP) was collected into fresh tube and prostaglandin E1 (PGE1, final conc.1 µM) was added, and mixed gently by inverting tubes. PGE1-PRP was then centrifuged at 800 × *g* for 10 min to pellet the platelets. After centrifugation, platelet pellets were washed with modified Tyrode's buffer (134 mmol L^{-1} NaCl, 2.9 mmol L^{-1} KCl, 2.9 mmol L^{-1} $CaCl_2$, 0.34 mmol L^{-1} Na_2HPO_4, 12 mmol L^{-1} $NaHCO_3$, 20 mmol L^{-1} HEPES, 1.0 mmol L^{-1} $MgCl_2$, 5.0 mmol L^{-1} glucose, pH 7.35) containing 1 µM PGE1. After washing, the platelet pellets were resuspended in modified Tyrode's buffer and counted on ADVIA 120 Hematology System (Siemens Healthineers, Malvern, PA).

Platelet aggregation assay. Washed platelets were prepared as above and resuspended in Tyrode buffer to a final concentration of 2.5 × 10^8 platelets per mL. For the platelet aggregation studies, 400 µL of washed platelets were stirred at 1200 rpm at 37 °C along with collagen (1 µg mL^{-1}), histone H4 (10 µg mL^{-1}), selected RNA rounds and/or KU7 or KU9 in a cuvette of an aggregometer (Chrono-log Model 560-VS) and light transmittance was recorded. Aggregation was measured as percent change in light transmission, where 100% refers to transmittance through blank solution.

Neutrophil isolation. Healthy donor blood (50 mL) was collected in 3.2% sodium citrate (9:1, v/v) vacutainer tubes (BD Scientific, San Jose, CA). The blood was mixed with equal volume of room temperature dextran/saline solution in 50 mL conical tubes (CellTreat, Pepperell, MA). The solution was then mixed by inverting 10 times and incubating upright for 20 min at room temperature. The upper layer (leukocyte-rich plasma) was carefully collected and transferred into a new 50 mL conical tube. The leukocyte-rich plasma solution was then centrifuged at 5 °C for 10 min at 250 × *g*. The supernatant was discarded and the cells were immediately resuspended in 30 mL of 0.9% saline. A 10 mL ficoll-hypaque solution (Sigma-Aldrich, catalog number: 10771) was added beneath the cell suspension and then centrifuged at 20 °C for 30–40 min at 400 × *g* with no breaks. The top layer was aspirated leaving the neutrophil and red blood cell (RBC) pellet behind. The cell pellet was resuspended in 20 mL of ice-cold water for exactly 30 s followed by 20 mL of cold 1.8% NaCl solution to restore isotonicity (0.9%). The neutrophil-containing solution was then centrifuge at 5 °C for 6 min at 250 × *g*. If the pellet was white, we resuspended in 5–10 mL of ice-cold PBS and counted the cells. If the pellet was red, we repeated the ice-cold water treatment as detailed above to remove RBC.

NETosis induction. Neutrophils were plated on 150 cm × 150 × 20 mm tissue culture dishes. After 30 min, when cells had adhered to the bottom of the dishes, they were stimulated for 4 h with 500 nM PMA. Conditioned medium was gently aspirated and the neutrophil/NET monolayer was collected with ice-cold PBS-Ca^{2++}/Mg^{2++} and centrifuged for 10 min at 450 × *g* at 4 °C to sediment cells. The cell-free but NET-rich supernatant was centrifuged for 10 min at 18,000 × *g* at 4 °C and the pellet containing NETs was suspended in Opti-MEM and DNA quantified by measuring absorbance at 260 nm using a NanoDrop spectrophotometer.

Imaging of NETs. To visualize NET formation, neutrophils were seeded on 12 mm coverslips inserted into 12-well plates (300,000 cells per well)[65]. After cells had adhered, they were stimulated with PMA as described above and aptamer binding to NET-associated chromatin was visualized by immunofluorescence[66]. Briefly, after fixing with 4% paraformaldehyde and permeabilizing with 0.5% Triton X-100, coverslips were blocked with 5% normal goat serum overnight at 4 °C. They were then sequentially incubated for 2.5 h each with anti-histone H3 (Cayman #13784, 1:50) antibody and 2 µM KU7–647 aptamer diluted in blocking buffer. After washing with PBS, cells/NETs were incubated with goat anti-rabbit IgG-Alexa Fluor 488 (1:360) for 1 h and counterstained with 1.33 µg mL^{-1} DAPI. All incubations were performed in a humidified chamber at 37 °C and were followed by three 5 min washes in PBS. Cells were mounted onto glass slides using Vectashield with DAPI. Images were captured using Leica LMD7000 confocal microscope under 40× oil per 2.8× zoom magnification and processed using Fiji Imaging software.

Cytotoxicity assays. EA.Hy926 cells were seeded in a 96-well flat bottom plate (CellTreat, Pepperell, MA) at a density of 8,000 cells per well in 100 µL of medium. After 24 h the medium was removed and replaced with 50 µL of Opti-MEM (GIBCO, Gaithersburg, MD) containing either calf thymus histones (Sigma-Aldrich, St. Louis, MO) and/or aptamer. After 24 h the medium was removed and MTS reagent (Abcam, Cambridge, MA) was added for 1 h according to manufacturer's protocol and quantified using a Thermo Max Microplate Reader (Molecular Devices, Sunnyvale, CA) at 490 nm.

EA.Hy926 cells were seeded in a 96-well flat bottom plate (CellTreat, Pepperell, MA) at a density of 8000 cells per well in 100 µL of medium. After 24 h, the medium was removed and replaced with 50 µL of Opti-MEM (GIBCO, Gaithersburg, MD) containing 8 µg of NET material (determined by DNA concentration) and/or 8 µg (10.66 µM) of aptamer. After 24 h, the medium was removed and MTS reagent (Abcam, Cambridge, MA) was added for 1 h according to the manufacturer's protocol and quantified using a Thermo Max Microplate Reader (Molecular Devices, Sunnyvale, CA) at 490 nm.

EA.Hy926 cells were seeded in a 96-well flat bottom plate (CellTreat, Pepperell, MA) at a density of 16,000 cells per well in 100 µL of medium. After 24 h, the medium was removed and replaced with 40 µL of Opti-MEM (GIBCO, Gaithersburg, MD) containing 200 µg mL^{-1} calf thymus histones (Sigma-Aldrich, St. Louis, MO). Quadruple wells received 10 µL of either vehicle (negative control), heparin (positive control, 1:1), KU7 aptamer (1:2) or KU9 aptamer (1:2) at time points 0, 5, 10, 15, 30, 45, 60, 90, 120 and 180 min. After 3 h, all wells were washed with media, followed by incubation in MTS reagent (Abcam, Cambridge, MA) for 1 h according to the manufacturer's protocol and quantified using a Thermo Max Microplate Reader (Molecular Devices, Sunnyvale, CA) at 490 nm.

Intracellular calcium influx measurements. Intracellular calcium concentration ($[Ca^{2+}]i$) was measured in single EA.hy926 cells using ratiometric calcium indicator Fura 2-AM (Life Technologies, Carlsbad, CA). Cells grown on 35 mm glass-bottom plates (MatTek, Ashland, MA) were loaded with 1 µM Fura 2-AM in calcium buffer (140 mM NaCl, 2.8 mM KCl, 2 mM $CaCl_2$, 2 mM $MgCl_2$, 10 mM glucose and 10 mM HEPES) for 15 min, washed and incubated in calcium buffer for another 15 min. Fura 2-AM-loaded cells were illuminated in calcium buffer by alternating 340/380-nm light delivered every 300 ms by a DG-4 argon exciter (Sutter Instruments, Novato, CA) under the control of MetaFluor software, and fluorescence images were captured at an emission of 510 nm with a Photometrics Cool SNAP HQ charge coupled device camera (Roper Scientific, Tucson, AZ) based on a Nikon TE2000 fluorescent microscope. Calf thymus histones (50 µg mL^{-1}) without or with 3 min of pre-incubation with RNA aptamer KU7 at various concentrations were added to loaded cells and calcium images were recorded for 10 min for each treatment condition. $[Ca^{2+}]i$ was reported as the ratio of Fura 2 fluorescence emission at 340 and 380 nm (F340/F380) normalized to baseline. All procedures were performed at room temperature.

TLR activation studies. TLR activation as measured by IL-6 production. EA.Hy926 cells were seeded in a 96-well flat bottom plate at a density of 15,000 cells per well in 100 µL of medium. After 24 h, the medium was removed and replaced with 100 µl of Opti-MEM containing either calf thymus histones and/or aptamers. After another 24 h, the supernatant was collected, processed and quantified according to the manufacturer's protocol used in the human IL-6 Quantikine® ELISA kit (R&D Systems, Minneapolis, MN).

Animals. The 8- to 12-week-old BALB/cJ mice (Jackson Laboratory, Bar Harbor, ME) were used for this study. All procedures conformed to standards established in the Guide for Care and Use of Laboratory Animals (National Academy Press, Washington, D.C. 2011). The Institutional Animal Care and Use Committees of the University of Iowa, accredited by AAALAC (Association for Assessment and Accreditation of Laboratory Animal Care International), reviewed and approved all protocols. All efforts were made to minimize the number of animals used and to avoid experiencing pain or distress.

Mouse model of multiple organ dysfunction. Mice received a tail vein injection of calf thymus histones at 50 mg kg^{-1} and/or aptamer at 25 or 12.5 mg kg^{-1} or vehicle (100 µL per mouse). The mice were monitored for distress and were killed 6 h post injection with isoflurane overdose if they survived histone toxicity.

Mice received retro-orbital injection of calf thymus histones at 62.5 mg kg^{-1} or vehicle (100 µL per mouse). After 30 min, mice received a follow-up retro-orbital injection (opposite eye) of either vehicle or aptamer at 31.25 mg kg^{-1} (100 µL per mouse). The mice were monitored for distress and were killed 6 h post injection with isoflurane overdose if they survived histone toxicity.

Mouse weights were recorded prior to tail vein injections using a digital laboratory balance (Denver Instrument MXX-601, Bohemia, NY). Organs were harvested and weighed after killing and normalized to the vehicle-treatment weight of each animal.

Histology was performed at the Comparative Pathology and Histology Research Laboratories (University of Iowa; http://www.medicine.uiowa.edu/pathology/research/dcp/). Tissues (lung, liver and spleen) were excised and fixed in 4% paraformaldehyde (PFA) (Affymetrix, Santa Clara, CA) for at least 1 week at 4 °C. All fixed tissues were processed in a series of alcohol and xylene baths, paraffin embedded and 7 µm sections were stained with H&E. A veterinary pathologist (David K. Meyerholz) examined all tissue sections. Dr. Meyerholz was blinded to the sample IDs. High-resolution digital images were acquired with a DP71 camera (Olympus) mounted on a BX51 microscope (Olympus) with MicroSuite Pathology Edition Software (Olympus).

Organs (lung, liver and spleen) were dissected out immediately after death or killing. A block of tissue (5 mm × 5 mm × 5 mm) from each organ was fixed in 4% PFA for 5 h and then cryo-protected overnight in 30% sucrose in PBS at 4 °C. Frozen 20 µm coronal sections were cut with a cryostat and mounted on Colorfrost Plus microscope slides (Fisher Scientific, Hampton, NH). Procedures like those described in previous publications were used for different combinations of multiple-label immunofluorescent staining for histone H3, myeloperoxidase (MPO, a marker for activated neutrophils), CD41 (a marker for platelets) and IL-6, and fluorescent staining for cytoskeleton (phalloidin-Alexa Fluor 568) and nucleus (TO-PRO®−3). Briefly, sections were incubated in 10% donkey serum with a mixture of primary antibodies that were made in different species. The antibody for histone H3 was purchased from Cell Signaling (Danvers, MA, dilution 1:200), MPO from Abcam (Cambridge, MA, dilution 1: 200), CD41 from BD Biosciences (San Jose, CA, dilution 1:400) and IL-6 from Novus Biologicals (Littleton, CO, dilution 1:100). After washing with PBS, sections were incubated in a mixture of fluorophore-conjugated secondary antibodies (Alexa Fluor 488 conjugated donkey anti-rabbit IgG and/or Alexa Fluro 594 conjugated donkey anti-rat IgG, both from Jackson ImmunoResearch, Westgrove, PA; dilution 1:200) against species from which the primary antibodies were made. Stained sections were covered using coverslips and Prolong Diamond Anti-Fade Reagents (Invitrogen, Carlsbad, CA) after the final washes with 1× PBS. Negative controls consisted of tissue processed in the absence of primary antibodies.

Fluorescent immuno-stained slides were examined with a Zeiss LSM 710 confocal laser scanning microscope. Sections were scanned sequentially in different channels to separate labels. Images from different channels were each assigned a pseudo-color and then were superimposed. Confocal images were obtained and processed with software provided with the Zeiss LSM 710.

Mouse organs (liver, lungs and spleen) were excised and immediately flash frozen. The organs were ground using a mortar and pestle (RPI, Mount Prospect, IL) over dry ice, followed by total cellular RNA extraction using the RNeasy Mini Kit (Qiagen, Valencia, CA). The purity and concentration of isolated RNA was measured using a NanoDrop 2000c spectrophotometer (ThermoFisher Scientific, Waltham, MA). The RNA was then reverse-transcribed into complementary DNA using SuperScript III Reverse Transcriptase (ThermoFisher Scientific, Waltham, MA). Real-time PCR was used to quantify the mRNA expression levels of the immune-responsive gene *IL-6*. Briefly, 100 ng of cDNA was used per 20 µL reaction of Power SYBR Green (Applied Biosystems, Foster City, CA). All PCR cycle programs were as follows: 95 °C for 10 min (95 °C for 15 s, 60 °C for 50 s) × 40 cycles, followed by a melting curve (95 °C for 15 s, 60 °C for 1 min, 95 °C for 1 s). Each reaction was performed in triplicate, and relative gene expression data were calculated as fold change to β-actin (control) expression data. The mouse-specific primers used in this study were: *β-Actin* (forward: CGG TTC CGA TGC CCT GAG GCT CTT; reverse: CGT CAC ACT TCA TGA TGG AAT TGA), *IL-6* (forward: GAG GAT ACC ACT CCC AAC AGA CC; reverse: AAG TGC ATC ATC GTT GTT CAT ACA).

Statistical analysis. Results are expressed as mean± SEM. Statistical comparisons were performed by a two-tailed *t*-test, or one-way or two-way analysis of variance (ANOVA) with correction for multiple comparisons using GraphPad Prism v.7.04. A p value of <0.05 was considered significant.

Reporting summary. Further information on experimental design is available in the Nature Research Reporting Summary linked to this article.

Data availability

The datasets generated during and/or analyzed during the current study are available from the corresponding author on request.

Received: 7 March 2018 Accepted: 12 December 2018
Published online: 10 January 2019

References

1. Frohlich, M. et al. Epidemiology and risk factors of multiple-organ failure after multiple trauma: an analysis of 31,154 patients from the TraumaRegister DGU. *J. Trauma Acute Care Surg.* **76**, 921–927; discussion 927–928 (2014).
2. Xu, J. et al. Extracellular histones are major mediators of death in sepsis. *Nat. Med.* **15**, 1318–1321 (2009).
3. Semeraro, F. et al. Extracellular histones promote thrombin generation through platelet-dependent mechanisms: involvement of platelet TLR2 and TLR4. *Blood* **118**, 1952–1961 (2011).
4. Chen, R., Kang, R., Fan, X. G. & Tang, D. Release and activity of histone in diseases. *Cell Death Dis.* **5**, e1370 (2014).

5. Murray, M. J. & Coursin, D. B. Multiple organ dysfunction syndrome. *Yale J. Biol. Med.* **66**, 501–510 (1993).
6. Alhamdi, Y. et al. Circulating histones are major mediators of cardiac injury in patients with sepsis. *Crit. Care Med.* **43**, 2094–2103 (2015).
7. Xu, J., Zhang, X., Monestier, M., Esmon, N. L. & Esmon, C. T. Extracellular histones are mediators of death through TLR2 and TLR4 in mouse fatal liver injury. *J. Immunol.* **187**, 2626–2631 (2011).
8. Yang, X., Li, L., Liu, J., Lv, B. & Chen, F. Extracellular histones induce tissue factor expression in vascular endothelial cells via TLR and activation of NF-kappaB and AP-1. *Thromb. Res.* **137**, 211–218 (2016).
9. Allam, R., Kumar, S. V., Darisipudi, M. N. & Anders, H.-J. Extracellular histones in tissue injury and inflammation. *J. Mol. Med.* **92**, 465–472 (2014).
10. Lv, X. et al. Extracellular histones are clinically relevant mediators in the pathogenesis of acute respiratory distress syndrome. *Respir. Res.* **18**, 165 (2017).
11. Thålin, C. et al. Citrullinated histone H3 as a novel prognostic blood marker in patients with advanced cancer. *PLoS ONE* **13**, e0191231 (2018).
12. Li, X. et al. Patients with HBV-related acute-on-chronic liver failure have increased concentrations of extracellular histones aggravating cellular damage and systemic inflammation. *J. Viral Hepat.* **24**, 59–67 (2017).
13. Ekaney, M. L. et al. Impact of plasma histones in human sepsis and their contribution to cellular injury and inflammation. *Crit. Care* **18**, 543 (2014).
14. Johansson, P. I., Windelov, N. A., Rasmussen, L. S., Sorensen, A. M. & Ostrowski, S. R. Blood levels of histone-complexed DNA fragments are associated with coagulopathy, inflammation and endothelial damage early after trauma. *J. Emerg. Trauma Shock* **6**, 171–175 (2013).
15. Kawai, C. et al. Circulating extracellular histones are clinically relevant mediators of multiple organ injury. *Am. J. Pathol.* **186**, 829–843 (2016).
16. Xu, J. et al. Extracellular histones are major mediators of death in sepsis. *Nat. Med.* **15**, 1318 (2009).
17. Huang, H. et al. Histones activate the NLRP3 inflammasome in Kupffer cells during sterile inflammatory liver injury. *J. Immunol.* **191**, 2665–2679 (2013).
18. Wildhagen, K. C. et al. Nonanticoagulant heparin prevents histone-mediated cytotoxicity in vitro and improves survival in sepsis. *Blood* **123**, 1098–1101 (2014).
19. Abrams, S. T. et al. Circulating histones are mediators of trauma-associated lung injury. *Am. J. Respir. Crit. Care Med.* **187**, 160–169 (2013).
20. Li, X., Egorina, E., Bertelsen, E. L., Dahlen, H. & Hannestad, K. Antinucleosome autoantibodies bind directly to cell lines in vitro and via the FcgammaRIIB receptor to B lymphocytes in vivo: a role for immune complexes in interactions between antinucleosome IgG2a and B cells of BXSB lupus mice. *Scand. J. Immunol.* **60**, 121–133 (2004).
21. Losman, M. J., Fasy, T. M., Novick, K. E. & Monestier, M. Relationships among antinuclear antibodies from autoimmune MRL mice reacting with histone H2A-H2B dimers and DNA. *Int. Immunol.* **5**, 513–523 (1993).
22. Opal, S. M., Dellinger, R. P., Vincent, J. L., Masur, H. & Angus, D. C. The next generation of sepsis clinical trial designs: what is next after the demise of recombinant human activated protein C?*. *Crit. Care Med.* **42**, 1714–1721 (2014).
23. Afifi, S. et al. Role of histone deacetylase inhibitors in relapsed refractory multiple myeloma: a focus on vorinostat and panobinostat. *Pharmacotherapy* **35**, 1173–1188 (2015).
24. Bongartz, T. et al. Anti-TNF antibody therapy in rheumatoid arthritis and the risk of serious infections and malignancies: systematic review and meta-analysis of rare harmful effects in randomized controlled trials. *JAMA* **295**, 2275–2285 (2006).
25. Shields, L. B. et al. Adverse effects associated with high-dose recombinant human bone morphogenetic protein-2 use in anterior cervical spine fusion. *Spine (Phila. Pa 1976)* **31**, 542–547 (2006).
26. Keefe, A. D., Pai, S. & Ellington, A. Aptamers as therapeutics. *Nat. Rev. Drug Discov.* **9**, 537–550 (2010).
27. Dassie, J. P. & Giangrande, P. H. Current progress on aptamer-targeted oligonucleotide therapeutics. *Ther. Deliv.* **4**, 1527–1546 (2013).
28. Thiel, K. W. & Giangrande, P. H. Therapeutic applications of DNA and RNA aptamers. *Oligonucleotides* **19**, 209–222 (2009).
29. Sundaram, P., Kurniawan, H., Byrne, M. E. & Wower, J. Therapeutic RNA aptamers in clinical trials. *Eur. J. Pharm. Sci.* **48**, 259–271 (2013).
30. Esposito, C. L. et al. A neutralizing RNA aptamer against EGFR causes selective apoptotic cell death. *PLoS ONE* **6**, e24071 (2011).
31. Povsic, T. J. et al. A phase 2, randomized, partially blinded, active-controlled study assessing the efficacy and safety of variable anticoagulation reversal using the REG1 system in patients with acute coronary syndromes: results of the RADAR trial. *Eur. Heart J.* **34**, 2481–2489 (2013).
32. Vavalle, J. P. & Cohen, M. G. The REG1 anticoagulation system: a novel actively controlled factor IX inhibitor using RNA aptamer technology for treatment of acute coronary syndrome. *Future Cardiol.* **8**, 371–382 (2012).
33. Chan, M. Y. et al. Phase 1b randomized study of antidote-controlled modulation of factor IXa activity in patients with stable coronary artery disease. *Circulation* **117**, 2865–2874 (2008).
34. Chan, M. Y. et al. A randomized, repeat-dose, pharmacodynamic and safety study of an antidote-controlled factor IXa inhibitor. *J. Thromb. Haemost.* **6**, 789–796 (2008).
35. Povsic, T. J. et al. Pegnivacogin results in near complete FIX inhibition in acute coronary syndrome patients: RADAR pharmacokinetic and pharmacodynamic substudy. *Eur. Heart J.* **32**, 2412–2419 (2011).
36. Tuerk, C. & Gold, L. Systematic evolution of ligands by exponential enrichment: RNA ligands to bacteriophage T4 DNA polymerase. *Science* **249**, 505–510 (1990).
37. Ellington, A. D. & Szostak, J. W. In vitro selection of RNA molecules that bind specific ligands. *Nature* **346**, 818–822 (1990).
38. Zuker, M. Mfold web server for nucleic acid folding and hybridization prediction. *Nucleic Acids Res.* **31**, 3406–3415 (2003).
39. Semeraro, N., Ammollo, C. T., Semeraro, F. & Colucci, M. Coagulopathy of acute sepsis. *Semin. Thromb. Hemost.* **41**, 650–658 (2015).
40. Freeman, C. G. et al. The accumulation of circulating histones on heparan sulphate in the capillary glycocalyx of the lungs. *Biomaterials* **34**, 5670–5676 (2013).
41. Gillrie, M. R. et al. Plasmodium falciparum histones induce endothelial proinflammatory response and barrier dysfunction. *Am. J. Pathol.* **180**, 1028–1039 (2012).
42. Kleine, T. J., Lewis, P. N. & Lewis, S. A. Histone-induced damage of a mammalian epithelium: the role of protein and membrane structure. *Am. J. Physiol.* **273**, C1925–C1936 (1997).
43. Kleine, T. J., Gladfelter, A., Lewis, P. N. & Lewis, S. A. Histone-induced damage of a mammalian epithelium: the conductive effect. *Am. J. Physiol.* **268**, C1114–C1125 (1995).
44. Abrams, S. T. et al. Human CRP defends against the toxicity of circulating histones. *J. Immunol.* **191**, 2495–2502 (2013).
45. Fuchs, T. A., Bhandari, A. A. & Wagner, D. D. Histones induce rapid and profound thrombocytopenia in mice. *Blood* **118**, 3708–3714 (2011).
46. Nakahara, M. et al. Recombinant thrombomodulin protects mice against histone-induced lethal thromboembolism. *PLoS ONE* **8**, e75961 (2013).
47. Sollberger, G., Tilley, D. O. & Zychlinsky, A. Neutrophil extracellular traps: the biology of chromatin externalization. *Dev. Cell* **44**, 542–553 (2018).
48. Saffarzadeh, M. et al. Neutrophil extracellular traps directly induce epithelial and endothelial cell death: a predominant role of histones. *PLoS ONE* **7**, e32366 (2012).
49. McDonald, B. et al. Platelets and neutrophil extracellular traps collaborate to promote intravascular coagulation during sepsis in mice. *Blood* **129**, 1357–1367 (2017).
50. Rusconi, C. P. et al. RNA aptamers as reversible antagonists of coagulation factor IXa. *Nature* **419**, 90–94 (2002).
51. Rusconi, C. P., Yeh, A., Lyerly, H. K., Lawson, J. H. & Sullenger, B. A. Blocking the initiation of coagulation by RNA aptamers to factor VIIa. *Thromb. Haemost.* **84**, 841–848 (2000).
52. Huang, H. et al. Damage-associated molecular pattern-activated neutrophil extracellular trap exacerbates sterile inflammatory liver injury. *Hepatology* **62**, 600–614 (2015).
53. Caudrillier, A. et al. Platelets induce neutrophil extracellular traps in transfusion-related acute lung injury. *J. Clin. Invest.* **122**, 2661–2671 (2012).
54. Allam, R. et al. Histones from dying renal cells aggravate kidney injury via TLR2 and TLR4. *J. Am. Soc. Nephrol.* **23**, 1375–1388 (2012).
55. Bosmann, M. et al. Extracellular histones are essential effectors of C5aR-and C5L2-mediated tissue damage and inflammation in acute lung injury. *FASEB J.* **27**, 5010–5021 (2013).
56. Ng, E. W. et al. Pegaptanib, a targeted anti-VEGF aptamer for ocular vascular disease. *Nat. Rev. Drug Discov.* **5**, 123–132 (2006).
57. Ng, E. W. & Adamis, A. P. Anti-VEGF aptamer (pegaptanib) therapy for ocular vascular diseases. *Ann. NY Acad. Sci.* **1082**, 151–171 (2006).
58. Pallan, P. S. et al. Unexpected origins of the enhanced pairing affinity of 2′-fluoro-modified RNA. *Nucleic Acids Res.* **39**, 3482–3495 (2010).
59. Krutzfeldt, J. et al. Specificity, duplex degradation and subcellular localization of antagomirs. *Nucleic Acids Res.* **35**, 2885–2892 (2007).
60. Krutzfeldt, J. et al. Silencing of microRNAs in vivo with 'antagomirs'. *Nature* **438**, 685–689 (2005).
61. Da Rocha Gomes, S. et al. (99m)Tc-MAG3-aptamer for imaging human tumors associated with high level of matrix metalloprotease-9. *Bioconjug. Chem.* **23**, 2192–2200 (2012).
62. Mittelberger, F. et al. RAID3--An interleukin-6 receptor-binding aptamer with post-selective modification-resistant affinity. *RNA Biol.* **12**, 1043–1053 (2015).
63. Meyer, C. et al. Stabilized Interleukin-6 receptor binding RNA aptamers. *RNA Biol.* **11**, 57–65 (2014).

64. Thiel, W. H. et al. Rapid identification of cell-specific, internalizing RNA aptamers with bioinformatics analyses of a cell-based aptamer selection. *PLoS ONE* **7**, e43836 (2012).
65. Najmeh, S., Cools-Lartigue, J., Giannias, B., Spicer, J. & Ferri, L. E. Simplified human neutrophil extracellular traps (NETs) isolation and handling. *J. Vis. Exp.* **98**, e52687 (2015).
66. Brinkmann, V., Laube, B., Abed, U. A., Goosmann, C. & Zychlinsky, A. Neutrophil extracellular traps: how to generate and visualize them. *J. Vis. Exp.* **36**, pii: 1724 (2010).

Acknowledgements

The authors would like to acknowledge the use of the University of Iowa Pathology Core and the University of Iowa Central Microscopy Research Facility, resources supported by the Vice President for Research & Economic Development, the Holden Comprehensive Cancer Center and the Carver College of Medicine. We would like to thank the labs of Drs. Adam Dupuy, George Wiener and the Iowa City VA Microscopy Core for the use of equipment (Bio-Rad Imager, plate reader and confocal microscope). K.T.U. was supported by the American Heart Association (AHA) pre-doctoral fellowship (17PRE33410335). This work was supported by grants to P.H.G. and F.J.M. from the Department of Defense Congressionally Directed Medical Research Programs (PR150627 and PR150627P1), University of Iowa Carver College of Medicine (CCOM) (Carver Collaborative Pilot Grant Award 2015) and University of Iowa Award from The Office of the Vice President for Research and Economic Development (OVPRED 2015). F.J.M. is also supported by the Office of Research and Development, Department of Veterans Affairs (2I01BX001729). This study was also supported in part by the National Institutes of Health grants AG049784 to S.D. and HL121105 to J.K.-T.

Author contributions

Conceptualization: F.J.M. and P.H.G.; methodology: F.J.M., P.H.G., S.D., M.E.W., J.A.S. and L.-H.L.; data acquisition, curation and analysis: K.T.U., G.N.B., L.-H.L., J.P.D., S.S., W.H.T., Y.C., V.K.S., B.L., J.A.S., S.M., W.R.G., J.K.-T., F.J.M. and P.H.G.; resources: F.J.M. and P.H.G.; writing (original draft): K.T.U., G.N.B. and L.-H.L.; writing (review and editing): J.K.-T., F.J.M., P.H.G., S.S. and L.-H.L.; supervision: F.J.M. and P.H.G.

Additional information

Supplementary Information accompanies this paper at https://doi.org/10.1038/s41467-018-08030-y.

Competing interests: The authors declare no competing interests.

Reprints and permission information is available online at http://npg.nature.com/reprintsandpermissions/

Journal peer review information: *Nature Communications* thanks the anonymous reviewers for their contribution to the peer review of this work. Peer reviewer reports are available.

Publisher's note: Springer Nature remains neutral with regard to jurisdictional claims in published maps and institutional affiliations.

RNA aptamer based detection of histone biomarker for early diagnosis of sepsis

Running head: Histone aptamer and sepsis diagnosis

Shambhavi Shubham[1], Li-Hsien Lin[1], Piedad del Carmen Gomez Contreras[1], Kevin T. Urak[1,2], Giselle Blanco[1], Felicia Ruffin [3], Vance G. Fowler Jr.[3], Julia Klesney-Tait[1], Colette Galet[4], Patrick W. McGonagill[4], Francis J Miller Jr[3], Paloma H. Giangrande,[1,2, 5,6,7,8]

[1]Internal Medicine, University of Iowa, Iowa City, IA, USA,
[2]Molecular & Cellular Biology Program, University of Iowa, Iowa City, IA, USA
[3] Departments of Internal Medicine and Pharmacology and Cancer Biology, Duke University, Durham, NC, USA,
[4]Department of Surgery, Acute Care Surgery Division, University of Iowa, Iowa City, IA, USA
[5]Holden Comprehensive Cancer Center, University of Iowa, Iowa City, IA, USA,
[6]Radiation Oncology, University of Iowa, Iowa City, IA, USA,
[7]Environmental Health Sciences Research Center (EHSRC), University of Iowa, Iowa City, IA, USA
[8]Abboud Cardiovascular Research Center, University of Iowa, Iowa City, IA, USA,

[§] Equal contribution

***Corresponding authors:**
Paloma H Giangrande, PhD
University of Iowa
375 Newton Rd
5202 MERF
Iowa City, IA 52242
Phone: +1-319-384-3242 (office)
Fax: +1-319-353-5552
Email: paloma-giangrande@uiowa.edu

Francis J Miller, Jr., MD
Duke University
508 Fulton St, Bldg. 15,
Room 306, Durham, NC 27705
Phone: +1-919-668-2688 (office)
Email: francis.miller@duke.edu

ABSTRACT

Sepsis remains a major public health problem, striking an estimated 31.5 million patients and killing 5.3 million worldwide annually. Delayed diagnosis and treatment of sepsis result in an extremely high rate of morbidity and mortality worldwide. Currently, sepsis is diagnosed via time-consuming bacterial culture of blood specimens or antibody-based molecular analysis. The use of nucleic acid aptamer biosensors that bind sepsis biomarkers in the circulation with high affinity and specificity could provide a robust and rapid method to diagnose sepsis. We previously used the systematic evolution of ligands by exponential enrichment (SELEX) technology to develop chemically-modified RNA aptamers to extracellular histones implicated in sepsis (histones H3 and H4). Here, we show that these aptamers can detect low levels (< 10 μg/mL) of circulating histones in serum samples from septic patients. Importantly, with the aptamer-based detection assay, we establish a well-defined correlation between sepsis severity and serum levels of circulating histones. Early diagnosis of sepsis has a major impact on the clinical course, prompting earlier antibiotic administration, ensuring more rapid surgical source control, and improving patient outcomes. Given the potential impact of early diagnosis of sepsis on patient outcomes, these aptamers represent a vital tool to predict adverse effects of sepsis and to help improve patient management.

INTRODUCTION

Sepsis is a systemic inflammatory response to infection. .Sepsis has a tremendous impact on healthcare systems worldwide, impacting an estimated 31.5 million patients and killing 5.3 million annually.[1] Early detection and treatment of sepsis key to prevent its progression to severe sepsis or septic shock, which lead to tissue damage and organ failure. Currently, sepsis is diagnosed via microbiological evaluation of bodily fluids to identify the causative bacterial strain. However, this diagnosis method is limited by the length of time required for the cultures to grow to identifiable quantities. Cultures are also reported to be insensitive under several conditions,[2-5] including slow-growing and non-cultivatable microorganisms and microorganisms present at very low concentrations. In light of these disadvantages, alternative diagnostic methods using molecular-based tests have been developed to enable the diagnosis of sepsis. C reactive protein (CRP) and procalcitonin (PCT) are two of many biomarkers used for the diagnosis of sepsis; however, these tests still lack accuracy and present prolonged turnaround times.[6] To overcome these issues, an array of multiple biomarkers can be used in combination to provide definitive diagnostic test results.

One such potential biomarker that has garnered the attention is circulating extracellular histones. Histones are major chromosomal proteins found in cell nuclei. They are highly conserved across species. Five histone proteins have been identified: H2A, H2B, H3, and H4, also known as “core histones,” and histone 1 and its homolog H5, which are known as linker Histones. [ref] Histones form the nucleosome as they wrap around cellular DNA. Nucleosomes contain one H3/H4 tetramer and two H2A/H2B dimers, while H1 binds to non-nucleosomal DNA and facilitates numerous nucleosomes to form higher order chromatin structures. [ref] Histones typically provide the structural framework within the nucleus and are inert. However, when released in the extracellular space, they lead to significant pathogenic effects. Studies identified extracellular histones as some of the major mediators of sepsis progression.[7 8]

Circulating extracellular histones originate from apoptotic or necrotic cells, as well as neutrophils activated to make neutrophil extracellular traps (NETs). They induce septic shock through cytotoxicity, excessive inflammation, and coagulation dysfunction. [9] They act as cytotoxic damage-associated molecular pattern (DAMP) proteins by activating Toll-like receptors (TLRs), promoting pro-inflammatory cytokine pathways and altering phospholipid membrane permeability. H3 and H4 histones are known as the most cytotoxic amongst all histone isoforms. (ref]

Circulating histones are usually present at low concentrations in healthy individuals, but circulating levels increase in patients who suffer from severe trauma, systemic inflammation, sepsis, or tissue damage.[1,10] While histones have been measured in patient plasma samples,[8,11] determination of histone concentration in serum has been difficult . Additionally, there is still no consensus regarding the disease-induced concentration threshold of histones in the serum. Immunoassays have been used for detection of free histone proteins.[12,13] However, results show poor reproducibility, wide error range, and low sensitivity.[13] Considering these limitations, a technique devised to detect circulating histones with high accuracy and sensitivity is paramount in a clinical setting.

Currently available techniques to detect histones rely on antibody-based detection methods. Although widely used, these techniques are limited by sensitivity, expense, and lengthy detection.

Aptamers are short nucleic acid sequences that are known to bind to their cognate targets with high affinity and specificity. They are selected by an *in vitro* selection process called Systematic evolution of ligands through exponential enrichment (SELEX).[14,15] They possess key advantages over antibodies as follows: 1) They can tolerate pH and temperatures unlike

antibodies; 2***)*** They are easy and economical to produce and their small size leads to a high number of moles of target substance bound per gram of aptamer; **3)** They are stable at ambient temperature, yielding a much longer shelf-life than other biologics, and can tolerate transportation without refrigeration. Since their discovery aptamers have been explored not just as therapeutics drugs but have been efficiently integrated on sensing platforms for use in detection of biological molecules. {REF}Several aptamers have been selected against sepsis-associated bacterial strains[16,17] and sepsis biomarkers.[18] Although these studies show high affinity and specific binding to their targets, clinical studies are still warranted to corroborate their use in clinical settings.

We recently selected 2'Fluoro-modified RNA aptamers (KU7 and KU9) to recombinant histone proteins, H3 and H4. KU7 and KU9 bind to H3 and H4 histones with high affinity (low nM) and specificity. (unpublished data) The selection protocol was designed to eliminate sequences binding to abundant serum proteins and enrich for sequences specifically binding to histones. Owing to their high affinity and specificity, these aptamers function as excellent tools for the detection of circulating histones in the serum. In this study, we used KU7 and KU9 aptamers to quantify low µg/mL levels of circulating histones in the serum of septic patients and demonstrated a correlation between sepsis severity and histone levels. Early diagnosis of sepsis using this technique will enable better prognosis of septic patients, potentially reducing sepsis-related morbidity and mortality.

RESULTS

Detection of histones H3 and H4 in human serum using ELISA

ELISA is widely used to quantify H3 and H4 histones.[11] Although, popularly used, there are conflicting reports of the histone concentrations in plasma of patients with severe sepsis.[8,19] Based on our assessment, quantification of histone levels in serum was difficult using ELISA. As shown in **Fig. 1A**, the presence of serum severely impaired the measurement of histones by ELISA even when diluting samples 1- to 25 folds. Filtrating the serum to remove proteins to which histones can bind (REF) allowed us to detect histones at concentrations matching those of histone concentrations in PBS **(Fig. 1A)**. Our data show that detecting histones in the serum by ELISA is not reliable as histones bind to proteins present in the serum.

Serum albumin is the most abundant serum protein and is negatively charged.[20] Given the cationic characteristic of histones, we tested whether bovine serum albumin (BSA) alone could be responsible for the low signal observed when detecting histone in the serum. As shown in **Fig. 1B**, detection of both H3 and H4 histones was significantly reduced in the presence of BSA**.** Interestingly, the detection of histone H4 was more severely decreased in the presence of albumin **(Fig. 1B, left panel)** than that of histone H3 **(Fig. 1B, right panel)**. These results suggest that ELISA is not a reliable method to detect extracellular histones in clinical samples.

Detection of histones in human serum using western blot

We next attempted to detect histones under denaturing conditions using western blot. The rationale was that denaturation and size-based separation of proteins will enable easy access and recognition of histone epitopes by anti-histone antibodies. Although, we detected CTH and histone H3 in 10% serum **(Fig. 2A),** we were unable to quantify histones. Even at lower concentrations of histones, we did not obtain a linear correlation between signal intensity and histone concentration **(Fig 2B)**. Apart from being non-quantitative, western blot involved long

processing times and, comparatively, was less sensitive than ELISA assay. Our results suggest that western blot would be an unsuitable technique for quantifying histones in serum.

Detection of histones in human serum using RNA aptamers

We next attempted to detect histones using RNA aptamers in the presence and absence of serum using a double filter binding assay. As shown in **Fig. 3**, aptamers effectively detected histones in undiluted (100%) serum. Importantly, KU7 detected recombinant histones (H3 and H4) and CTH with similar sensitivities in undiluted serum **(Fig. 3 A, B, C, left panel)**. Using KU9, we were only able to detect CTH in serum **(Fig. 3 A, B, C right panel)**. This suggests that KU7 and KU9 bind to non-overlapping epitopes on histone proteins. Our results indicate that KU7 binds to an epitope that is readily accessible even in the presence of serum proteins. While we failed to detect recombinant H3 and H4 in serum using KU9, CTH was detected **(Fig. 3C, right panel).**

Detection of histones in serum samples from septic patients using RNA aptamers

We next tested whether KU7 and KU9 aptamers could be used to detect histones in serum samples from septic patients**.** Patients' characteristics are presented in **Table 1 (Duke population).** Consistent with our earlier observation, we could detect histones (10–40 µg/mL) in patient samples using aptamers and histone concentrations correlated with sepsis severity **(Fig. 4A, left panel)**. Moreover, when assessing histones levels based on bacterial infection type, histone levels were significantly different in patients inflicted with gram negative and gram-positive bacteria (**Supplementary Fig. 1A)**. Both groups were similar in term of age, gender, and APACHE II scores (data not shown). These results suggest that histone levels could predict the infection type.

Considering the increased incidence of sepsis infections in males, we compared histone levels between males and females; no significant difference was observed (**Fig. 4A; right panel**), likely reflecting similar APACHE II scores in males and females.

We next verified the robustness of this assay by measuring histone levels using KU7 aptamer in serum samples from patients presenting with severe sepsis (**Table 1: Iowa population**)**.** High levels (50 µg/mL) of histones were detected in serum samples of patients presenting with severe sepsis and high APACHE scores (**Fig. 4B; left panel**)**.** Combining data from both University of Iowa and Duke University, we showed that histone levels significantly and positively correlated with APACHE II scores **(Supplementary Fig. 2).** Lactate dehydrogenase (LDH) has been identified as one of the biomarkers for sepsis severity.[25] As shown in **Fig. 4B; right panel,** LDH levels were higher in serum samples from patients with severe sepsis than those in serum samples from healthy donors, the difference was not statistically significant**.** Our results suggest that detection of histones using aptamer is more sensitive in detecting severe sepsis than the currently used biomarker, LDH.

DISCUSSION

Sepsis is characterized by several clinical stages, and mortality rates are different for each stage. Ref Early identification of sepsis would improve patient management, leading to reduced mortality rates.[21] Currently, sepsis is diagnosed by either culturing bacterium from patient blood samples or by detection of sepsis biomarkers using antibody-based molecular techniques. Although regularly used, these methods present slow turnaround times as well as low sensitivity and specificity. Thus, tools that provide high sensitivity, accuracy, and rapid detection are urgently needed. Herein, we developed an RNA aptamer based assay for the detection of histones with high sensitivity (<10 µg/mL) and specificity in serum samples from septic patients. ELISA is popularly used for the detection of histones in plasma samples from septic patients. However, there is a lack of consensus regarding the threshold of histone levels detected in plasma samples from septic patients. As with others, we were not able to detect histones in serum using ELISA. Histones are inherently cationic in nature[27] and studies have shown that they adhere to proteins circulating in the serum.[28,29] Therefore, we reasoned that serum proteins might be masking the epitopes recognized by anti-histone antibodies resulting in the attenuation of the signal. Histones could only be detected when the serum was diluted to a minimum of 25%. Thus, we concluded that ELISA cannot be used to accurately measure circulating histones in undiluted serum samples.

Detection of histones in serum proved to be difficult using ELISA primarily due to epitope masking. Therefore, we attempted to detect circulating histones using western blot wherein we would denature histones and later detect them by using anti-histone antibodies. Similarly, to ELISA, we failed to detect histones in undiluted serum using western blot. Additionally, western blot is a semi-quantitative method which requires additional sample preparation and longer run-times.

Chemically modified RNA aptamers (KU9 and KU7) selected in our laboratory bind to histone proteins (H3, H4, and CTH) with low nM affinity (5 nM and 4 nM, respectively). These aptamers are highly specific as they differentially bind to histones in comparison to abundantly present serum albumin. (under review). Previously, our colleagues demonstrated the efficacy of these aptamers as potential therapeutics for treatment of multiple organ dysfunction syndrome (MODS). (REF) These aptamers have been shown to function well *in vivo.* (REF) Thus, we further evaluated their ability to detect histones in serum. Binding of these aptamers to histones in the presence and absence of serum was tested using the double filter binding assay. We successfully detected histones in serum and, more importantly, histones were detected in undiluted serum. We noticed that KU9 was only able to detect CTH in serum, while we detected H3, H4, and CTH in serum using KU7. This suggests that KU7 and KU9 bind to non-overlapping epitopes on histone proteins. Our results indicate that KU7 binds to an epitope that is readily accessible even in the presence of serum proteins. CTH includes all histone proteins (H1, H2a, H2b, H3, and H4) which, due to histone fold motif, assemble into a multi-subunit complex. Based on our results, we speculate that KU9 binds to an epitope presented on the complex that is stabilized, but not masked by serum proteins. Together, these data confirm that KU7 and KU9 effectively detect histones in pure serum with high sensitivity and could potentially be utilized to detect histones in clinical samples.

Clinical severity of sepsis is determined based on APACHE II scores. APACHE II score assesses the overall health state in an inpatient setting, using factors that are most predictive of mortality.[22] We next tested the accuracy and robustness of the aptamer assay by testing serum samples from septic patients. Aptamers detected histones (10–40 µg/mL) in patient samples and histone concentrations correlated with sepsis severity (Sup Fig2). Moreover, when assessing histones levels based on bacterial infection type, we noticed a significant difference in

histone levels in patients infected with gram negative and gram-positive bacteria. These results suggest that levels of histones could be predictive of the type of infection.

Epidemiological studies demonstrate gender differences with respect to the development of septic complications and multiple organ failure in trauma patients.(REF) In this respect, male gender has been identified as an independent risk factor for the development of severe infection in surgical patients.[23] In another study, a significantly higher incidence of bacteremia has been reported in males compared to that in females.[24] No significant difference in histone levels was observed between male and female septic patients in our study. This lack of significance might be linked to the small sample size. Moreover, the patients tested were similar in terms of sepsis severity, which might explain the lack of significant difference. LDH is one of the regularly tested biomarkers of sepsis. Higher levels of LDH (≥ 2mM) are indicative of sepsis severity and patient mortality.[26] Upon analysis of the clinical data from septic patients we did not observe any statistical difference in the levels of LDH between healthy and septic patients and this could be due to small patient sample size. This preliminary study shows that the aptamers can efficiently detect histones in serum samples and can be translated to further detect histones in clinical samples as well. This study can be further expanded by testing larger patient population to test for the correlation between histones levels and sepsis severity. Since, we were limited w.r.t to information regarding the demographics of the patients we were unable to look at other factors that could be contributing to the increased level of sepsis. While, we used filter binding assay for detection of histones, the aptamers can be further developed for integration onto a biosensor platform which is quicker and can be easily used in a hospital setting. In summary, This study demonstrates an efficacious, high affinity aptamer-based assay that warrants further prospective evaluation in hospitalized patients as an early detector of sepsis.

METHODS

Enzyme-linked immunosorbent Assays (ELISA)

Filtration: High molecular weight proteins were removed from 10% or 25% human serum (Sigma-Aldrich, St. Louis, MO) with an Amicon Ultra centrifugal filter that had a cut-off at 30,000 molecular weight (Millipore, Burlington, MA). Filtrate was collected after the unit was centrifugated at 14,000g at 4^{o}C for 15 min.

Histone H3 ELISA: Calf thymus histones (CTH, Sigma-Aldrich, St. Louis, MO) was spiked into filtered or un-filtered 10% human serum (to test the effect of filtration) or into 0.5% bovine serum albumin (BSA, Sigma-Aldrich, St. Louis, MO, to test the effect of BSA) or PBS (control) at a final concentration of 10 µg/mL. A commercial H3 ELISA kit, PathScan Total Histone H3 Sandwich ELISA kit (Cell Signaling, Danvers, MA) was utilized to detect serum histone H3 following the manufacturer's protocol. Absorbance at 450 nm was immediately measured spectrophotometrically by using a plate reader.

Histone H4 ELISA: Human recombinant H4 histone (New England Biological, Ipswich, MA) was spike into filtered or un-filtered 25% human serum or 0.5% BSA or PBS at a final concentration of 10 µg/ml. A commercial H4 ELISA kit (Cloud-Clone Corp., Katy, TX) was utilized histone H4 detection following the manufacturer's protocol. Absorbance at 450 nm was immediately measured spectrophotometrically with a plate reader.

Immunoblotting

For standard curve generation, 10% serum samples were spiked with varying concentrations of (CTH and H3) (100, 50, 25, 12.5, 6.25, 3.125, 1.56, and 0.78 µg/mL). These samples were then treated and loaded onto 4-20% NuPAGE Bis Tris gel following the manufacturer's

instructions (Thermo Scientific, Waltham, MA). Proteins were transferred to nitrocellulose membranes as for 1 hr. at 100V at 4 ˚C

Immunoblots were probed for H3 histones as follows: All steps were carried out at room temperature with gentle shaking. After 60 min in blocking buffer (5% skim milk in PBS), membranes were incubated for 1h with H3 primary (1:2000, Cell Signaling, Danvers, MA) in blocking buffer. After thorough washing in PBS containing 1% Tween 20 (wash buffer), filters were incubated for 1h in a 1:4000 dilution of the second antibody, horseradish peroxidase (HRP)-conjugated donkey anti-rabbit IgG (Jackson Immunosearch, West Grove, PA) in wash buffer. Streptavidin-HRP conjugate (Amersham, PA) was included at 1h in 1:3000 dilution in each of the second antibody solutions to allow detection of the biotinylated protein standards. Blots were developed by the enzyme chemiluminescence (ECL) method according to the manufacturer's instructions (Amersham, PA).

Double-filter binding assay

The binding affinity (K_D) of the aptamers for their target was assessed by double-filter binding assay. The dephosphorylated RNA and synthetic aptamers (KU7 and KU9) were radiolabeled with gamma-^{32}P-ATP using T4 polynucleotide kinase (PNK) following the manufacturer's instructions. Labeling efficiency was determined by a scintillation counter. All radiolabeled RNAs were diluted in 1× bromophenol blue (BB) to 2,000 cpm/mL. Five microliters of 2,000 cpm/mL radiolabeled RNA were incubated at 37°C for 5 min with 15 µL of either human histone H3.2 (positive selection targets), Calf Thymus Histone alone or spiked within 100% serum (Sigma-Aldrich, St. Louis, MO) serially diluted in 1× BB. The binding reactions were loaded onto a dot blot apparatus (composed of nitrocellulose membrane on the top, nylon membrane (Sigma-Aldrich, St. Louis, MO) in the middle, and Whatman paper (Sigma-Aldrich, St. Louis, MO) on the bottom). The nitrocellulose membrane was pretreated with 0.5 M KOH (Sigma-Aldrich, St.

Louis, MO) for 20 min, quickly washed with diH_2O. The membrane was then equilibrated in 0.1 M Tris HCl 7.5 for 45 min, washed with diH_2O, and transferred to 1×BB for 20 min before it was loaded onto manifold (Sigma-Aldrich, St. Louis, MO). The nylon was incubated in 1× BB for 20 min before being loaded on the manifold. Before loading the RNA/protein samples, the wells were washed with 100 µL of 1× BB. The amount of RNA bound (nitrocellulose) versus unbound (nylon) was determined by densitometric analysis of the imaged membrane on a Fuji Phosphor imager.

Patient samples

This study was approved by the University of Iowa and Duke University Institutional Review Board (IRB # xxx and #xxx). Forty-one and ten samples from septic patients were obtained from Duke University and University of Iowa, respectively. Healthy donor samples were obtained from University of Iowa (IRB # 201505719). Clinical data including demographic information, survival, laboratory results, Acute Physiologic Assessment and Chronic Health Evaluation II Score (APACHE II), Sequential Organ Failure Assessment (SOFA) were collected from septic patients.

Statistical Analysis

Descriptive statistics were obtained for human specimens. Results are expressed as mean ± SEM unless otherwise indicated. Statistical comparisons were performed by a two-tailed t-test, or one-way or two-way analysis of variance (ANOVA) with appropriate post-hoc analysis. Statistical analyses were performed using GraphPrism (Graph Pad, San Diego, CA) or SPSS 25.0 (SPSS, Chicago, IL). A p value of < 0.05 was considered significant.

Data Availability

The datasets generated during and/or analyzed during the current study are available from the

corresponding author on request.

ACKNOWLEDGMENTS

The authors would like to acknowledge the use of the University of Iowa Pathology Core, a core resource supported by the Vice President for Research & Economic Development, the Holden Comprehensive Cancer Center, and the Carver College of Medicine.

AUTHOR CONTRIBUTIONS

Conceptualization: FJM and PHG; Methodology: FJM, PHG, JKT; Data Acquisition, Curation and Analysis: SS, KTU, GNB, LHL, SS, PCGC, CG, and PHG; Resources: FJM and PHG; Writing – original draft: SS and LHL, PHG; Writing – review and editing: FJM, PHG, SS, CG, PWM, LHL; Supervision: FJM and PHG.

FUNDING SOURCES

This work was supported by grants to PHG and FJM from Department of Defense Congressionally Directed Medical Research Programs (PR150627 and PR150627P1), University of Iowa Carver College of Medicine (CCOM) (Carver Collaborative Pilot Grant Award 2015) and University of Iowa Award from The Office of the Vice President for Research and Economic Development (OVPRED 2015). FJM is also supported by the Office of Research and Development, Department of Veterans Affairs (2I01BX001729).

CONFLICT OF INTEREST

The authors declare no conflicts of interest

REFERENCES

1

2 Maubon, D. *et al.* Therapeutic impact and diagnostic performance of multiplex PCR in patients with malignancies and suspected sepsis. *Journal of Infection* **61**, 335-342 (2010).

3 Martini, A. *et al.* Procalcitonin levels in surgical patients at risk of candidemia. *Journal of Infection* **60**, 425-430 (2010).

4 von Lilienfeld-Toal, M. *et al.* Utility of a commercially available multiplex real-time PCR assay to detect bacterial and fungal pathogens in febrile neutropenia. *Journal of clinical microbiology* **47**, 2405-2410 (2009).

5 Pierrakos, C. & Vincent, J.-L. Sepsis biomarkers: a review. *Critical care* **14**, R15 (2010).

6 Chan, T. & Gu, F. Early diagnosis of sepsis using serum biomarkers. *Expert review of molecular diagnostics* **11**, 487-496 (2011).

7 Xu, J. *et al.* Extracellular histones are major mediators of death in sepsis. *Nature medicine* **15**, 1318 (2009).

8 Ekaney, M. L. *et al.* Impact of plasma histones in human sepsis and their contribution to cellular injury and inflammation. *Critical care* **18**, 543 (2014).

9 Xu, Z., Huang, Y., Mao, P., Zhang, J. & Li, Y. Sepsis and ARDS: the dark side of histones. *Mediators of inflammation* **2015** (2015).

10 García-Giménez, J. *et al.* A new mass spectrometry-based method for the quantification of histones in plasma from septic shock patients. *Scientific Reports* **7**, 10643 (2017).

11 Nakahara, M. *et al.* Recombinant thrombomodulin protects mice against histone-induced lethal thromboembolism. *PloS one* **8**, e75961 (2013).

12 Romac, J., Bouley, J. & Van Regenmortel, M. Enzyme-linked immunosorbent assay in the study of histone antigens and nucleosome structure. *Analytical biochemistry* **113**, 366-371 (1981).

13 Costa, O. & Monier, J. in *Annales de l'Institut Pasteur/Immunologie.* 365-376 (Elsevier).

14 Tuerk, C. & Gold, L. Systematic evolution of ligands by exponential enrichment: RNA ligands to bacteriophage T4 DNA polymerase. *science* **249**, 505-510 (1990).

15 Ellington, A. D. & Szostak, J. W. In vitro selection of RNA molecules that bind specific ligands. *nature* **346**, 818 (1990).

16 Graziani, A. C. *et al.* High Efficiency Binding Aptamers for a Wide Range of Bacterial Sepsis Agents. *Journal of microbiology and biotechnology* **27**, 838-843 (2017).

17 Marton, S., Cleto, F., Krieger, M. A. & Cardoso, J. Isolation of an Aptamer that Binds Specifically to E. coli. *PLoS One* **11**, e0153637 (2016).

18 Zamarreno, C. *et al.* in *SENSORS, 2013 IEEE.* 1-4 (IEEE).

19 Abrams, S. T. *et al.* Circulating histones are mediators of trauma-associated lung injury. *American journal of respiratory and critical care medicine* **187**, 160-169 (2013).

20 Khargharia, S., Baumhover, N., Crowley, S., Duskey, J. & Rice, K. The uptake mechanism of PEGylated DNA polyplexes by the liver influences gene expression. *Gene therapy* **21**, 1021 (2014).

21 Sebat, F. *et al.* Effect of a rapid response system for patients in shock on time to treatment and mortality during 5 years. *Critical care medicine* **35**, 2568-2575 (2007).

22 Dyagilev, K. & Saria, S. in *AMIA Annual Symposium Proceedings.* 1890 (American Medical Informatics Association).

23 Offner, P. J., Moore, E. E. & Biffl, W. L. Male gender is a risk factor for major infections after surgery. *Archives of Surgery* **134**, 935-940 (1999).

24 McGowan Jr, J. E., Barnes, M. W. & Finland, M. Bacteremia at Boston City Hospital: occurrence and mortality during 12 selected years (1935-1972), with special reference to hospital-acquired cases. *Journal of Infectious Diseases* **132**, 316-335 (1975).

25 Duman, A. *et al.* Prognostic value of neglected biomarker in sepsis patients with the old and new criteria: predictive role of lactate dehydrogenase. *The American journal of emergency medicine* **34**, 2167-2171 (2016).

26 Blum, A., Zoubi, A. A., Kuria, S. & Blum, N. High serum lactate level may predict death within 24 hours. *Open medicine* **10** (2015).

27 Campos, E. I. & Reinberg, D. Histones: annotating chromatin. *Annual review of genetics* **43** (2009).

28 Chen, R., Kang, R., Fan, X. & Tang, D. Release and activity of histone in diseases. *Cell death & disease* **5**, e1370 (2014).

29 Watson, K., Gooderham, N. J., Davies, D. S. & Edwards, R. J. Nucleosomes bind to cell surface proteoglycans. *Journal of Biological Chemistry* **274**, 21707-21713 (1999).

FIGURE LEGENDS

Figure 1. Detection of histones H3 and H4 in human serum using ELISA

A) Measurement of 10 µg/mL of H3 & H4 histones (PBS, 25% Serum,10% Serum) pre- and post- filtration of serum proteins using ELISA. **B)** Detection of H3 & H4 Histone in the presence and absence of 5 mg/ml BSA using ELISA.

Figure 2. Detection of histones in human serum using Western blot

A) Western blot of serially diluted Calf thymus histones (CTH) (100, 50, 25, 12.5, 6.25, 3.125, 1.56, 0.78) µg/mL in 10% serum using H3 antibody. **B)** Western blot of serially diluted H3 histones (100, 50, 25, 12.5, 6.25, 3.125, 1.56, 0.78) µg/mL in 10% serum using H3 antibody. **C)** Immunoblot of serially diluted H3 histones (6.25, 3.125, 1.56, 0.78) µg/mL in 10% serum using H3 antibody.

Figure 3. Detection of histones in human serum using RNA aptamers

A) Detection of serially diluted H3 Histones in the presence and absence of 100% serum through KU7 and KU9 aptamers using double filter binding assays. **B)** Detection of serially diluted H4 Histones in the presence and absence of 100% serum through KU7 and KU9 aptamers using double filter binding assays. C) Detection of serially diluted Calf thymus histones (CTH) in the presence and absence of 100% serum through KU7 and KU9 aptamers using double filter binding assays.

Figure 4. **Detection of histones in serum samples from septic patients using RNA aptamers**

A) Serum samples obtained from Duke University. Left panel: Correlation between sepsis severity (APACHEII scores) and concentration of extracellular histones. Right panel: Comparison of histone levels in male patients in comparison to female patients. **(Table 1)**

B) Serum samples obtained from University of Iowa **(Table 2)**. Left panel: Detection of histones in high sepsis severity patient serum samples. Right panel: Evaluation of LDH in high sepsis severity patient serum samples.

Figure 1

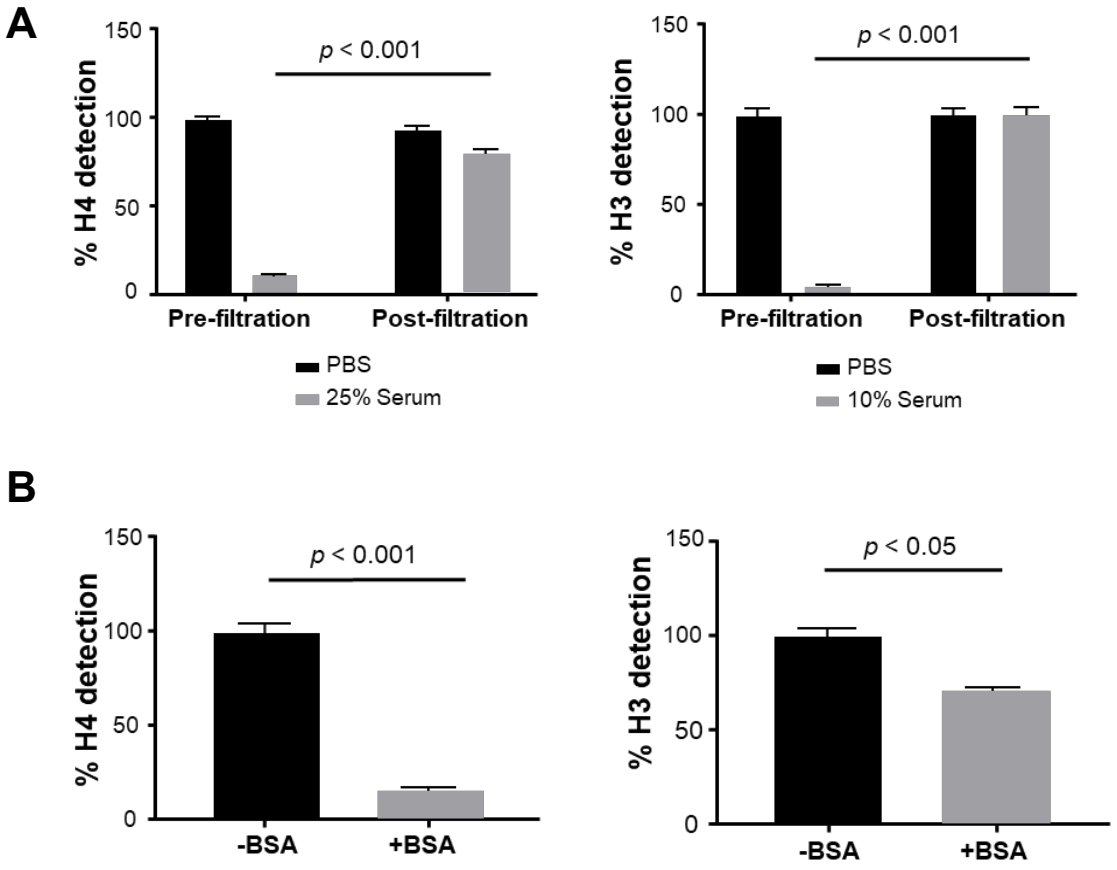
A
% H4 detection
150
100
50
0
p < 0.001
Pre-filtration
Post-filtration
PBS
25% Serum
% H3 detection
150
100
50
0
p < 0.001
Pre-filtration
Post-filtration
PBS
10% Serum
B
% H4 detection
150
100
50
0
p < 0.001
-BSA
+BSA
% H3 detection
150
100
50
0
p < 0.05
-BSA
+BSA

Figure 2

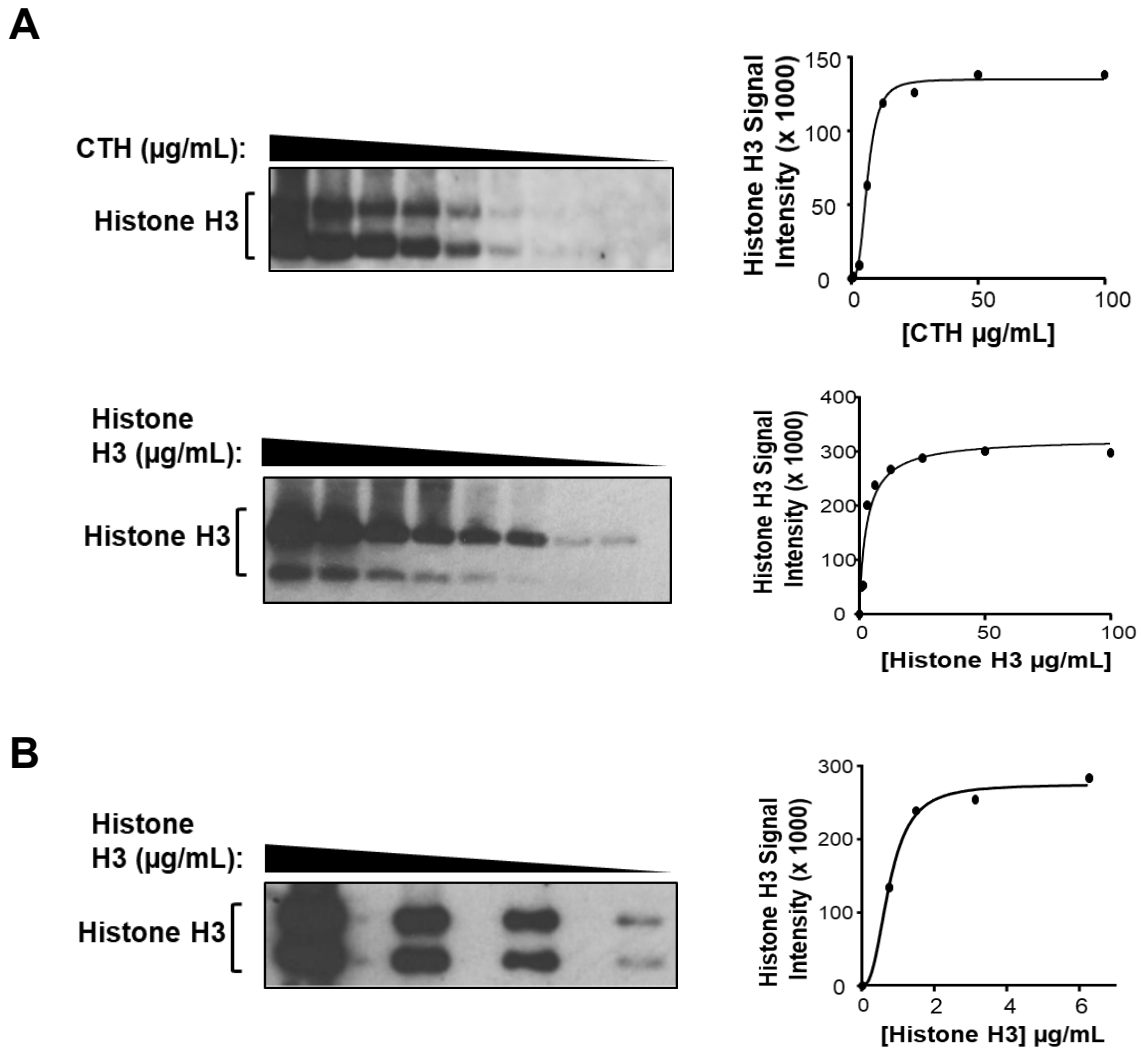
A
CTH (µg/mL):
Histone H3
Histone H3 Signal Intensity (x 1000)
150
100
50
0
0
50
100
[CTH µg/mL]
Histone H3 (µg/mL):
Histone H3
Histone H3 Signal Intensity (x 1000)
400
300
200
100
0
0
50
100
[Histone H3 µg/mL]
B
Histone H3 (µg/mL):
Histone H3
Histone H3 Signal Intensity (x 1000)
300
200
100
0
0
2
4
6
[Histone H3] µg/mL

Figure 3

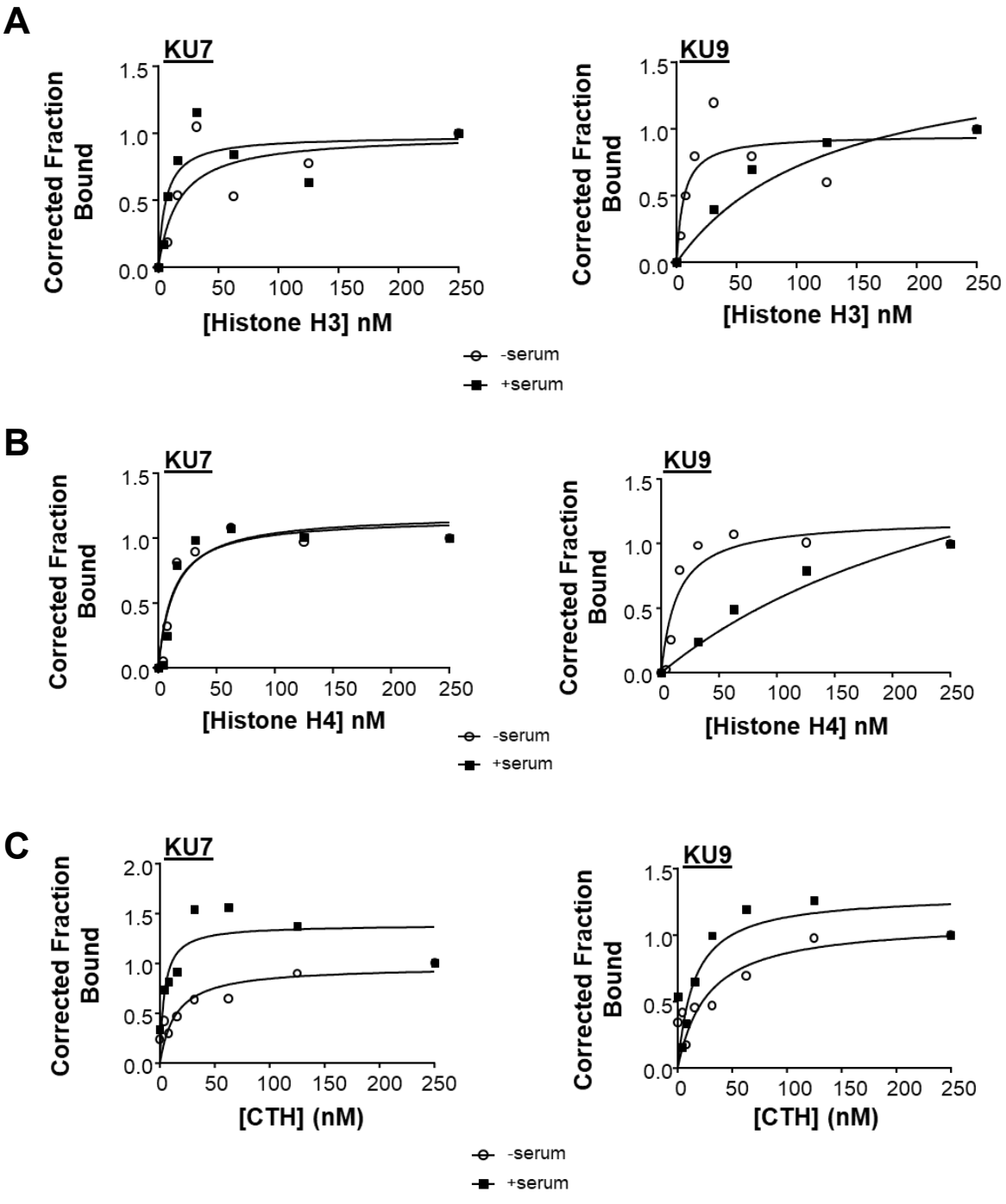
A
KU7
KU9
Corrected Fraction Bound
[Histone H3] nM
-serum
+serum
B
KU7
KU9
Corrected Fraction Bound
[Histone H4] nM
-serum
+serum
C
KU7
KU9
Corrected Fraction Bound
[CTH] (nM)
-serum
+serum

Figure 4

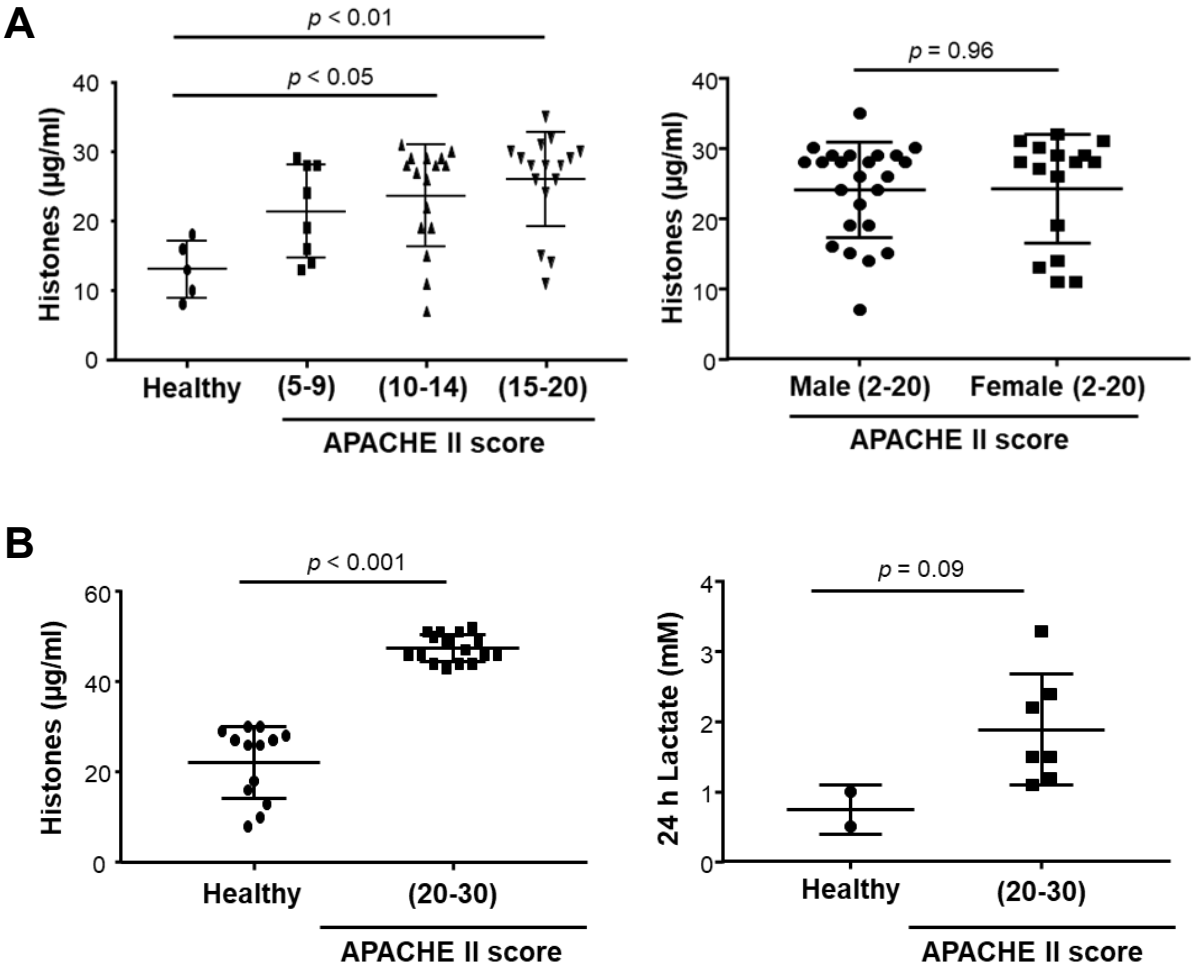
A
p < 0.01
p < 0.05
Histones (µg/ml)
40
30
20
10
0
Healthy
(5-9)
(10-14)
(15-20)
APACHE II score
p = 0.96
Histones (µg/ml)
Male (2-20)
Female (2-20)
APACHE II score
B
p < 0.001
Histones (µg/ml)
60
40
20
0
Healthy
(20-30)
APACHE II score
p = 0.09
24 h Lactate (mM)
4
3
2
1
0
Healthy
(20-30)
APACHE II score

RNA inhibitors of extracellular histones to prevent multiple organ dysfunction syndrome

Francis J Miller, MD[1,2], Kevin T Urak[3], Giselle N Blanco[3], Li-Hsien Lin[3], Beilei Lei, PhD[1], and Paloma H Giangrande, PhD[3]

[1]Duke University, Durham, NC
[2]Veterans Administration Medical Center, Durham, NC
[3]University of Iowa, Iowa City, IA

Background: Severe tissue injury, including major trauma, sepsis, burns, radiation, inhalation of toxic substances, or radiation, will often result in the development of multiple organ dysfunction syndrome (MODS) or acute respiratory distress syndrome (ARDS). MODS/ARDS is primarily managed with supportive care, as there is no treatment to prevent or reverse its development, and the associated morbidity and mortality is high. Following cellular injury, nuclear proteins, of which histones are the most abundant, are released by dying cells. In the extracellular space, histones act as cytotoxic damage-associated molecular pattern proteins by activating platelets to cause thrombi formation; toll-like receptors resulting in cytokine production; and with cellular membranes triggering calcium influx and cell death. These effects of circulating histones result in remote cellular injury and a positive feedback loop of additional histone release. We hypothesized that RNA aptamers could selectively bind extracellular histones and abrogate histone-mediated injury. RNA aptamers are chemically-stabilized nucleic acid bio-drugs that bind with high affinity and specificity to their targets. As a therapeutic, aptamers possess several key advantages over other biologics: (1) they are self-refolding, single-chain, and redox-insensitive. Unlike proteins, they do not aggregate, and they tolerate pH and temperatures that proteins do not, making them ideal for field administration. (2) They have high selectivity for their target, eliminating potential for off-target effects. (3) They are easy to synthesize and their production does not depend on bacteria, cell cultures or animals. (4) Cross-species reactive aptamers can be easily engineered, thus expediting testing of the same reagent in preclinical animal models and human clinical trials.
Methods: Systematic evolution of ligands by exponential enrichment technology was used to select for RNA aptamers that bind to the histones primarily responsible for MODS/ARDS (H3 and H4), but not to other serum proteins. The RNA aptamers were evaluated for efficacy against histone-mediated toxicity *in vitro* using cultured human cells. *In vivo* efficacy was examined in a mouse model of MODS consisting of intravenous injection of histones into the tail vein. The dose of histones used were similar to that measured in serum of patients with MODS due to trauma or sepsis.
Results: First, we developed nuclease-resistant, 2′ fluoro-modified RNA aptamers with high affinity (K_D = nanomolar) for histones H3 and H4. These anti-histone aptamers inhibited histone-induced platelet aggregation in a dose-dependent manner. In contrast, the aptamers did not inhibit platelet aggregation induced by collagen. The aptamers also inhibited histone-induced toll-like receptor activation in cultured endothelial cells, as measured by IL-6 production. Extracellular histones induce cytotoxicity through their interaction with the plasma membrane, leading to calcium influx, cell swelling, and cytolysis. Aptamers significantly inhibited the histone-induced increase of intracellular

calcium as measured by the calcium indicator fura 2-AM. We confirmed that administration of histones to human endothelial and epithelial cell lines caused dose-dependent cell death. RNA aptamers had a dose-dependent protective effect in neutralizing histone-induced cytotoxicity. Next, we tested the efficacy of the RNA aptamer in a mouse model of MODS/ARDS. Tail vein injection of histones resulted in dose-dependent organ dysfunction and death in mice. Histologic staining of lung and liver revealed tissue edema, inflammatory cell infiltration, microthrombi, and hemorrhage. The administration of RNA aptamers at the same time or 30 minutes after histones prevented death and reduced the histopathologic findings of tissue injury. *Conclusion:* These data confirm that RNA aptamers, selected to bind to extracellular histones, can attenuate histone-mediated injury in human platelets and endothelial cells *in vitro* and protect from morbidity in a mouse model of MODS. Given the many etiologies of severe tissue injury, these aptamers could have a significant impact on the treatment of numerous clinical conditions associated with MODS/ARDS.

RNA Inhibitors of Extracellular Histones to Prevent Multiple Organ Dysfunction Syndrome

Francis J Miller[1,2], Kevin T Urak[3], Giselle N Blanco[3], Li-Hsien Lin[3], Beilei Lei[1], Paloma H Giangrande[3]

[1]Duke University, Durham, NC, [2]Veterans Administration Medical Center, Durham, NC, [3]University of Iowa, Iowa City, IA

Introduction

- A challenging problem in critically ill patients is that following a severe injury or illness, even those organs not directly affected by the original problem become dysfunctional. This condition, known as multiple organ dysfunction syndrome (MODS), may be reversible, but there is no treatment to prevent it from happening.
- The most common organ involved in MODS is the lungs. Mortality rates associated with MODS and acute respiratory distress syndrome (ARDS) approach 50%.
- The cellular release of histone proteins into the extracellular space with tissue injury or neutrophil extracellular traps (NETosis) facilitate MODS/ARDS.
- Circulating histones act as cytotoxic damage-associated molecular pattern (DAMP) proteins, activating Toll-like receptors (TLRs), promoting pro-inflammatory cytokine pathways and altering membrane permeability.
- RNA aptamers are chemically-stabilized, single-stranded nucleic acid (<60 nt) bio-drugs that bind with high affinity and specificity to their targets.

Goal of Study

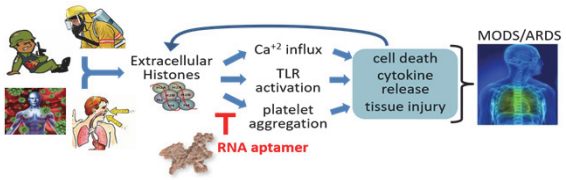

Figure 1. Histones are released into the extracellular space following tissue injury and contribute to the development of MODS and ARDS. Our goal is to identify RNA aptamers with high affinity and specificity for histones to bind and neutralize circulating histones thereby reducing the morbidity and mortality with MODS and ARDS.

Results

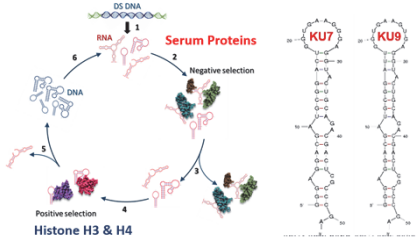

	KU7 (nM)	KU9 (nM)
H4	0.4	7.6
H3	2.5	11.2
H2B	8.4	ND
H2A	ND	ND
H1	5	5.3
Albumin	ND	ND

Figure 2. Identification of histone-specific RNA aptamers. In vitro Systematic Evolution of Ligands by Exponential Enrichment (SELEX) procedure: Step 1. Double-stranded DNA template library is transcribed in the presence of 2′ Fluoro pyrimidines and 2′ OH purines to generate the 2′ Fluoro-modified Round 0 RNA library. Step 2. The Round 0 RNA library was incubated with human albumin and IgG to remove RNAs that bind to human serum proteins. Step 3. RNA-bound to serum proteins was discarded. Step 4. RNA not bound to serum proteins was incubated with human histones H3 and H4 and reverse-transcribed into DNA (Step 5). Step 6. Round 1 DNA was then transcribed into RNA for the subsequent round of selection for eight rounds. Right panels show the theoretical secondary RNA structures for KU7 and KU9 histone aptamers and binding constants of KU7 and KU9 to recombinant histones. ND = not detected.

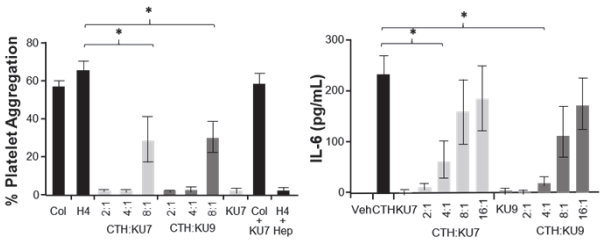

Figure 3. *In vitro* efficacy of RNA aptamers - platelet aggregation and TLR activation. Human platelet aggregation measurements in response to collagen (Col), histone H4 (H4), histone aptamers (KU7 and KU9), and heparin (Hep). *P <0.05 vs H4. Right panel: ELISA detection of IL-6 protein levels as a measurement of TLR activation in supernatants of EA.Hy926 cells treated with media alone (Veh), calf thymus histones (CTH), histone aptamers alone or in combination. * P <0.05 vs CTH. **p <0.01 *vs.* CTH.

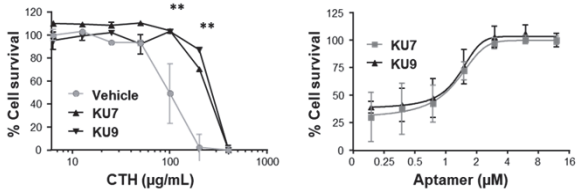

Figure 4. *In vitro* efficacy of RNA aptamers – endothelial cell viability. Aptamer inhibition of histone-mediated cytotoxicity of EA.hy926 cells treated with 1.2 μM of aptamers and varying amounts of CTH as measured by MTS assay. Right panel shows EA.hy926 cells treated with 180 μg/mL of CTH and increasing amounts of aptamers. N = 4. **P <0.01 *vs*. vehicle.

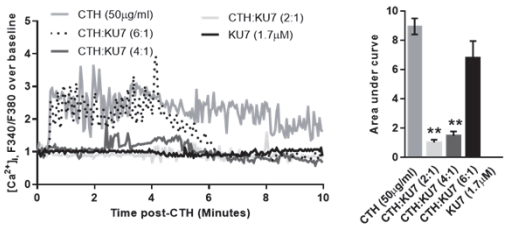

Figure 5. *In vitro* efficacy of RNA aptamers - calcium influx. Dynamic changes of intracellular calcium in fura 2-AM loaded endothelial cells measured by fluorescence microscopy. Right panel shows summary data from multiple EA.hy926 cells, n = 19 - 69 cells per bar. **p <0.01 vs. CTH.

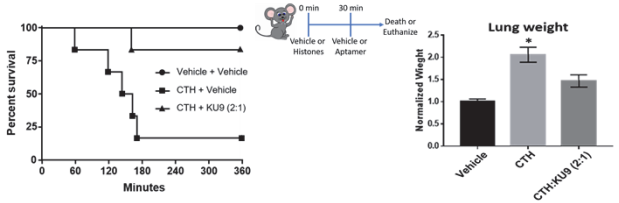

Figure 6. Efficacy of anti-histone aptamer in a murine model of MODS/ARDS. Survival curves of mice injected IV with vehicle or calf thymus histones (CTH, 62.5 mg/kg), followed 30 min by IV injection of vehicle or aptamer KU9 (31.25 mg/kg). Surviving mice euthanized at three house. Right panel shows lung weights of the treatment groups normalized to pre-treatment body weight. n = 6 per each group. *p <0.05 *vs.* CTH + vehicle.

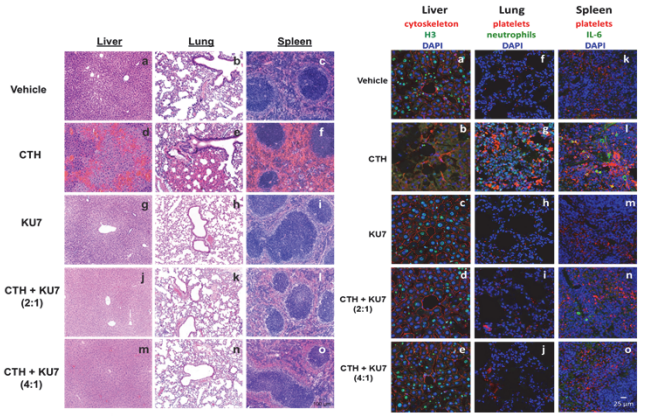

Figure 7. Histological efficacy of histone aptamer in murine model of MODS. Light microscopy of H&E stained sections of the liver, lung, and spleen collected three hours after the interventions noted. Vascular congestion, thrombi and hemorrhaging are observed in histone treated (CTH) mice and prevented by co-administration of aptamers. Right panel shows immunostaining of mouse liver. lung, and spleen stained with TO-PRO3 (nucleus, pseudo blue stain), cytoskeleton and platelets (pseudo red stain), histone H3, neutrophils and IL-6 (pseudo green stain)

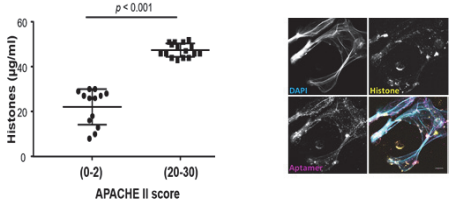

Figure 8. Aptamer KU7 binds human derived-histones. We developed an aptamer-based detection assay, and find that serum histone levels are associated with the severity of illness, in patients. Right panel shows confocal microscopy images of human neutrophil-derived NETs. Single images are shown in grey scale. Merged image showing labeling of DNA (cyan), histones (yellow) and KU7 (magenta). White areas in the merged image represent close-proximity of all three. Scale bar is 10 μm.

Conclusions and Summary

- We developed nuclease-resistant RNA aptamers that bind with high affinity and specificity to human histones H3 and H4.
- RNA aptamers inhibit histone-induced platelet aggregation, TLR activation, cell death and calcium influx in human cells in culture.
- Anti-histone aptamers reduce mortality and tissue injury in a murine model of MODS/ARDS.

Anti-histone aptamer bio-drugs could potentially impact the treatment of numerous MODS-inducing clinical conditions relevant to the military including, acute lung injury, transfusion related acute lung injury, sepsis, trauma, burns, ischemia/reperfusion and chemical-mediated tissue injury.

This work is supported by Peer Reviewed Medical Research Program/Investigator-Initiated Research Award W81XWH-16-1-0179.

Inhalation of an RNA Biodrug Targeting Extracellular Histones Protects from Acute Lung Injury

Francis J. Miller, MD[1,2], Beilei Lei, MD, PhD[2], Kamie Snow[2], Robert M. Tighe[2], MD, Paloma H. Giangrande, PhD.[3]
[1]Veterans Affairs Medical Center, Durham, NC
[2]Duke University, Durham, NC
[3]University of Iowa, Iowa City, IA

There are multiple diverse causes of acute lung injury (ALI), including inhalation of toxic substances, bacterial infection, aspiration of gastric contents, radiation, and epidemic viruses. Despite extensive research into its pathogenesis and clinical trials of new therapeutics, there remains no effective pharmacotherapy to interrupt the progression of ALI. Patients with severe ALI often develop acute respiratory distress syndrome (ARDS) which is accompanied by a high incidence of morbidity and mortality. The early exudative phase of ALI is characterized by increased alveolar-capillary permeability with clinical manifestation of this barrier disruption manifested by pulmonary edema, impairment of lung compliance and hypoxemia. Damage to lung tissue causes release of damage-associated molecular patterns (DAMPs), which act as endogenous danger signals to promote and exacerbate the inflammatory response. One of these DAMPs are the histone proteins. Extracellular histones are implicated in the propagation of ALI and serum levels of histones in critically ill patients predicts mortality. Histones normally reside in the nucleus where they partner with DNA, but when released from damaged cells, histones cause additional tissue injury via activation of Toll-like receptors, calcium influx, platelet aggregation, and cell death. The goal of this study was to develop a therapeutic to inactivate circulating histones for administration in field situations to prevent the morbidity and mortality associated with ALI/ARDS. Because histones (cationic proteins) normally associate with DNA in the nucleosome, we hypothesized that oligonucleotides such as RNA aptamers (anionic molecules) will have extraordinarily high affinity and specificity for histones, making them the preferred reagent for binding and neutralizing circulating histones. Aptamers are single-stranded nucleic acids whose binding properties are comparable to antibody/antigen interactions. Using Systemic Evolution of Ligands by Exponential Enrichment (SELEX) technology, we identified chemically stabilized RNA aptamers that bind with high affinity and specificity to the histone subunits mostly commonly implicated in tissue damage (H3 and H4) but do not bind to other serum proteins. Exposure of cultured human endothelial or epithelial cells to calf thymus-derived histones (CTH, 50 µg/ml) caused (1) calcium influx, as measured by the calcium indicator fura 2-AM; (2) toll-like receptor activation, as measured by IL-6 production, and (3) cell death, as measured by MTT assay. Administration of a histone-targeted RNA aptamer (KU7) after CTH exposure significantly protected cultured cells from all of these toxic effects. We next induced histone-mediated ALI in mice by the oropharyngeal aspiration of CTH (300 µg in 50 µL saline). Within hours, aspiration of CTH increased the number of neutrophils and levels of albumin and cytokines in the broncheoalveolar lavage fluid (BALF). Histologic analysis of the lungs showed evidence of alveolar edema, inflammatory infiltrate, and alveolar disruption. We next evaluated the retention and distribution of RNA aptamers in the lung following delivery by oropharyngeal aspiration. A single administration of fluorescent-labeled KU7 aptamer was distributed throughout all of the lung segments and remained present in BALF and in the alveoli for 24 hours. Importantly, the RNA aptamer alone did not cause inflammatory cell infiltration or alveolar injury. Treatment of mice with KU7 (4:1 Molar ratio CTH:KU7) 30 minutes prior to, or 30 minutes after CTH, attenuated barrier disruption, as evident by a reduction in BALF albumin. In summary, we have developed an RNA aptamer with high specificity and affinity to extracellular histones capable of protecting from histone-mediated lung injury. As a potential therapeutic for ALI, aptamers do not have the same limitations of other biologics and have the potential for rapid and easy delivery in field situations.

- Patients with severe ALI often develop acute respiratory distress syndrome (ARDS) which is accompanied by a high incidence of morbidity and mortality.
- The cellular release of histone proteins into the extracellular space with tissue injury or neutrophil extracellular traps (NETosis) facilitate ARDS.
- Circulating histones act as cytotoxic damage-associated molecular pattern (DAMP) proteins, activating Toll-like receptors (TLRs), promoting pro-inflammatory cytokine pathways and altering membrane permeability.

Acute Respiratory Distress Syndrome (ARDS)

- Activation of resident alveolar macrophages.
- Neutrophil infiltration
- Release of proinflammatory cytokines
- Epithelial cell injury
- Endothelial cell injury
- Loss of barrier function
- Interstitial and intraalveolar flooding

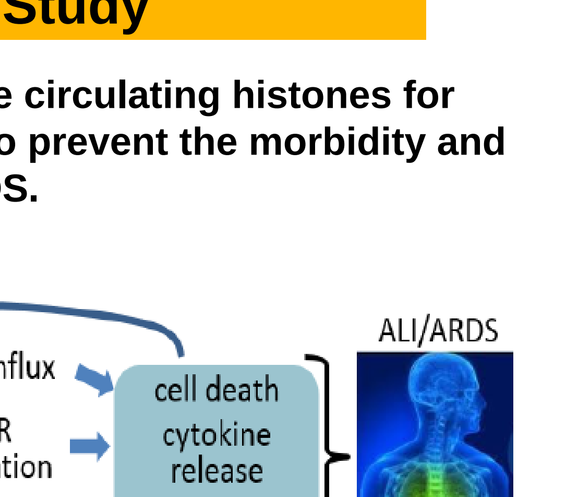

Thompson, NEJM, 2017

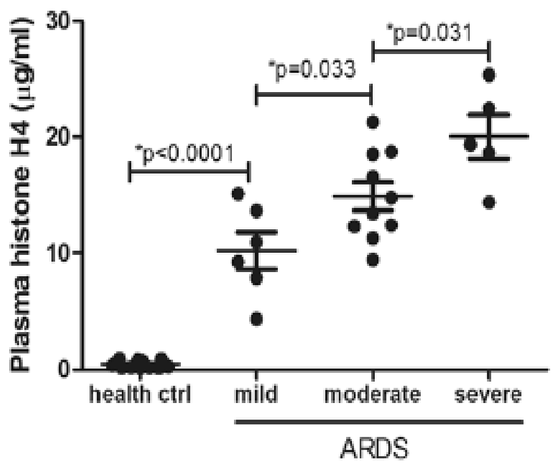

- Plasma levels of histones are associated with severity and mortality of ARDS
- Normally associated with DNA
- Released into the extracellular space in response to tissue injury/stress

Zhang, Anesthesiology 2015

Goal of Study

Develop a therapeutic to inactivate circulating histones for administration in field situations to prevent the morbidity and mortality associated with ALI/ARDS.

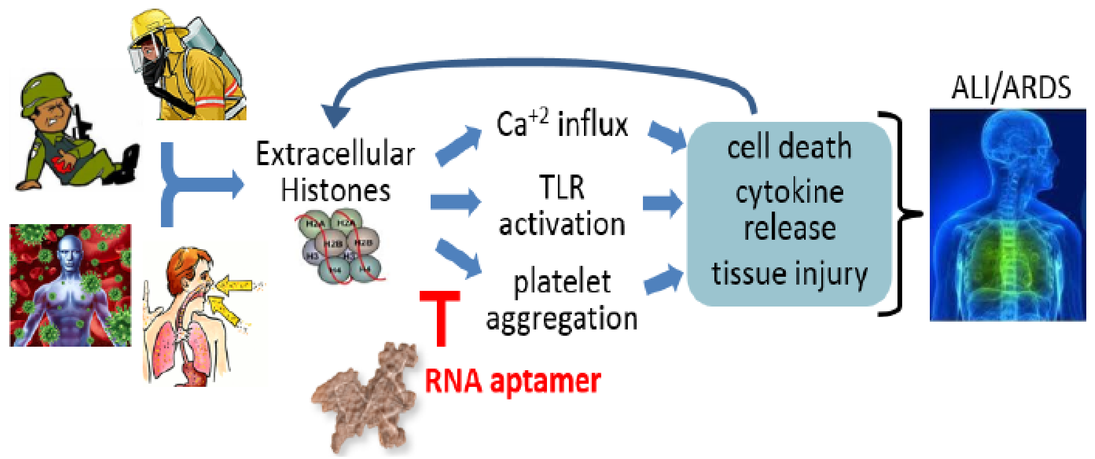

RNA aptamers are chemically-stabilized, single-stranded nucleic acid (<60 nt) bio-drugs that bind with high affinity and specificity to their targets

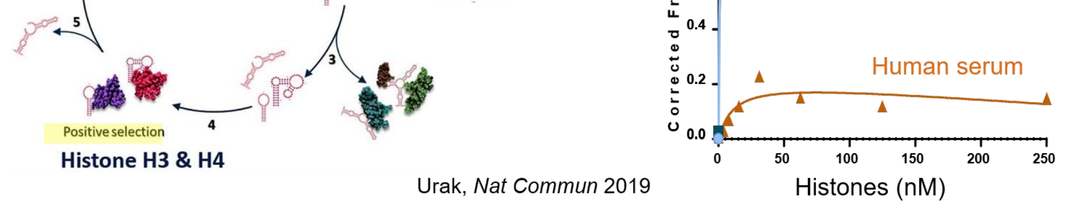

Urak, *Nat Commun* 2019

Figure 1. Identification of histone-specific RNA aptamers. In vitro Systematic Evolution of Ligands by Exponential Enrichment (SELEX) procedure. Right panels show the theoretical secondary RNA structure for KU7 histone aptamer and binding constants of KU7 to recombinant histones and serum protein. ND = not detected, H3 = histone 3, H4 = histone 4.

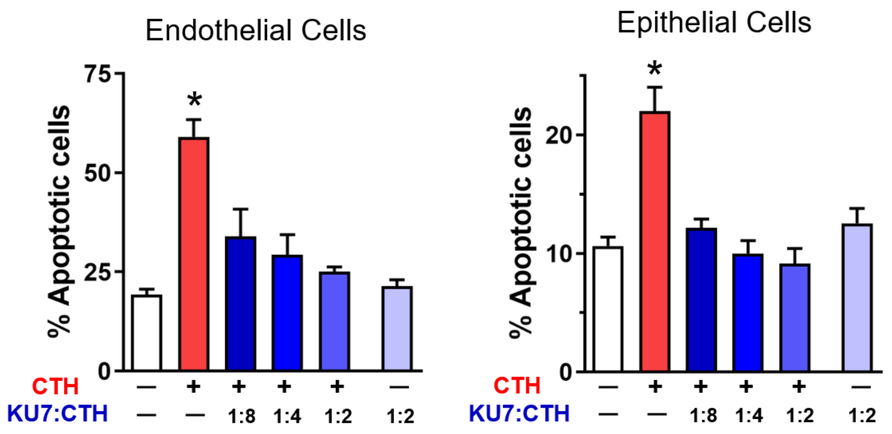

Figure 2. KU7 prevents histone-mediated apoptosis. Calf thymus histones (CTH, 75 µg/ml) caused apoptosis of human endothelial (4 hours) and epithelial cells (24 hours) as measured by Annexin V. The addition of aptamer KU7 30 minutes after CTH prevented histone-mediated toxicity. Ratio refers to molar ratio of KU7 to CTH. N = 4-8. *p<0.05 *vs*. control.

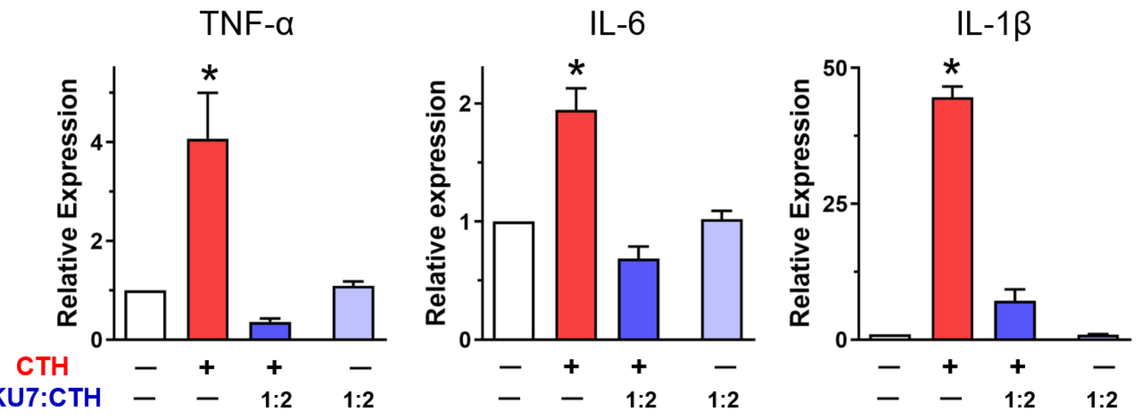

Figure 3. KU7 prevents histone-mediated TLR activation. Calf thymus histones (CTH, 50 µg/ml) increased mRNA expression of cytokines after 4 hours in human pulmonary microvascular endothelial cells as measured by PCR. The addition of aptamer KU7 30 minutes after CTH prevented histone-mediated cytokine activation. Ratio refers to molar ratio of KU7 to CTH. N = 3-4. *p<0.05 *vs*. control.

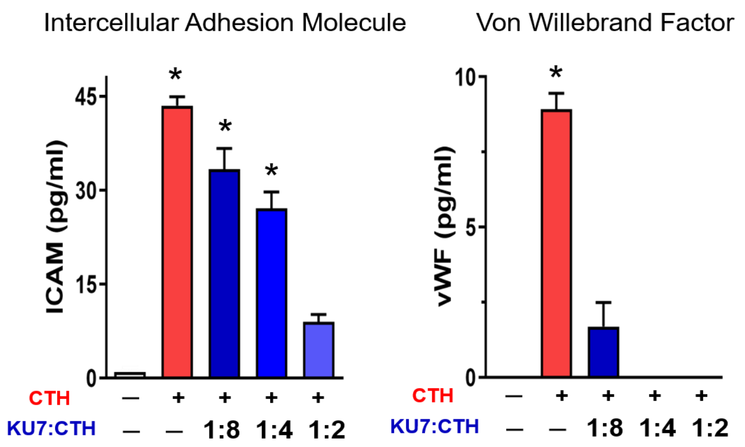

Figure 4. KU7 protects from histone-mediated endothelial cell dysfunction. Markers of endothelial cell dysfunction were measured by ELISA of supernatant of human endothelial cells 6 hours after calf thymus histones (CTH, 50 µg/ml). Aptamer KU7 was added 60 minutes after CTH. Ratio refers to molar ratio of KU7 to CTH. N = 4. *p<0.05 *vs*. control.

Figure 5. KU7 prevents histone-mediated human platelet acti
Human platelets were exposed to calf thymus histones (CTH, 50 µg/ml minutes and P-selectin expression measured by flow cytometry. Aptam was added at the same time as the CTH. Ratio refers to molar ratio of CTH. N = 3-5. *p<0.05 *vs*. control.

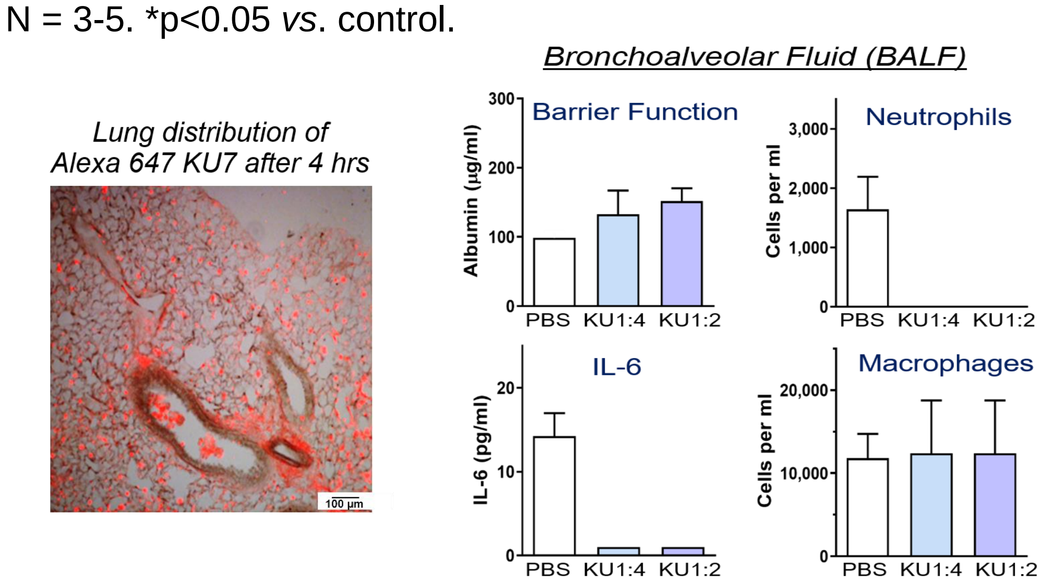

Figure 6. Inhalation of KU7 does not cause alveolar damage in
Intratracheal aspiration of fluorescent-tagged aptamer KU7 by mic distributed in the alveoli (left panel). KU7 did not increase broncho fluid (BALF) levels of albumin, cytokines or inflammatory cells.

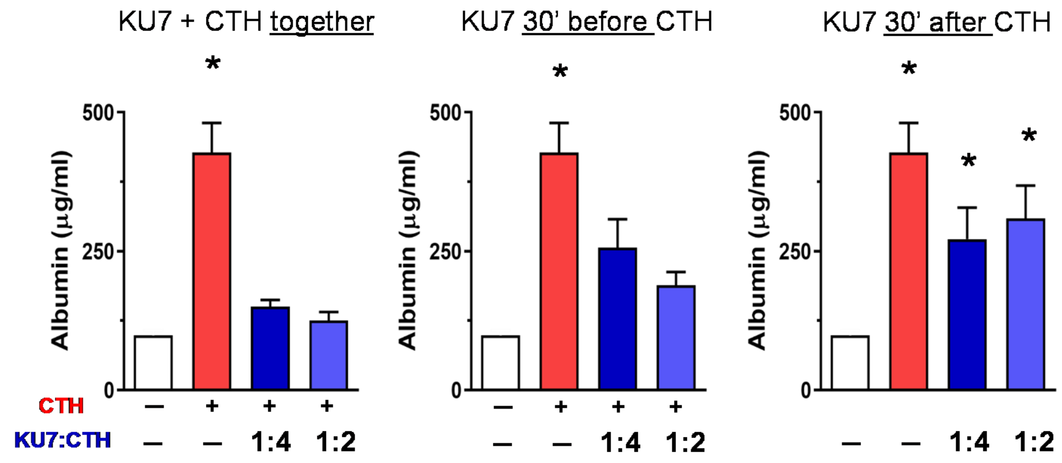

Figure 7. Inhalation of KU7 prevents histone-mediated barrier disr in mice. Albumin was measured in bronchoalveolar fluid (BALF) 8 after intratracheal aspiration of calf thymus histones (CTH, 300 µg/50 µ KU7 was delivered by similar method at the indicated times. Ratio re molar ratio of KU7 to CTH. N = 3-11. *p<0.05 *vs*. control.

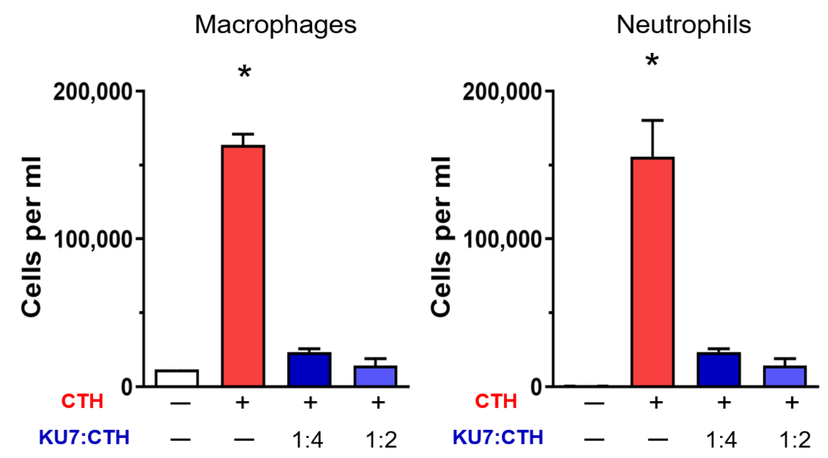

Figure 8. Inhalation of KU7 prevents histone-mediated inflammato infiltration in mice. Cell counts were measured in bronchoalveol (BALF) 8 hours after intratracheal aspiration of calf thymus histones 300 µg/50 µl PBS). KU7 was delivered with the CTH. Ratio refers to ratio of KU7 to CTH. N = 3-7. *p<0.05 *vs*. control.

Inhalation of an RNA Aptamer Targeting Extracellular Histones Protects from Acute Lung Injury

Beilei Lei, M.D., Ph.D.

Duke University

Financial Disclosure: No relationships to disclose

Acute Respiratory Distress Syndrome (ARDS)

- Acute onset of respiratory failure, pulmonary edema, hypoxemia
- Occurs in 10% of all patients admitted to the ICU
- 85% of cases due to sepsis, pneumonia, or aspiration of gastric contents
- Mortality of ~50% in patients with severe ARDS

No therapy beyond supportive care

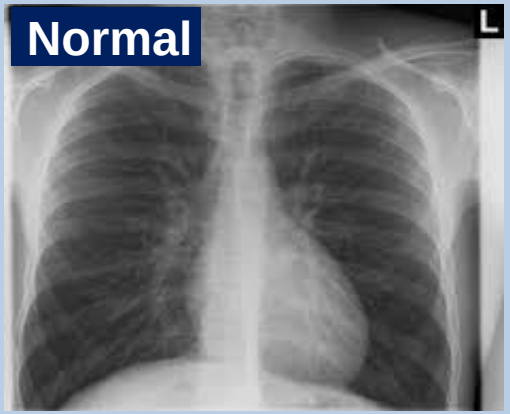

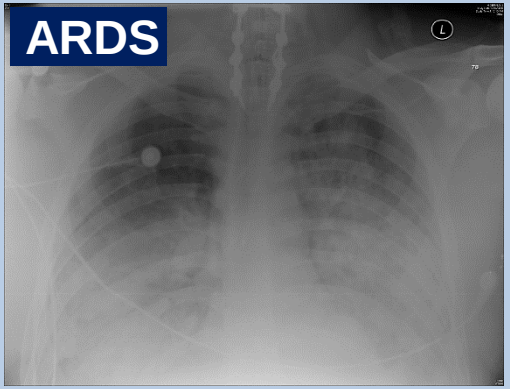

Thompson, NEJM, 2017

Acute Respiratory Distress Syndrome (ARDS)

- Activation of resident alveolar macrophages.
- Neutrophil infiltration
- Release of proinflammatory cytokines
- Epithelial cell injury
- Endothelial cell injury
- Loss of barrier function
- Interstitial and intraalveolar flooding

Alveoli

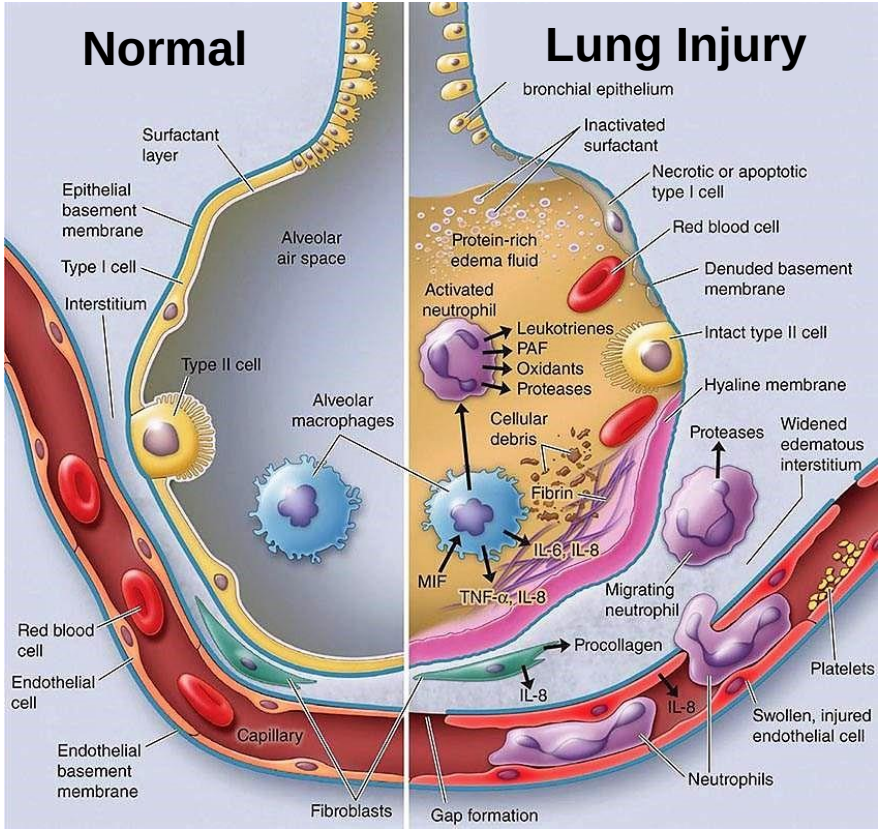

Thompson, NEJM, 2017

Extracellular Histones are Implicated in ARDS

Source of histones

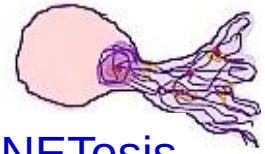

NETosis

Cell necrosis

Macrophage exosomes

- Normally associated with nuclear DNA
- Can be released into the extracellular space in response to tissue injury/stress
- Act as damage-associated molecular patterns (DAMPs)
- Increase intracellular Ca++, cytotoxic, activate TLRs

Plasma levels of histones are associated with severity and mortality of ARDS in patients

Zhang, Anesthesiology 2015

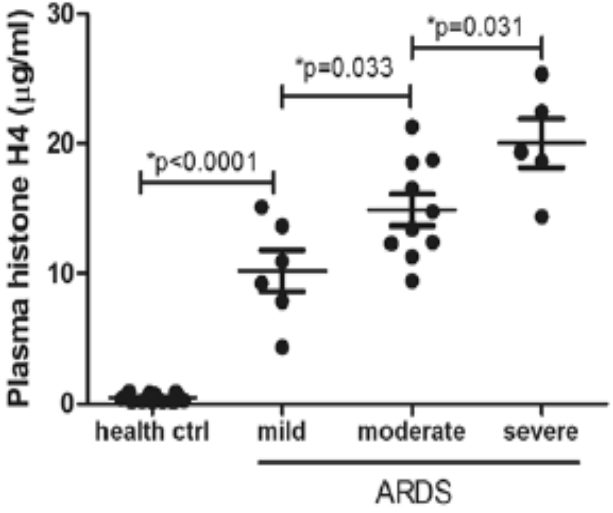

Hypothesis

Inhalation of RNA aptamers that bind histones will prevent lung injury.

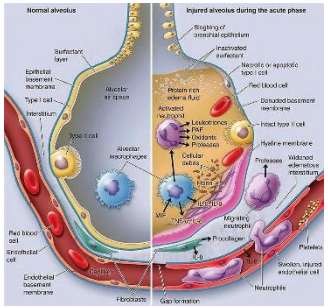

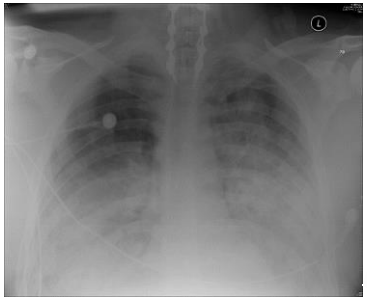

Identification of Histone-specific RNA Aptamers

Systematic Evolution of Ligands by Exponential Enrichment (SELEX)

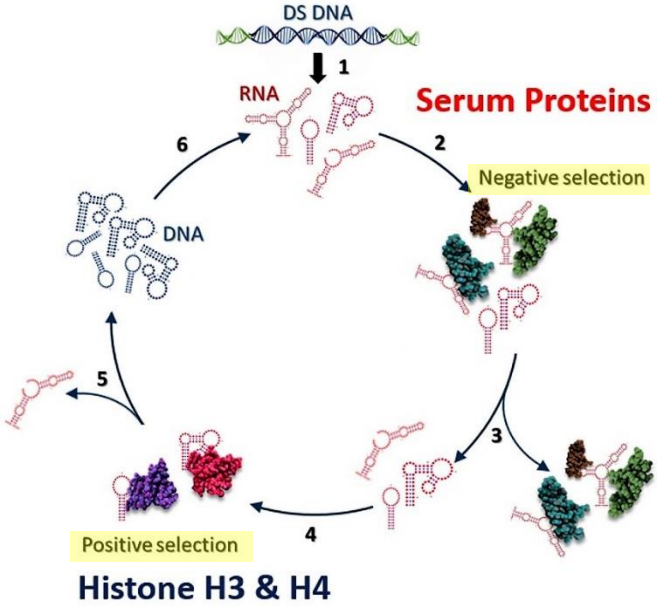

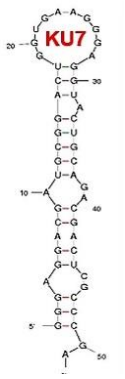

Binding constants

	KU7 (nM)
H4	0.4
H3	2.5
H2B	8.4
H2A	ND
H1	5
Albumin	ND

Filter binding assay

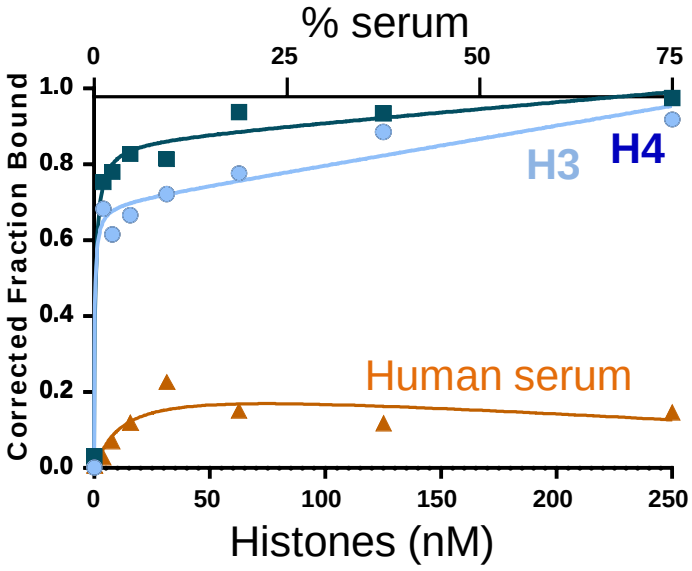

Urak, *Nat Commun* 2019

Aptamer KU7 Prevents Histone-mediated Apoptosis

In Vitro

Annexin V Staining

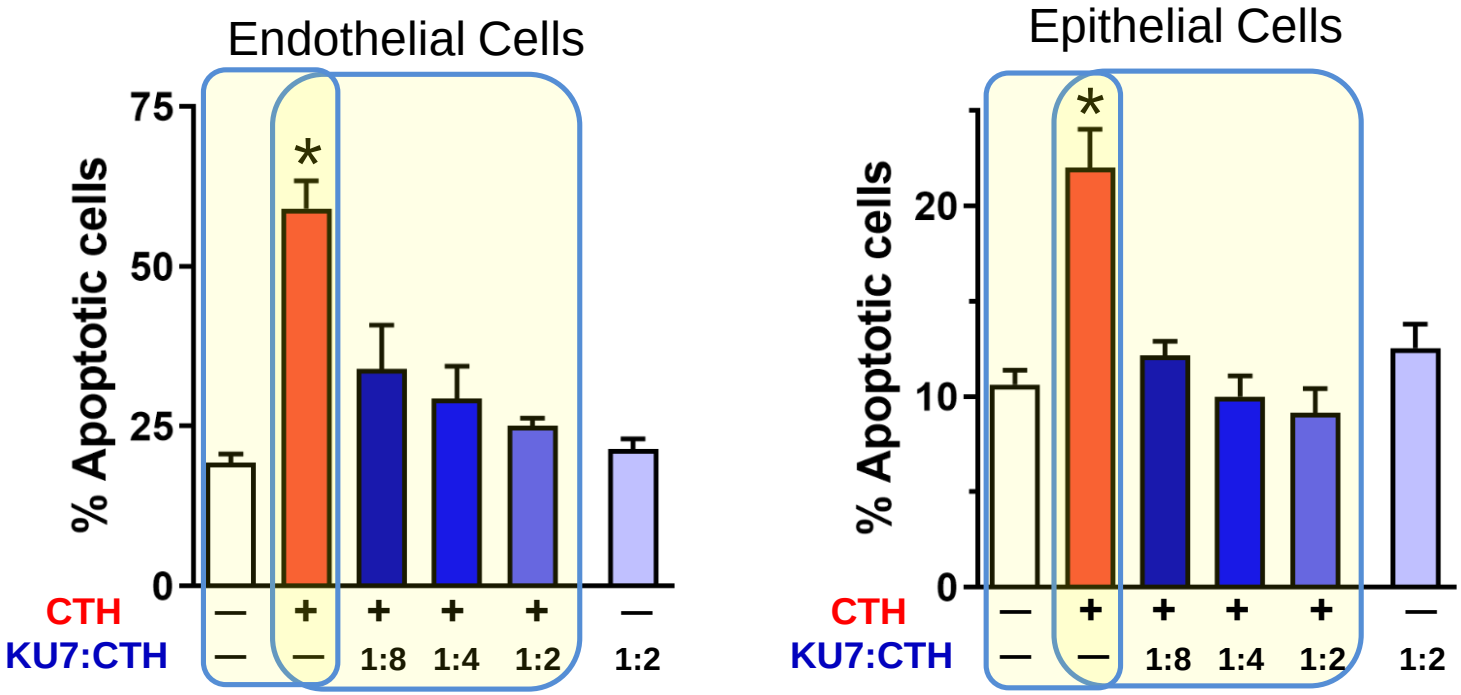

KU7 added 30 minutes after CTH (calf thymus histones)

∗ *p<0.05 vs control*

KU7 Prevents Impaired Cell Metabolic Activity

In Vitro

MTT Assay

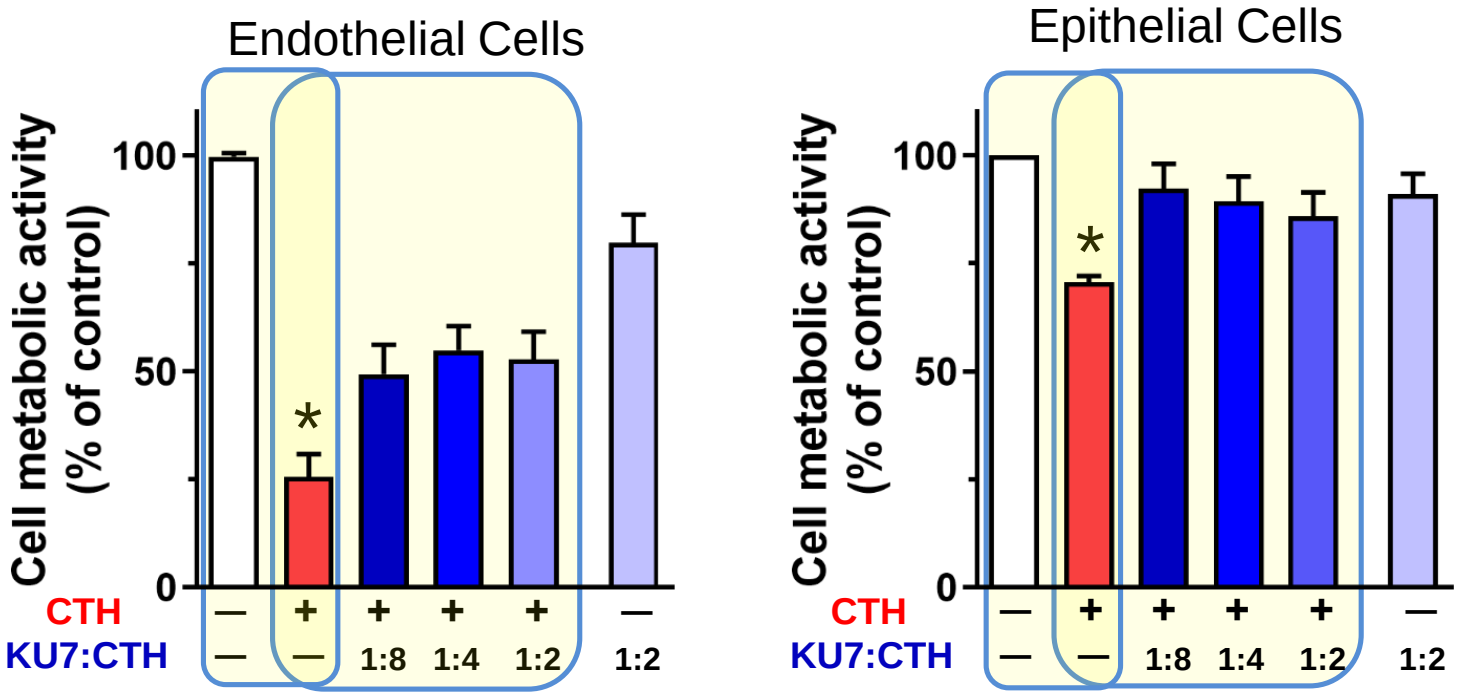

KU7 added 30 minutes after CTH (calf thymus histones)

∗ *p<0.05 vs control*

KU7 Inhibits Histone-mediated TLR Activation

In Vitro

mRNA Levels in PMVEC

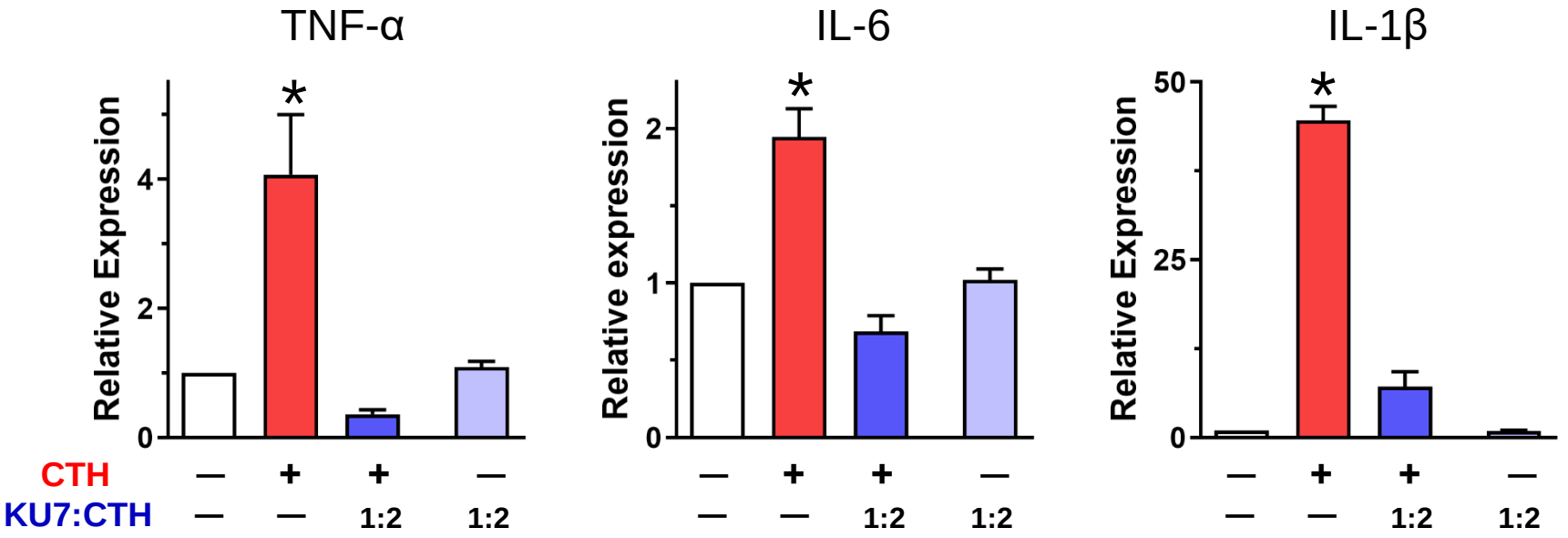

KU7 added 30 minutes after CTH (calf thymus histones)

Human pulmonary microvascular endothelial cells

∗ *p<0.05 vs control*

KU7 Protects from Histone-mediated EC Dysfunction

In Vitro

ELISA of Supernatant

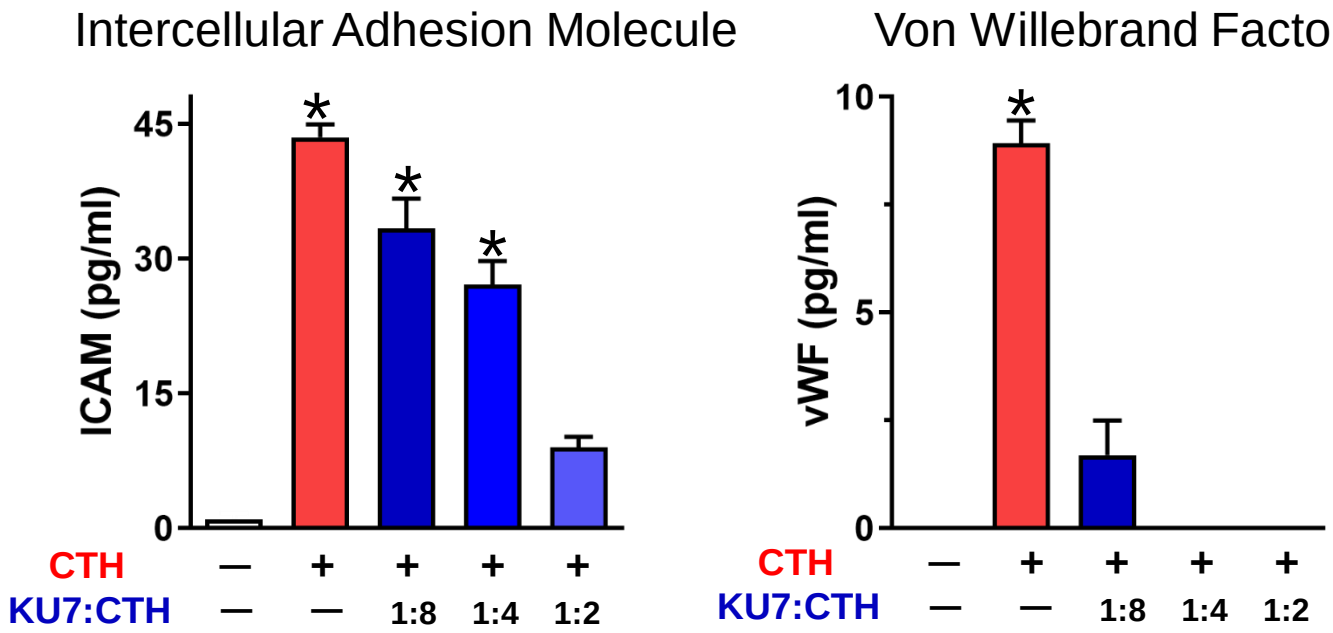

KU7 added 60 minutes after CTH (calf thymus histones)
Human endothelial cell line

∗ *p<0.05 vs control*

KU7 Does Not Induce Alveolar Damage in Mice

Intratracheal Aspiration of KU7

Lung distribution of Alexa 647 KU7 after 4 hrs

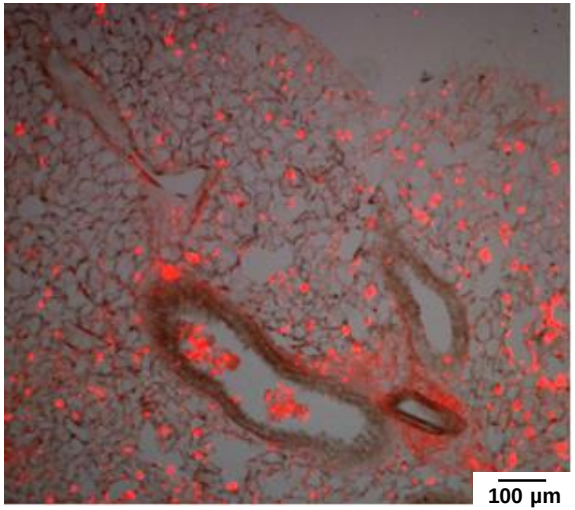

Bronchoalveolar Fluid (BALF)

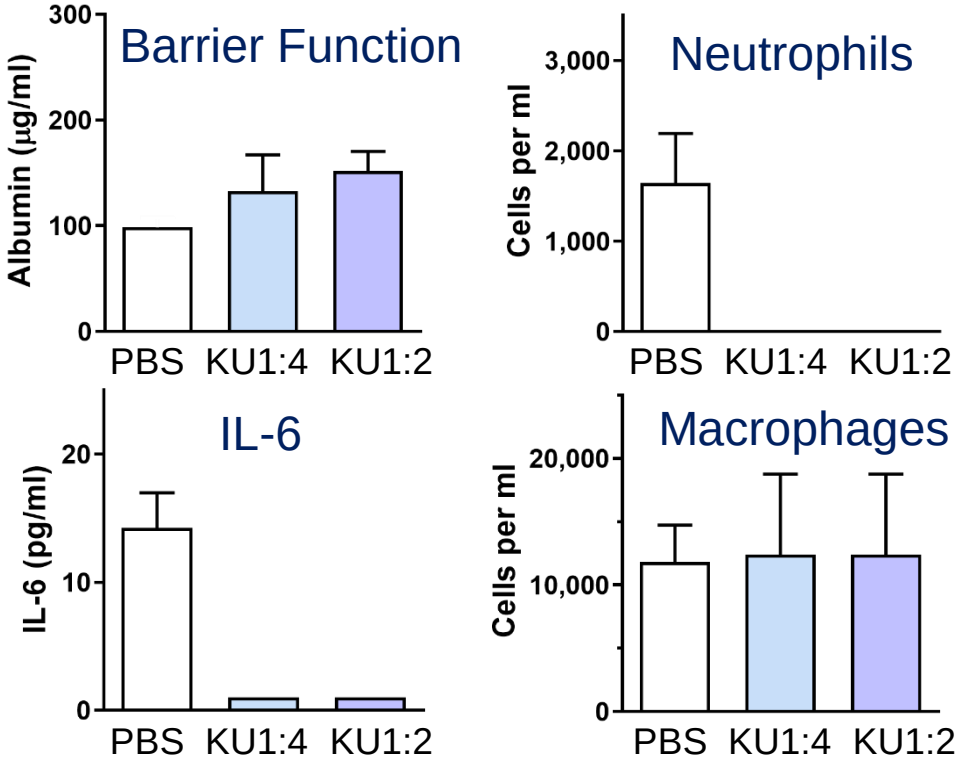

KU7 Prevents Histone-mediated Barrier Disruption

Albumin in Bronchoalveolar Lavage Fluid – 8 hours after CTH

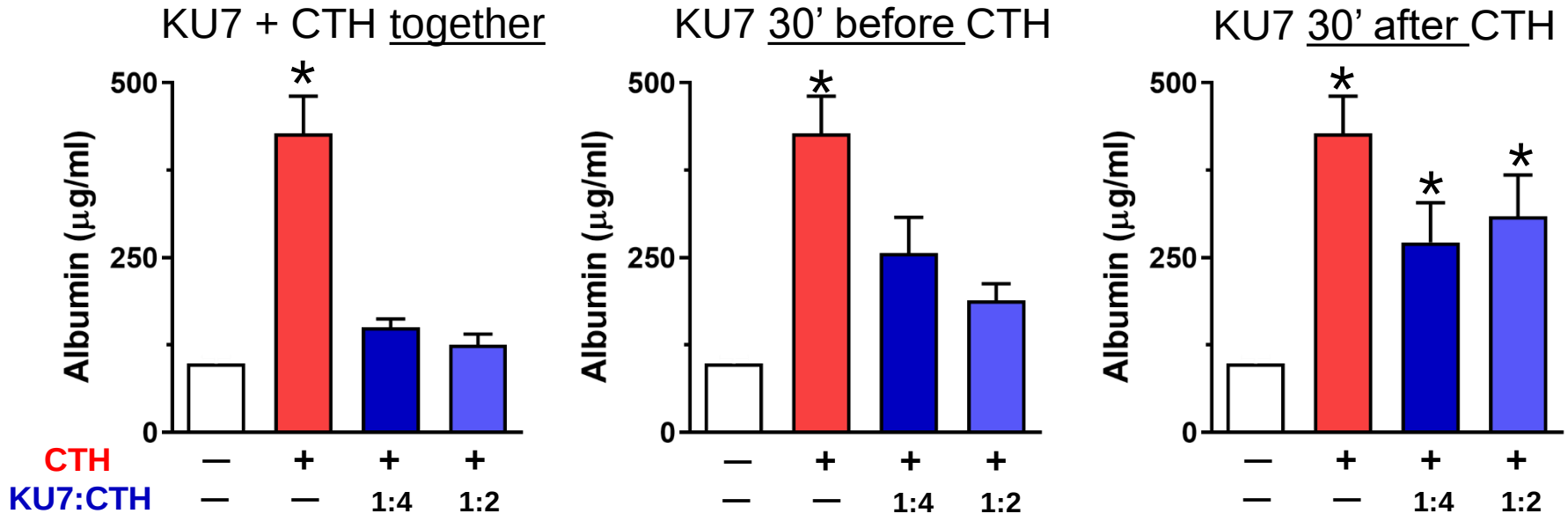

CTH = calf thymus histones

*$p<0.05$ vs control

KU7 Prevents Histone-mediated WBC Infiltration

WBC in Bronchoalveolar Lavage Fluid

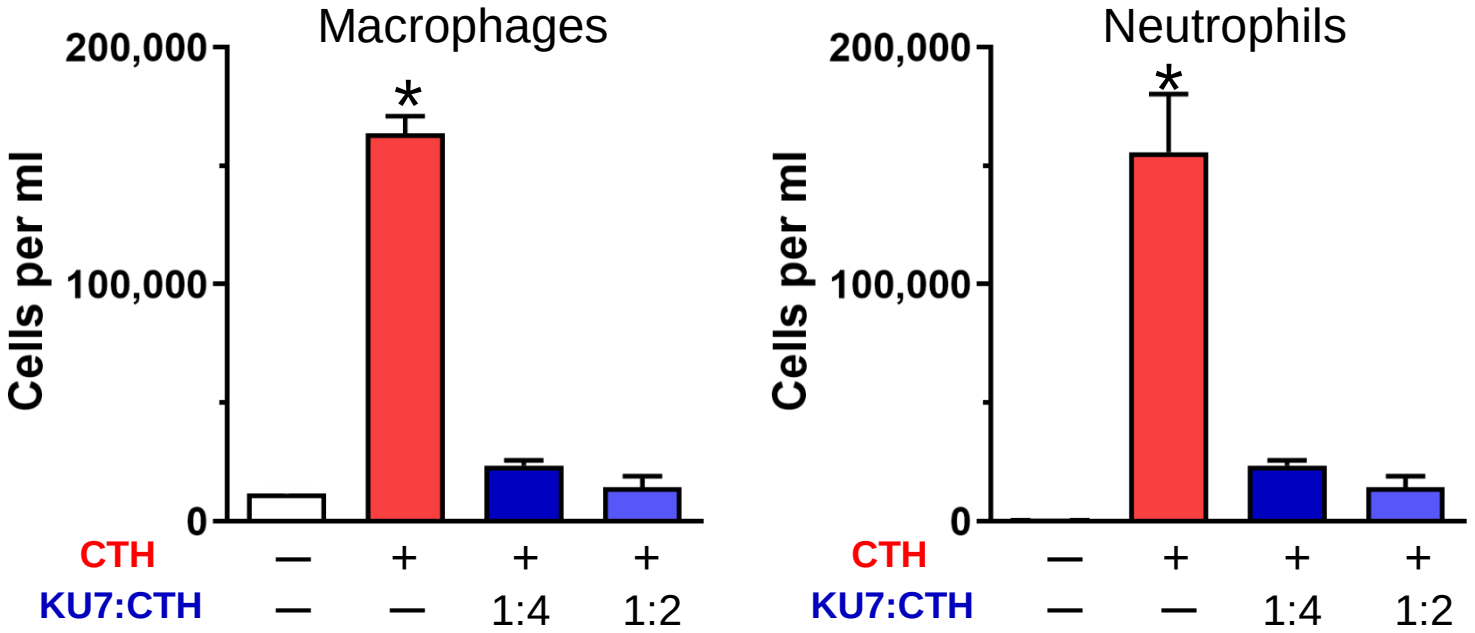

KU7 + CTH Together

CTH = calf thymus histones

*$p<0.05$ vs control

KU7 Protects from Histone-mediated Alveolar Damage

H&E Staining of Mouse Lung

Saline

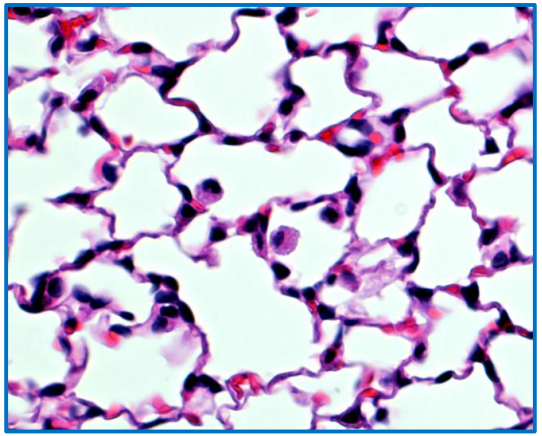

CTH

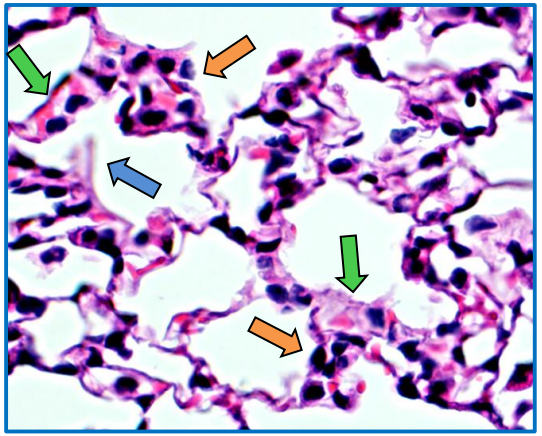

KU7+CTH

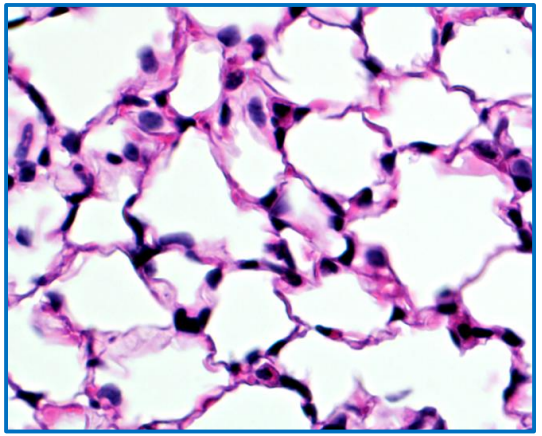

Neutrophil infiltrate
Alveolar destruction
Interstitial edema

Summary

- The RNA aptamer, KU7, protects endothelial cells and epithelial cells from histone-mediated toxicity *in vitro*.
- Aspiration of histones by mice causes disruption of the alveolar-capillary barrier, WBC infiltration and proinflammatory cytokine release.
- Inhalation of KU7 protects from histone-mediated lung injury in mice.

Inhalation of RNA aptamer KU7 may reduce the progression of acute lung injury to ARDS in patients.

Acknowledgements

Duke University

Francis Miller
Beilei Lei
Kamie Snow
Chaojian Wang
Jacob Fang

Duke Rodent Inhalation Core

Robert Tighe
Jaime Daly
Barbara Theriot

University of Iowa

Paloma Giangrande
Kevin Urak

Funding

DoD PR150627 (FM)
and PR150627P1 (PG)

Study Design

Experimental Aims: complete no observed adverse event level (NOAEL) study, evaluation of hematologic parameters and gross organ pathology in response to high dose KU7.

Experimental Subjects: Subjects were 20 mice, 6-8 weeks old at study start, 10 males, 10 females, BALB/c, Charles River Laboratories.

Housing and Husbandry: Subjects were housed in room 1033 in Vivarium on the Duke campus. Their room was climate/temp controlled and on a 12-hour light dark cycle. Food and bedding were changed weekly by DLAR staff.

Experimental Groups: To achieve the primary study aim, the study was divided into two parts:

- Safety study #1 Part 1: in which 10 mice were treated 500ug/mouse KU7 on Day 1 and consisted of the following groups:
    - Group 3: 5 males
    - Group 4: 5 females
- Safety Study #1 Part 2: in which 10 mice were treated with 200ug/mouse KU7 on Day 1 and consisted of the following groups:
    - Group 1: 5 males
    - Group 2: 5 females
- A control group consisted of 5 females which did not receive any treatment was used for clinical observation comparison and to decide the normal range for the blood analysis results (n=3 for blood analysis).

Endpoints: The endpoint for this study was sacrifice on day 7 after monitoring the mice for the last clinical observation and recording the last weight measurements. Mice were anesthetized using isoflurane 1-4%, then blood was collected through thoracotomy and cardiac puncture using a 25G needle. 100 ul of the collected blood was collected into a tube containing EDTA. The rest of the blood was stored in a serum separator tube. The blood samples were sent to the lab within less than 4 hours for CBC, Chemistry and electrolyte analysis. After collecting the blood sample, the mouse was perfused with 10 ml saline followed by 10 ml NBF. Then the following organs were collected and stored in NBF: Brain, Lungs, Heart, Liver, Spleen, Kidney, Ovaries and Testes.

Experimental Procedures

Treatment Preparation: KU7 was given to the PTRU as frozen aliquot and was stored in -20 freezer. For the Safety Study #1 Part1, 1020 ul sterile saline was added to KU7 500 ug labeled tubes. For the Safety Study #1 Part2, 1128 ul sterile saline was added to KU7 200 ug labeled tubes. The drug was mixed with saline by pipetting.

Treatment Administration: For Part 1 of the study the mice received a single dose of 500ug KU7 in 200ul dose volume. For part 2 of the study the mice received a single dose of 200ug KU7 in 200ul dose volume. The

drug was administered i.v. through the retro-orbital sinus on day one after anesthetizing the mice using isoflurane (1-4 %).

Data

Collection: Data for this study consisted of the clinical observation notes, Weight, collected organs histology, CBC, electrolytes and chemistry panel results. Data was entered and maintained in Excel.

Analysis software: Final analysis for data was performed in Prism software suite.

Day numbers: Calendar dates were assigned day numbers beginning with day 0 for the KU7 administration day (12/3/2019 for part 1 of the study, and 12/4/2019 for part 2 of the study). Mice were anesthetized and sacrificed on day 7 (12/10/2019 for part 1 of the study and 12/11/2019 for part 2 of the study).

Subject Weights: Weight: was measured daily using a digital scale. The mice weight in both study part remains within the normal weight range of the breed.

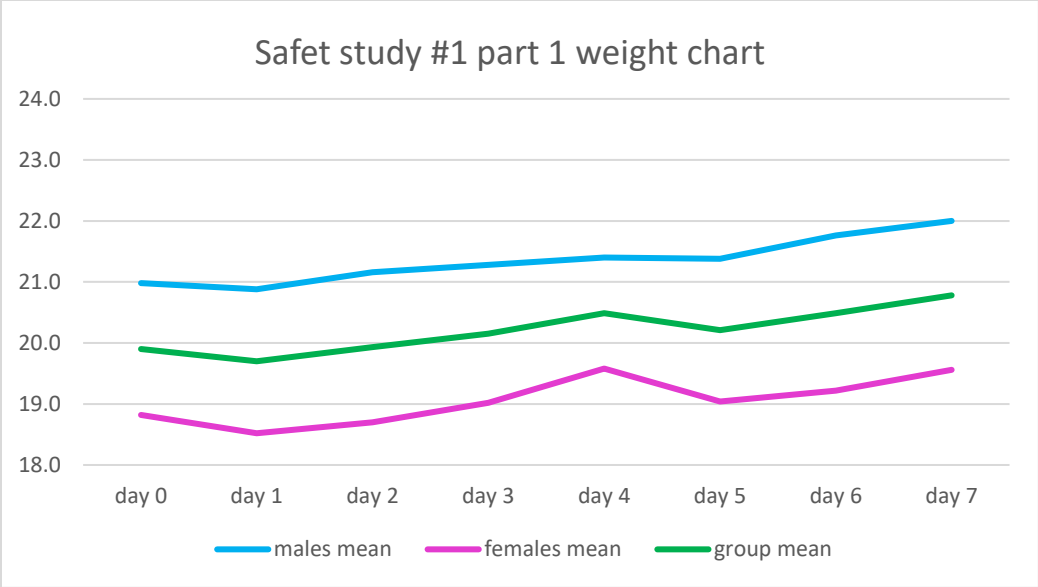

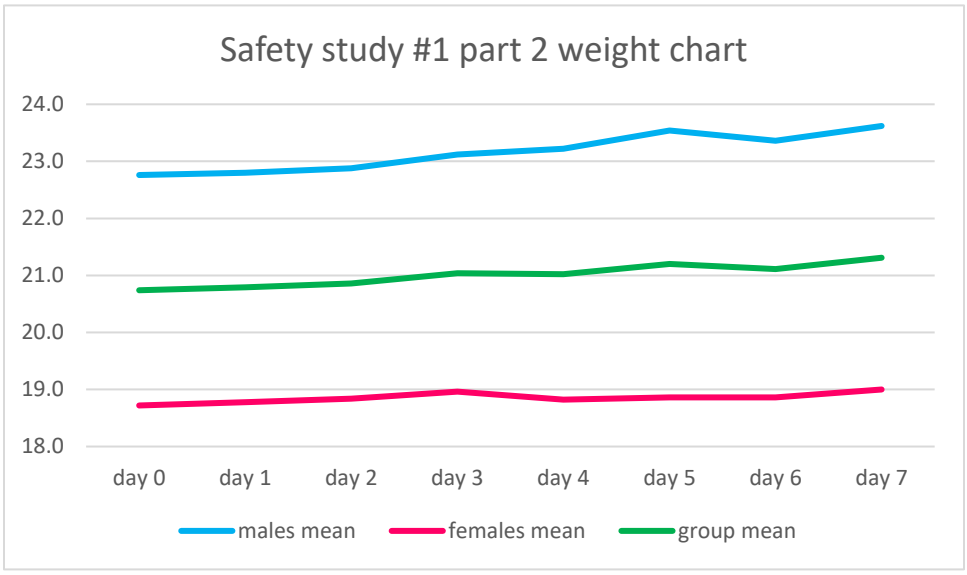

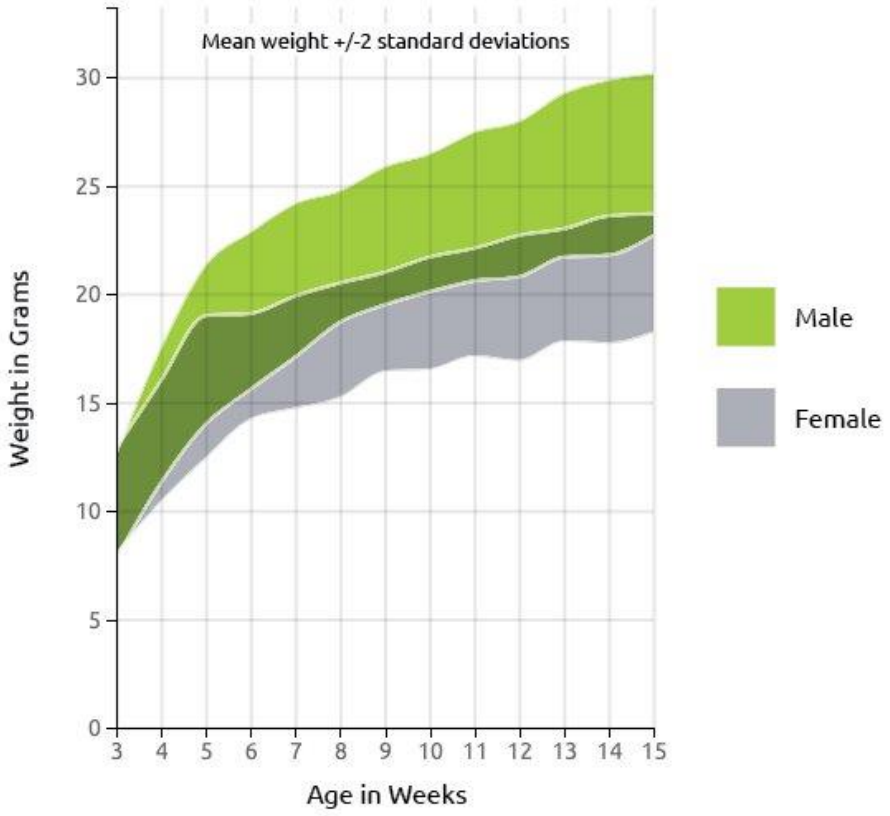

BALB/c strain weight chart

Clinical Observations: Mice were monitored the 5 hours post injection then daily for one hour each day. The clinical observations were made by placing the mice in their home cage in a quiet dark room and compare their behavior to control mice which did not receive any treatment. Clinical observations consisted of the following:

- General body condition
- Posture
- Behavior: including response to external stimuli (tapping on the cage)

- Activity
- Grooming
- Feces

The treated mice clinical observation in both study parts were similar to control group clinical observation except in the first 10-20 minutes post injection on day 1 where the treated mice were still sedated for 1 minute after isoflurane flow was stopped and then assumed a hunched position for the next 10-20 minutes which could be due to the isoflurane sedation.

Collected Organs Histology: In process, to be added.

CBC, electrolytes and chemistry: the collected blood samples were sent to Dr. Asfaw's lab for CBC, electrolyte and chemistry panel analysis. The results of the treated mice were compared to the results of 3 control female mice which received no treatment. The results were as follow:

- **Chemistry:**
  - **Creatinine, BUN/Creatinine, Calcium, Total protein, Albumin, Cholesterol, GGT, Total bilirubin:** the samples were diluted 1:4 by Asfaw's Lab to perform the blood analyses for all these parameters and the results were reported as "less than: BUN <5.0 , Creatinine <0.2 , CA<3.3 , Total protein <2.0 , Albumin < 1.0 , Cholesterol < 50 , GGT < 10 , Total bilirubin < 0.1" in all groups including the control group, so it was impossible to estimate the actual value and subsequently all these parameters were excluded (one mouse in safety study #1 part 2 male group had a Total bilirubin=0.4)
  - **BUN:** the blood sample was diluted 4 times by Asfaw's lab to perform the BUN test and in some mice the results were reported as "< 0.5" and subsequently the BUN for these mice were excluded from the analysis. The male group in safety study #1 part 1 was excluded because it had only 1 mouse that was not reported as less than.
  - **CBC:** the blood samples for CBC for 3 males in toxicity study #1 part 1 coagulated so the CBC results for the male group in this study contains the results of 2 males only

*Raw data from Asfaw Lab, Excel file containing all the organized blood results, Prism analysis files and Pathology report will be included with this report.
* For BALB/c strain blood results please refer to the following link:
https://www.criver.com/sites/default/files/Technical%20Resources/Clinical%20Pathology%20Data%20for%20BALB_c%20Mouse%20Colonies%20in%20North%20America%20for%20January%202008%20-%20December%202012.pdf

In general, compared to values of normal animals in the link above, the following chemistries and CBCs appear to be low:

- **Potassium (normal values confirmed with CRL and Jax)**
- **WBCs**
- **Lymph**
- **Mono**
- **RDW %**
- **MCV**
- **Neu**

In general, compared to values of normal animals in the link above, the following appear to be high:

- **MCHC**

Other points to note:

- Regarding creatinine, the normal range for males and females is 0.2-0.4 and 0.2-0.5 mg/dL, respectively. The instrument used to evaluate this parameter was not sensitive enough to provide meaningful data, so all samples tested including controls were reported as 0.2 mg/dL in 4X diluted samples.

- Regarding part 1 female basophil%, a single animal skewed the results: 1 out of 5 mice had 1% basophils.

- All graphs below show mean +/- standard deviation.

- Min and max of the reported normal ranges are also reported where available, sourced from the Charles River link above.

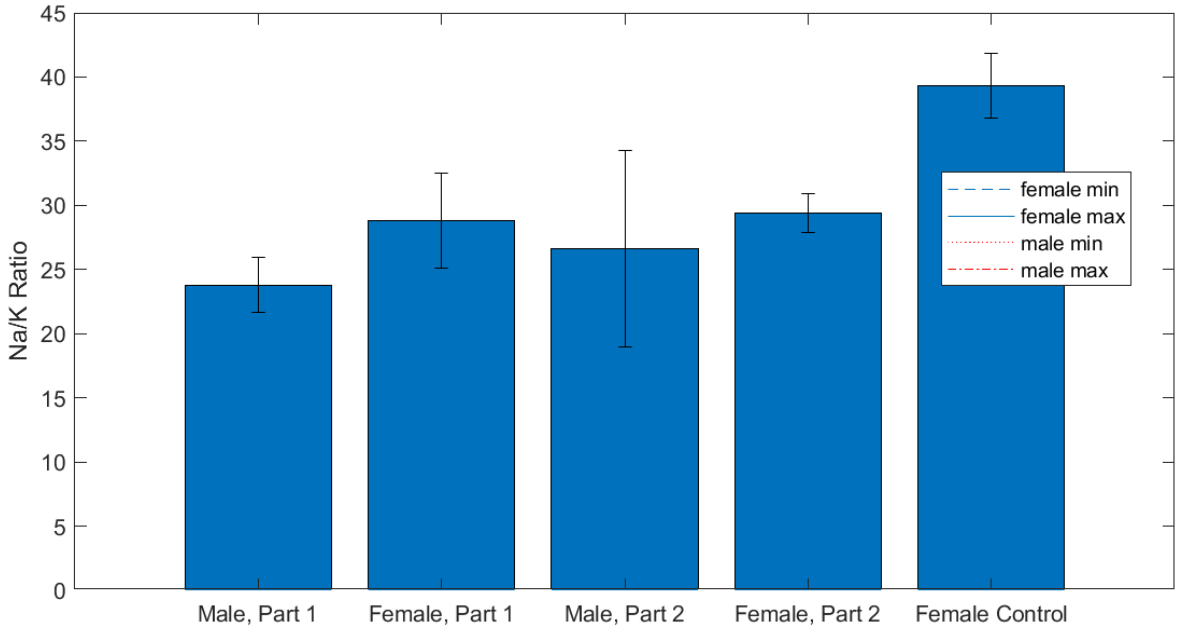

*Normal range not available

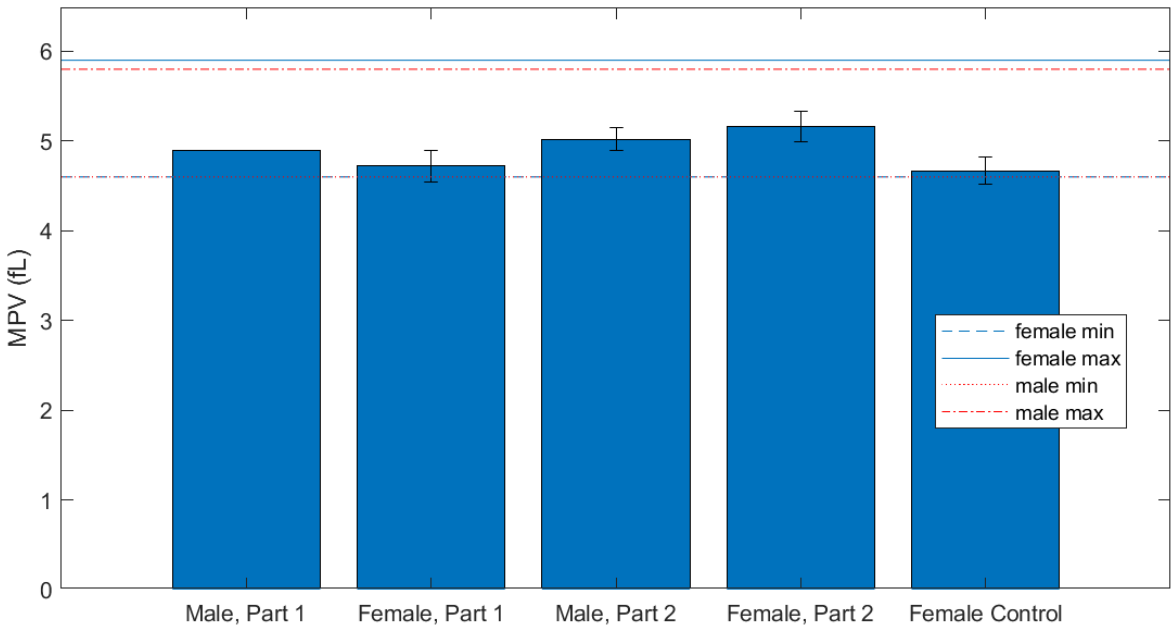
MPV (fL)
0
1
2
3
4
5
6
female min
female max
male min
male max
Male, Part 1
Female, Part 1
Male, Part 2
Female, Part 2
Female Control

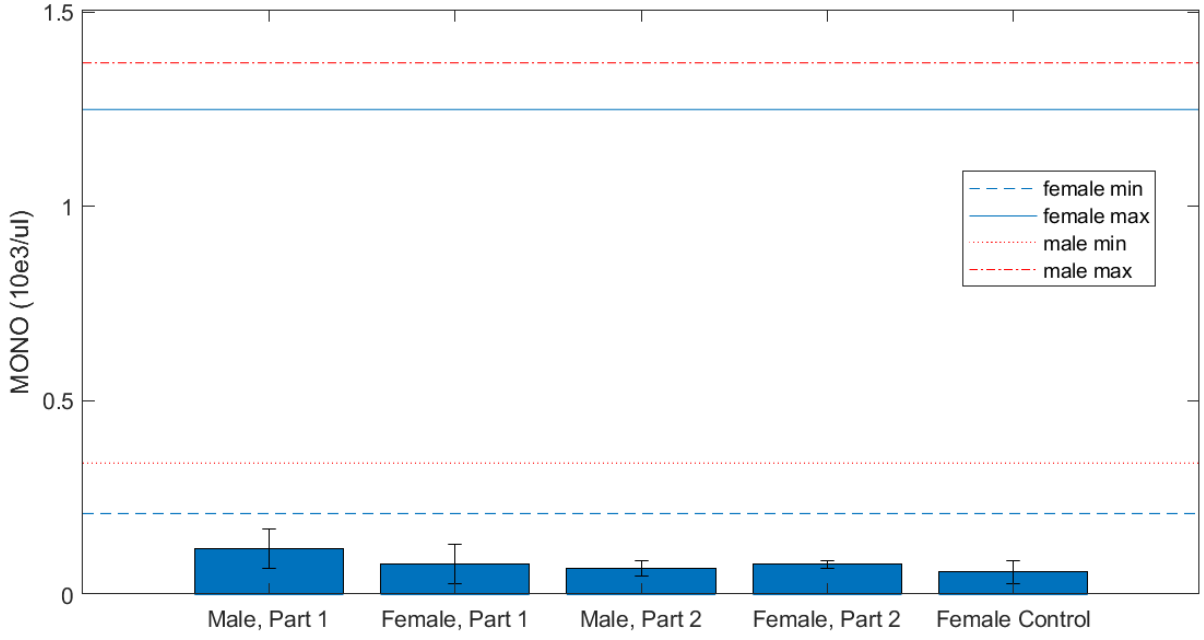
MONO (10e3/ul)
0
0.5
1
1.5
female min
female max
male min
male max
Male, Part 1
Female, Part 1
Male, Part 2
Female, Part 2
Female Control

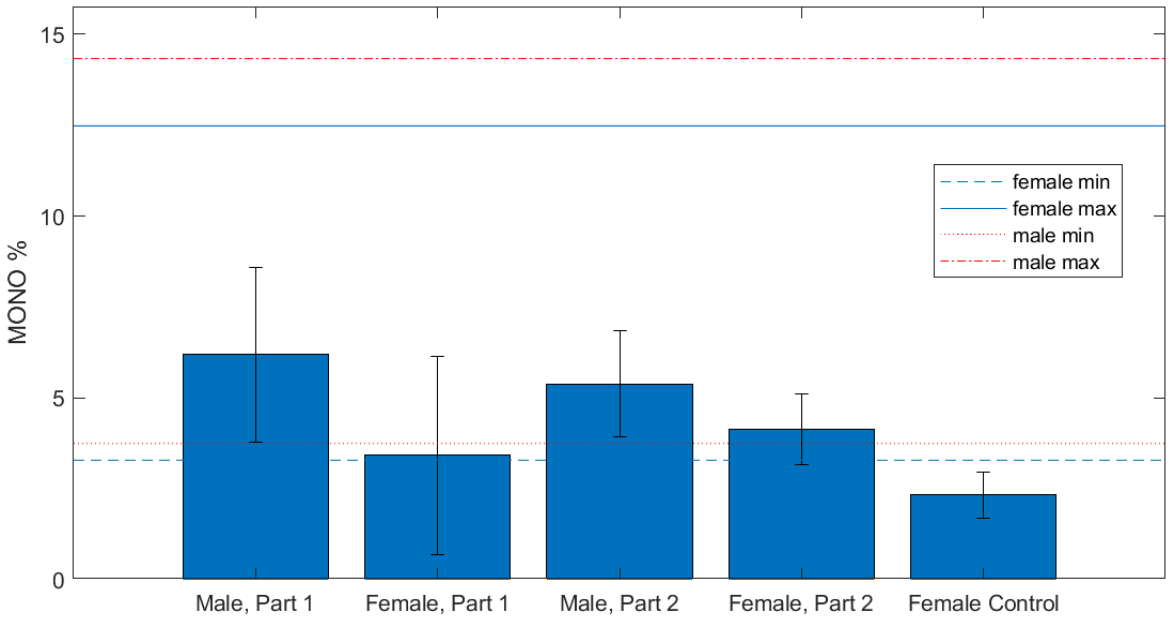
MONO %
15
10
5
0
female min
female max
male min
male max
Male, Part 1
Female, Part 1
Male, Part 2
Female, Part 2
Female Control

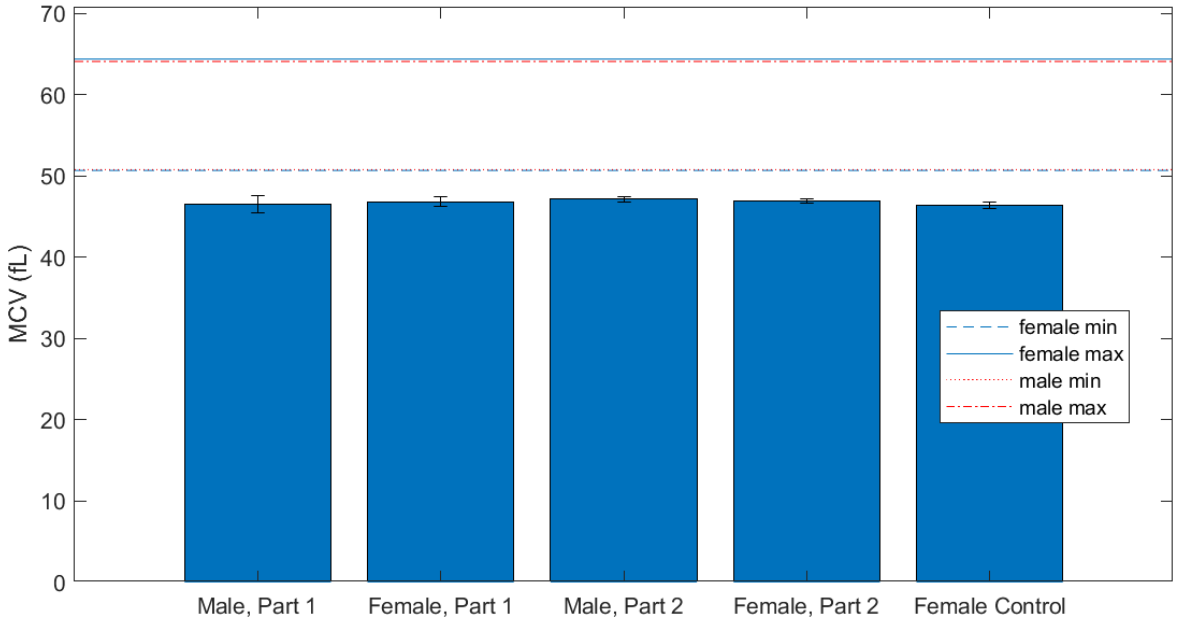
MCV (fL)
70
60
50
40
30
20
10
0
female min
female max
male min
male max
Male, Part 1
Female, Part 1
Male, Part 2
Female, Part 2
Female Control

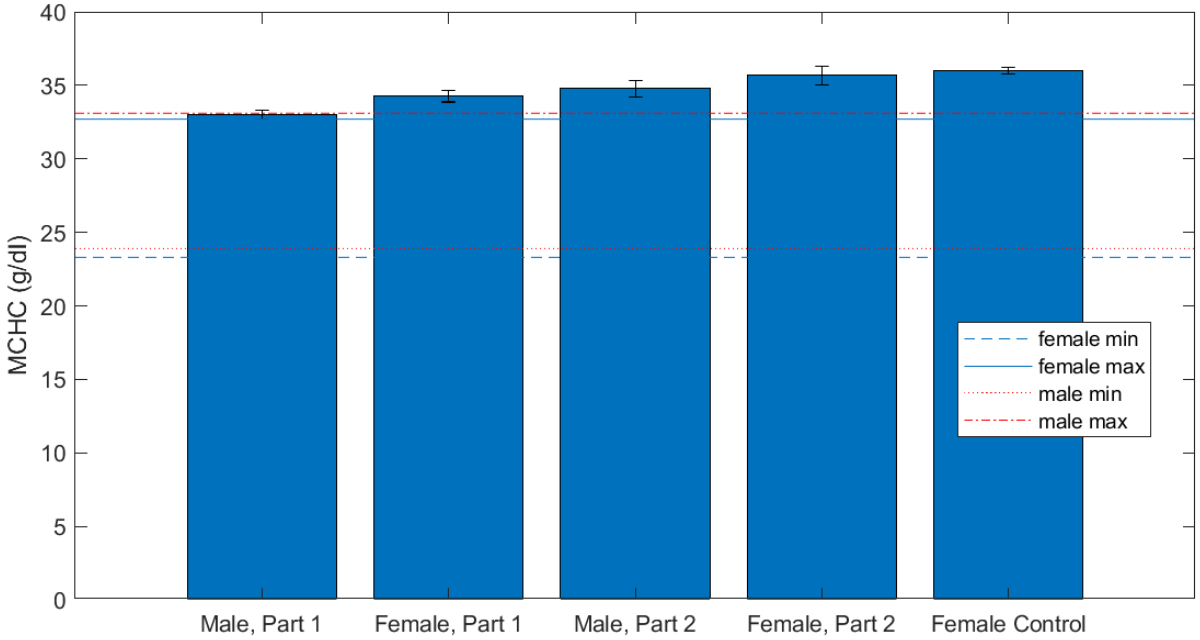
MCHC (g/dl)
40
35
30
25
20
15
10
5
0
female min
female max
male min
male max
Male, Part 1
Female, Part 1
Male, Part 2
Female, Part 2
Female Control

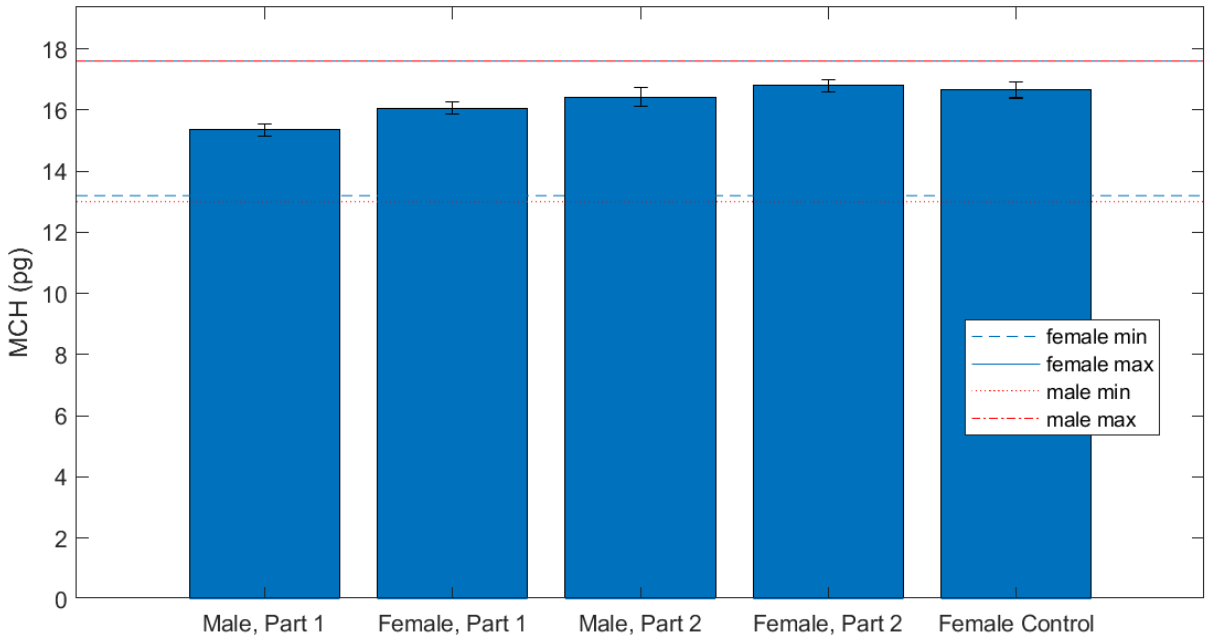
MCH (pg)
18
16
14
12
10
8
6
4
2
0
female min
female max
male min
male max
Male, Part 1
Female, Part 1
Male, Part 2
Female, Part 2
Female Control

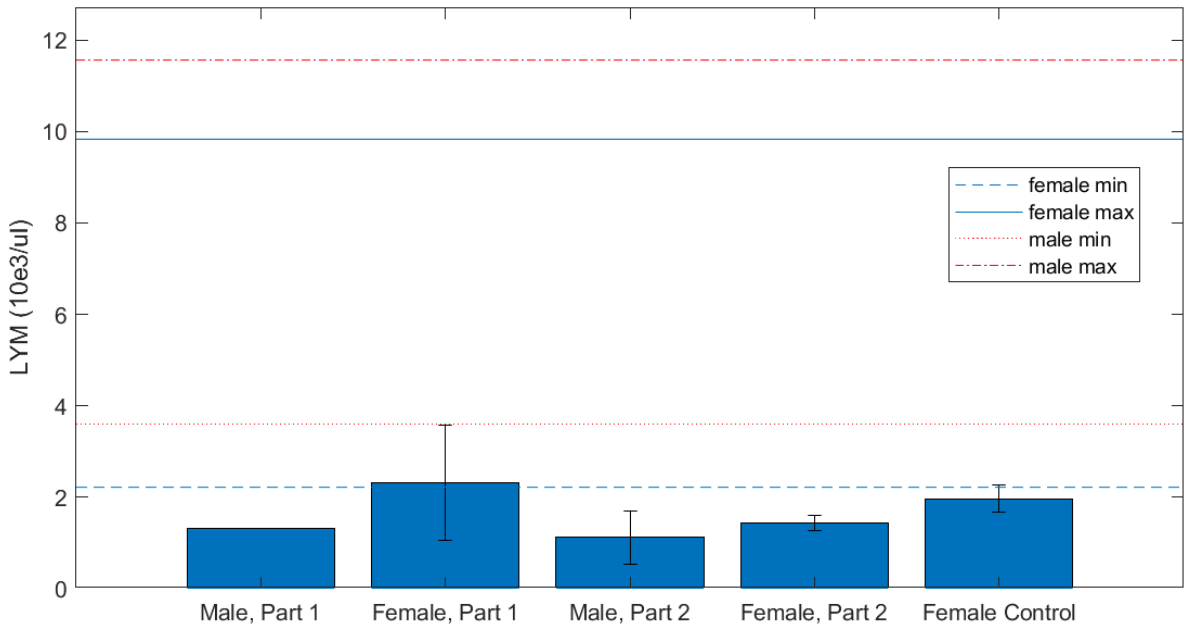
LYM (10e3/ul)
12
10
8
6
4
2
0
female min
female max
male min
male max
Male, Part 1
Female, Part 1
Male, Part 2
Female, Part 2
Female Control

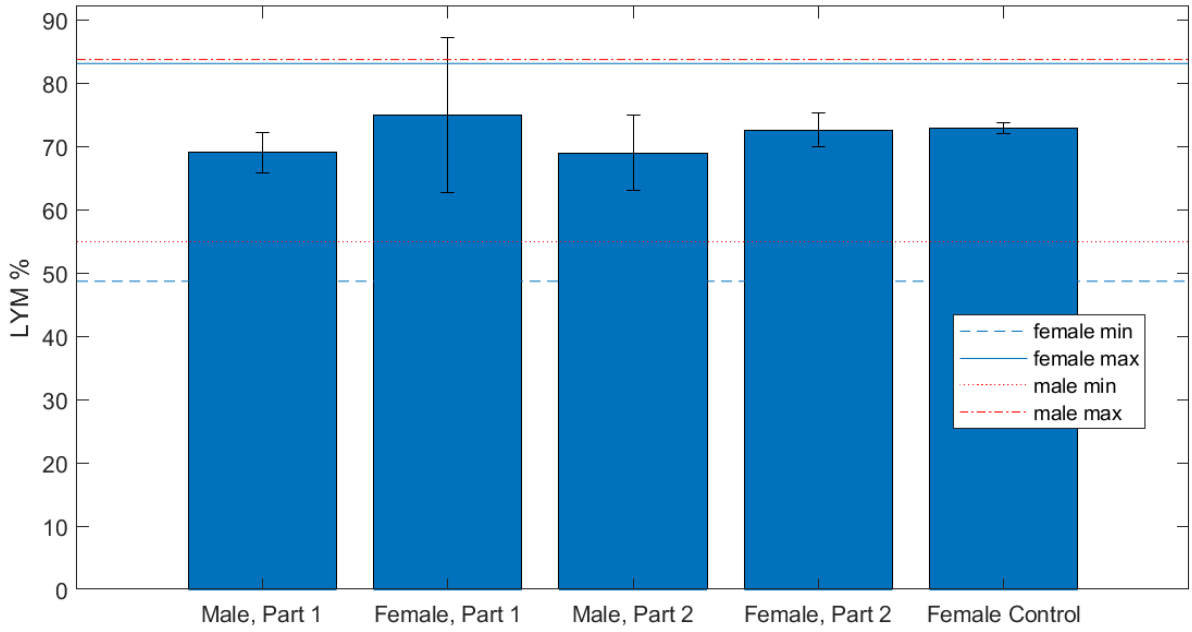
LYM %
90
80
70
60
50
40
30
20
10
0
female min
female max
male min
male max
Male, Part 1
Female, Part 1
Male, Part 2
Female, Part 2
Female Control

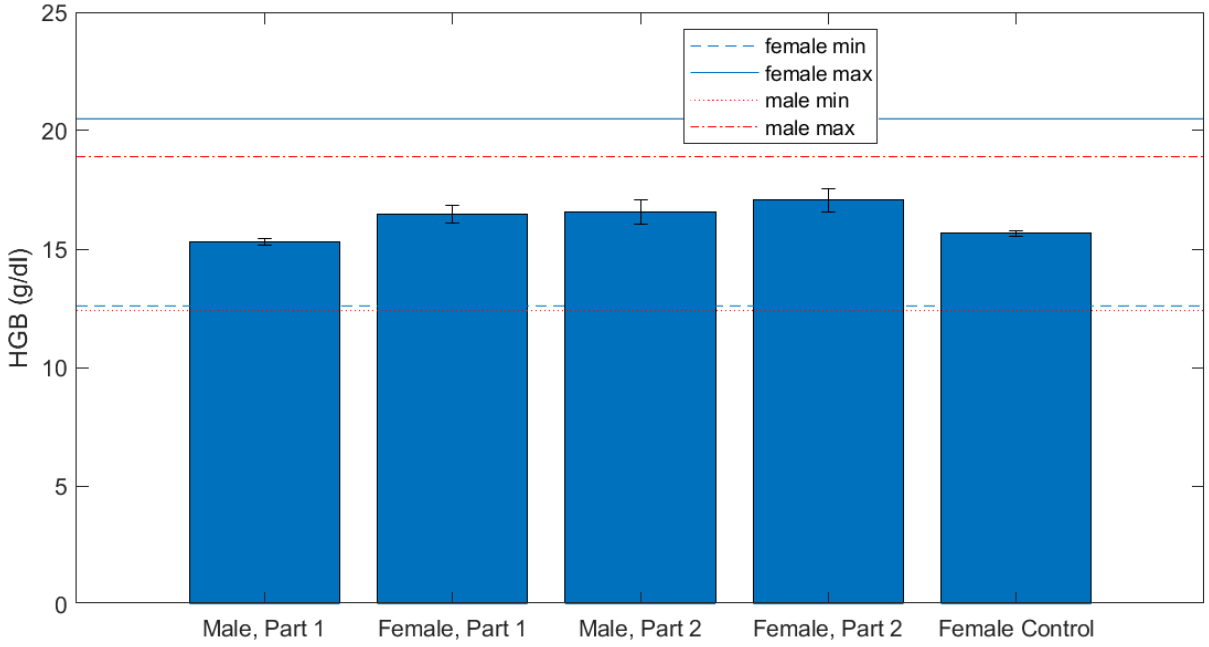
HGB (g/dl)
25
20
15
10
5
0
female min
female max
male min
male max
Male, Part 1
Female, Part 1
Male, Part 2
Female, Part 2
Female Control

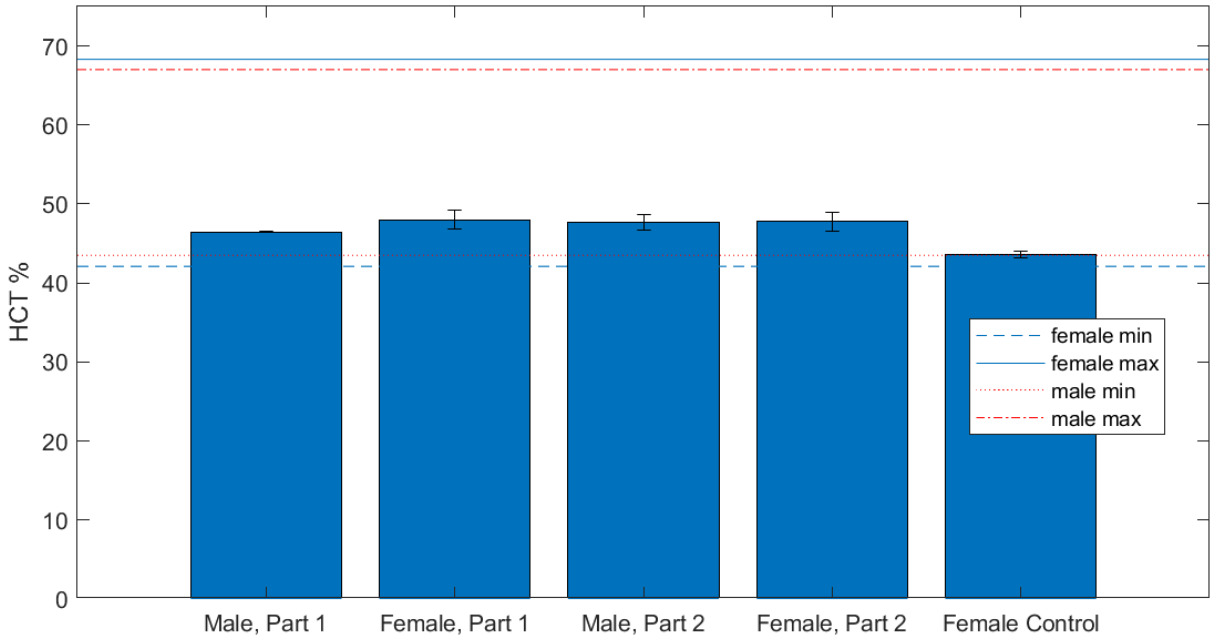
HCT %
70
60
50
40
30
20
10
0
female min
female max
male min
male max
Male, Part 1
Female, Part 1
Male, Part 2
Female, Part 2
Female Control

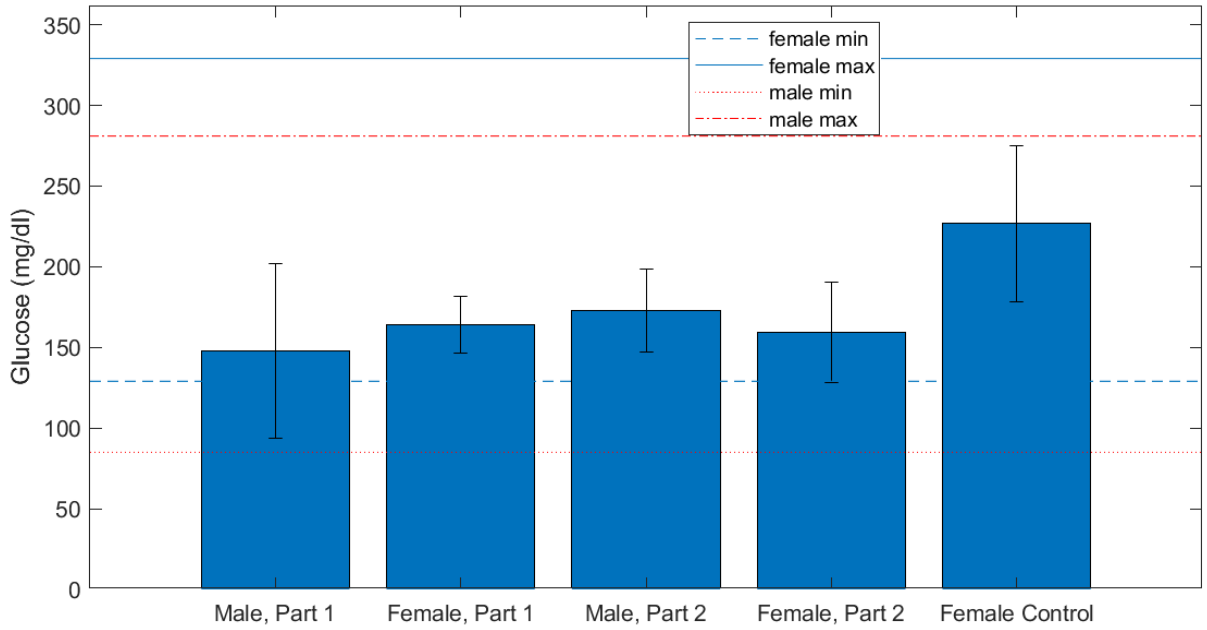
female min
female max
male min
male max
Glucose (mg/dl)
350
300
250
200
150
100
50
0
Male, Part 1
Female, Part 1
Male, Part 2
Female, Part 2
Female Control

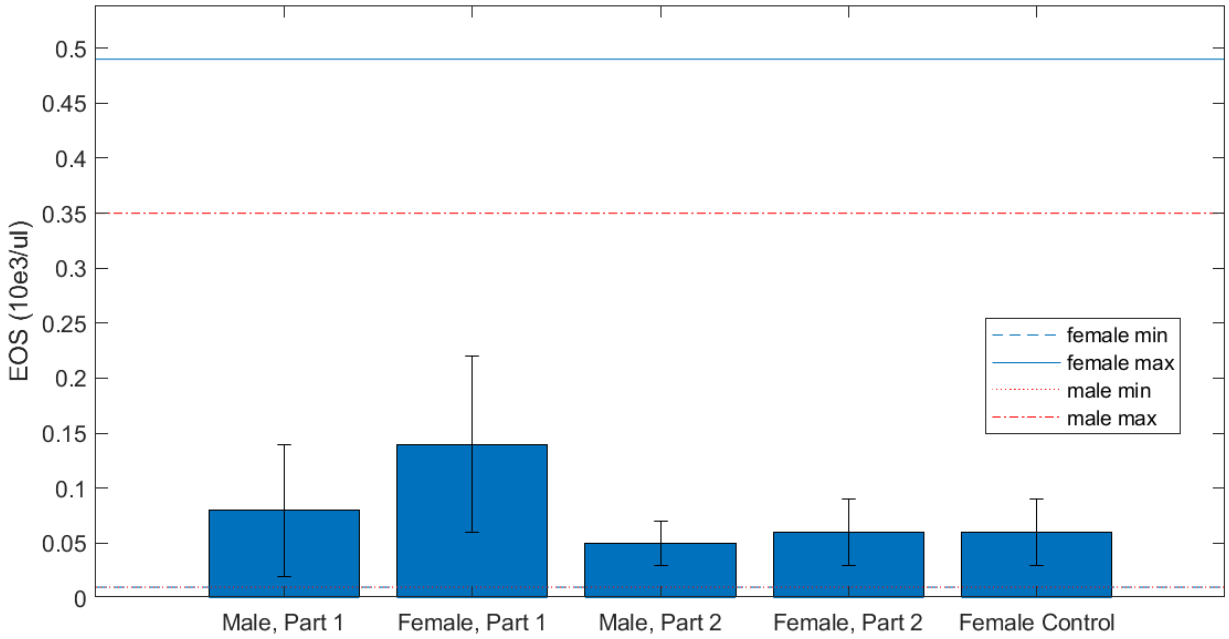
female min
female max
male min
male max
EOS (10e3/ul)
0.5
0.45
0.4
0.35
0.3
0.25
0.2
0.15
0.1
0.05
0
Male, Part 1
Female, Part 1
Male, Part 2
Female, Part 2
Female Control

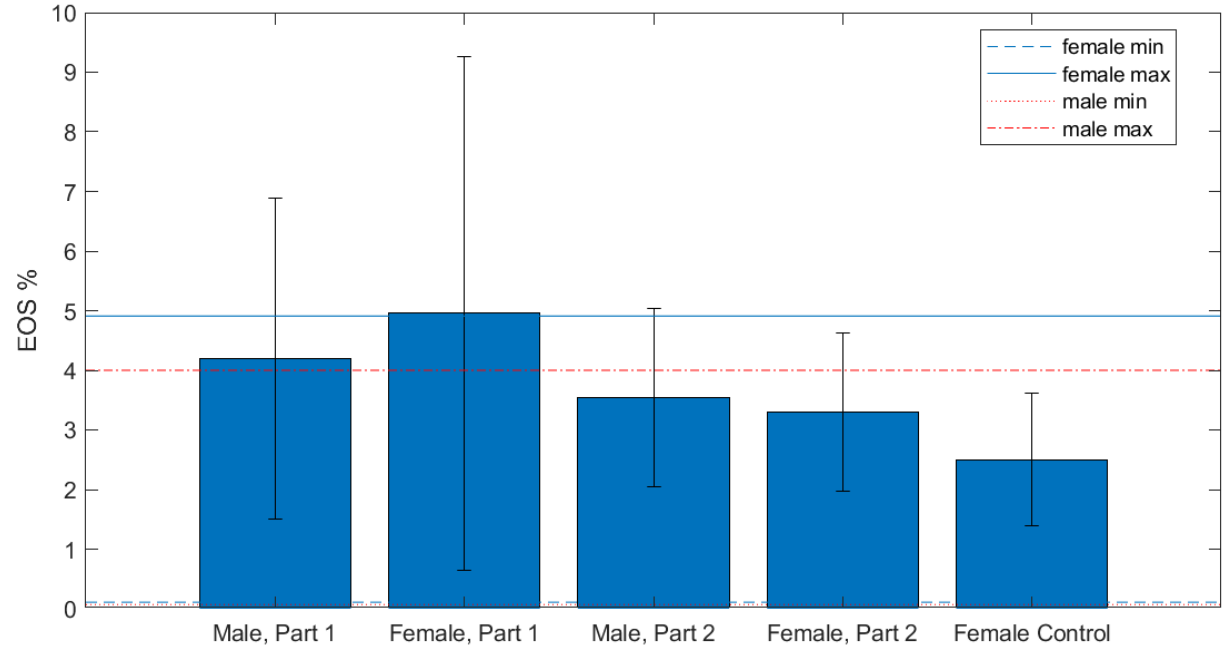
EOS %
10
9
8
7
6
5
4
3
2
1
0
female min
female max
male min
male max
Male, Part 1
Female, Part 1
Male, Part 2
Female, Part 2
Female Control

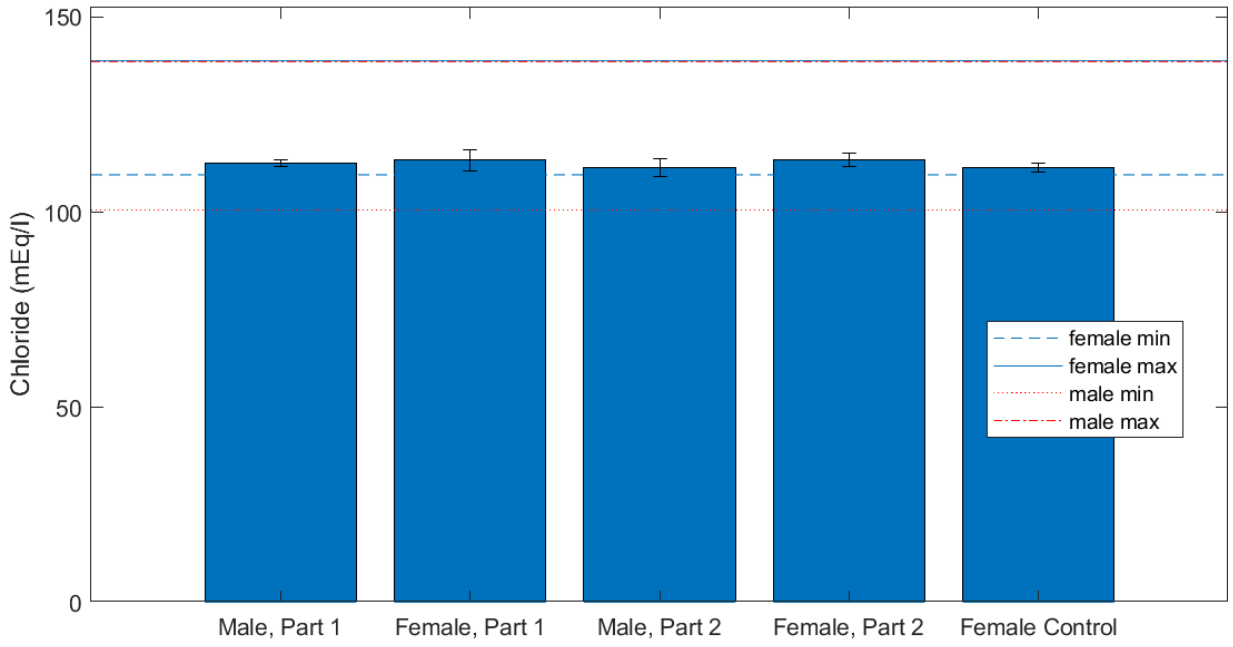
Chloride (mEq/l)
150
100
50
0
female min
female max
male min
male max
Male, Part 1
Female, Part 1
Male, Part 2
Female, Part 2
Female Control

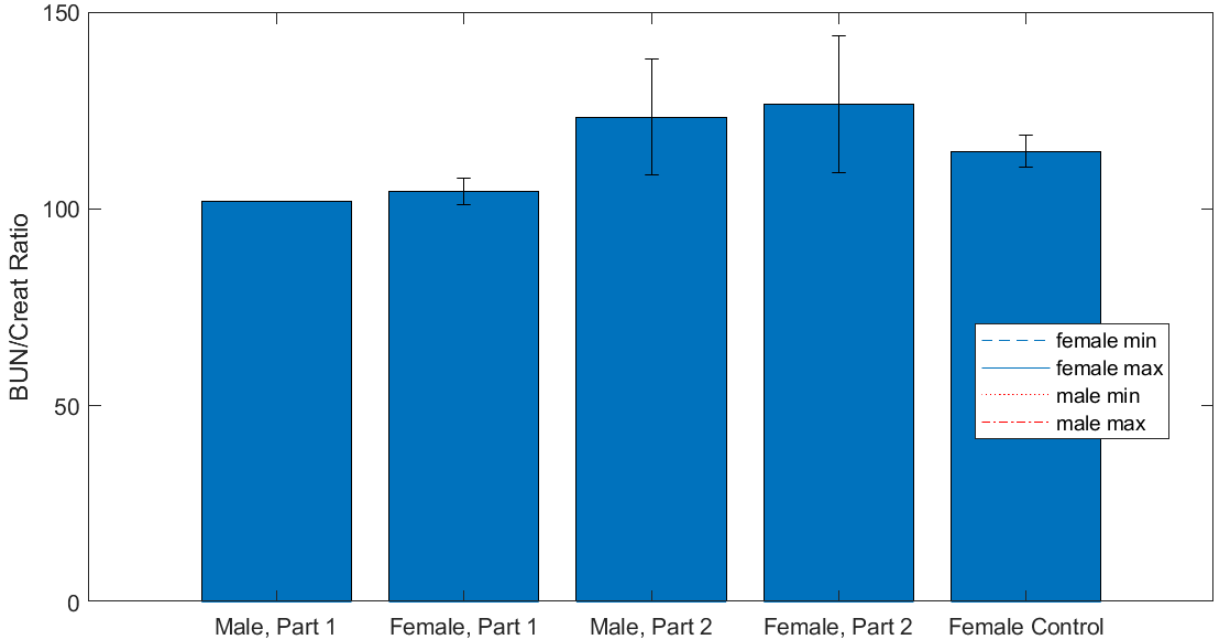
150
100
50
0
BUN/Creat Ratio
female min
female max
male min
male max
Male, Part 1
Female, Part 1
Male, Part 2
Female, Part 2
Female Control

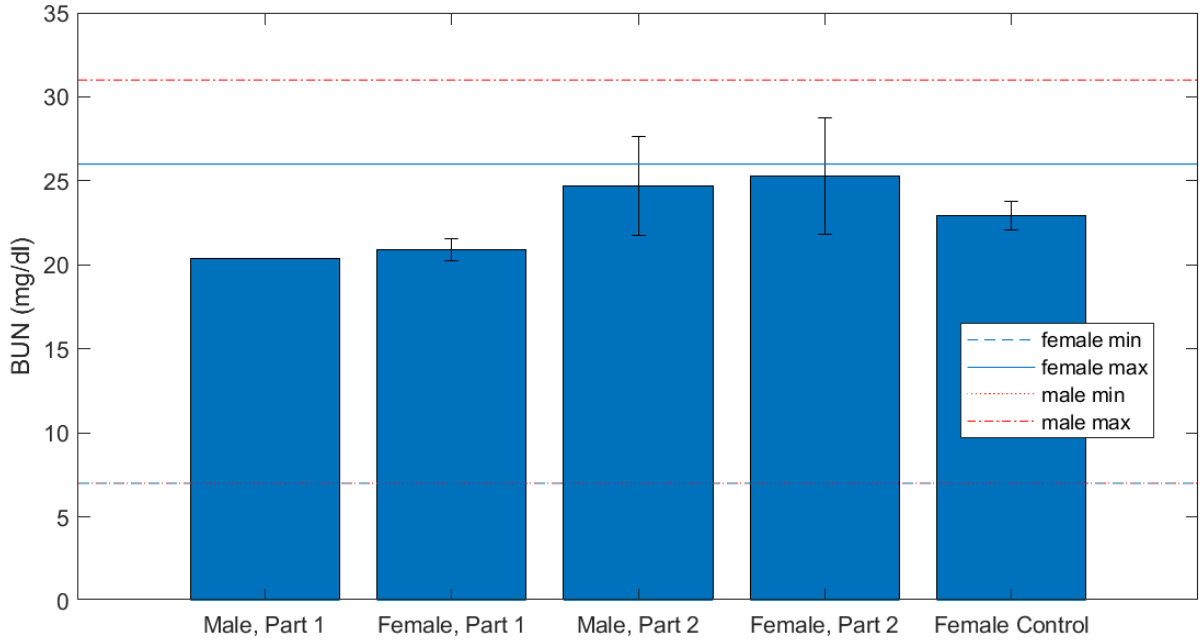
35
30
25
20
15
10
5
0
BUN (mg/dl)
female min
female max
male min
male max
Male, Part 1
Female, Part 1
Male, Part 2
Female, Part 2
Female Control

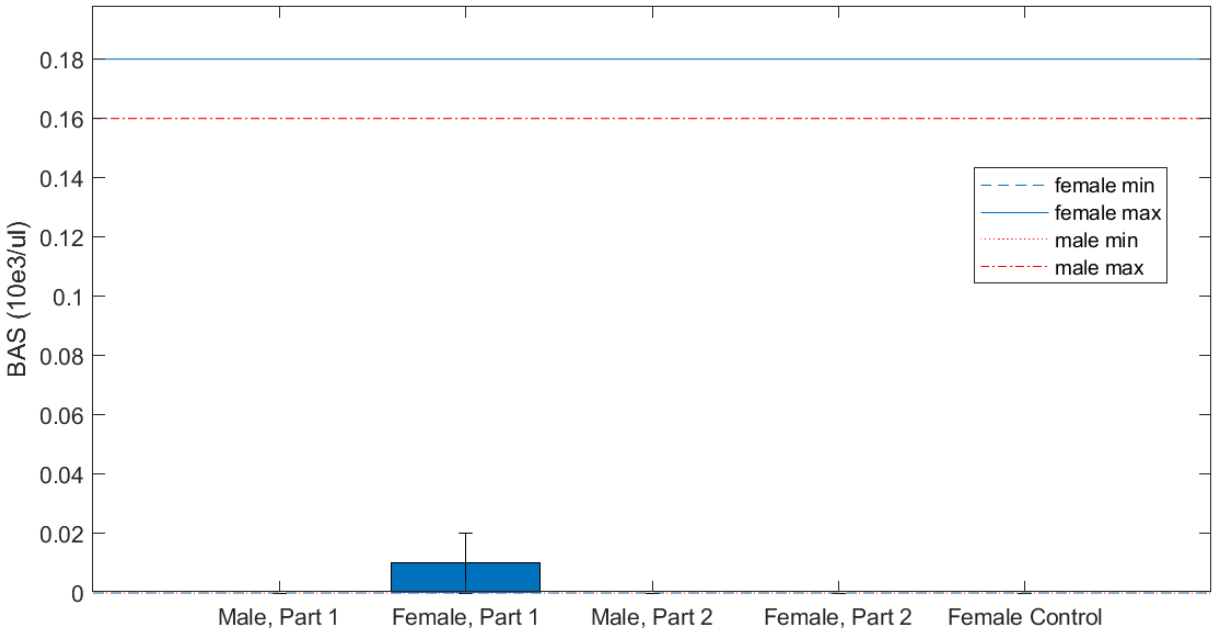
BAS (10e3/ul)
0.18
0.16
0.14
0.12
0.1
0.08
0.06
0.04
0.02
0
female min
female max
male min
male max
Male, Part 1
Female, Part 1
Male, Part 2
Female, Part 2
Female Control

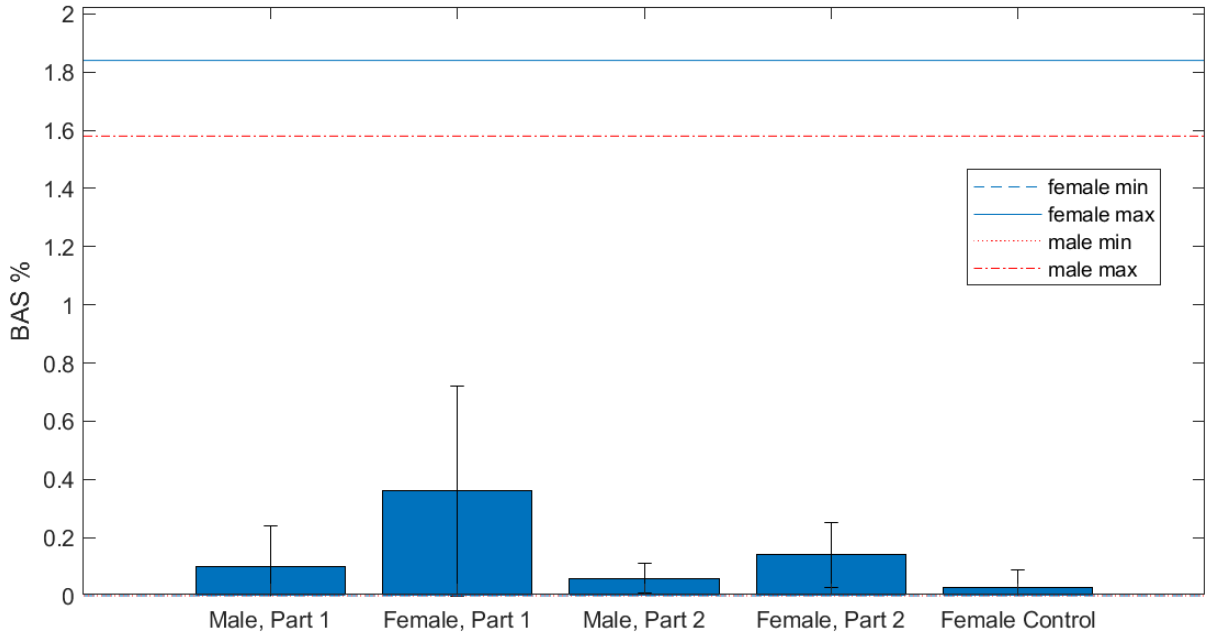
BAS %
2
1.8
1.6
1.4
1.2
1
0.8
0.6
0.4
0.2
0
female min
female max
male min
male max
Male, Part 1
Female, Part 1
Male, Part 2
Female, Part 2
Female Control

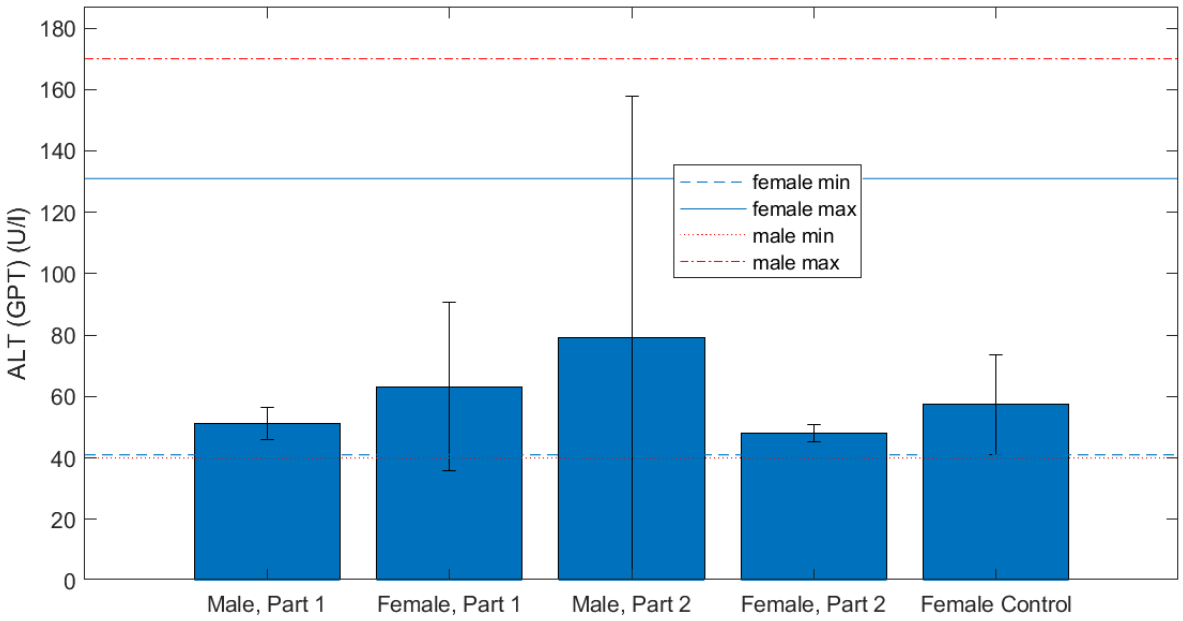
ALT (GPT) (U/l)
180
160
140
120
100
80
60
40
20
0
female min
female max
male min
male max
Male, Part 1
Female, Part 1
Male, Part 2
Female, Part 2
Female Control

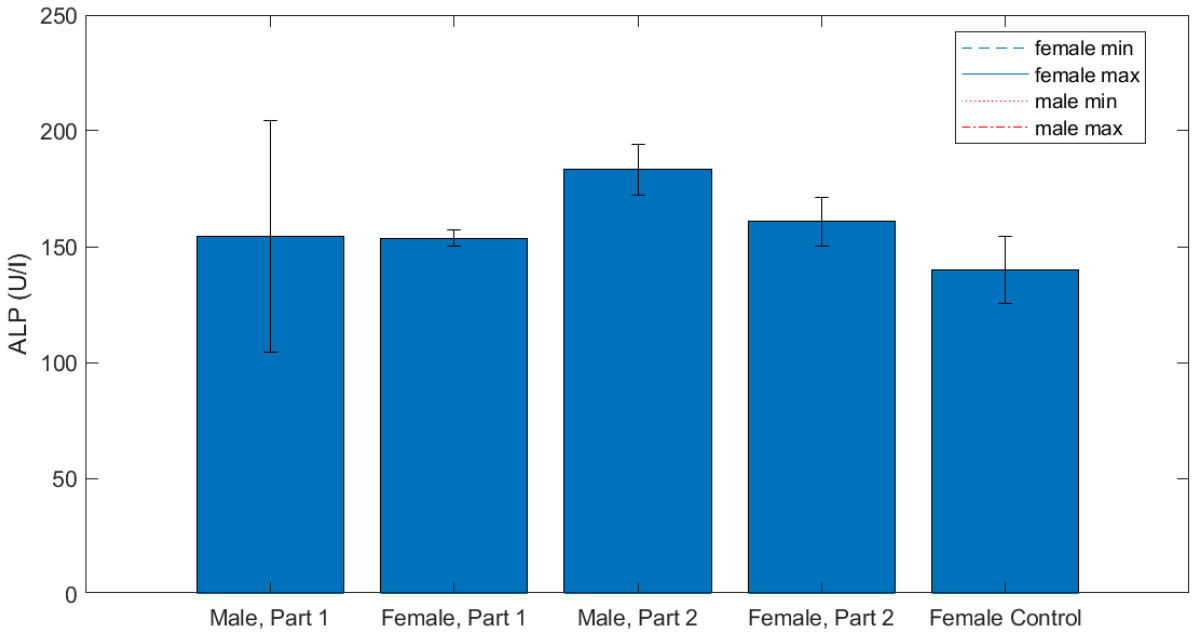
ALP (U/l)
250
200
150
100
50
0
female min
female max
male min
male max
Male, Part 1
Female, Part 1
Male, Part 2
Female, Part 2
Female Control

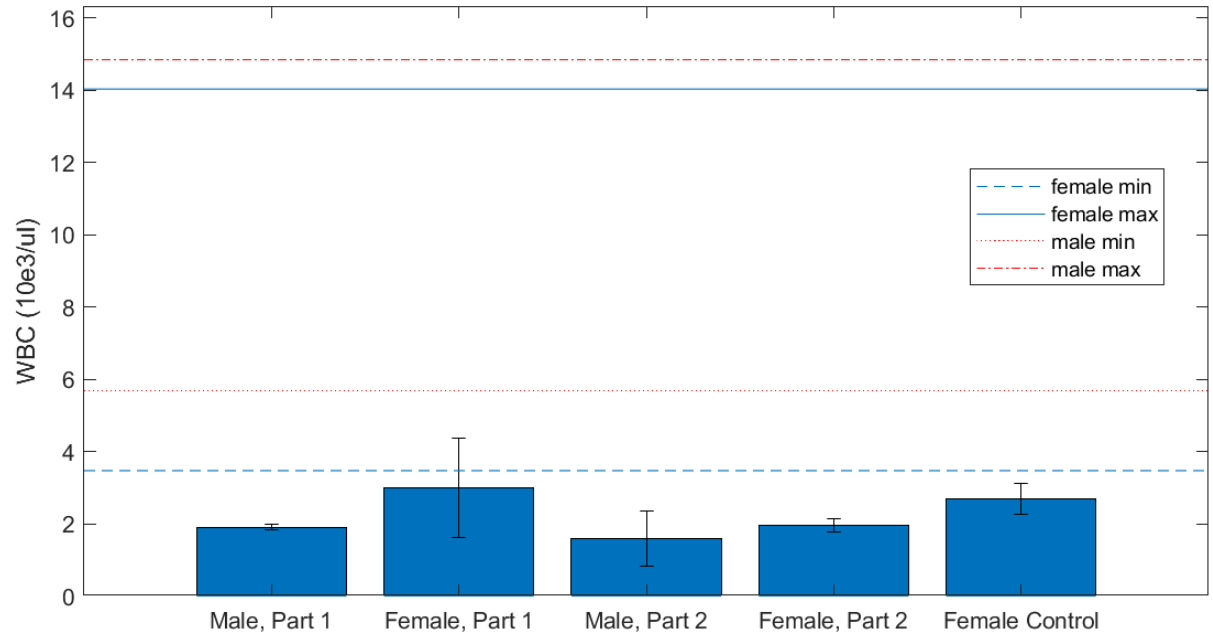
WBC (10e3/ul)
16
14
12
10
8
6
4
2
0
female min
female max
male min
male max
Male, Part 1
Female, Part 1
Male, Part 2
Female, Part 2
Female Control

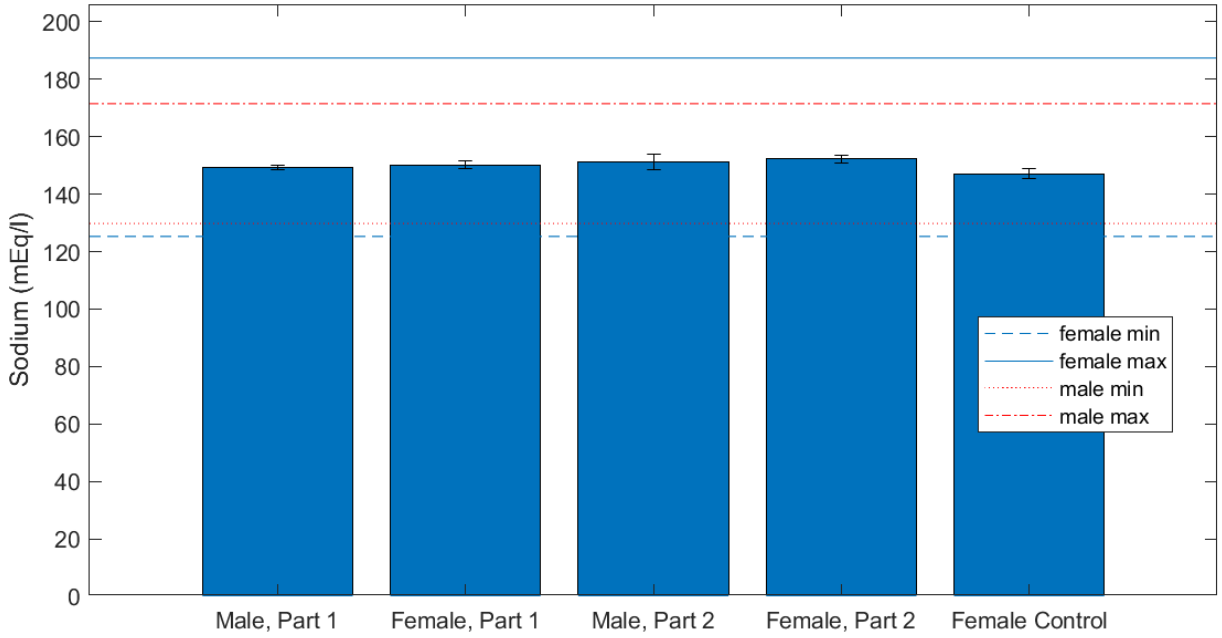
Sodium (mEq/l)
200
180
160
140
120
100
80
60
40
20
0
female min
female max
male min
male max
Male, Part 1
Female, Part 1
Male, Part 2
Female, Part 2
Female Control

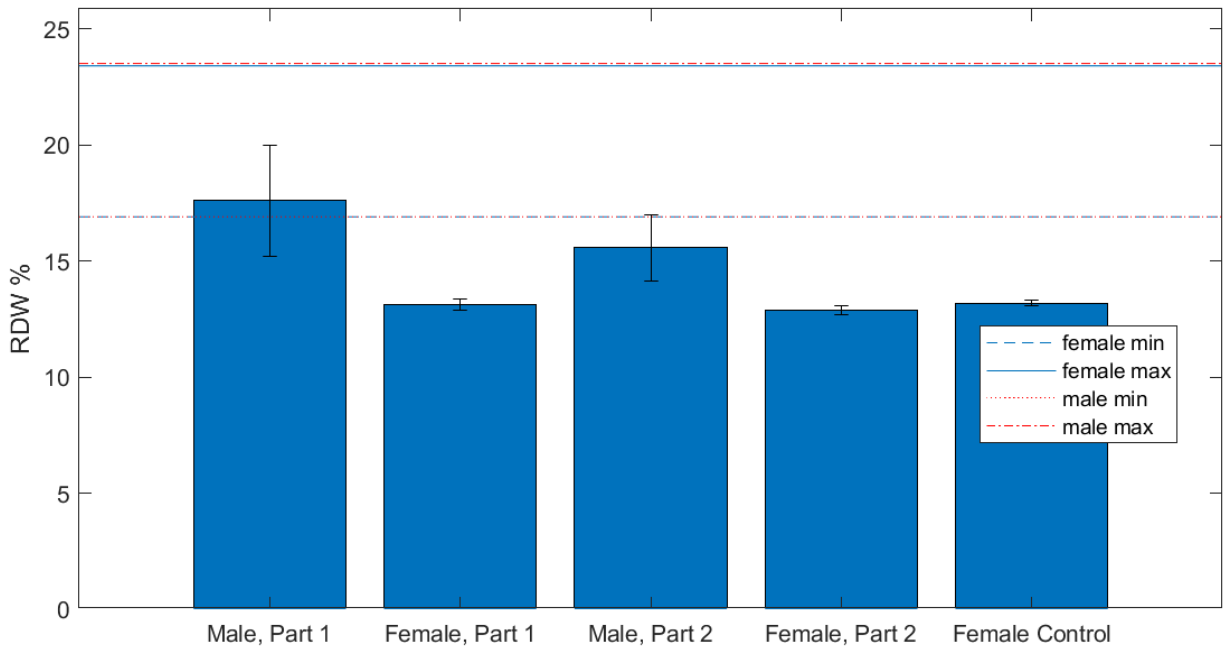
RDW %
25
20
15
10
5
0
female min
female max
male min
male max
Male, Part 1
Female, Part 1
Male, Part 2
Female, Part 2
Female Control

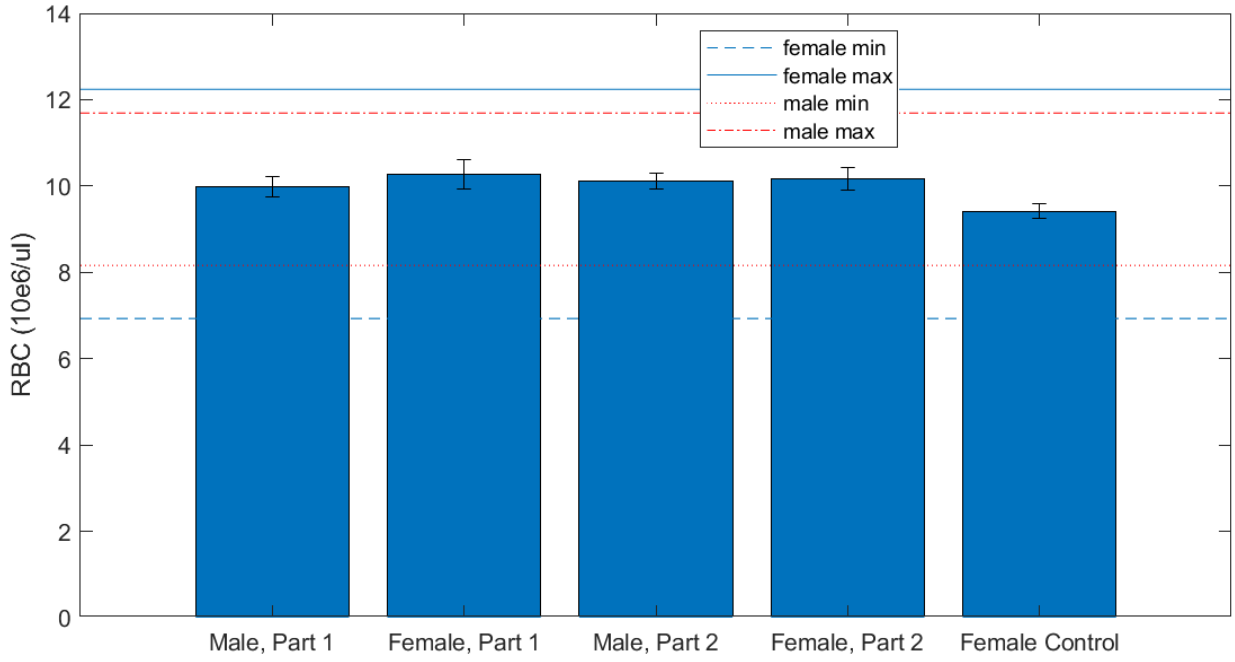
RBC (10e6/ul)
14
12
10
8
6
4
2
0
female min
female max
male min
male max
Male, Part 1
Female, Part 1
Male, Part 2
Female, Part 2
Female Control

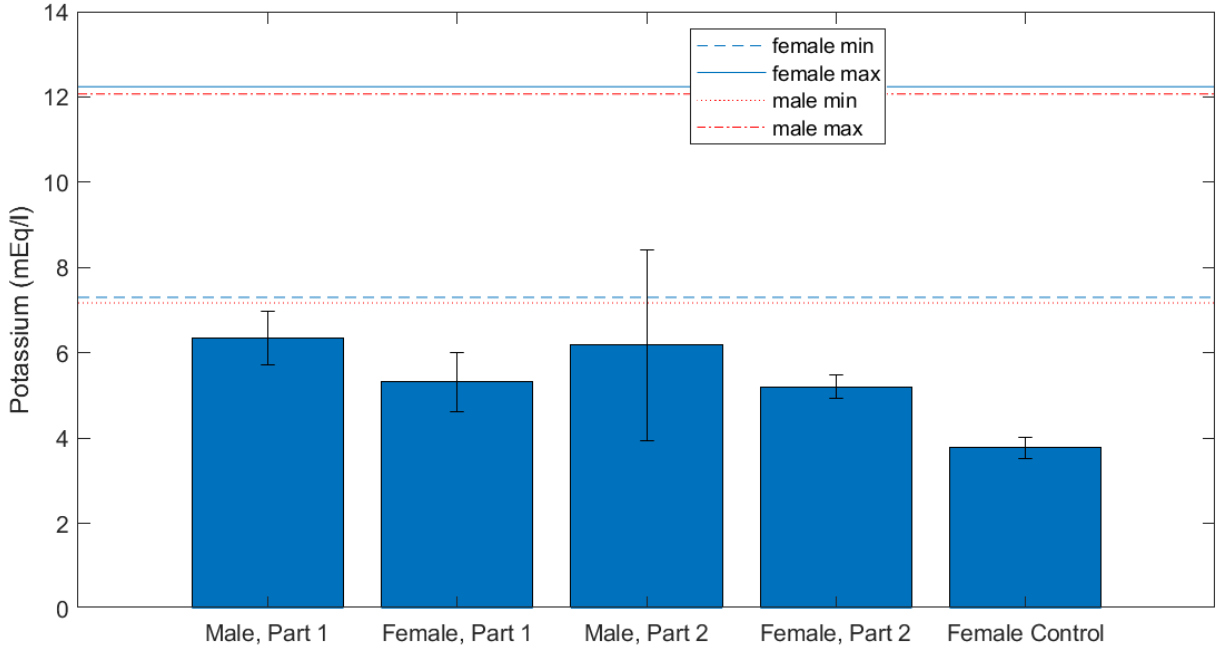
female min
female max
male min
male max
Potassium (mEq/l)
0
2
4
6
8
10
12
14
Male, Part 1
Female, Part 1
Male, Part 2
Female, Part 2
Female Control

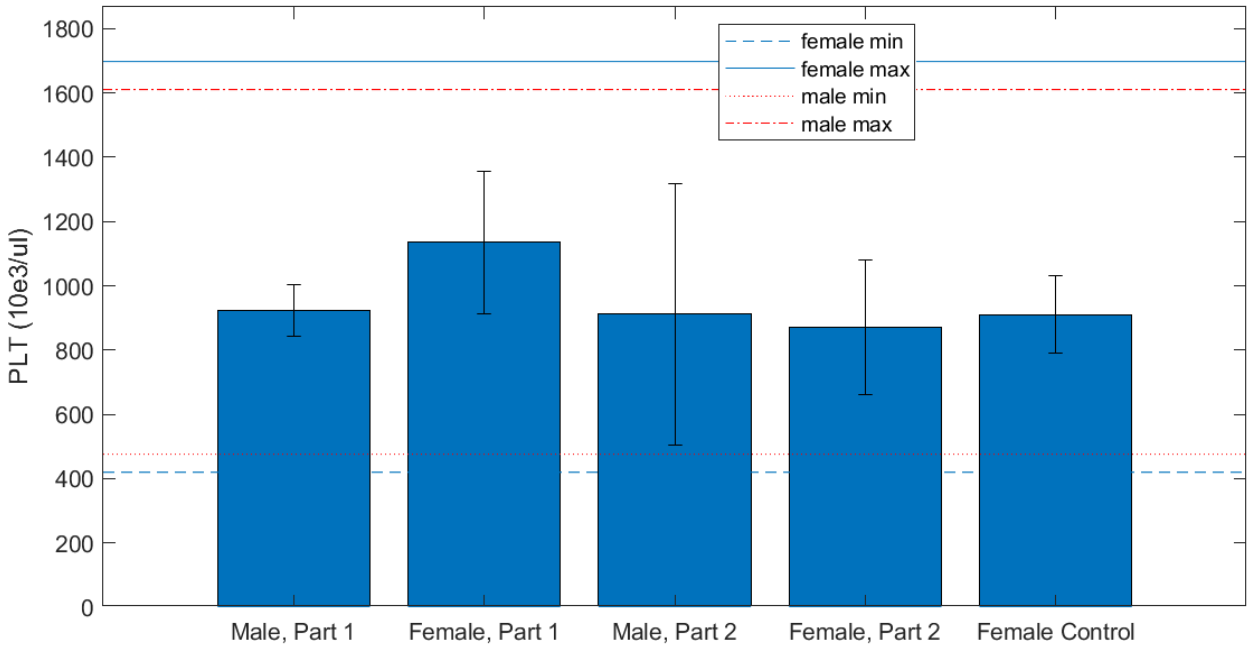
female min
female max
male min
male max
PLT (10e3/ul)
0
200
400
600
800
1000
1200
1400
1600
1800
Male, Part 1
Female, Part 1
Male, Part 2
Female, Part 2
Female Control

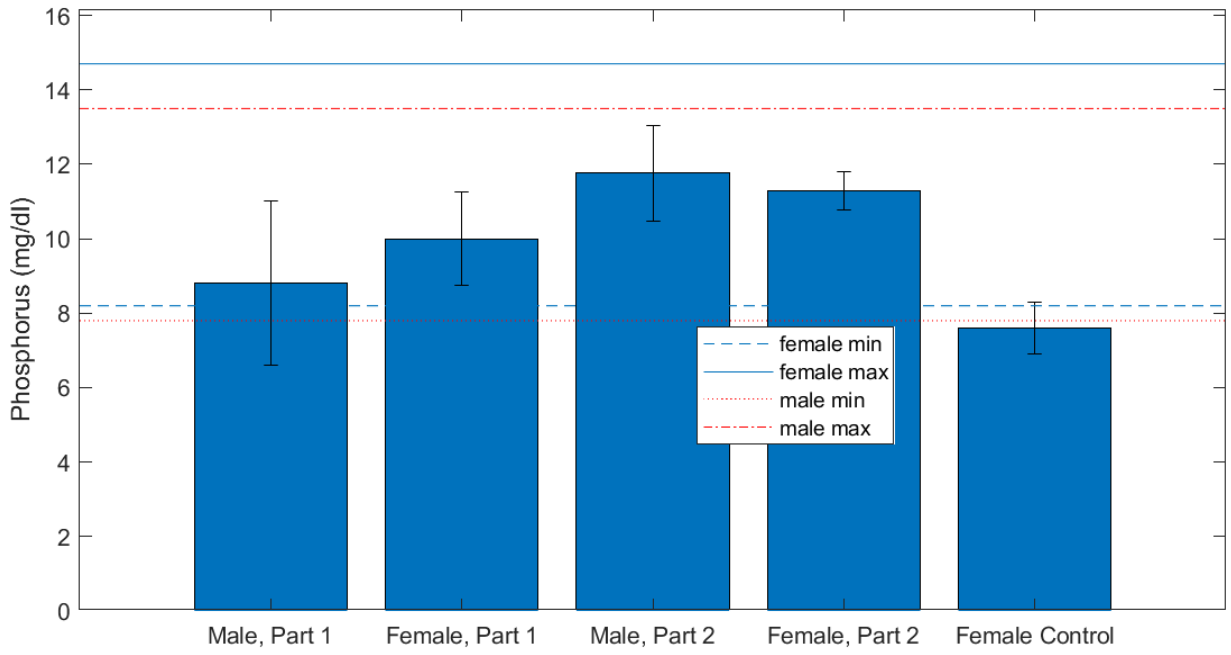
Phosphorus (mg/dl)
16
14
12
10
8
6
4
2
0
female min
female max
male min
male max
Male, Part 1
Female, Part 1
Male, Part 2
Female, Part 2
Female Control

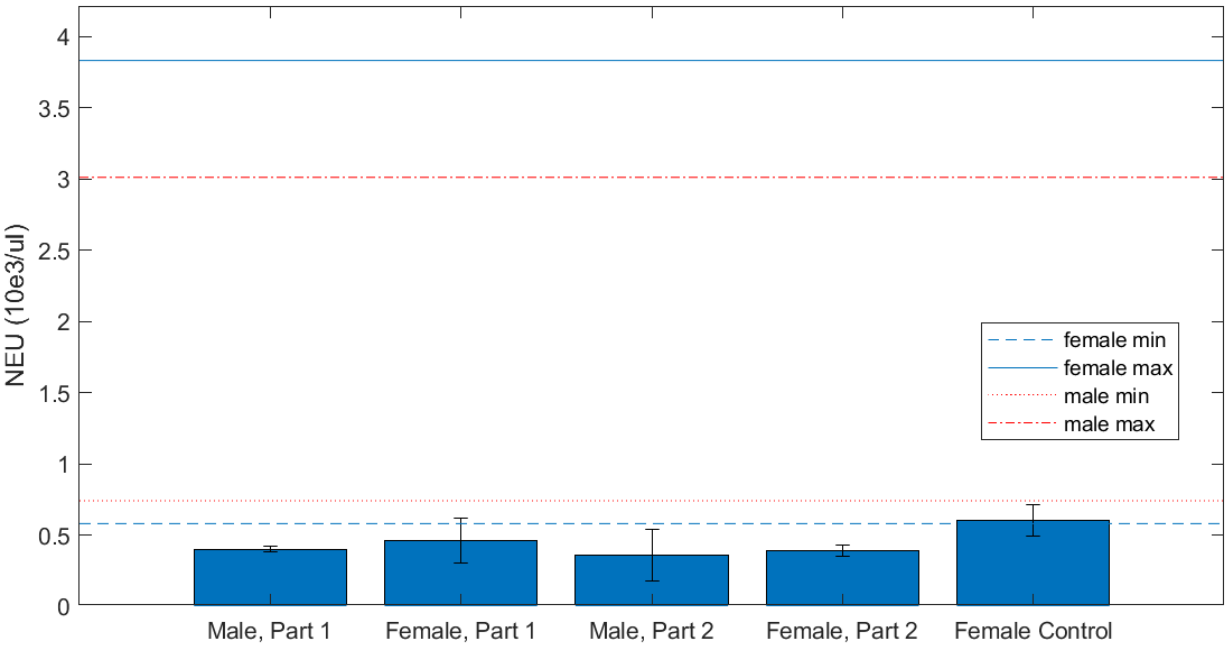
NEU (10e3/ul)
4
3.5
3
2.5
2
1.5
1
0.5
0
female min
female max
male min
male max
Male, Part 1
Female, Part 1
Male, Part 2
Female, Part 2
Female Control

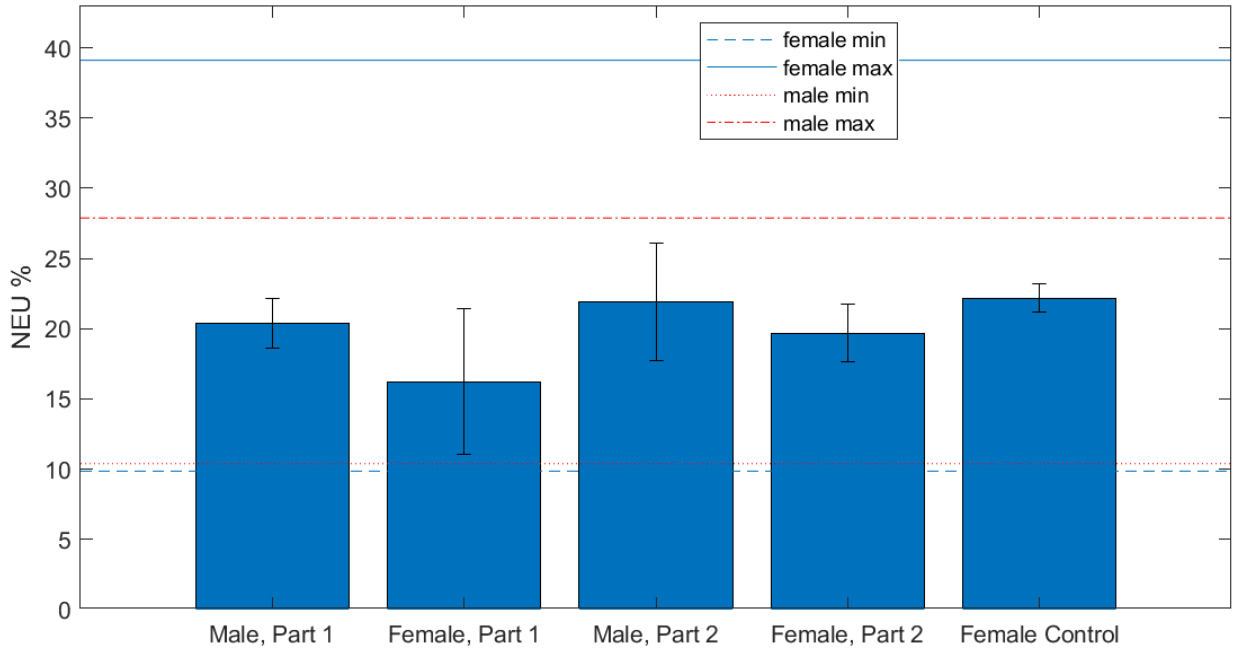
female min
female max
male min
male max
NEU %
0
5
10
15
20
25
30
35
40
Male, Part 1
Female, Part 1
Male, Part 2
Female, Part 2
Female Control

Study Design

Experimental Aims: complete no observed adverse event level (NOAEL) study, evaluation of hematologic parameters and gross organ pathology in response to high dose KU7.

Experimental Subjects: Subjects were 10 mice, 6-8 weeks old at study start, 5 males, 5 females, BALB/c, Charles River Laboratories.

Housing and Husbandry: Subjects were housed in room 1033 in Vivarium on the Duke campus. Their room was climate/temp controlled and on a 12-hour light dark cycle. Food and bedding were changed weekly by DLAR staff.

Experimental Groups: To achieve the primary study aim, mice were treated with a single dose of 500 ug/mouse KU7 in a 200ul dose volume. The mice were divided into two groups based on sex:

- Group 1: 5 males
- Group 2: 5 females

Endpoints: The endpoint for this study was sacrifice on day 2. Mice were anesthetized using isoflurane (1-4 %), then blood was collected through thoracotomy and cardiac puncture using a 25G needle. 100 ul of the collected blood was stored in EDTA tube. The rest of the collected blood was stored in a serum separator tube. The blood samples were sent to Asfaw's lab within less than 4 hours for CBC, Chemistry and electrolyte analysis.

Experimental Procedures

Treatment Preparation: KU7 Drug was given to the PTRU as frozen aliquot and was stored in -20 freezer. For the Safety Study #2, 1020 ul sterile saline was added to KU7 500 ug labeled tubes. The drug was mixed with saline by pipetting.

Treatment Administration: The mice received a single dose of 500ug KU7 in 200ul dose volume on day 0. The drug was administered I.V. through the retro-orbital sinus on day one after anesthetizing the mice using isoflurane (1-4%).

Data

Collection: Data for this study consisted of the CBC, electrolytes and chemistry panel results. Data was entered and maintained in Excel.

Analysis software: Final analysis for data was performed in Prism software suite.

Day numbers: Calendar dates were assigned day numbers beginning with day 0 for the KU7 administration day (12/12/2019). Mice were anesthetized and sacrificed on day 1 (12/13/2019).

CBC, electrolytes and chemistry: the collected blood samples were sent to Asfaw Lab for CBC, electrolyte, and chemistry panel analysis. The results of the treated mice were compared to the results of 3 control female mice which received no treatment. The results were as follows:

- **Chemistry:**
    - **Creatinine, BUN/Creatinine, Calcium, Total protein, Albumin, Cholesterol, GGT, Total bilirubin:** the samples were diluted 1:4 by Dr. Asfaw's Lab to perform the blood analyses for all these parameters and the results were reported as "less than: BUN <5.0 , Creatinine <0.2 , CA<3.3 , Total protein <2.0 , Albumin < 1.0 , Cholesterol < 50 , GGT < 10 , Total bilirubin < 0.1" in all groups including the control group so it was impossible to estimate the actual value and subsequently all these parameters were excluded (one mouse in safety study #1 part 2 male group had a total bilirubin = 0.4)
    - **BUN:** the blood sample was diluted 1:4 by Asfaw's lab to perform the BUN test and in some mice the results were reported as "< 0.5" and subsequently the BUN for these mice were excluded from the analysis. The male group in safety study #1 part 1 was excluded because it had only 1 mouse that was not reported as less than.
    - **CBC:** the blood samples for CBC for 3 males in toxicity study #1 part 1 coagulated so the CBC results for the male group in this study contains the results of 2 males only

*Raw data from Asfaw Lab, Excel file containing all the organized blood results, Prism analysis files and Pathology report will be included with this report.
* For BALB/c strain blood results please refer to the following link:
https://www.criver.com/sites/default/files/Technical%20Resources/Clinical%20Pathology%20Data%20for%20BALB_c%20Mouse%20Colonies%20in%20North%20America%20for%20January%202008%20-%20December%202012.pdf

In general, compared to values of normal animals in the link above, the following chemistries and CBCs appear to be low:

- **Potassium (normal values confirmed with CRL and Jax)**
- **Mono**
- **RDW %**
- **MCV**

In general, compared to values of normal animals in the link above, the following appear to be high:

- **MCHC**

Other points to note:

- Regarding creatinine, the normal range for males and females is 0.2-0.4 and 0.2-0.5 mg/dL, respectively. The instrument used to evaluate this parameter was not sensitive enough to provide meaningful data, so all samples tested including controls were reported as 0.2 mg/dL in 4X diluted samples.

- All graphs below show mean +/- standard deviation.

- Min and max of the reported normal ranges are also reported where available, sourced from the Charles River link above.

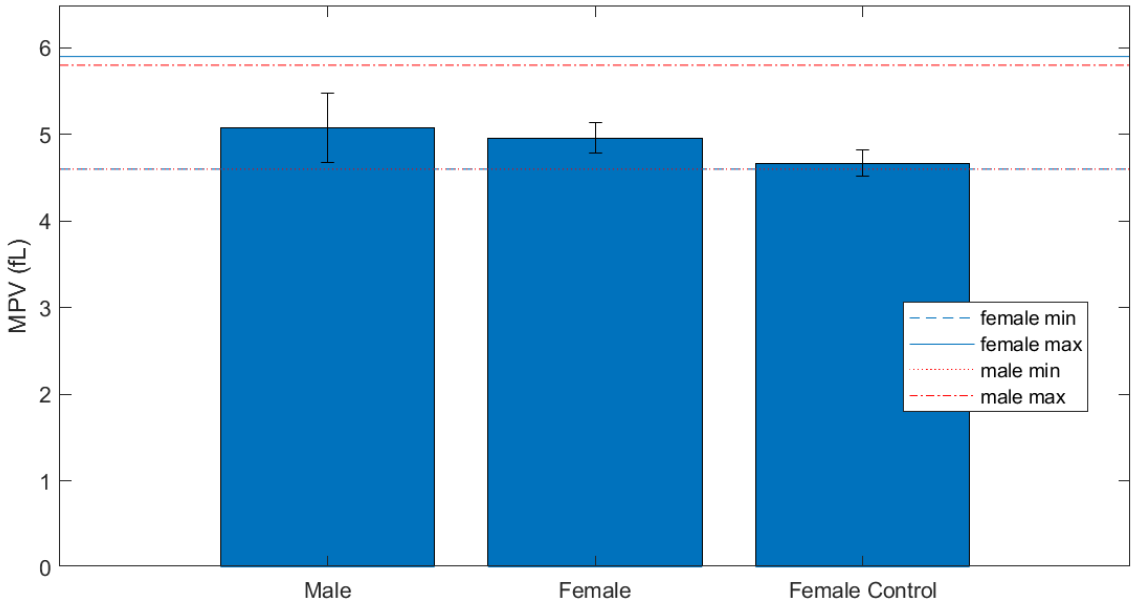
MPV (fL)
0
1
2
3
4
5
6
Male
Female
Female Control
female min
female max
male min
male max

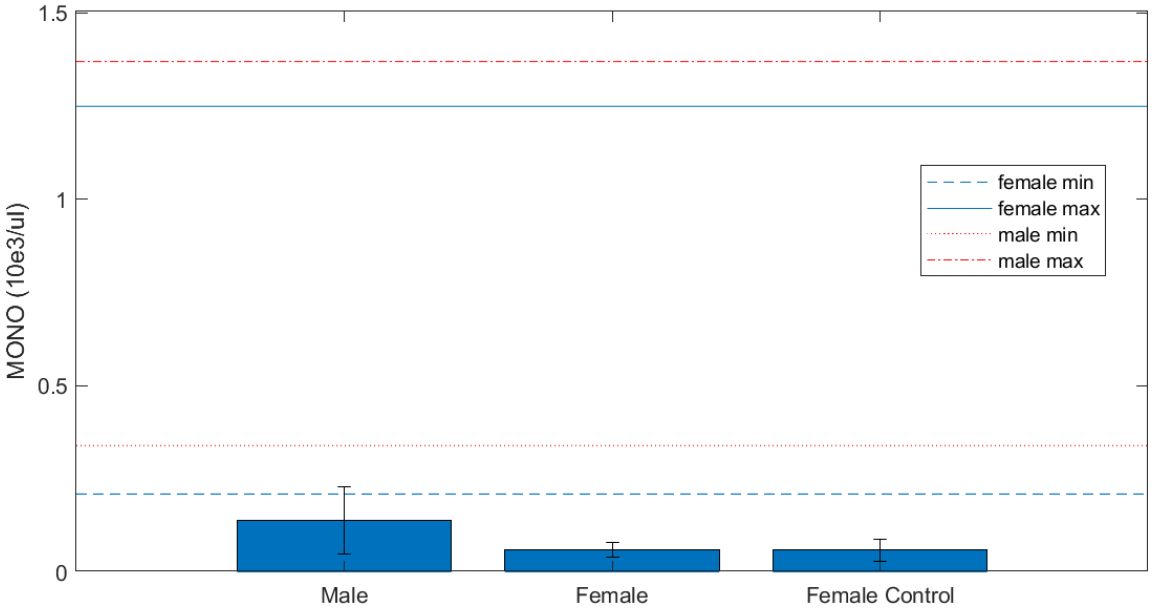
MONO (10e3/ul)
0
0.5
1
1.5
Male
Female
Female Control
female min
female max
male min
male max

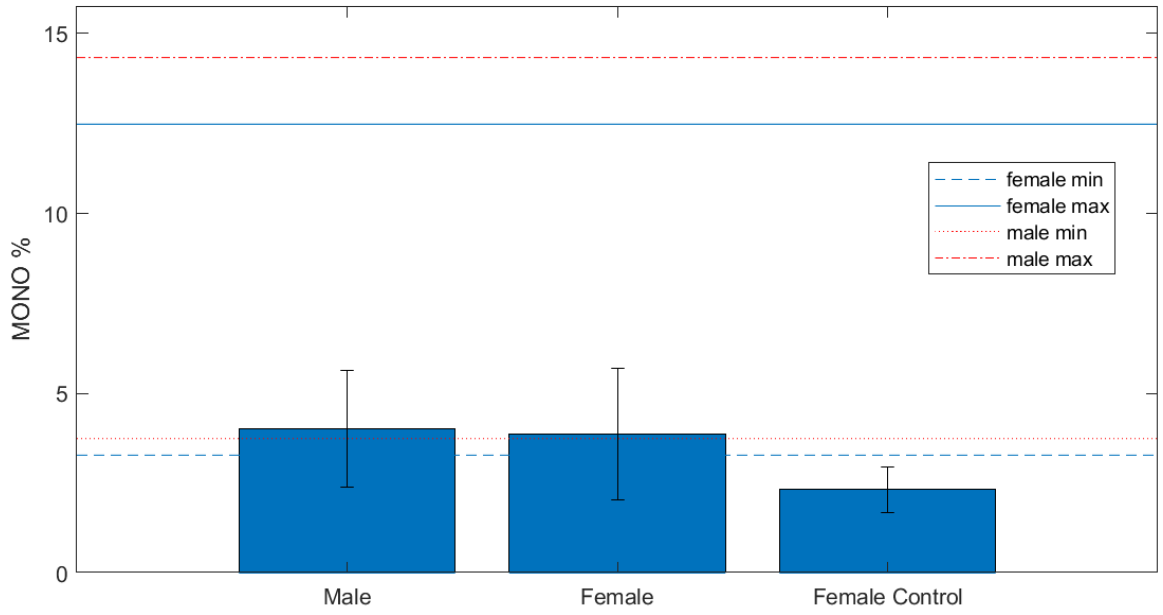
MONO %
15
10
5
0
female min
female max
male min
male max
Male
Female
Female Control

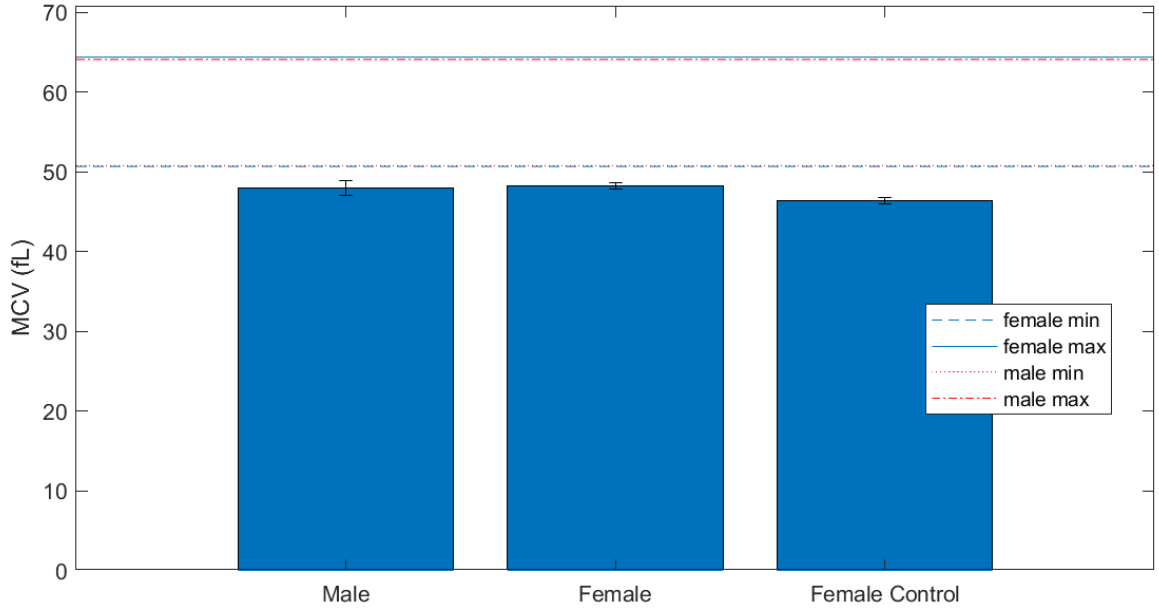
MCV (fL)
70
60
50
40
30
20
10
0
female min
female max
male min
male max
Male
Female
Female Control

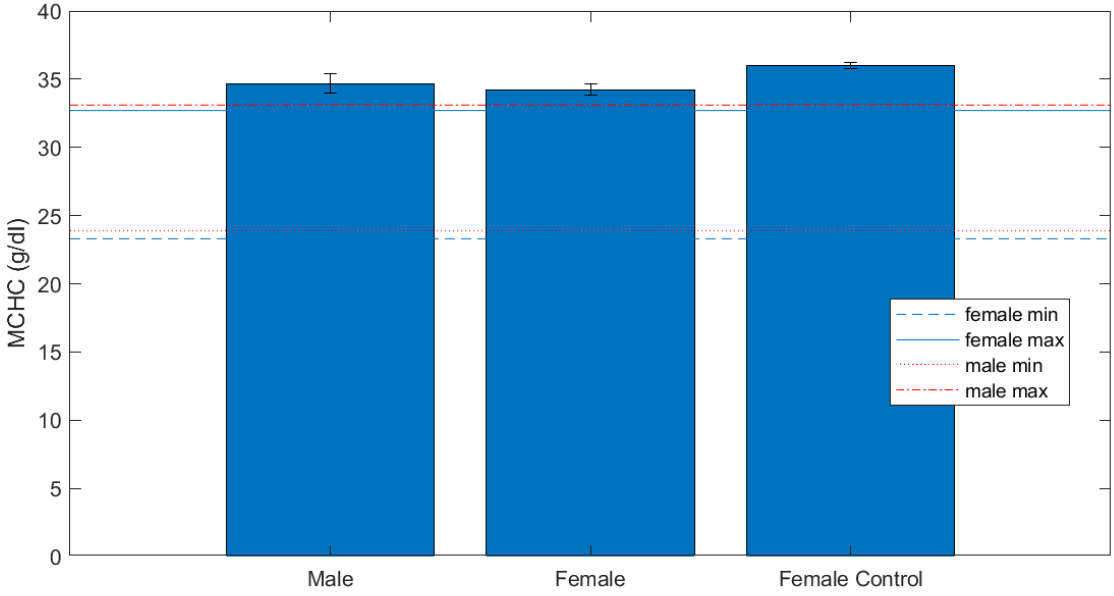
MCHC (g/dl)
40
35
30
25
20
15
10
5
0
Male
Female
Female Control
female min
female max
male min
male max

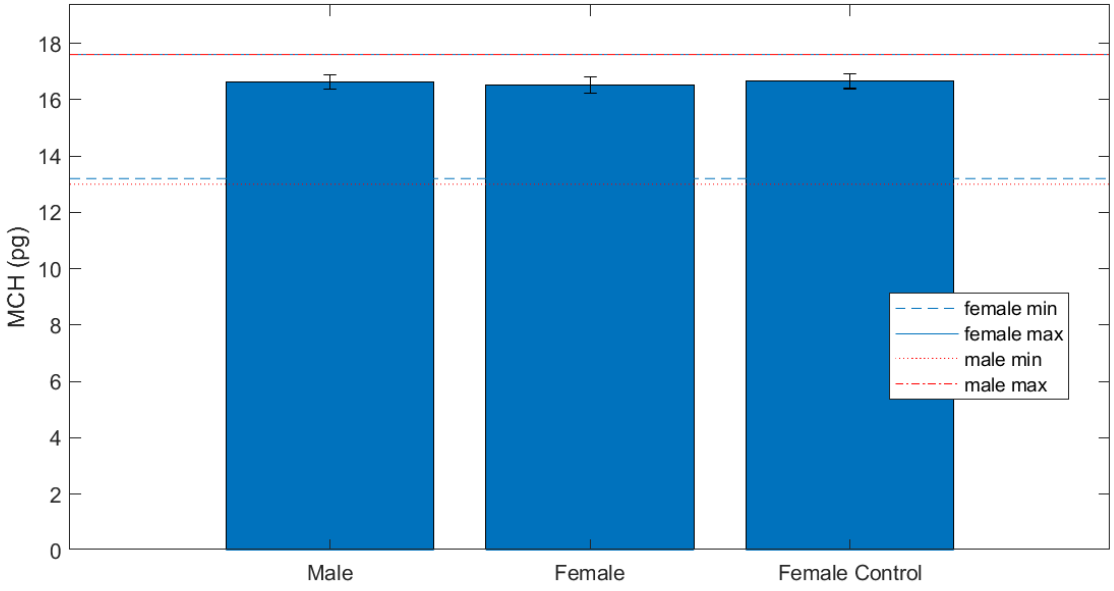
MCH (pg)
18
16
14
12
10
8
6
4
2
0
Male
Female
Female Control
female min
female max
male min
male max

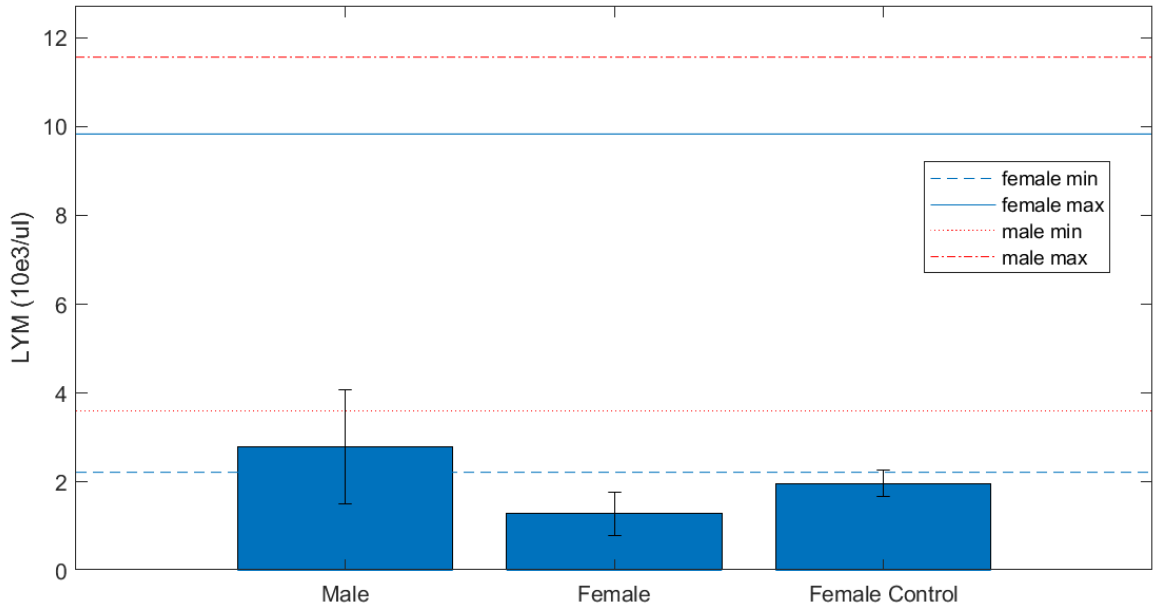
LYM (10e3/ul)
0
2
4
6
8
10
12
female min
female max
male min
male max
Male
Female
Female Control

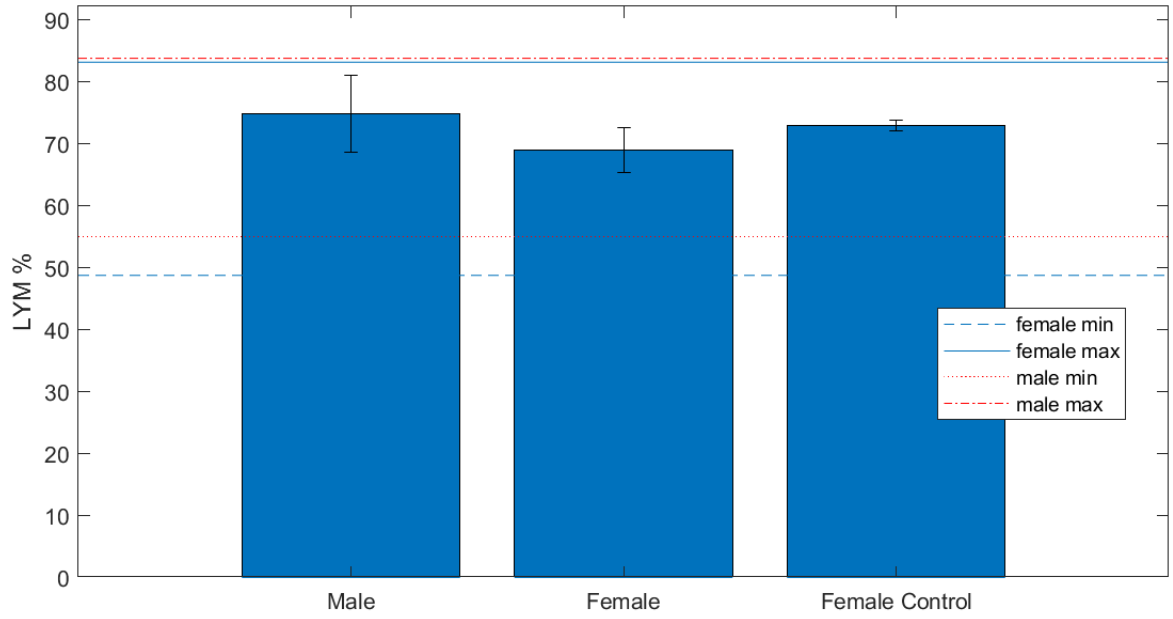
LYM %
0
10
20
30
40
50
60
70
80
90
female min
female max
male min
male max
Male
Female
Female Control

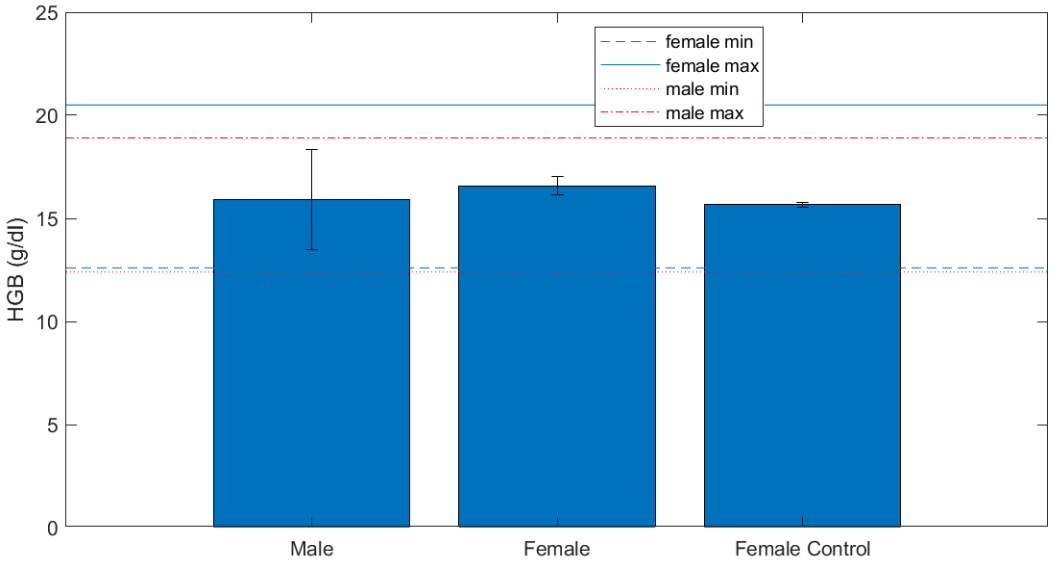
HGB (g/dl)
25
20
15
10
5
0
female min
female max
male min
male max
Male
Female
Female Control

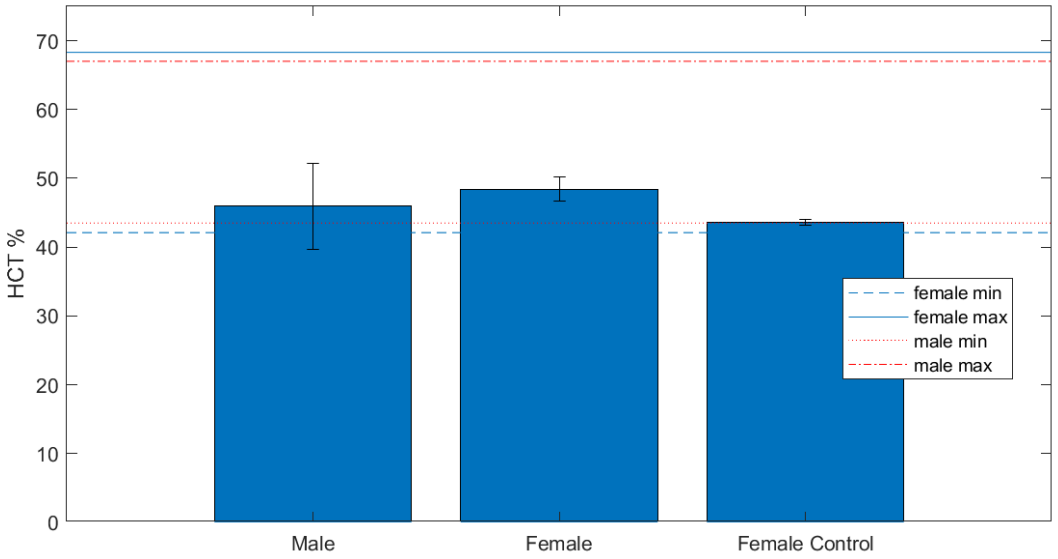
HCT %
70
60
50
40
30
20
10
0
female min
female max
male min
male max
Male
Female
Female Control

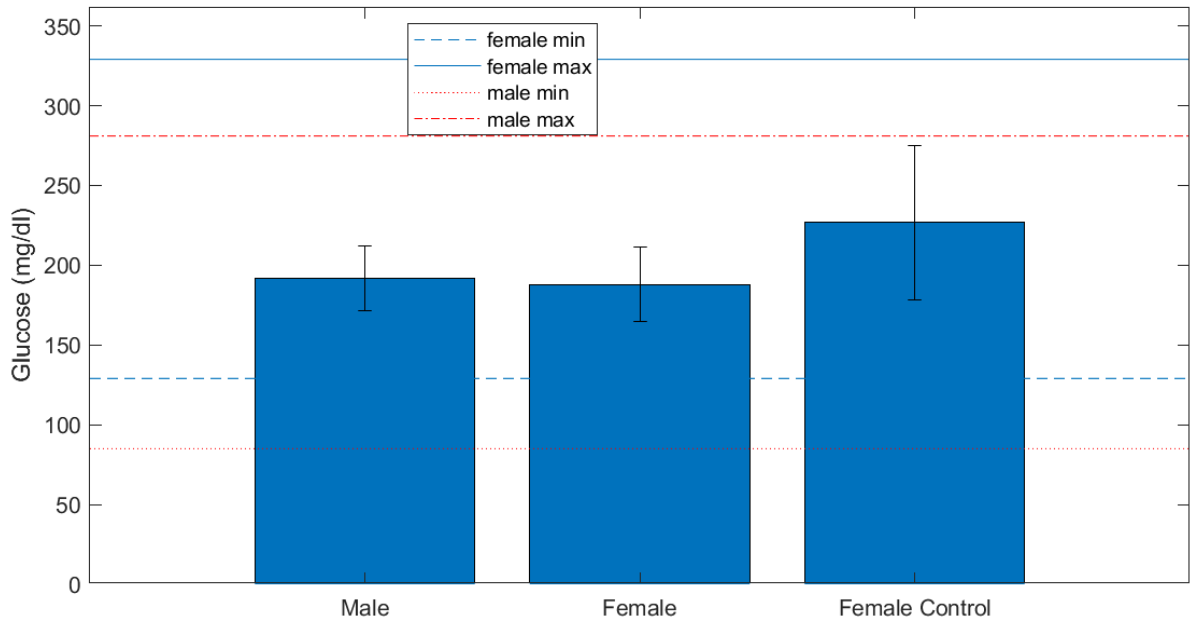
female min
female max
male min
male max
Glucose (mg/dl)
350
300
250
200
150
100
50
0
Male
Female
Female Control

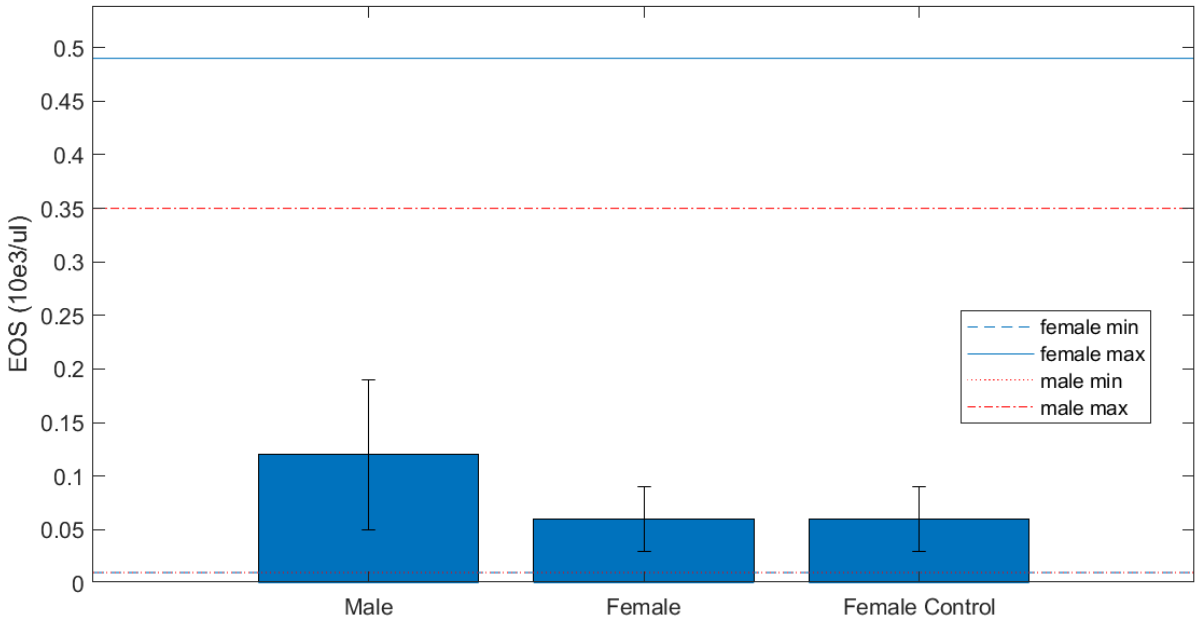
female min
female max
male min
male max
EOS (10e3/ul)
0.5
0.45
0.4
0.35
0.3
0.25
0.2
0.15
0.1
0.05
0
Male
Female
Female Control

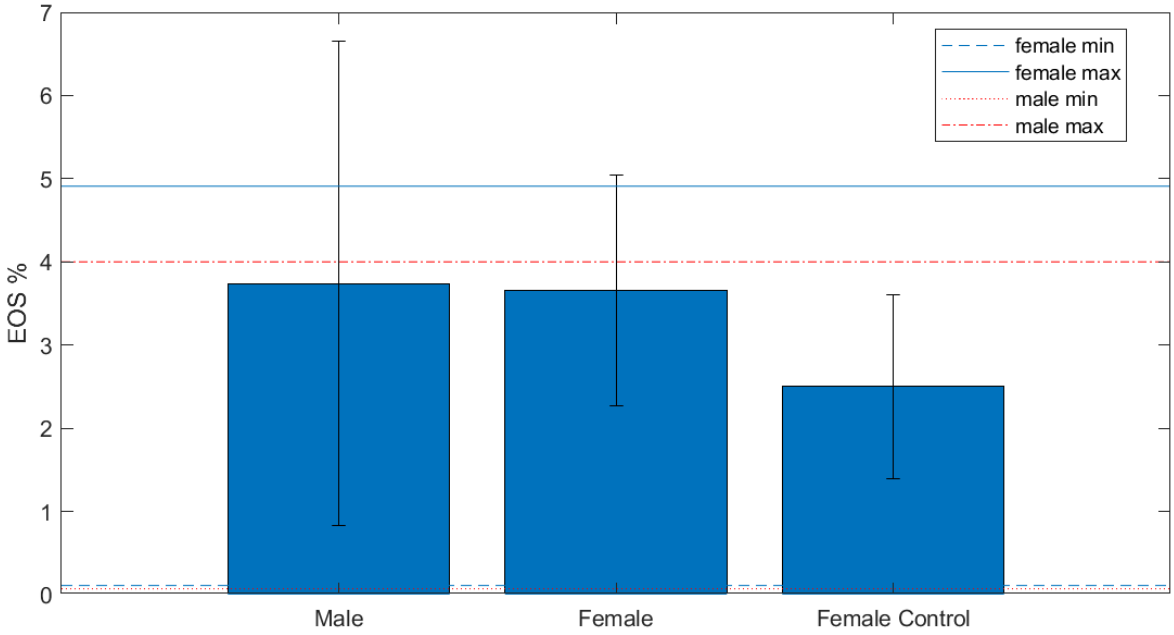
EOS %
0
1
2
3
4
5
6
7
Male
Female
Female Control
female min
female max
male min
male max

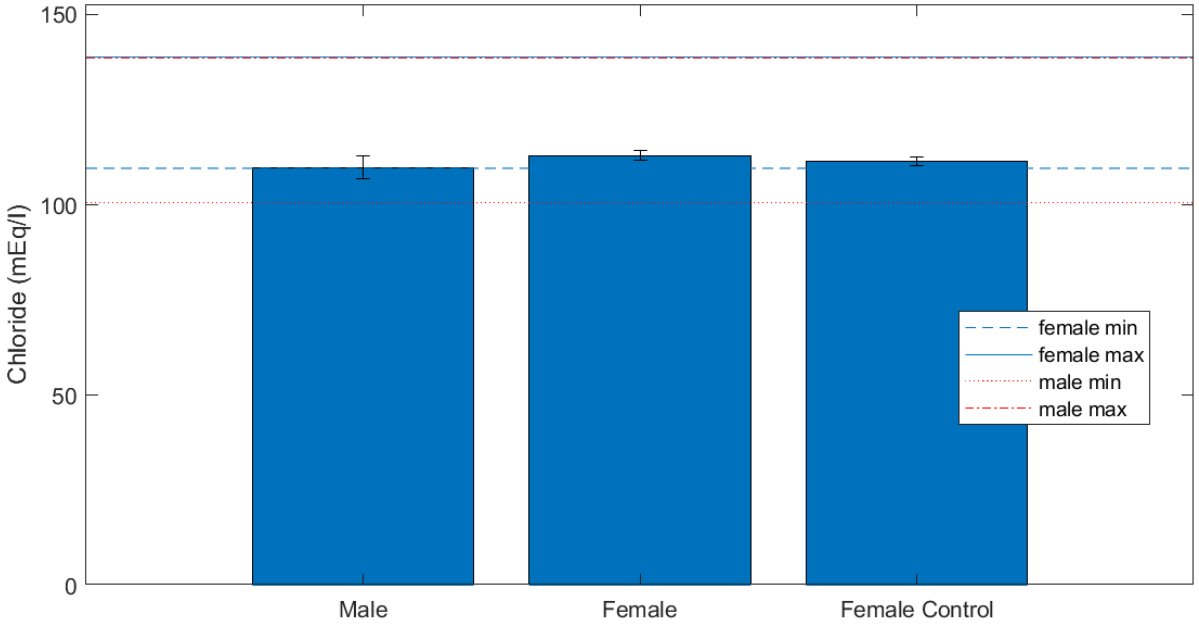
Chloride (mEq/l)
0
50
100
150
Male
Female
Female Control
female min
female max
male min
male max

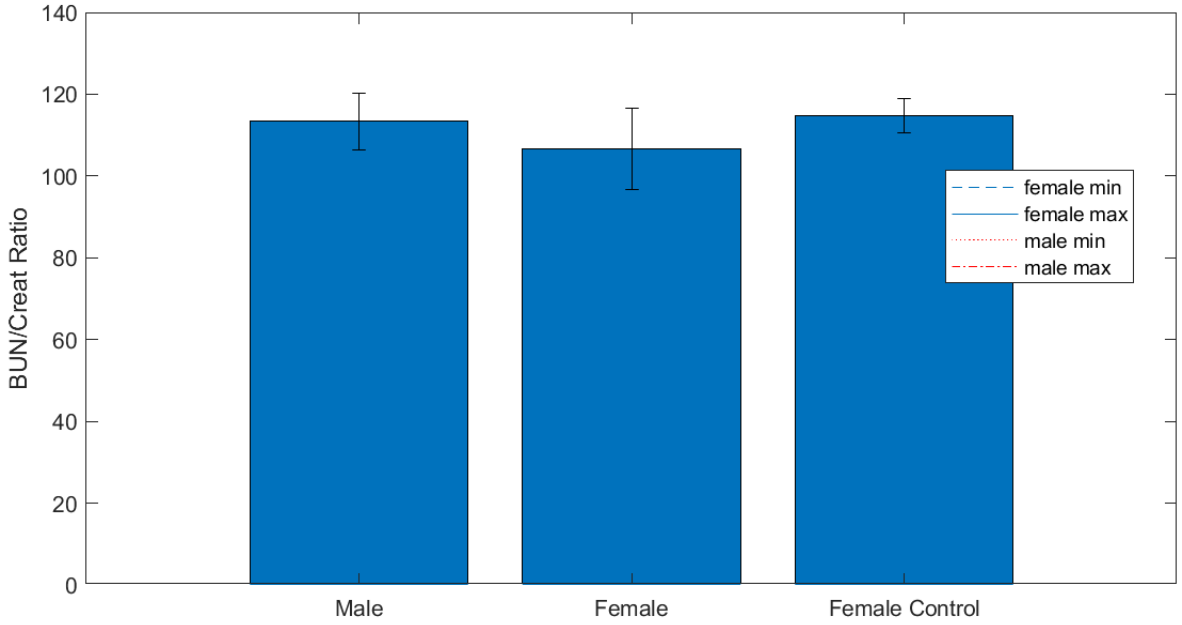
140
120
100
80
60
40
20
0
BUN/Creat Ratio
female min
female max
male min
male max
Male
Female
Female Control

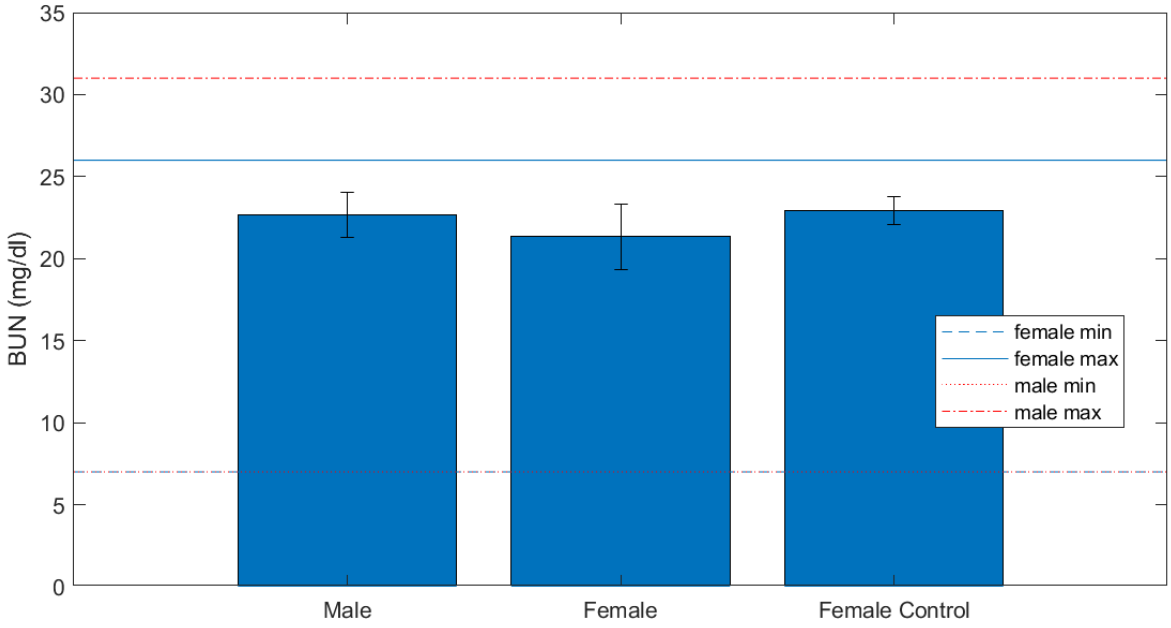
35
30
25
20
15
10
5
0
BUN (mg/dl)
female min
female max
male min
male max
Male
Female
Female Control

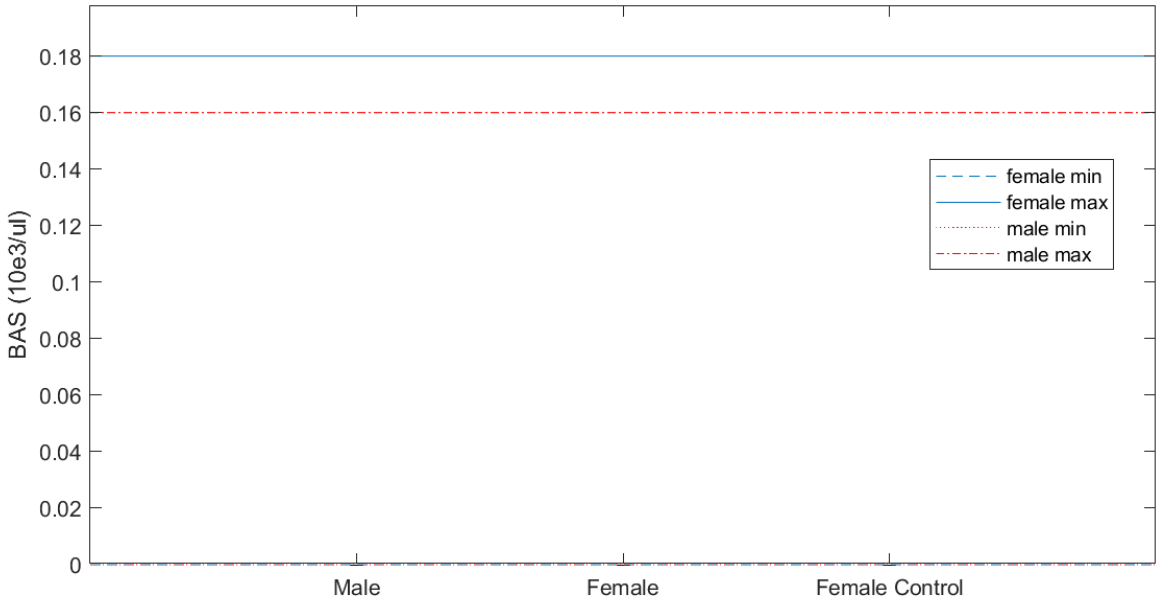
BAS (10e3/ul)
0.18
0.16
0.14
0.12
0.1
0.08
0.06
0.04
0.02
0
female min
female max
male min
male max
Male
Female
Female Control

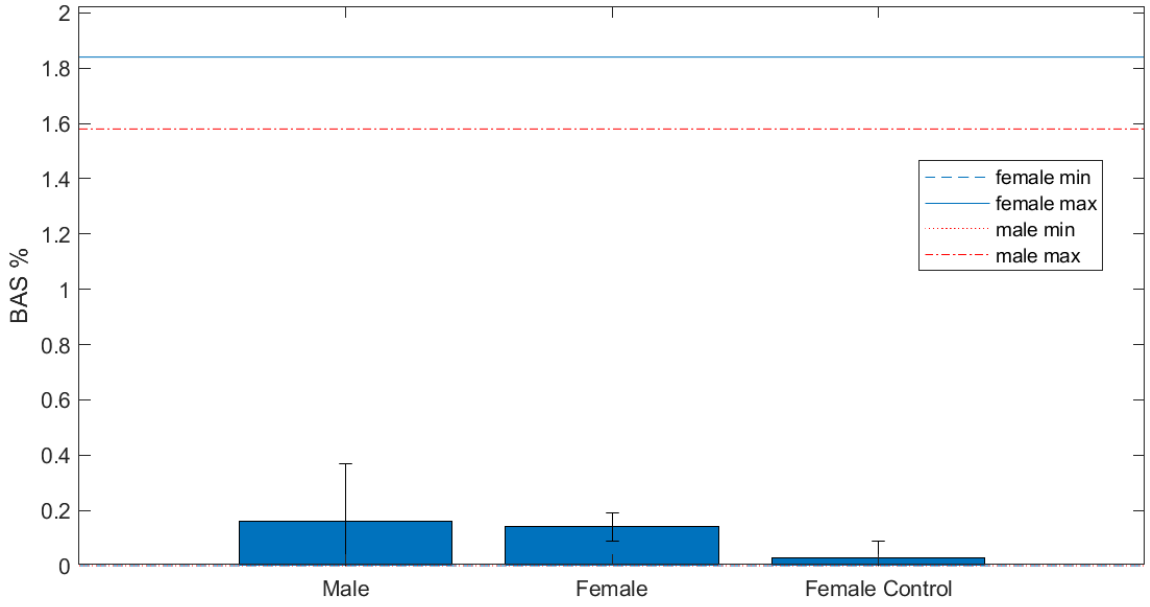
BAS %
2
1.8
1.6
1.4
1.2
1
0.8
0.6
0.4
0.2
0
female min
female max
male min
male max
Male
Female
Female Control

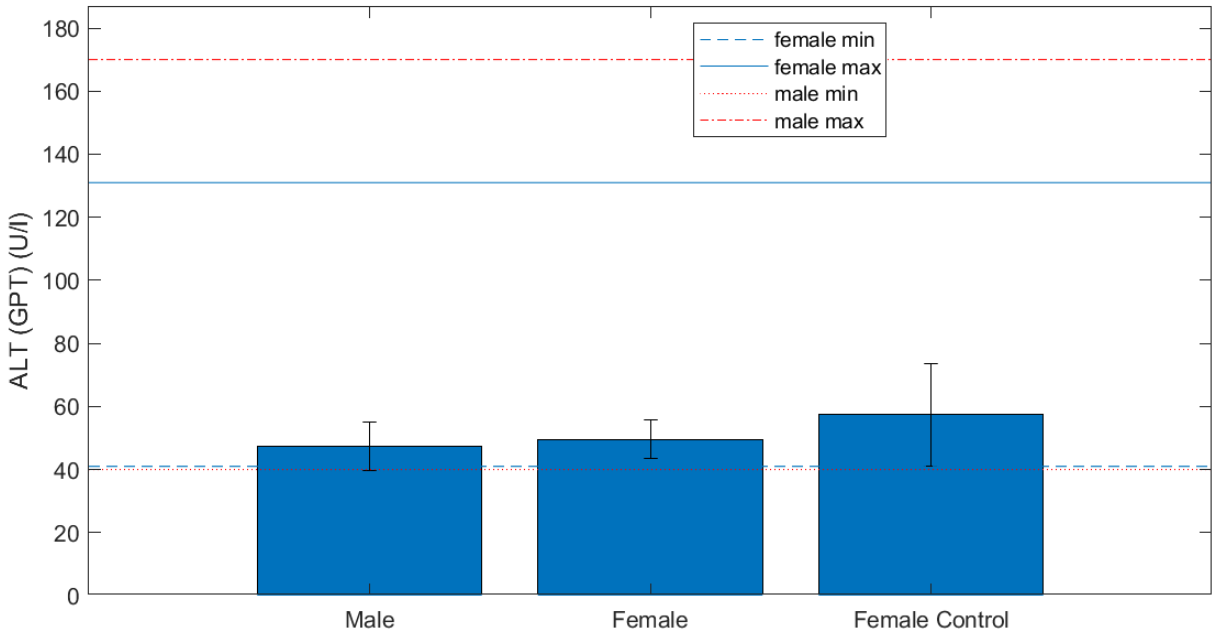
female min
female max
male min
male max
ALT (GPT) (U/l)
180
160
140
120
100
80
60
40
20
0
Male
Female
Female Control

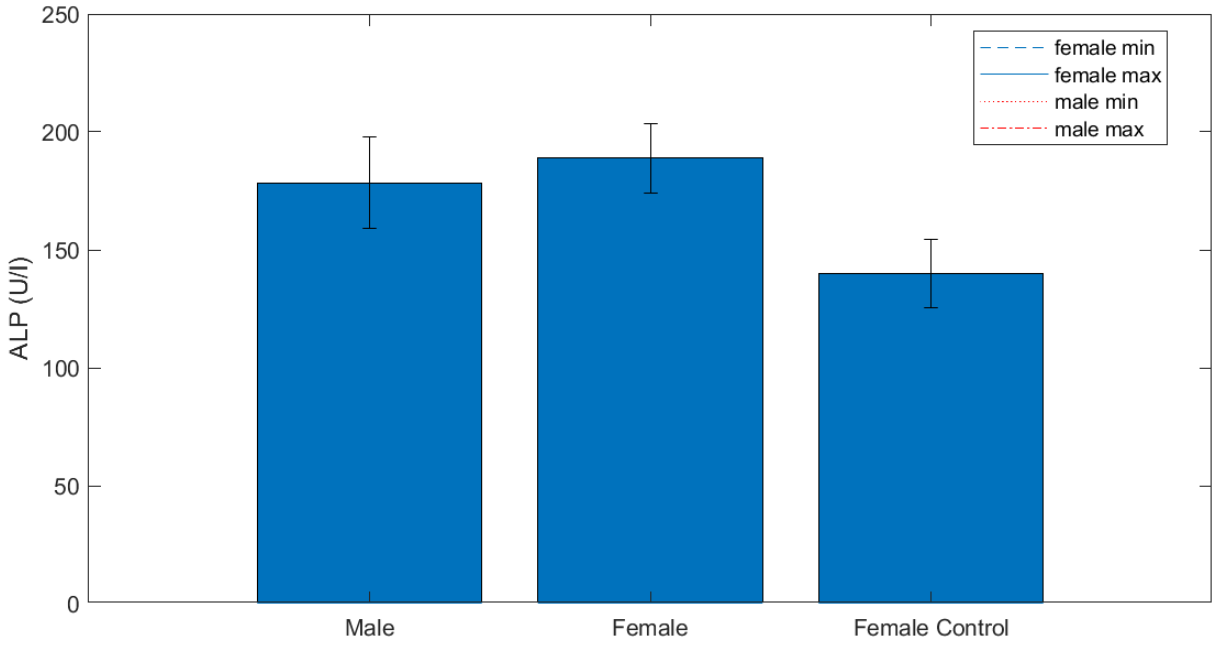
female min
female max
male min
male max
ALP (U/l)
250
200
150
100
50
0
Male
Female
Female Control

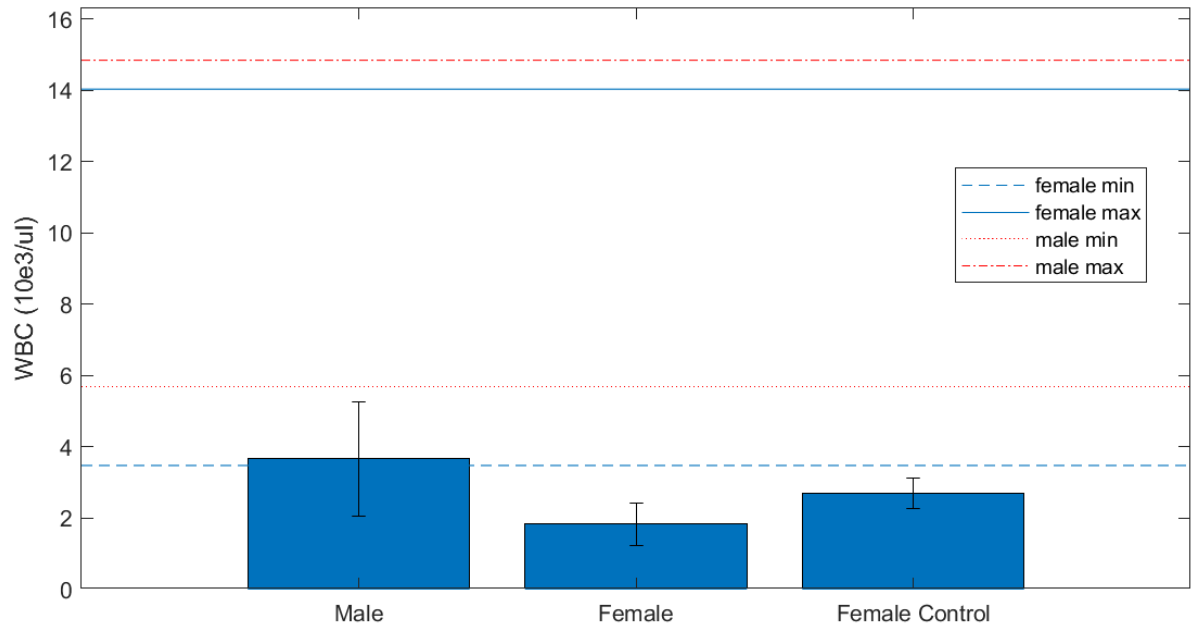
WBC (10e3/ul)
16
14
12
10
8
6
4
2
0
female min
female max
male min
male max
Male
Female
Female Control

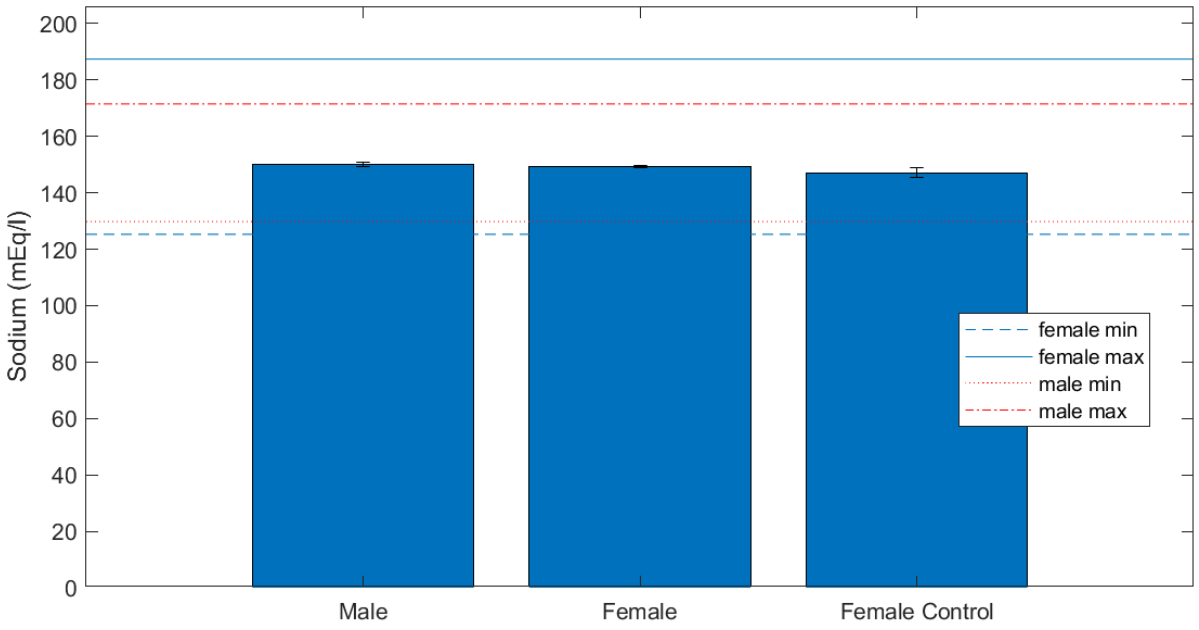
Sodium (mEq/l)
200
180
160
140
120
100
80
60
40
20
0
female min
female max
male min
male max
Male
Female
Female Control

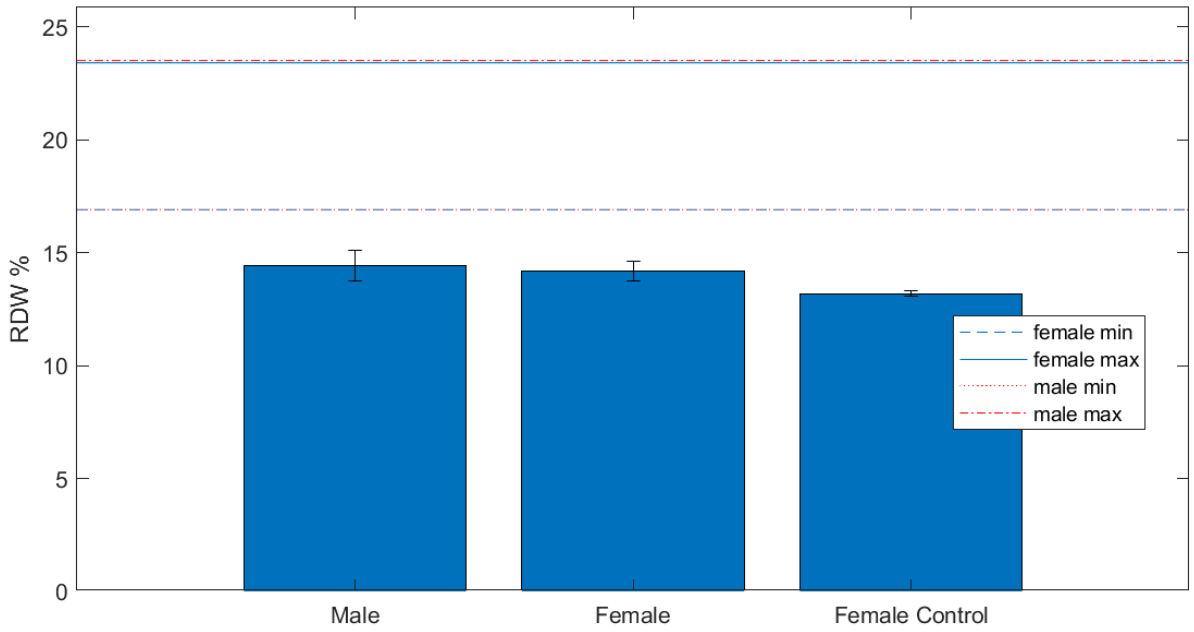
25
20
15
10
5
0
RDW %
female min
female max
male min
male max
Male
Female
Female Control

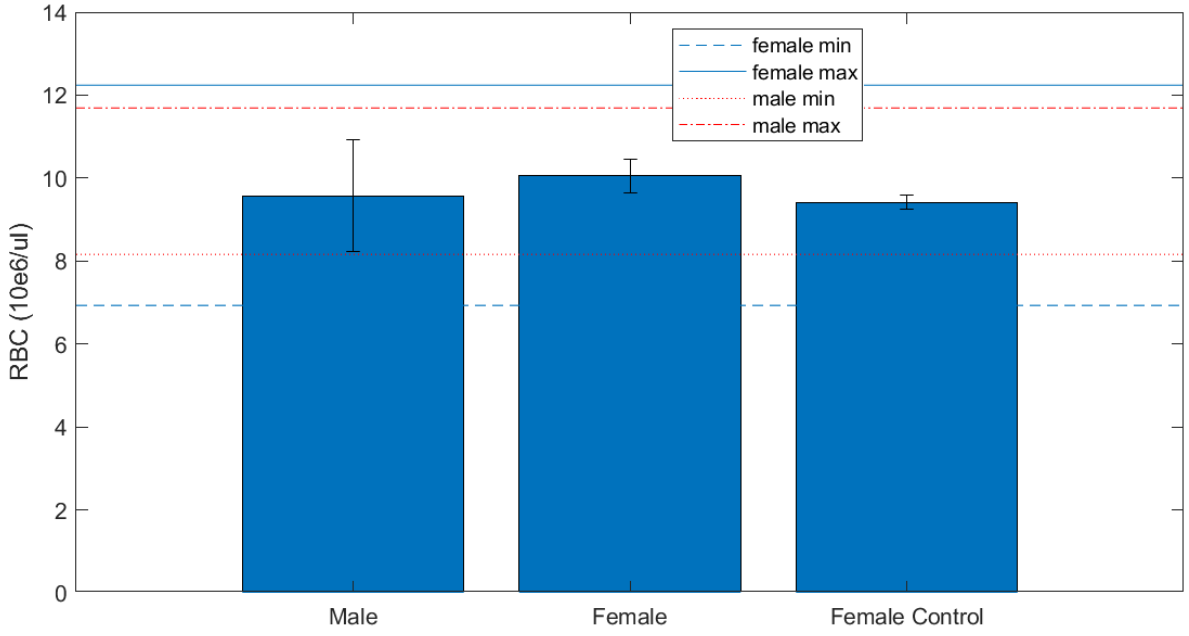
14
12
10
8
6
4
2
0
RBC (10e6/ul)
female min
female max
male min
male max
Male
Female
Female Control

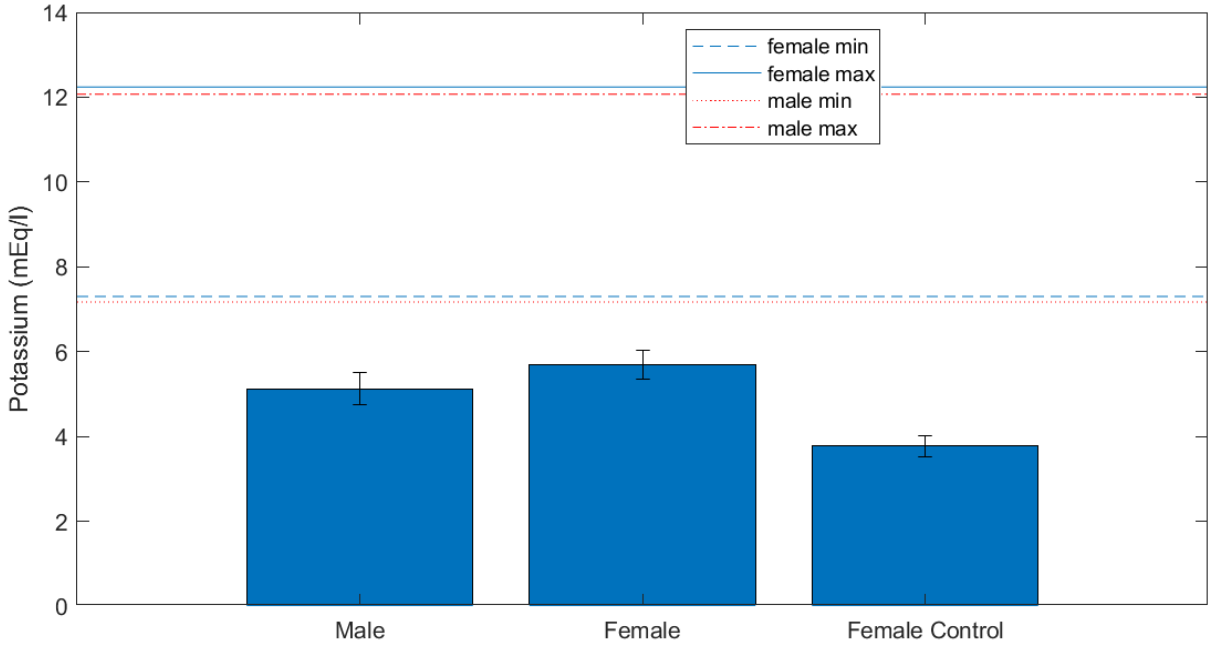
female min
female max
male min
male max
Potassium (mEq/l)
0
2
4
6
8
10
12
14
Male
Female
Female Control

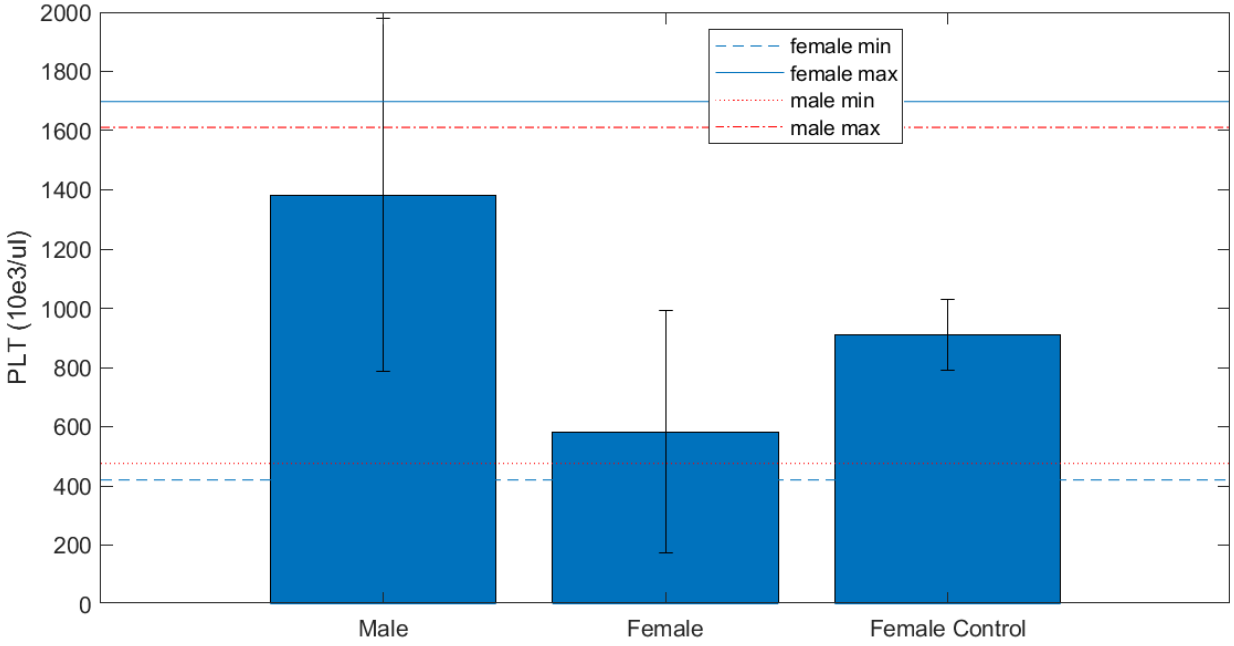
female min
female max
male min
male max
PLT (10e3/ul)
0
200
400
600
800
1000
1200
1400
1600
1800
2000
Male
Female
Female Control

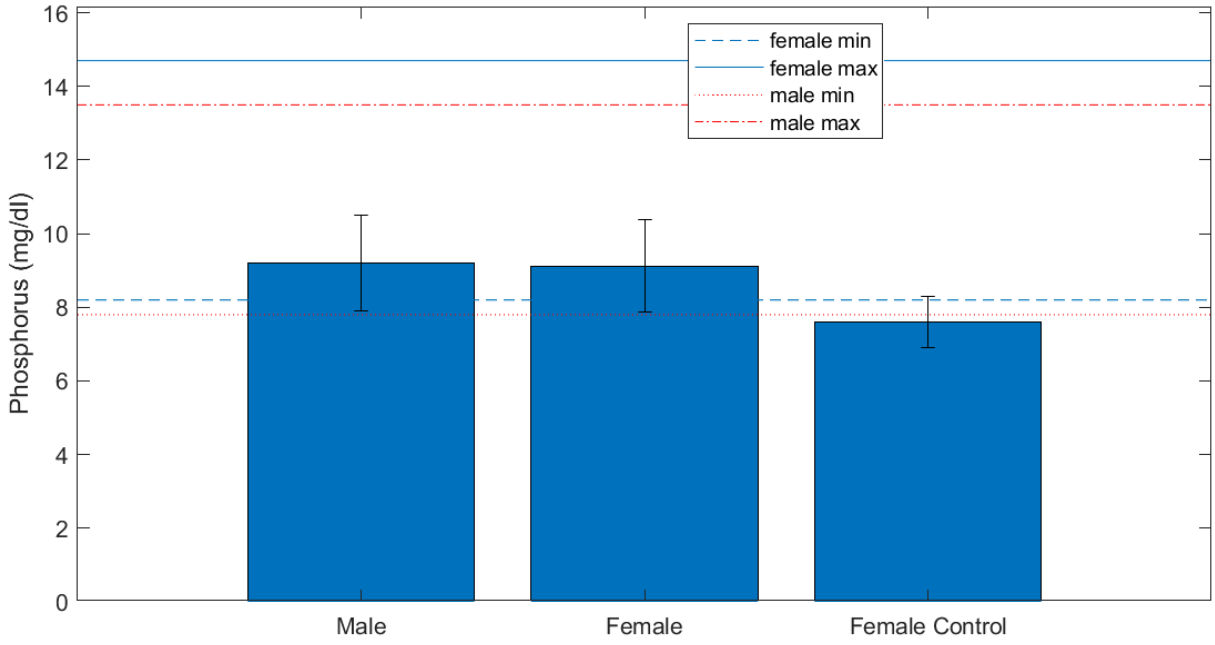
female min
female max
male min
male max
Phosphorus (mg/dl)
16
14
12
10
8
6
4
2
0
Male
Female
Female Control

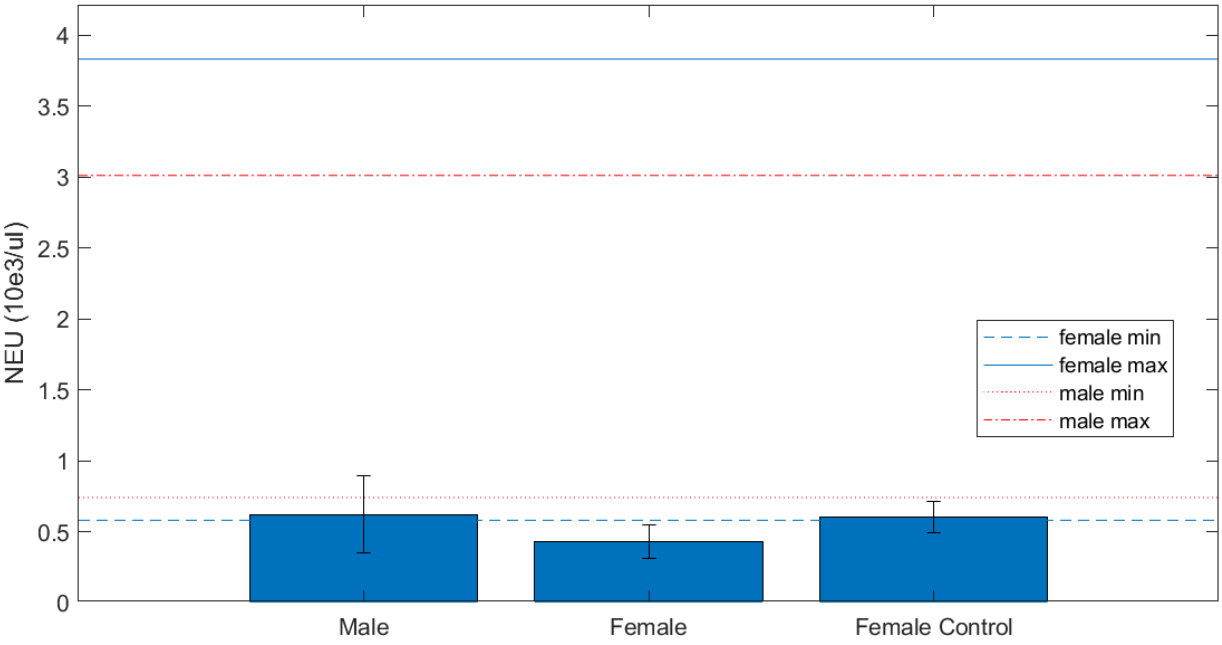
female min
female max
male min
male max
NEU (10e3/ul)
4
3.5
3
2.5
2
1.5
1
0.5
0
Male
Female
Female Control

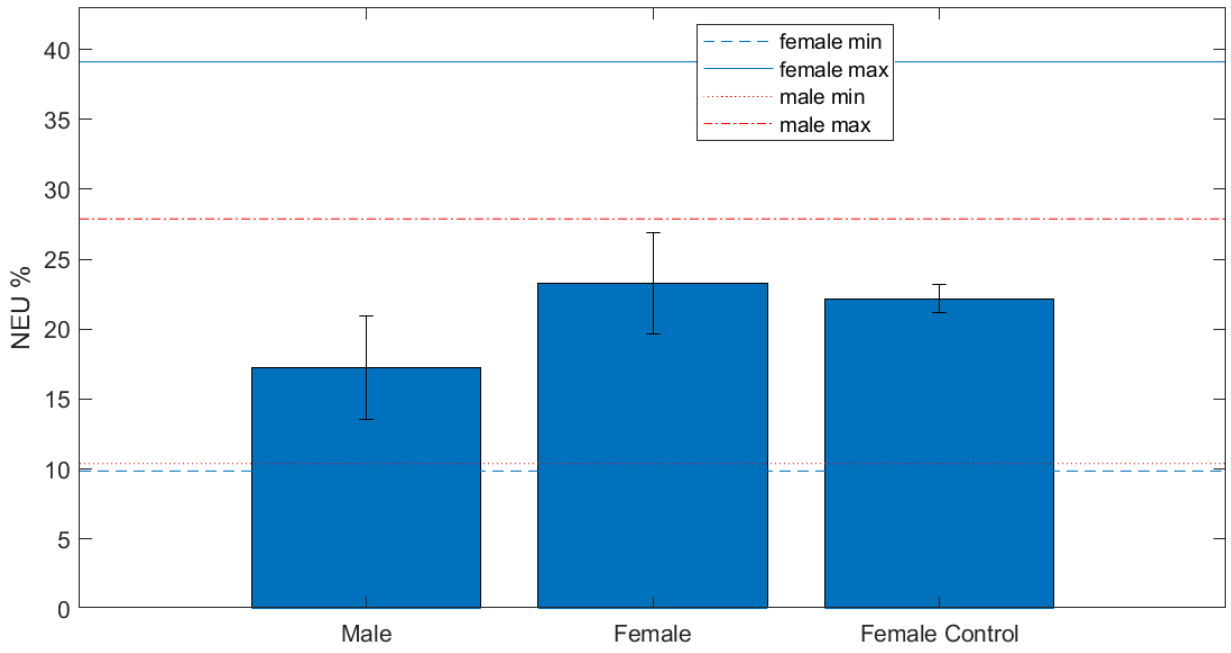
female min
female max
male min
male max
NEU %
0
5
10
15
20
25
30
35
40
Male
Female
Female Control

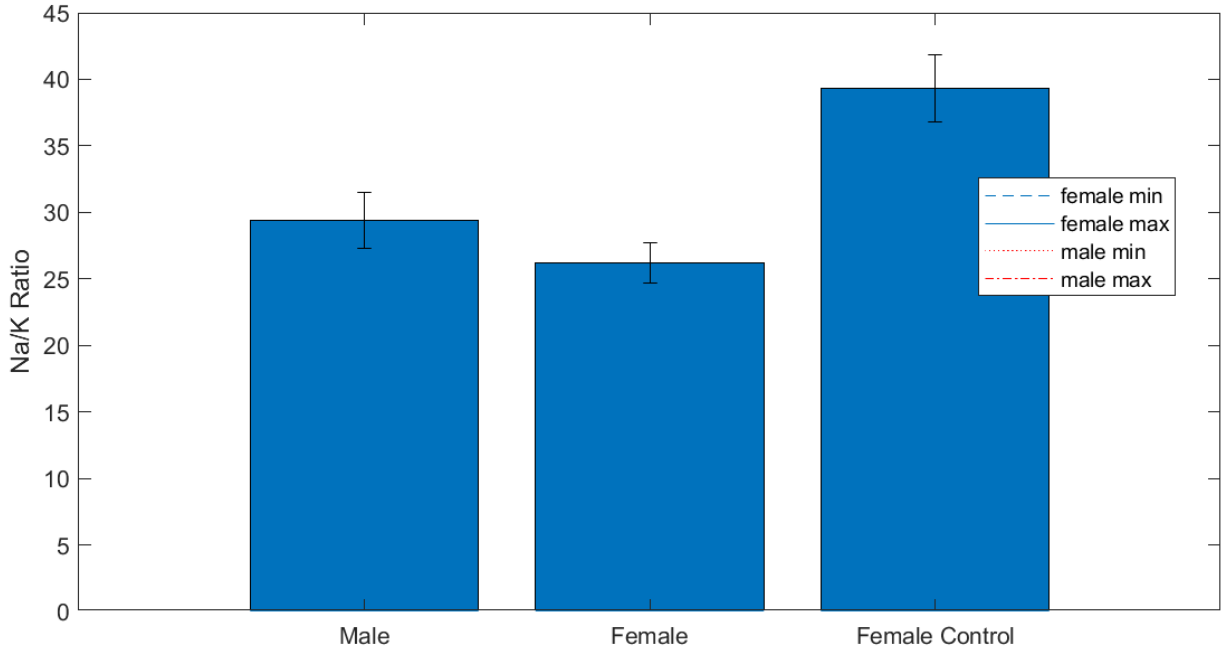
female min
female max
male min
male max
Na/K Ratio
0
5
10
15
20
25
30
35
40
45
Male
Female
Female Control

Study Design

Experimental Aims: complete no observed adverse event level (NOAEL) study, evaluation of hematologic parameters and gross organ pathology in response to high dose KU7.

Experimental Subjects: Subjects were 10 mice, 6-8 weeks old at study start, 5 males, 5 females, BALB/c, Charles River Laboratories.

Housing and Husbandry: Subjects were housed in room 1033 in Vivarium on the Duke campus. Their room was climate/temp controlled and on a 12-hour light dark cycle. Food and bedding were changed weekly by DLAR staff.

Experimental Groups:

- Mice were treated with 100 ug KU7 qd x 5, beginning day 1. Clinical observations were conducted on days 1 through 8 for changes in activity, posture, and grooming.
- A control group consisted of 5 females which did not receive any treatment was used for clinical observation comparison and to decide the normal range for the blood analysis results (n=3 for blood analysis).

Endpoints: The endpoint for this study was sacrifice on day 8 after monitoring the mice for the last clinical observation and recording the last weight measurements. Mice were anesthetized using isoflurane 1-4%, then blood was collected through thoracotomy and cardiac puncture using a 25G needle. 100 ul of the collected blood was collected into a tube containing EDTA. The rest of the blood was stored in a serum separator tube. The blood samples were sent to the lab within less than 4 hours for CBC, Chemistry and electrolyte analysis. After collecting the blood sample, the mouse was perfused with 10 ml saline followed by 10 ml NBF. Then the following organs were collected and stored in NBF: Brain, Lungs, Heart, Liver, Spleen, Kidney, Ovaries and Testes.

Experimental Procedures

Treatment Preparation: KU7 was given to the PTRU as frozen aliquot and was stored in -20 freezer. For Safety Study #3, 1164 ul sterile saline was added to KU7 100 ug labeled tubes. The compound was mixed with saline by pipetting.

Treatment Administration: Mice received 1 dose of 100ug KU7 each day for 5 consecutive days in a 200ul dose volume via the retro-orbital sinus after anesthetizing with isoflurane (1-4 %).

Data:

Data for this study consisted of the clinical observation notes, Weight, collected organs histology, CBC, electrolytes and chemistry panel results. Data was entered and maintained in Excel.

Analysis software: Final analysis for data was performed in Prism software suite.

Subject Weights: Body weights were measured daily using a digital scale. The mice weight in both study part remains within the normal weight range of the breed.

Body weight data from Charles River Laboratories:

Body weights of mice in Safety Study #3:

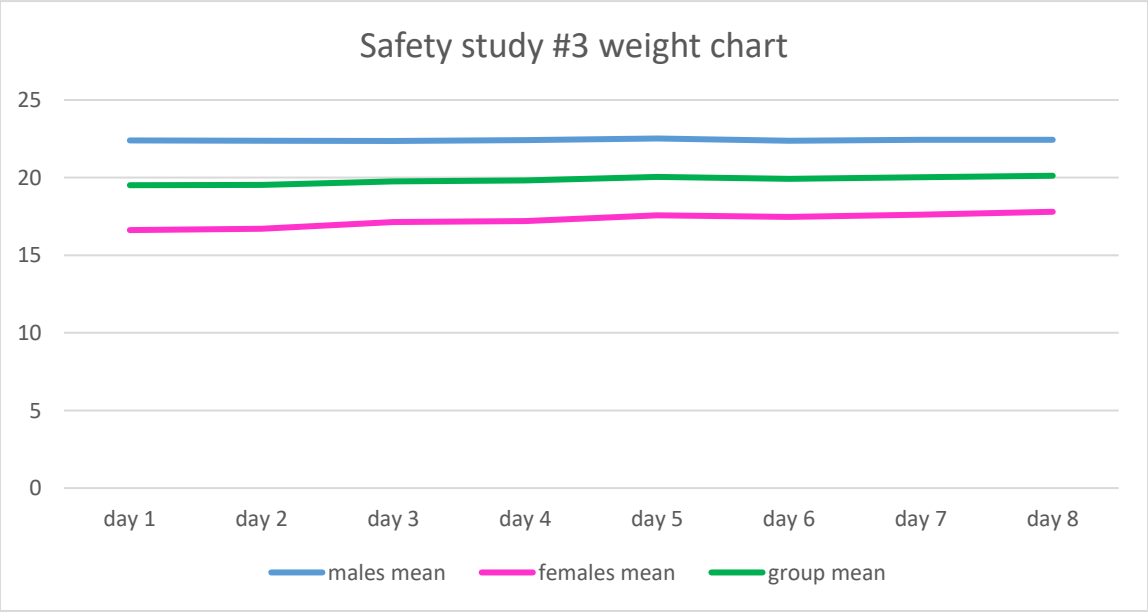

Collection

Day numbers: Calendar dates were assigned day numbers beginning with day 1 for the KU7 administration day (12/16/2019. Mice were anesthetized and sacrificed on day 8 (12/23/2019).

Clinical Observations: Mice were monitored the 5 hours post injection then daily for one hour each day. The clinical observations were made by placing the mice in their home cage in a quiet dark room and compare their behavior to control mice which did not receive any treatment. Clinical observations consisted of the following:

- General body condition
- Posture
- Behavior: including response to external stimuli (tapping on the cage)
- Activity
- Grooming
- Feces

The treated mice clinical observation in both study parts were similar to control group clinical observation except in the first 10-20 minutes post injection on day 1 where the treated mice were still sedated for 1 minute after isoflurane flow was stopped and then assumed a hunched position for the next 10-20 minutes which could be due to the isoflurane sedation.

Collected Organs Histology: In process, to be added.

CBC, electrolytes and chemistry: the collected blood samples were sent to Dr. Asfaw's lab for CBC, electrolyte and chemistry panel analysis. The results of the treated mice were compared to the results of 3 control female mice which received no treatment. The results were as follow:

- **<u>Chemistry:</u>**
    - **Creatinine, BUN/Creatinine, Calcium, Total protein, Albumin, Cholesterol, GGT, Total bilirubin:** the samples were diluted 1:4 by Asfaw's Lab to perform the blood analyses for all these parameters and the results were reported as "less than: BUN <5.0 , Creatinine <0.2 , CA<3.3 , Total protein <2.0 , Albumin < 1.0 , Cholesterol < 50 , GGT < 10 , Total bilirubin <

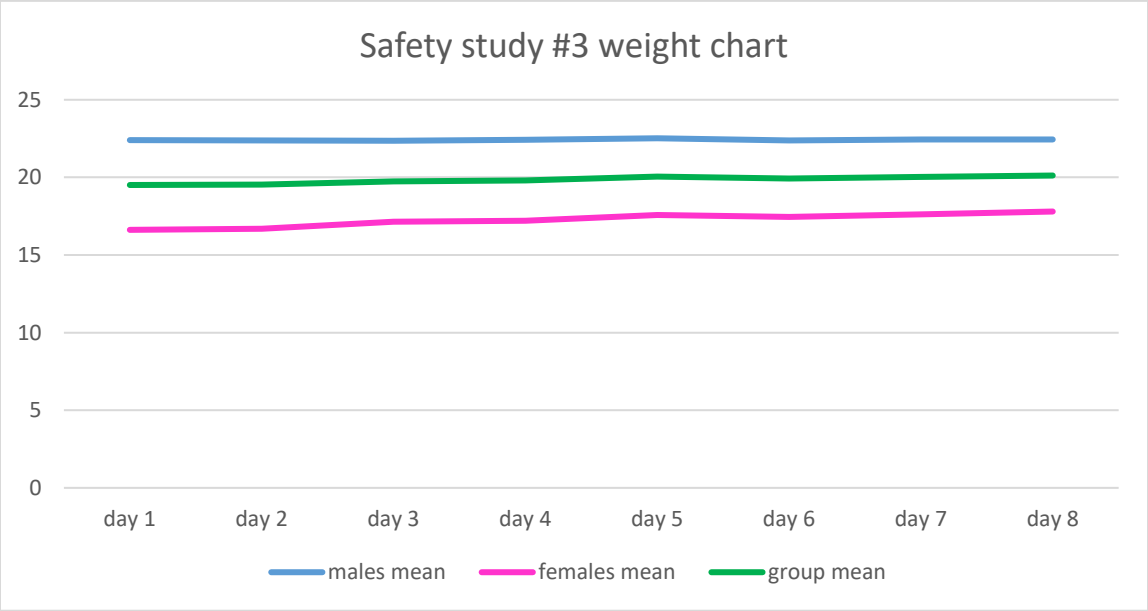

0.1" in all groups including the control group, so it was impossible to estimate the actual value and subsequently all these parameters were excluded (one mouse in safety study #1 part 2 male group had a Total bilirubin=0.4)

- **BUN:** the blood sample was diluted 4 times by Asfaw's lab to perform the BUN test and in some mice the results were reported as "< 0.5" and subsequently the BUN for these mice were excluded from the analysis. The male group in safety study #1 part 1 was excluded because it had only 1 mouse that was not reported as less than.
- **CBC:** the blood samples for CBC for 3 males in toxicity study #1 part 1 coagulated so the CBC results for the male group in this study contains the results of 2 males only

*Raw data from Asfaw Lab, Excel file containing all the organized blood results, Prism analysis files and Pathology report will be included with this report.
* For BALB/c strain blood results please refer to the following link:
https://www.criver.com/sites/default/files/Technical%20Resources/Clinical%20Pathology%20Data%20for%20BALB_c%20Mouse%20Colonies%20in%20North%20America%20for%20January%202008%20-%20December%202012.pdf

In general, compared to values of normal animals in the link above, the following chemistries and CBCs appear to be low:

- **Potassium (normal values confirmed with CRL and Jax)**
- **WBCs**
- **Lymph**
- **Mono**
- **RDW %**
- **MCV**
- **Neu**

In general, compared to values of normal animals in the link above, the following appear to be high:

- **MCHC**

Other points to note:

- Regarding creatinine, the normal range for males and females is 0.2-0.4 and 0.2-0.5 mg/dL, respectively. The instrument used to evaluate this parameter was not sensitive enough to provide meaningful data, so all samples tested including controls were reported as 0.2 mg/dL in 4X diluted samples.

- All graphs below show mean +/- standard deviation.

- Min and max of the reported normal ranges are also reported where available, sourced from the Charles River link above.

- Normal body weights, as shown by Charles River Laboratories:

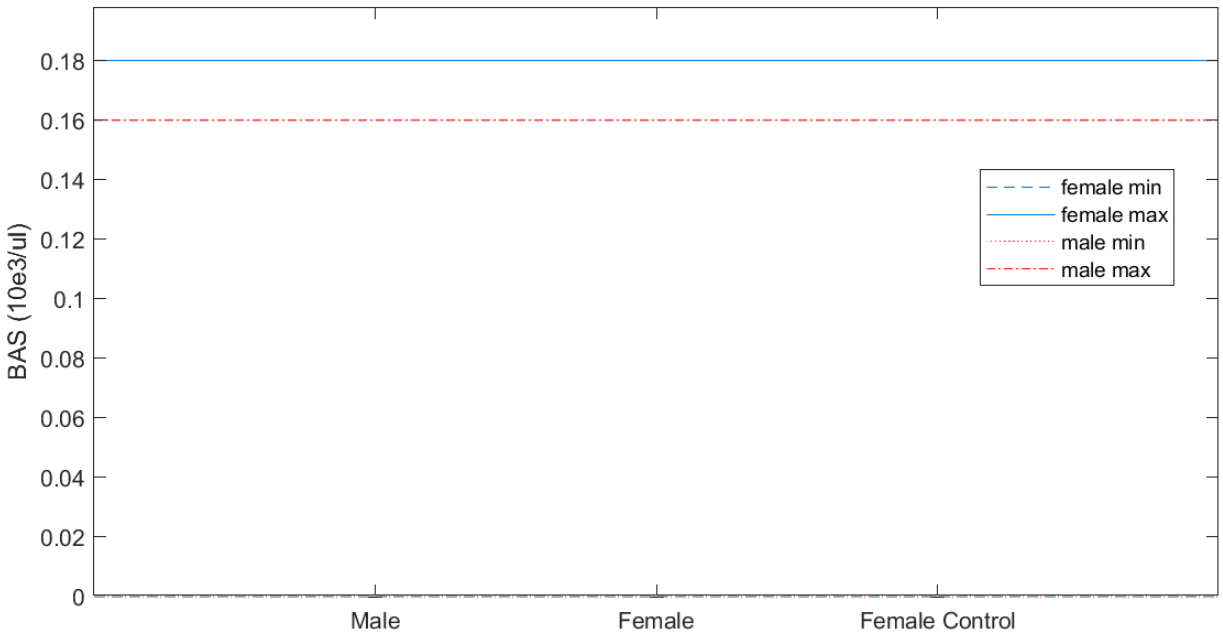
BAS (10e3/ul)
0.18
0.16
0.14
0.12
0.1
0.08
0.06
0.04
0.02
0
female min
female max
male min
male max
Male
Female
Female Control

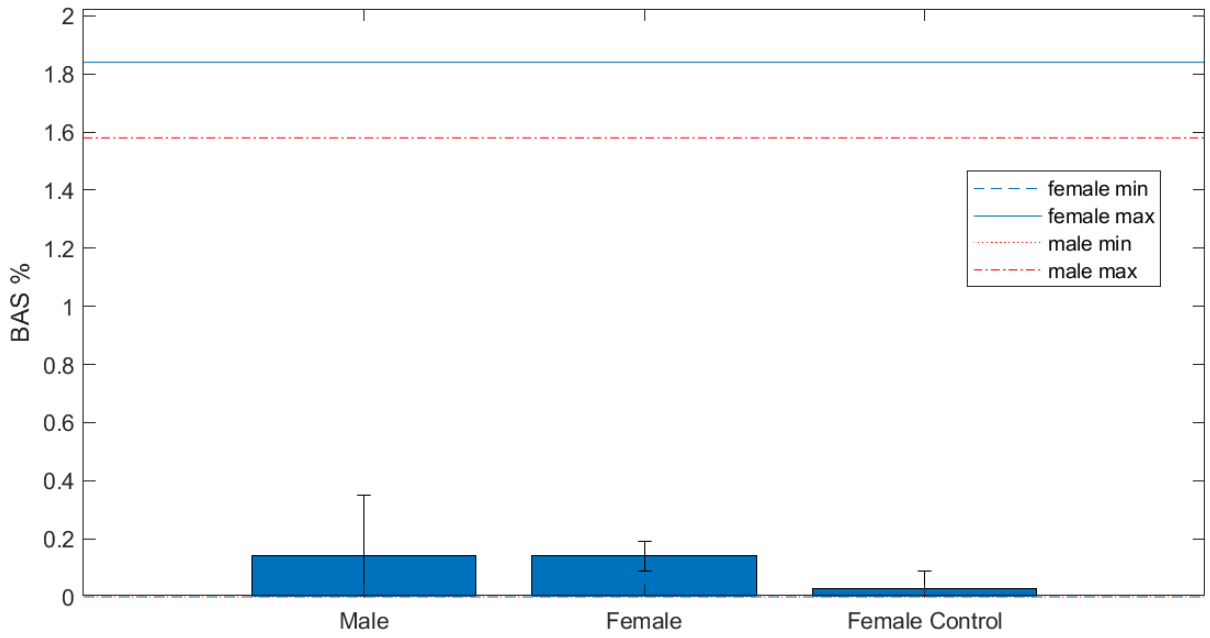
BAS %
2
1.8
1.6
1.4
1.2
1
0.8
0.6
0.4
0.2
0
female min
female max
male min
male max
Male
Female
Female Control

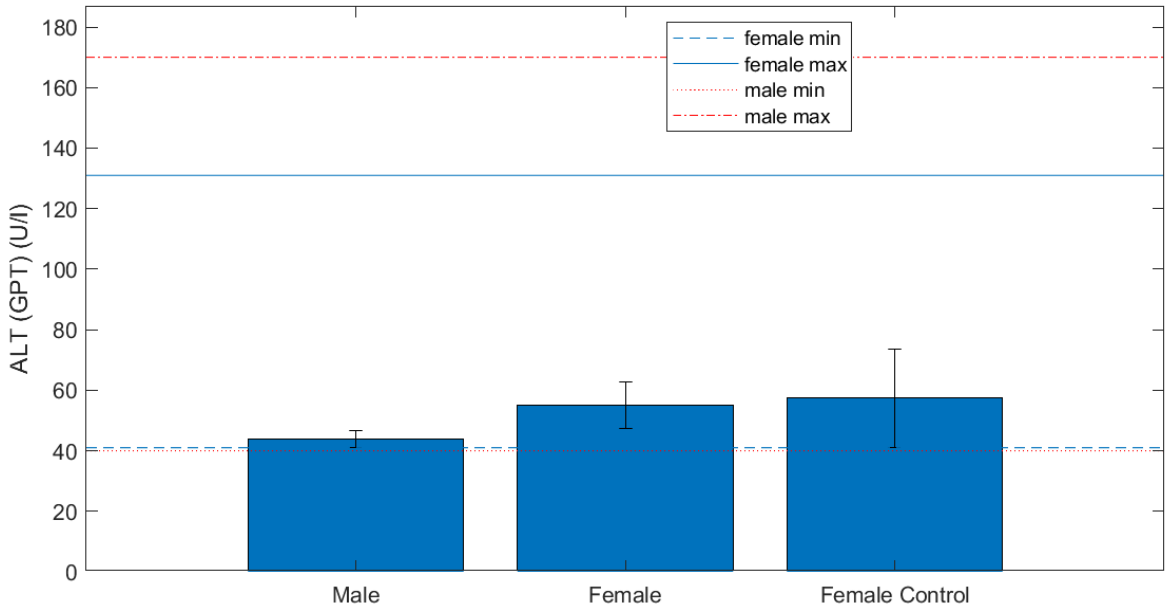
female min
female max
male min
male max
ALT (GPT) (U/l)
0
20
40
60
80
100
120
140
160
180
Male
Female
Female Control

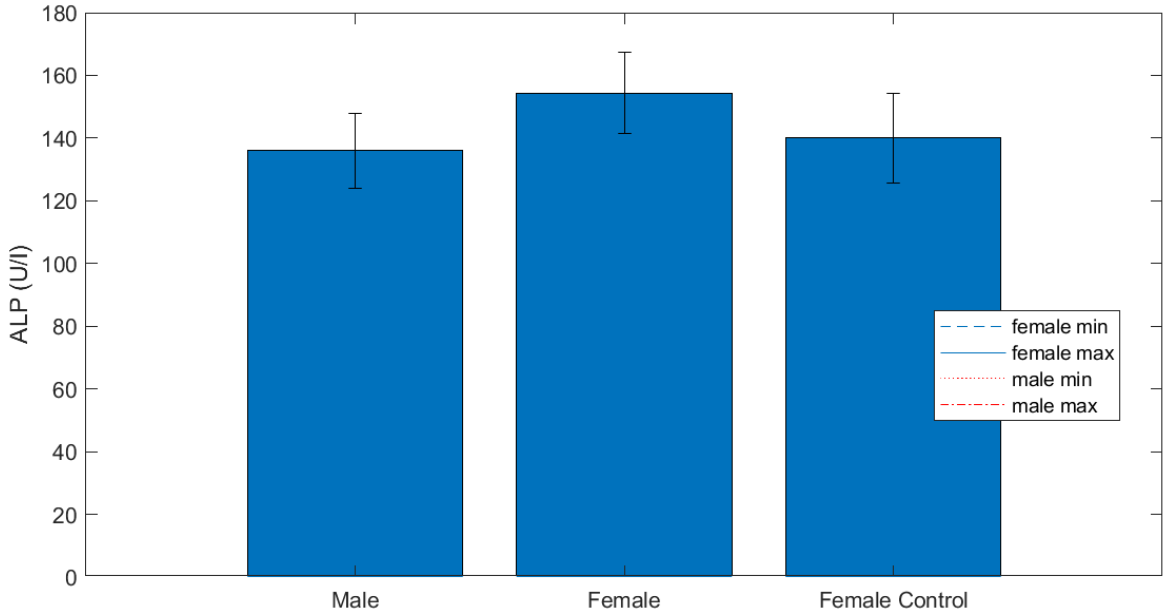
female min
female max
male min
male max
ALP (U/l)
0
20
40
60
80
100
120
140
160
180
Male
Female
Female Control

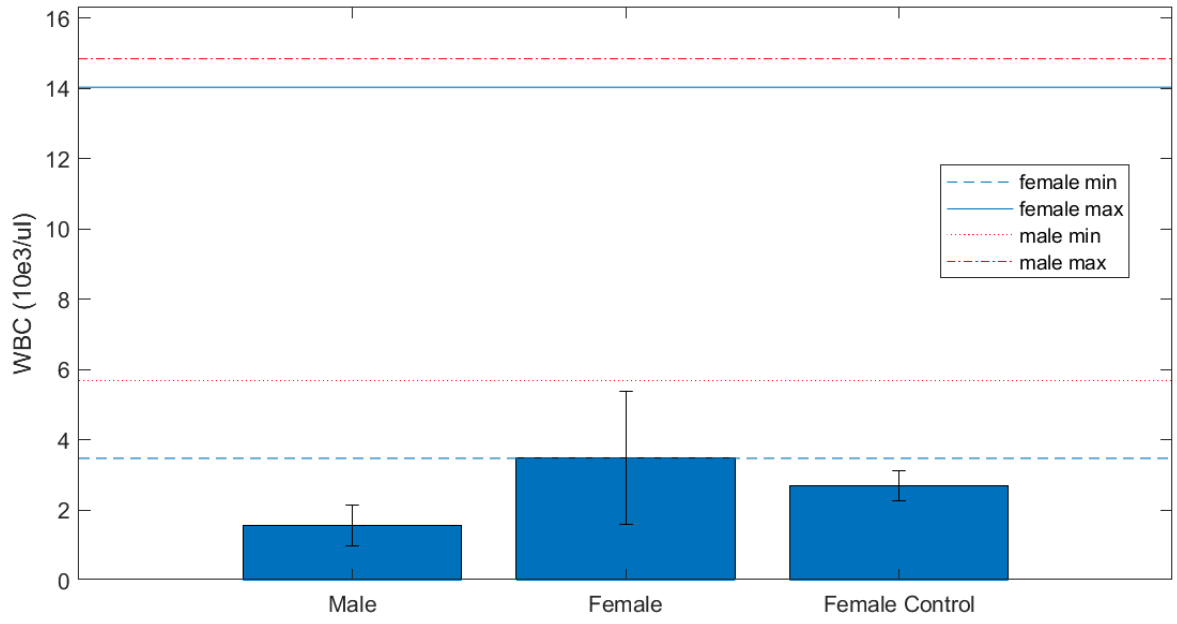
WBC (10e3/ul)
16
14
12
10
8
6
4
2
0
female min
female max
male min
male max
Male
Female
Female Control

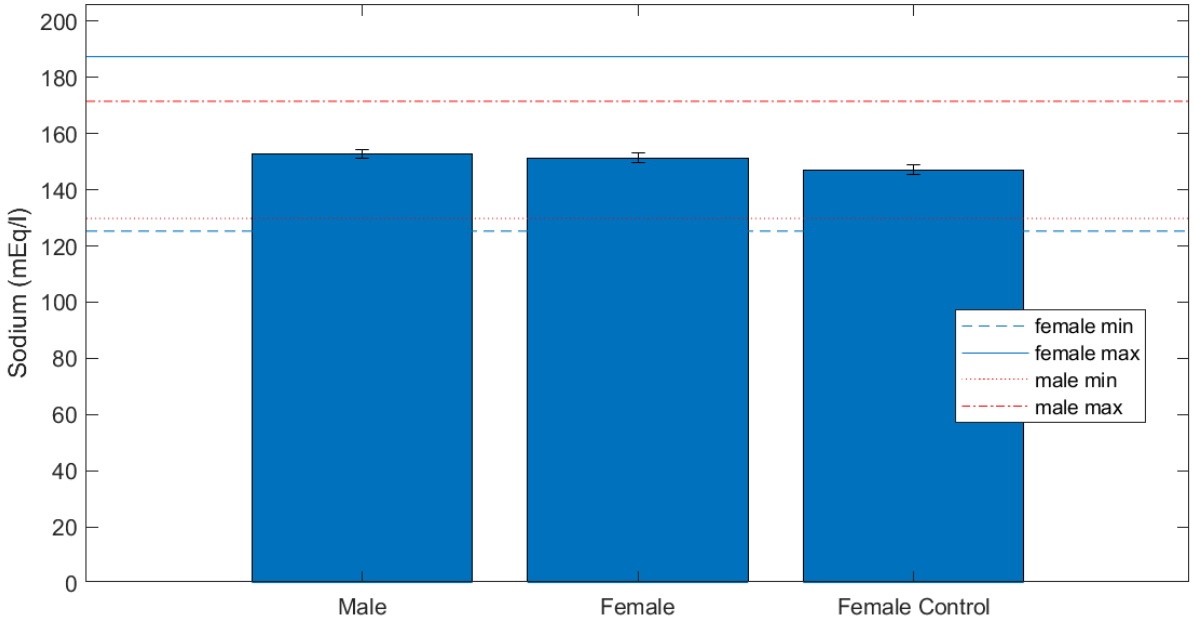
Sodium (mEq/l)
200
180
160
140
120
100
80
60
40
20
0
female min
female max
male min
male max
Male
Female
Female Control

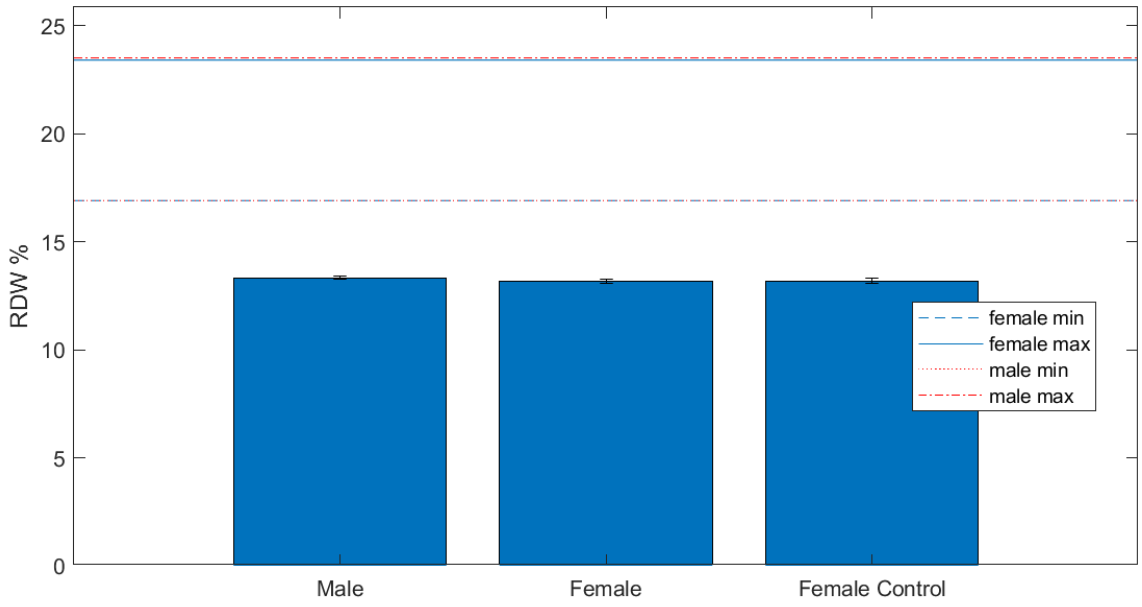
RDW %
25
20
15
10
5
0
Male
Female
Female Control
female min
female max
male min
male max

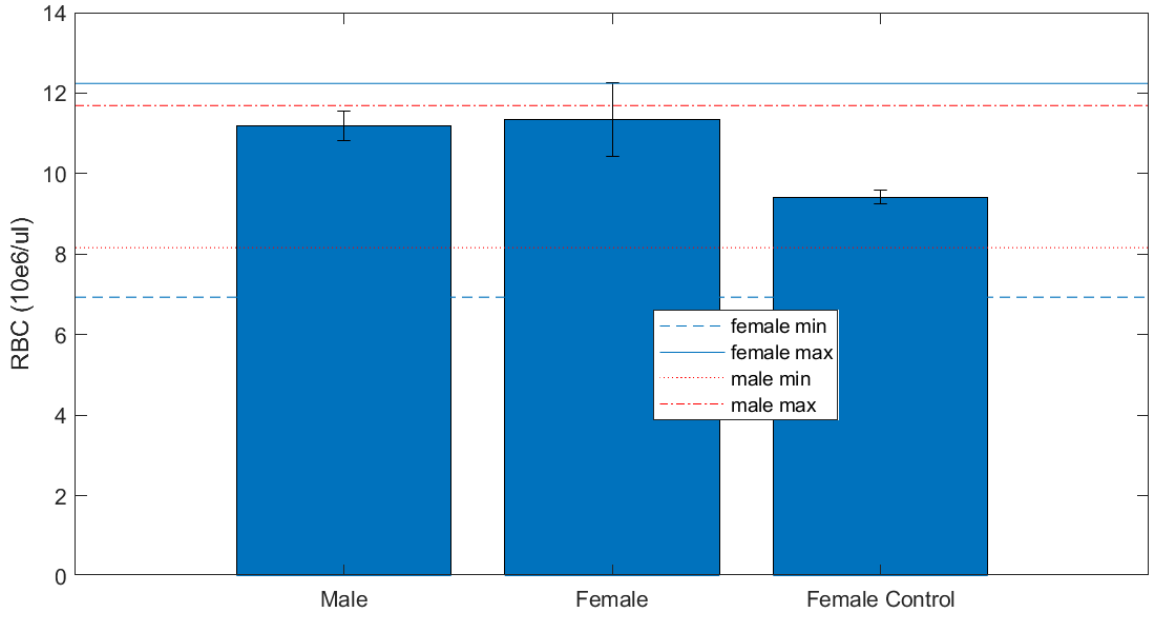
RBC (10e6/ul)
14
12
10
8
6
4
2
0
Male
Female
Female Control
female min
female max
male min
male max

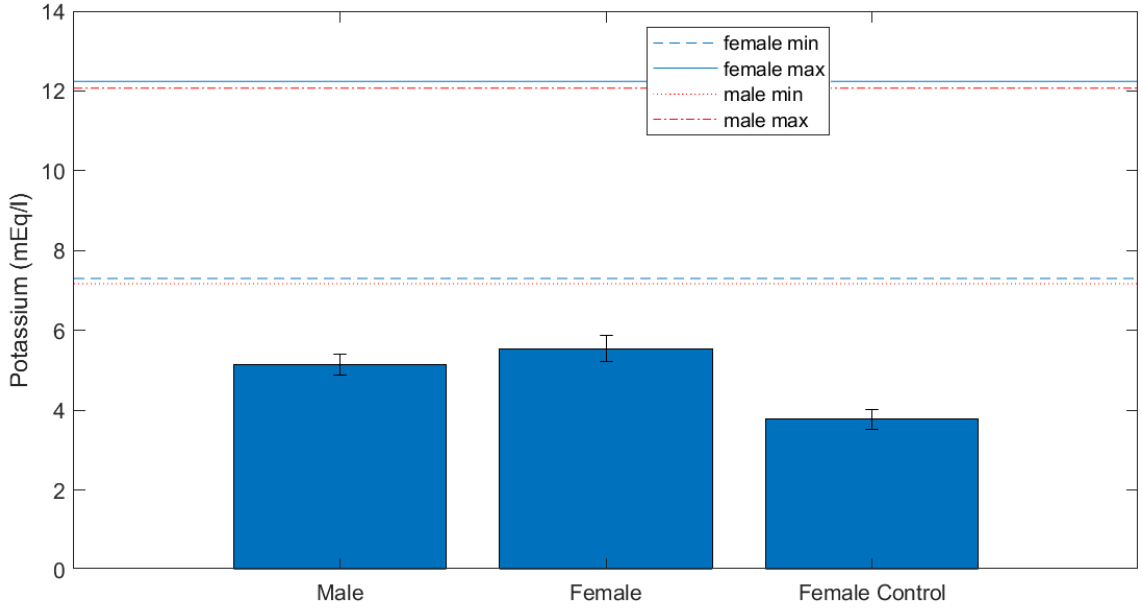
female min
female max
male min
male max
Potassium (mEq/l)
0
2
4
6
8
10
12
14
Male
Female
Female Control

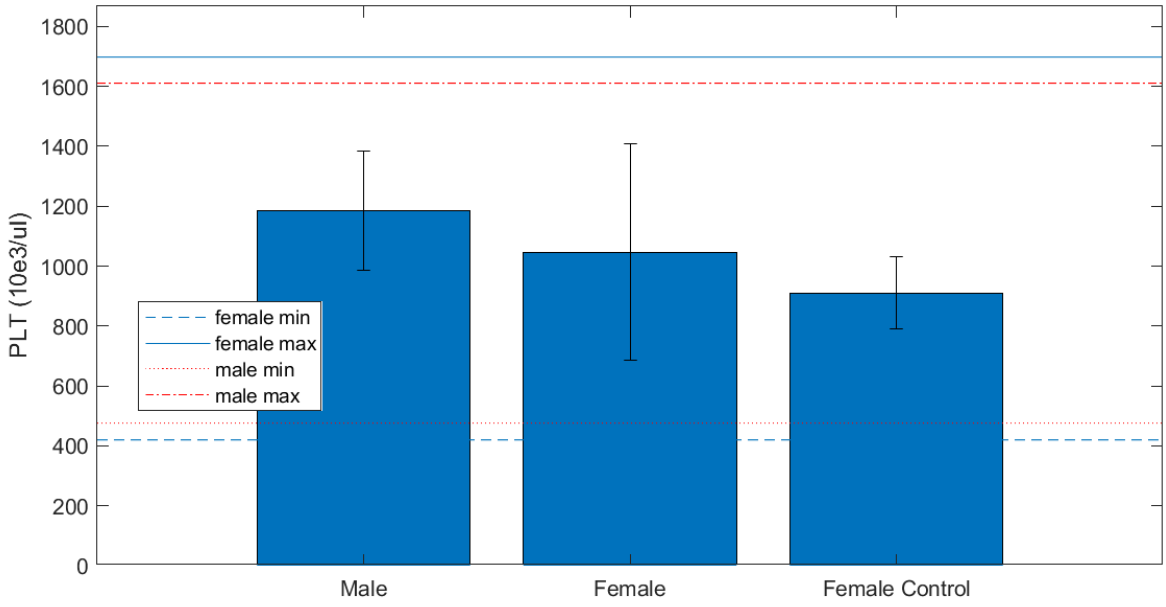
female min
female max
male min
male max
PLT (10e3/ul)
0
200
400
600
800
1000
1200
1400
1600
1800
Male
Female
Female Control

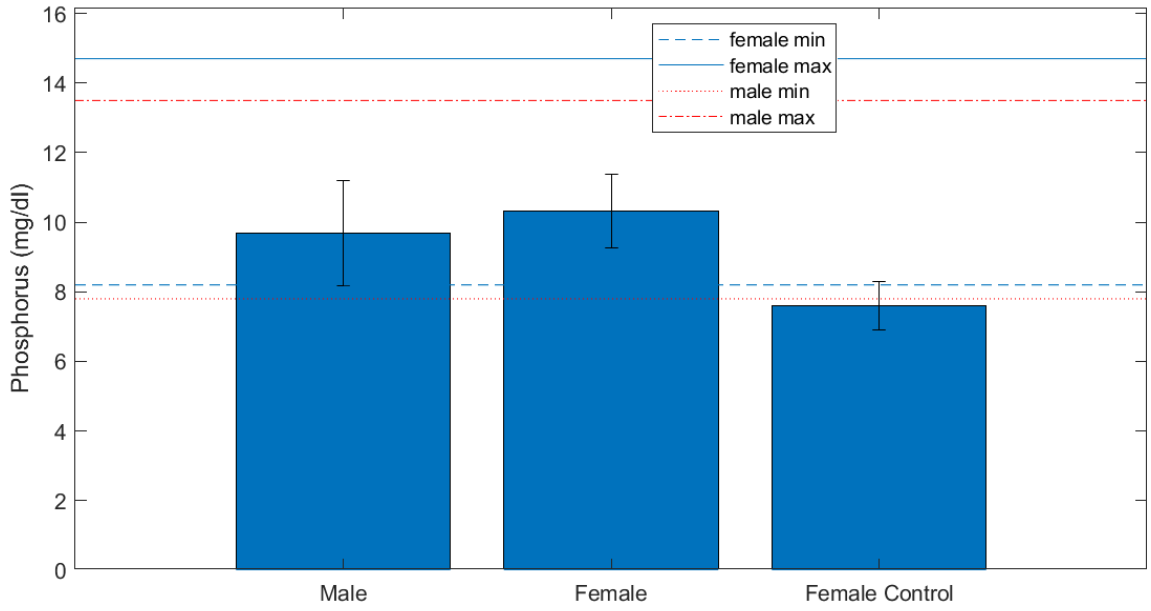
female min
female max
male min
male max
Phosphorus (mg/dl)
0
2
4
6
8
10
12
14
16
Male
Female
Female Control

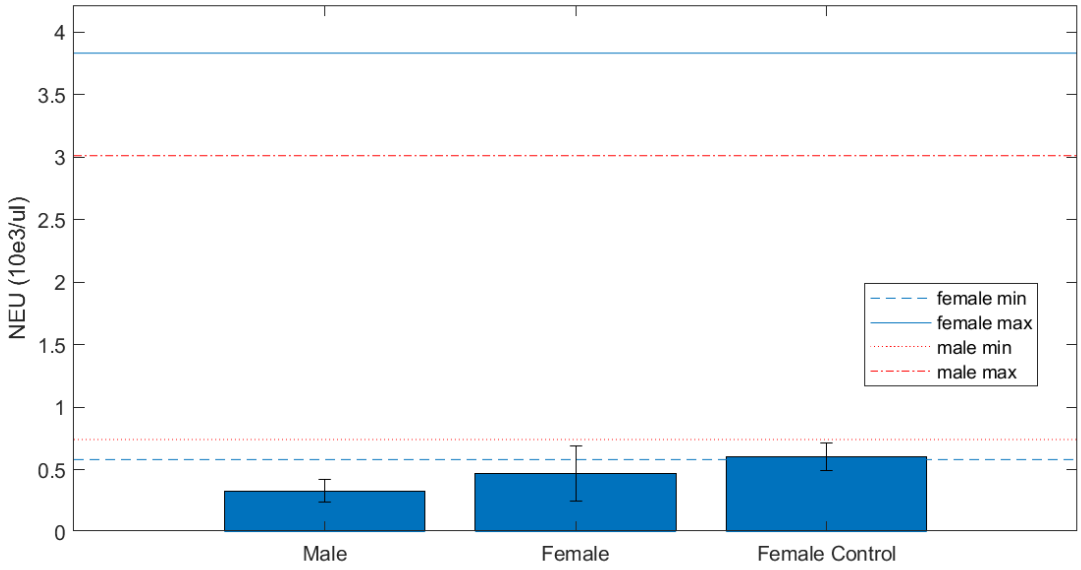
female min
female max
male min
male max
NEU (10e3/ul)
0
0.5
1
1.5
2
2.5
3
3.5
4
Male
Female
Female Control

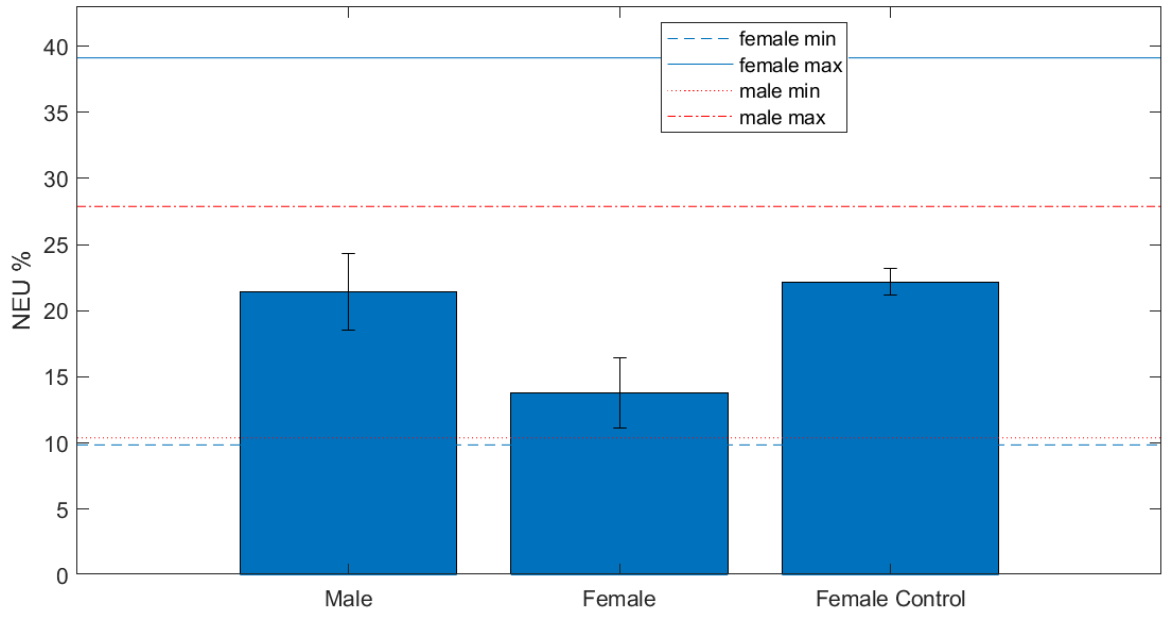
female min
female max
male min
male max
NEU %
0
5
10
15
20
25
30
35
40
Male
Female
Female Control

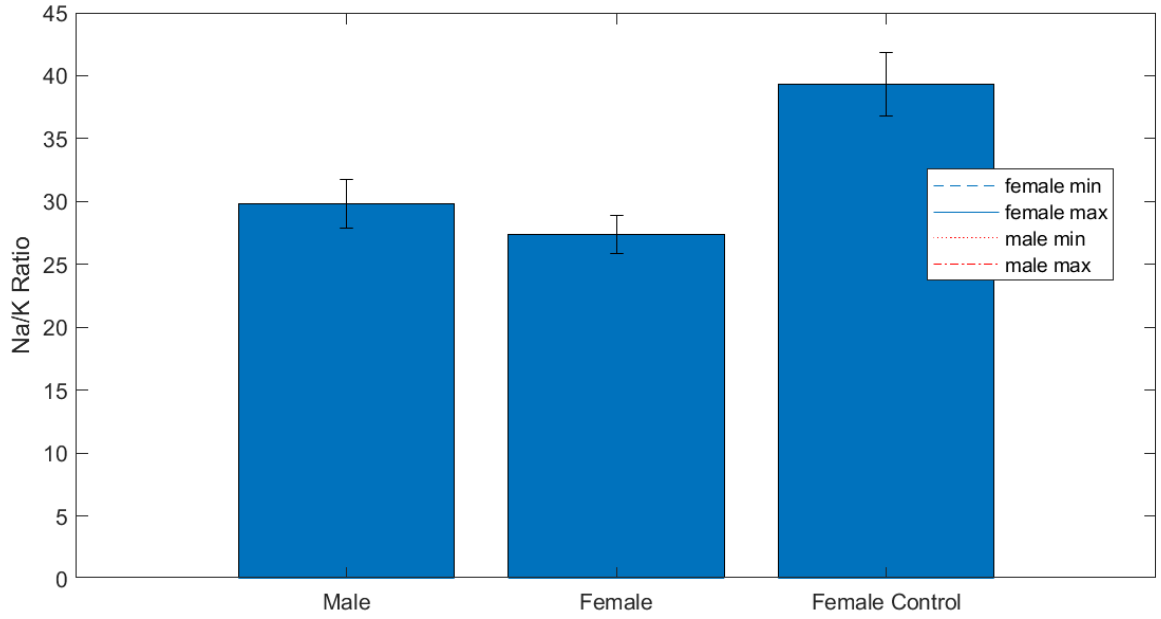
female min
female max
male min
male max
Na/K Ratio
0
5
10
15
20
25
30
35
40
45
Male
Female
Female Control

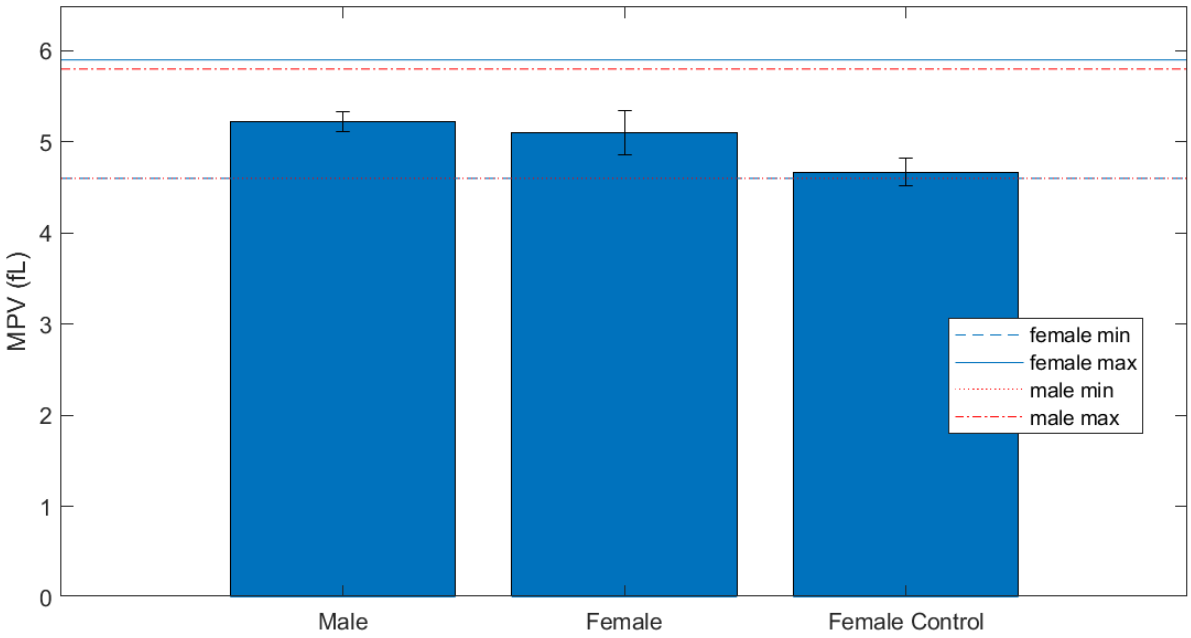
MPV (fL)
0
1
2
3
4
5
6
Male
Female
Female Control
female min
female max
male min
male max

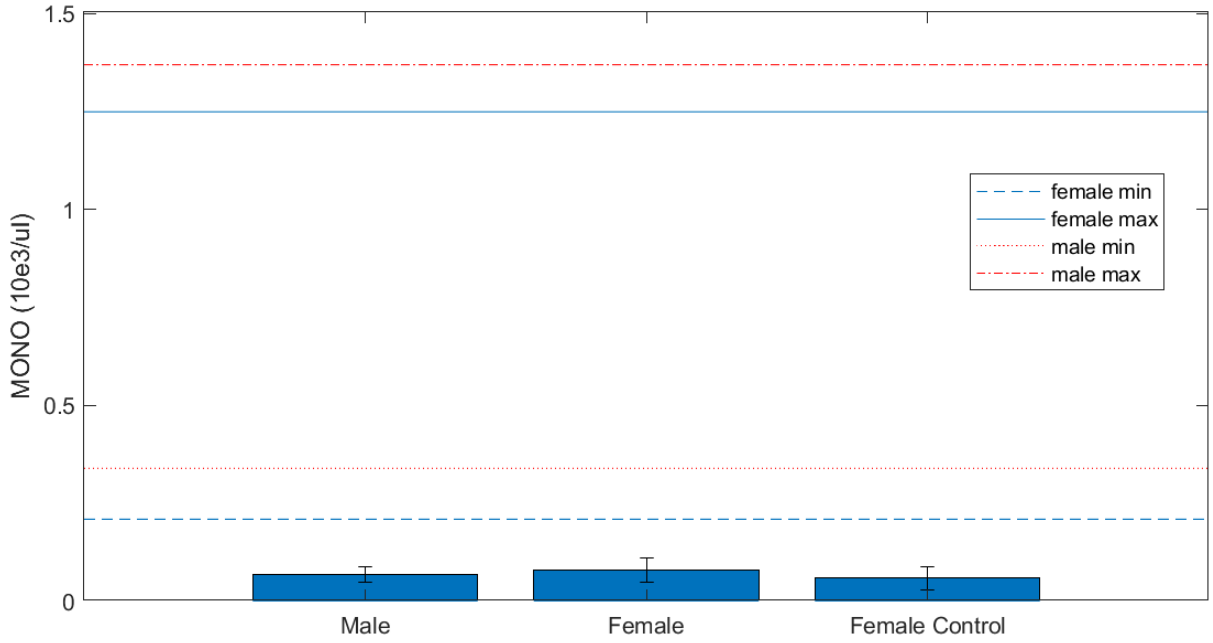
MONO (10e3/ul)
0
0.5
1
1.5
Male
Female
Female Control
female min
female max
male min
male max

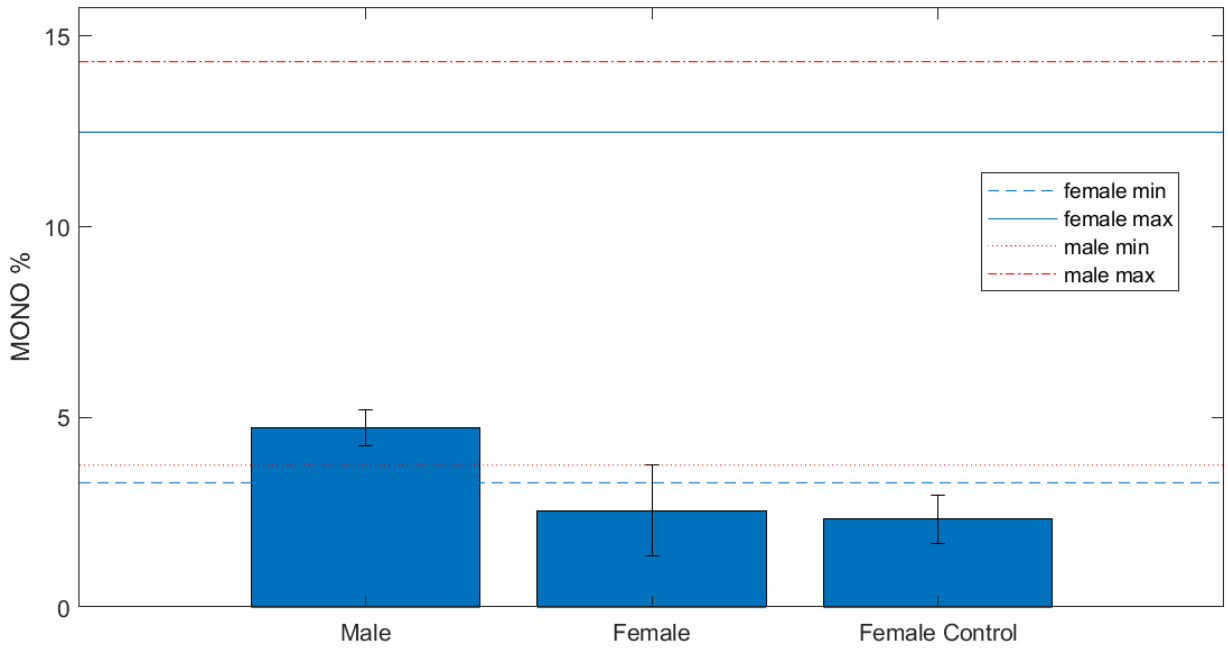
15
10
5
0
MONO %
female min
female max
male min
male max
Male
Female
Female Control

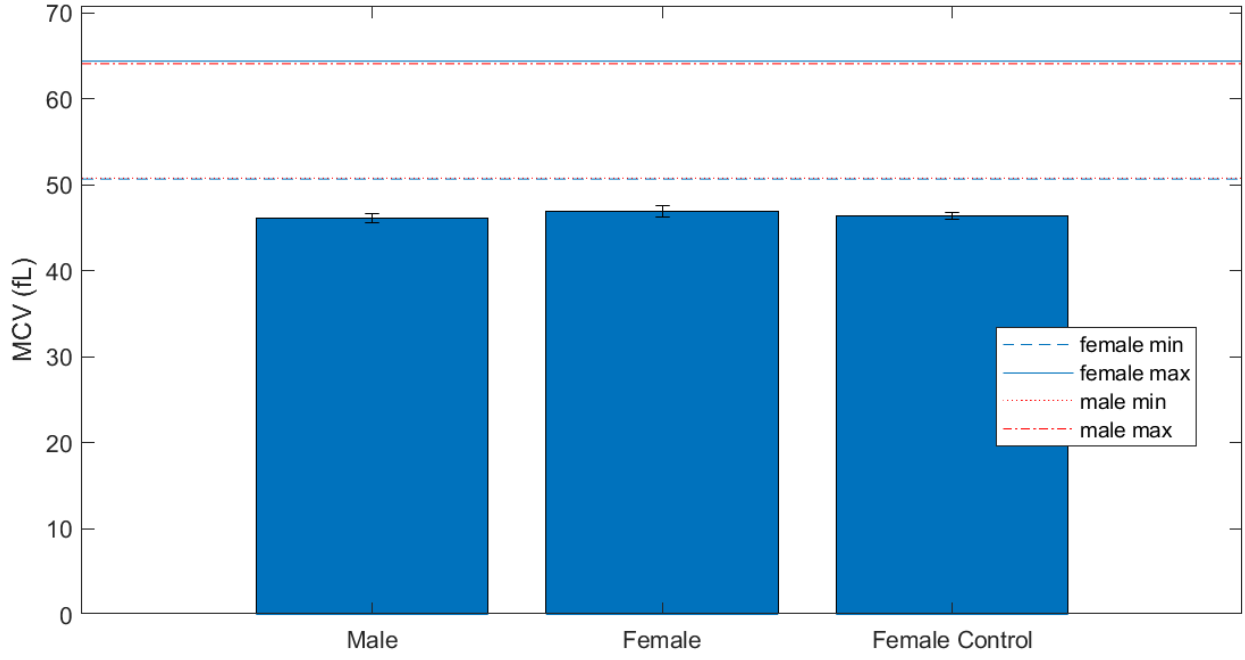
70
60
50
40
30
20
10
0
MCV (fL)
female min
female max
male min
male max
Male
Female
Female Control

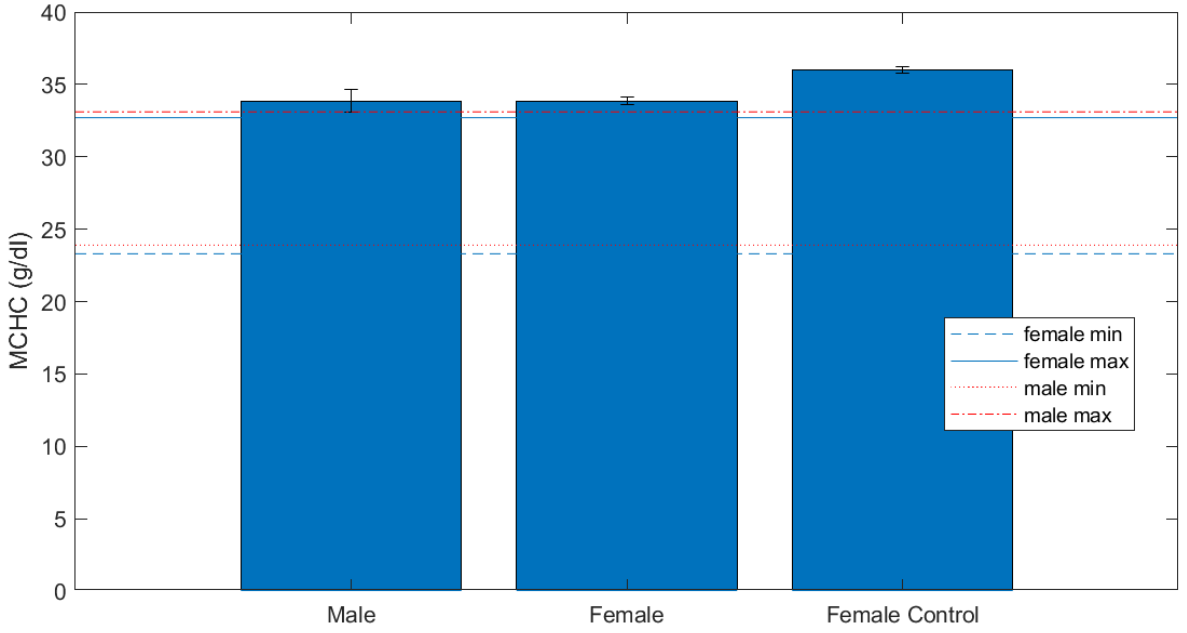
MCHC (g/dl)
40
35
30
25
20
15
10
5
0
Male
Female
Female Control
female min
female max
male min
male max

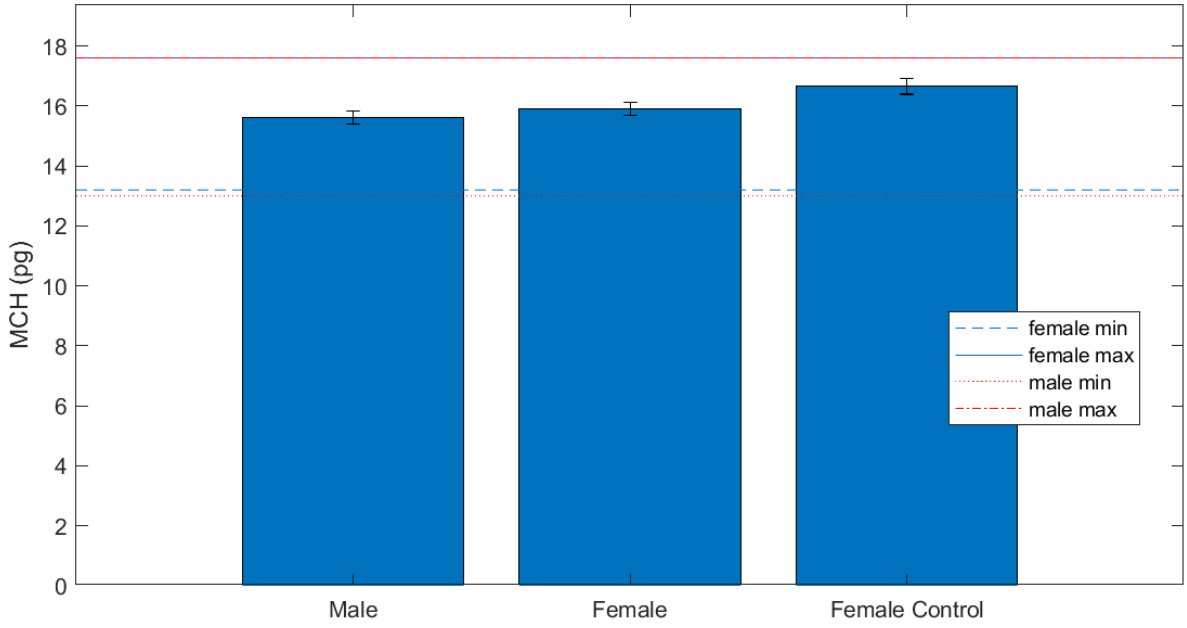
MCH (pg)
18
16
14
12
10
8
6
4
2
0
Male
Female
Female Control
female min
female max
male min
male max

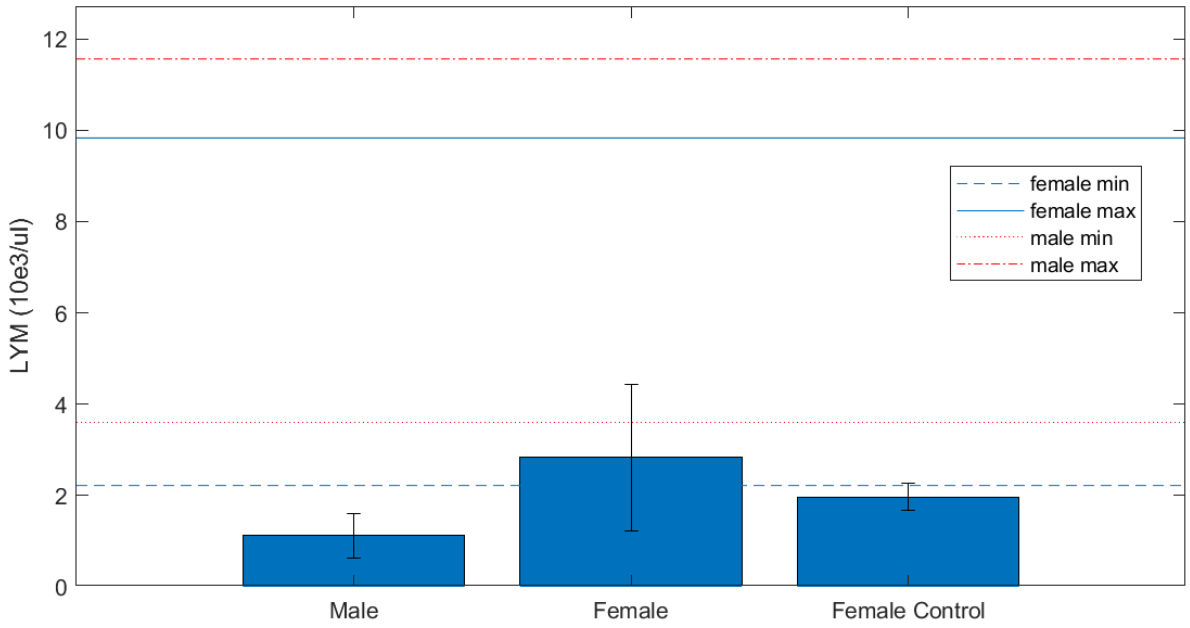
LYM (10e3/ul)
12
10
8
6
4
2
0
female min
female max
male min
male max
Male
Female
Female Control

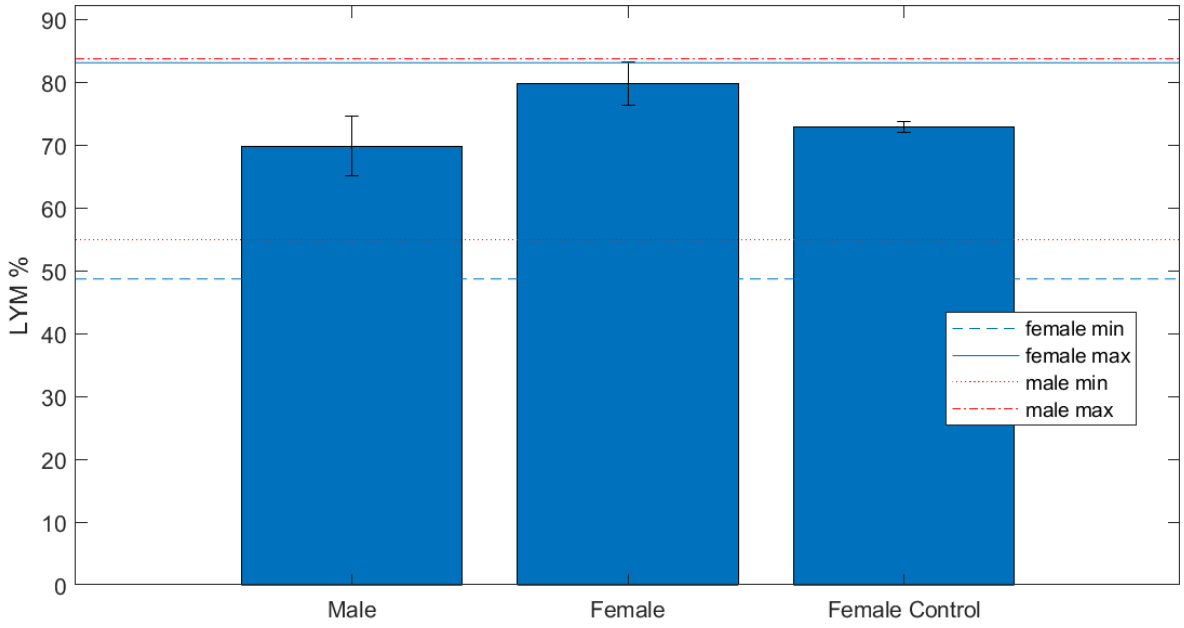
LYM %
90
80
70
60
50
40
30
20
10
0
female min
female max
male min
male max
Male
Female
Female Control

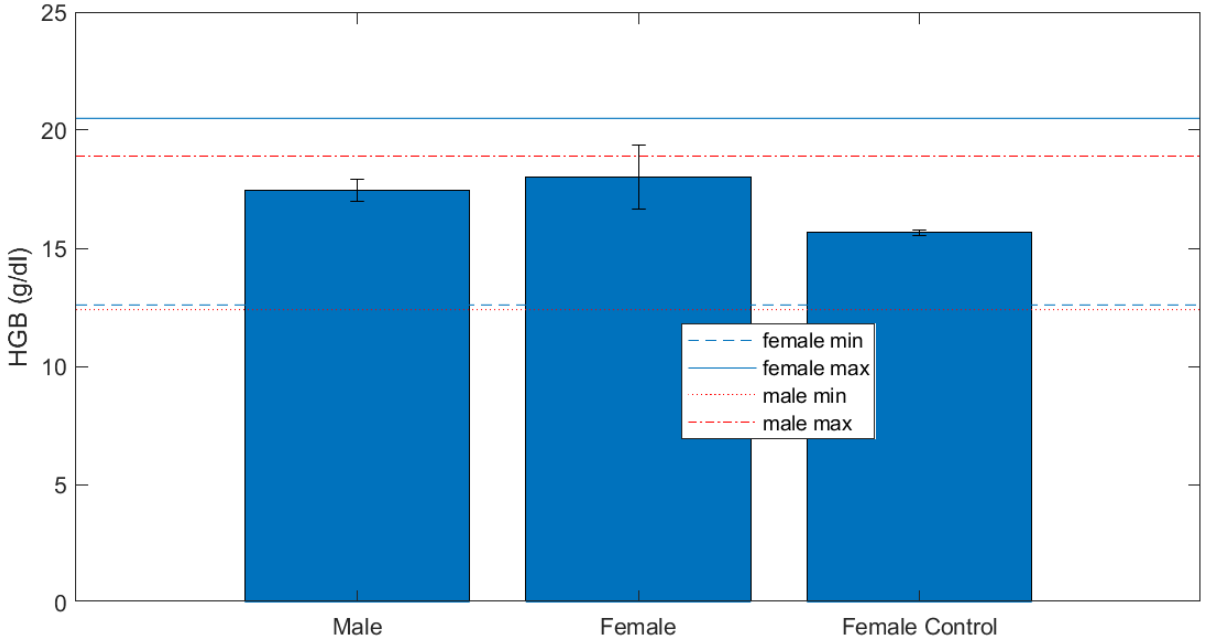
25
20
15
10
5
0
HGB (g/dl)
female min
female max
male min
male max
Male
Female
Female Control

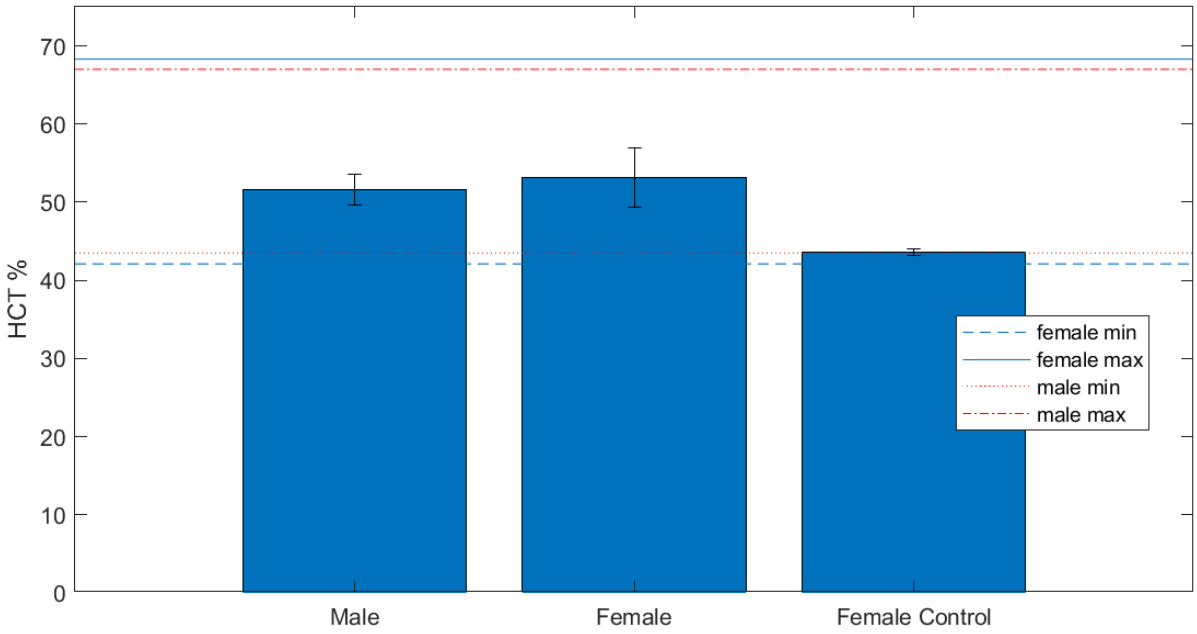
70
60
50
40
30
20
10
0
HCT %
female min
female max
male min
male max
Male
Female
Female Control

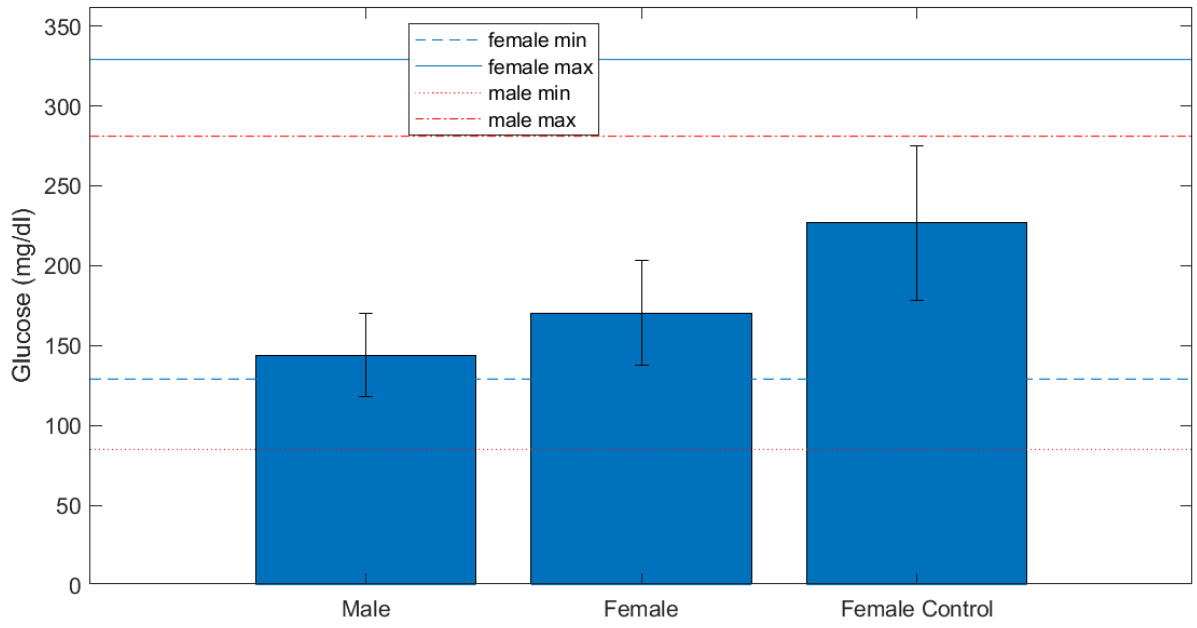
female min
female max
male min
male max
Glucose (mg/dl)
350
300
250
200
150
100
50
0
Male
Female
Female Control

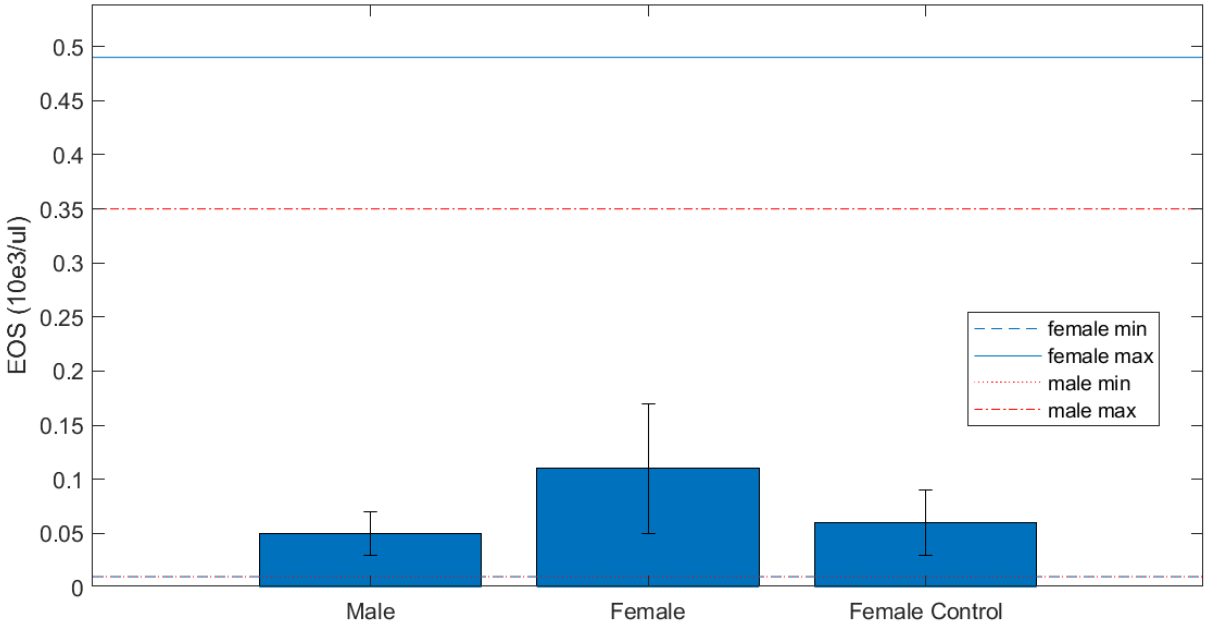
female min
female max
male min
male max
EOS (10e3/ul)
0.5
0.45
0.4
0.35
0.3
0.25
0.2
0.15
0.1
0.05
0
Male
Female
Female Control

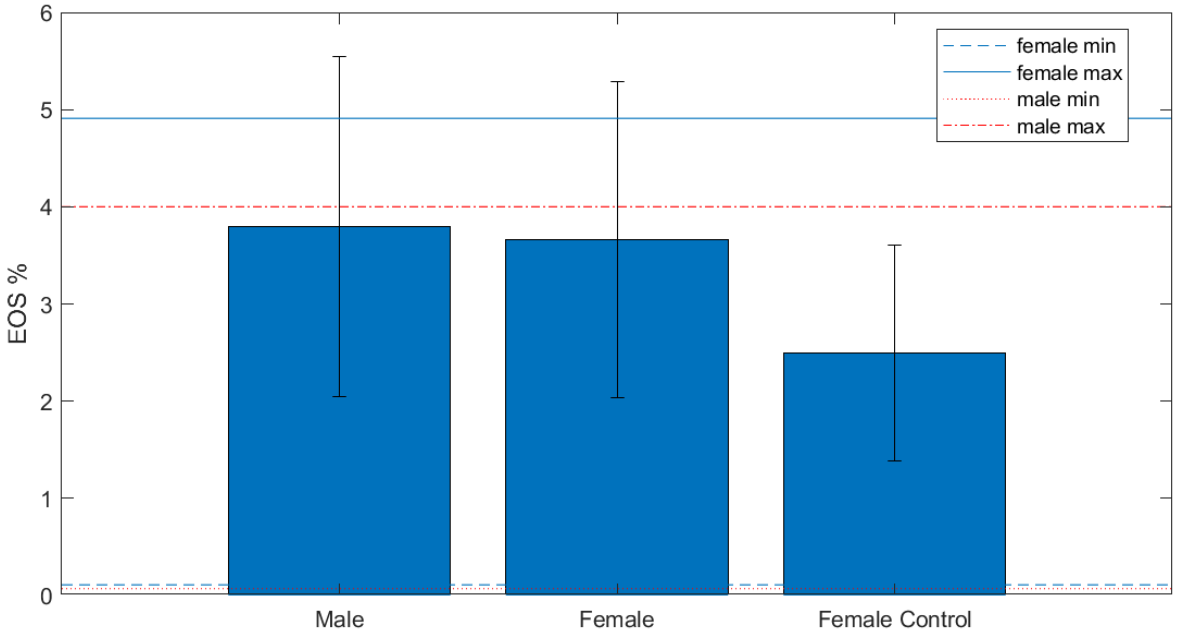
EOS %
6
5
4
3
2
1
0
female min
female max
male min
male max
Male
Female
Female Control

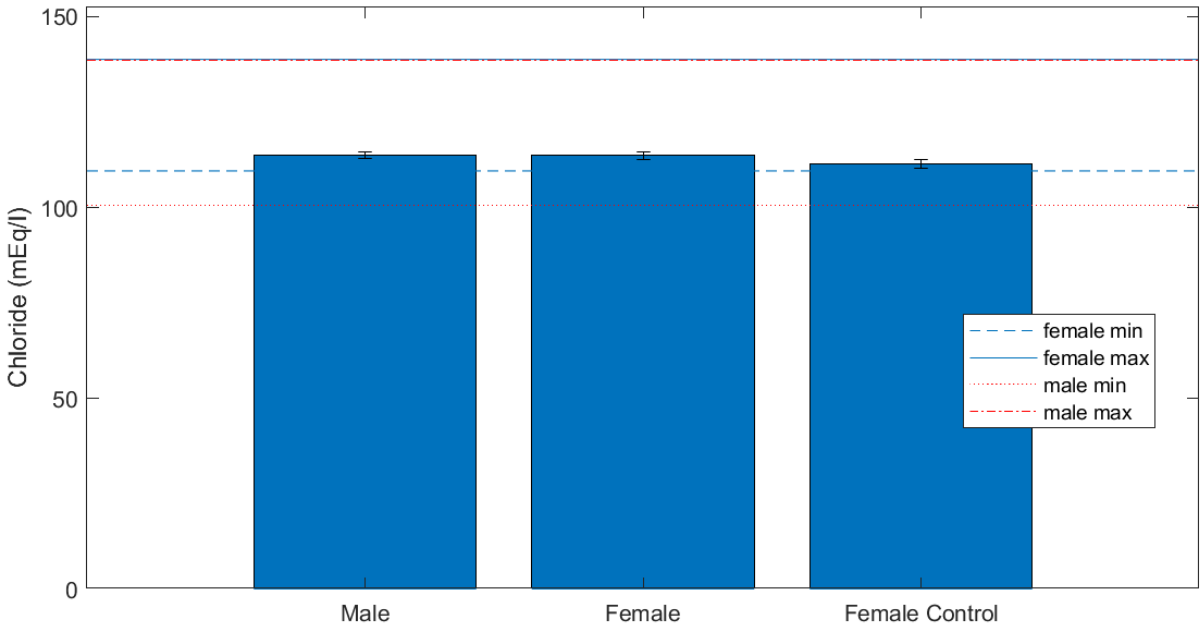
Chloride (mEq/l)
150
100
50
0
female min
female max
male min
male max
Male
Female
Female Control

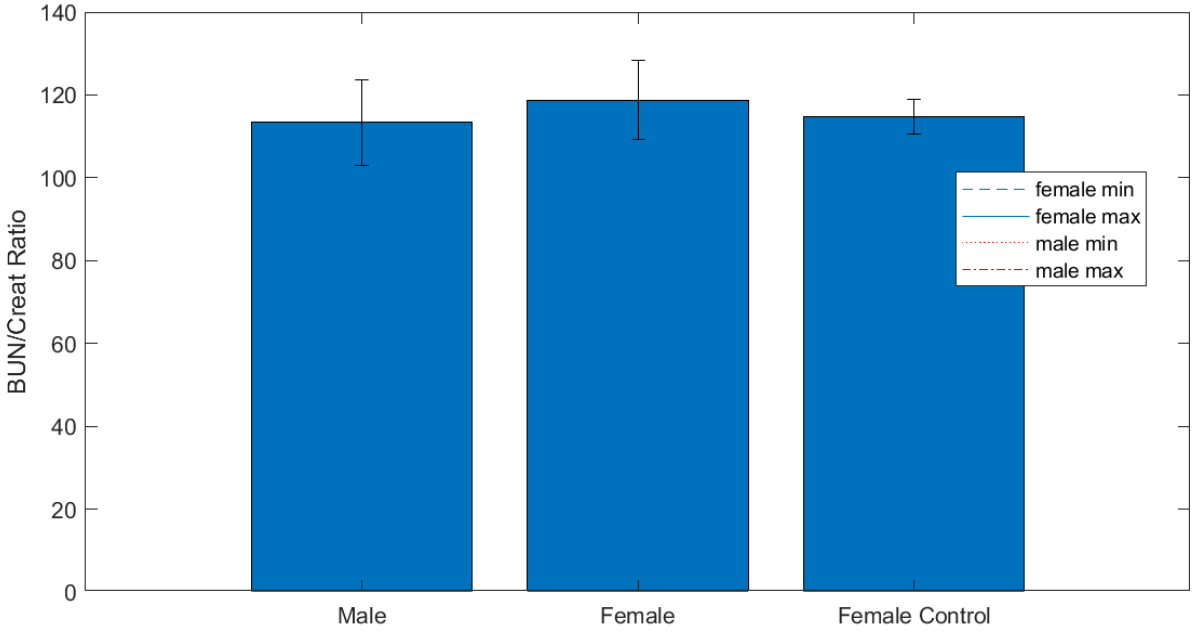
140
120
100
80
60
40
20
0
BUN/Creat Ratio
female min
female max
male min
male max
Male
Female
Female Control

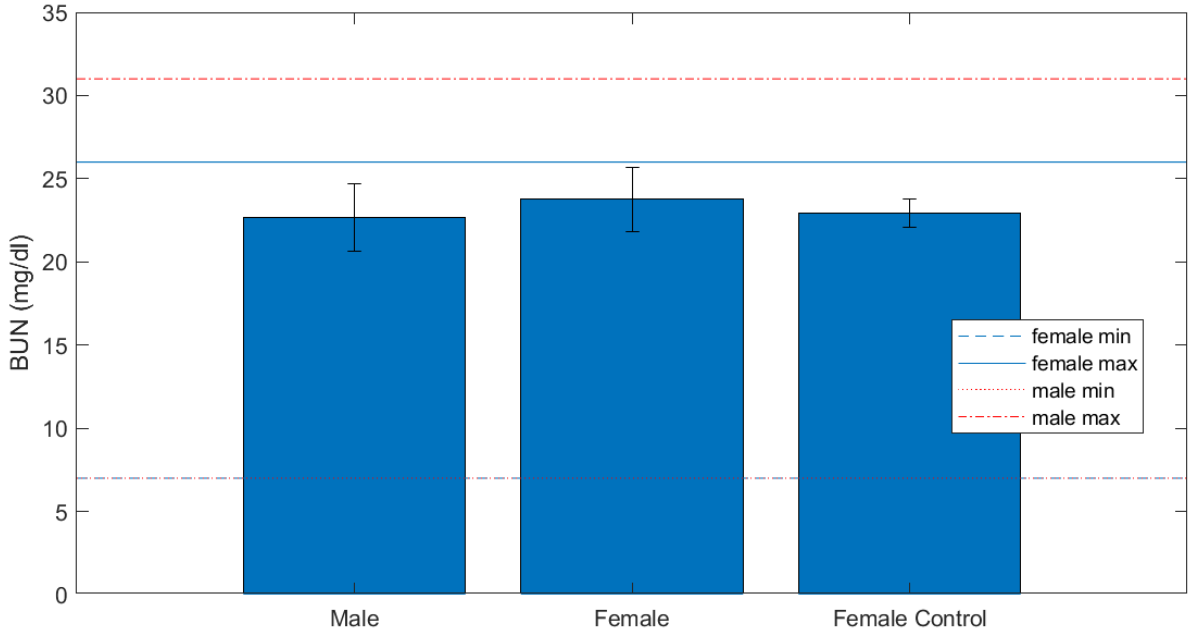
35
30
25
20
15
10
5
0
BUN (mg/dl)
female min
female max
male min
male max
Male
Female
Female Control